INDOOR POSITIONING AS A CONTRIBUTION TO BUILDING OCCUPANT MODELLING

MD. SHADAB MASHUK

BSC, MSC COMPUTER SCIENCE

THESIS SUBMITTED TO THE UNIVERSITY OF NOTTINGHAM

FOR THE DEGREE OF DOCTOR OF PHILOSOPHY

SEPTEMBER 2019



HORIZON CENTRE FOR DOCTORAL TRAINING

ABSTRACT

Assessing building performance related to energy consumption in the post-design-occupancy stage requires knowledge of occupancy patterns together with many other behavioural factors. Typically to evaluate building performance in the post-occupancy-evaluation (POE) period, it would require users to participate in occupancy detection trials covering the building and generate occupancy-related data. This would allow architects and built environment professionals to understand the current occupancy pattern and evaluate by comparing it with the predicted performance done at the design stage. Due to the limitations of passive sensors in detecting an individual's occupancy throughout the building, indoor positioning can provide a viable alternative but requires the deployment of a robust positioning solution. It also demands a user-friendly device capable of providing positioning-related data that users can carry around without any obstruction or hindrance to their daily work. Most modern smartphones come with an array of sensors quite capable of providing the desired solution. These requirements create the opportunity for research in new application areas of indoor positioning to solve real-world problems such as understanding building occupancy.

It is well-known that Global Navigation Satellite System (GNSS) based positioning performs poorly in the indoor environment, but alternative options making use of signals of opportunity from existing wireless devices and sensors can provide reliable and to some extent, very high accuracy indoor positioning solutions. Some common examples of indoor positioning systems widely researched are based on Wi-Fi and Bluetooth Low Energy (BLE), inertial navigation solutions using foot-mounted or smartphone Inertial Measurement Unit (IMU), Ultrawideband (UWB) or Radio Frequency Identification (RFID). Unfortunately, the use of such technology is dependent on the context of usage and most of them have not yet been commercialised. After careful exploration of the current state of research related to indoor positioning technology, techniques, positioning capability, infrastructure costs and ease of deployment, an indoor positioning system is proposed which makes use of

the smartphone and its built-in integrated sensors: Wi-Fi, Bluetooth, accelerometer, and gyroscope. The positioning system uses the traditional Wi-Fi and Bluetooth fingerprinting in combination together with pedestrian dead reckoning to develop a cheap but effective multi-floor indoor positioning solution. The combination of all these performance critical elements involved in the positioning system requires continuous collection of Wi-Fi and BLE signal observations from the fingerprint radio map, checking step events and heading and stairwell detection. These are all fused in a particle filter engine for positioning state estimation epoch-by-epoch in a multi-sensor pedestrian dead reckoning solution.

To test the capability of the proposed positioning system each of the dead reckoning elements; step detection and heading estimation have been thoroughly tested in an objective manner and the positioning system validated by carrying out experimental trials against ground truth obtained from a Robotic Total Station. The relevant positioning algorithms and techniques were carefully chosen to ensure ease of implementation with minimum complexity without compromising the core performance specification necessary for occupancy detection.

Real-life occupancy is very complex, and an extensive trial in a real-world setup is necessary. The potential of the proposed prototype positioning system was investigated by involving non-expert participants in real-world trials to show the limitations and effectiveness of using such systems for detecting occupancy. The trials were designed in the form of spatially distributed tasks to imitate real-life occupancy. Participants were required to move around without any guidance to cover different parts of an office building with multiple floors. The appropriate ethics approval was obtained for the study beforehand and participants were recruited with their explicit consent. In total, fifty trials were carried out by around twenty-two participants. The trials comprised of a variety of routes and floors of a sample office building within the limited time scale of the PhD research. All the trials were validated by comparing the estimated occupancy against real occupancy recorded by the researcher who shadowed the participants during the trials. The trial results were analysed to

demonstrate the level of accuracy achievable in terms of occupancy against a specific set of performance metrics. Sensor deployment challenges faced during the research are discussed as well.

Finally, to demonstrate a possible contribution, an agent-based building occupant model is developed to understand the local dynamics of electricity consumption using different lighting policies with inputs from the developed indoor positioning system. The model uses the Nottingham Geospatial Building's lighting and floor plan configuration as an example. The energy usage obtained from simulation for the default lighting policy is validated using real electricity data from the local energy supplier, the University Estates Department for any required calibration of the model. One example is then chosen to illustrate how the positioning data collected from observed individuals' trajectories from the original trials contribute to the understanding of electricity usage in multi-floor offices when a different lighting policy is applied on the base model and any potential impact analysed.

This research has intended to demonstrate how indoor positioning data can be applied to the improvement of building occupant modelling and what the shortcomings and limitations of this approach are. Shortcomings of the positioning system, when it comes to detecting occupancy, have been identified from the multi-user trials. Simplifications and assumptions made when implementing the algorithms for individual elements of the positioning system, especially motion detection and heading estimation, have been discussed together with their potential implications on the expected accuracy of the positioning system. Key areas of improvement, choice of technology, techniques and application methodology were identified for future work related to the development of the positioning solution.

ACKNOWLEDGEMENT

As I look back on the past five years of my life, i.e. half a decade spent with the University of Nottingham, Horizon CDT and most importantly Nottingham Geospatial Institute, I start to get a bit emotional. I remember a line from one of my favourite songs, Unchained Melody by Righteous Brothers “Time goes by so slowly and time can do so much”. Indeed, it is so true, and I have experienced a range of emotions within this period. I have been excited, nervous, tense, bored and excited again and if these emotions can be mapped into my PhD timeline, it would perfectly fit from starting on the very first day I got my PhD offer.

Time did go slowly when I got stuck, and things did not work out the way they were planned. Those flurry of emails and meetings with my supervisors and informal drop-ins on how to proceed with the PhD are all paperwork now in the form of supervision meeting forms. However, time has also made me do so much in the process; reading papers, writing codes, surveying, running experiments and simulations, designing trials and data collection but most importantly experiencing failures. All of them stitched together, finally take the shape of this PhD thesis. I must say I have learned a lot, not just from an academic perspective but also from an individual development point of view. I believe whatever I have learned will be translated as a life experience for whatever the future may hold, and I am grateful for that.

I would like to sincerely thank my supervisors, Professor Terry Moore, Dr James Pinchin and Dr Peer-Olaf Siebers, for their constant support and guidance throughout my research. Without their support it would have been very difficult to reach this stage. A big thanks to Professor Darren Robinson who originally came up with the idea of linking the indoor positioning part of my PhD with building occupancy modelling when I was struggling to connect the dots for this inter-disciplinary PhD. He was my supervisor until the first year but has since moved to the University of Sheffield. Special thanks to my internal examiner Dr Chris Hill, who has provided me with constructive feedback of my work during the annual reviews and advised me whenever I knocked. A big thank you to Emma Juggins and Andrea Haworth from Horizon CDT

and Alison Mellor from NGI for supporting me with all the administrative paperwork chores. Thanks to Lukasz Bonenberg and Sean Ince for assistance related to survey equipment's and trial setup and Chaz Dixon for managing my internship with Satellite Applications Catapult.

I want to thank my NGI colleagues, Pekka, Jialin, Ammar, Ioulia, Francesco, Ahmed Talabany, Roberto, Abdullahi, Habboub and many more for making my time spent in NGI worth it and enjoyable. A special mention for Jialin and Pekka again for their help with my work and data collection. It would have been difficult without your support. Thank you to my Horizon CDT colleagues, we had a wonderful year with the CDT and thank you to all who have graciously agreed to participate in my trials for data collection.

Friends are the light bulbs of my life and they need a special mention. Here is to all my dear friends from Nottingham who are very close to my heart and without whom my life would have been very dull at various points of my stay in the UK. Qur, Sanjana, Tamanna, Sakib, Tushar, Zenan, Meem, Nabil, Zarin, Shabnam, Asif, Bismoy, Rai, Nobel, Rishov, Samiha, Aunik, Sabrin and Nusrat Priya, you all have supported me and my family and made our life in Nottingham colourful. May Allah (SWT) shower you all with all the blessings and prosperity in life wherever you go.

Last but not the least I would like to extend my unconditional love and gratitude to my parents; Ammu, Abbu and my dear brother Shaan for who I am today and always believing in me, my in-laws; Maa, Baba, Adnan bhai and bhabi for always being so supportive and motivating, Mejo Fuppi, Prince Fuppa, Toma and Trina for always being there beside us in the UK whenever we needed but most importantly my dear Wife; Kashfia for always staying by my side and providing me with love, invaluable support and motivation throughout this journey. In the midst of all them, I must mention my biggest joy in life, my baby daughter Zeinaab, who came into this world on November 24, 2017, and gave me new hope and direction in life. Finally, all praise be to Allah (SWT) for His blessings and mercy and for my sound health, mind and body with the constant reminder that our life is fleeting just like the sands of time.

Contents

Chapter 1 INTRODUCTION 1

1.1 Overview 1

1.2 Background 2

1.3 Research Details and Approach 6

1.3.1 Problem Statement 6

1.3.2 Research Questions 8

1.3.3 Aim 9

1.3.4 Objectives 9

1.3.5 Steps for Achieving Objectives 9

1.4 Thesis Outline 11

Chapter 2 INDOOR POSITIONING OVERVIEW 14

2.1 Coordinate System 15

2.1.1 Earth-Centred Inertial Frame 16

2.1.2 Earth-Centred Earth-Fixed Frame 17

2.1.3 Local Navigation Frame 17

2.1.4 Body Frame 18

2.2 Attitude Representation 19

2.2.1 Euler Attitude 20

2.2.2 Coordinate Transformation Matrix 21

2.2.3 Quaternion Attitude 22

2.3 Kinematics 23

2.3.1 Angular Motion 23

2.3.2 Cartesian position 24

2.3.3 Velocity 25
2.3.4 Acceleration 26
2.4 Filter Algorithms in Navigation System 26
2.4.1 Kalman Filter 27
2.4.2 Closed Loop Kalman Filter 29
2.4.3 Extended Kalman Filter 29
2.4.4 Unscented Kalman Filter 29
2.4.5 Particle Filter 30
2.5 Inertial Navigation and Dead Reckoning 32
2.5.1 Pedestrian Dead Reckoning 35
2.6 Map Matching 37
2.7 Indoor Positioning Technology and Techniques 38
2.7.1 Measurement Techniques 39
2.7.2 Positioning Technology 44
2.8 Discussion on Application 50
2.9 Choice of Technology and Discussion 55
Chapter 3 BUILDING OCCUPANT MODELLING OVERVIEW 57
3.1 Background 57
3.2 Probabilistic Modelling approaches 58
3.3 Environmental Sensors 62
3.4 Localisation Sensor and Technology 63
3.5 Alternative Modelling Approaches 64
3.6 Conclusion 65
Chapter 4 INDOOR POSITIONING USING BLE and Wi-Fi 67
4.1 Introduction 67

4.2 Android Data Logger 68
4.2.1 Android Wi-Fi API 68
4.2.2 Android BLE API 69
4.2.3 Android Motion Sensor 70
4.2.4 Discussion 71
4.3 Wi-Fi and Bluetooth *RSS* characteristics 72
4.4 Radio Fingerprint Mapping and Analysis 82
4.4.1 Offline Phase 82
4.4.2 Online Phase 83
4.4.3 Training Point Data Collection 83
4.4.4 Gaussian Process Regression Fingerprint Database 86
4.5 Positioning algorithm comparison 92
4.6 Discussion 101
Chapter 5 LOCATION ENGINE ALGORITHMS 103
5.1 Introduction 103
5.2 Smartphone Motion Sensors 104
5.2.1 Experimental Setup 105
5.2.2 Results 106
5.3 Motion Detection 116
5.3.1 Background 116
5.3.2 Motion Detection Methodology 119
5.3.1 Peak-Valley motion detection 120
5.3.2 Discrete Fourier Transform based motion detection 121
5.3.3 Combined DFT and Peak-Valley motion detection 123
5.3.4 Testing the combined DFT and Peak-Valley method 125

5.4 Heading Estimation 130
5.4.1 Heading Estimation - Experimental Results 134
5.5 Particle Filter Engine 137
5.6 Location-Engine Validation 141
5.7 Discussion 143
Chapter 6 MULTI-USER POSITIONING TRIAL 145
6.1 Introduction 145
6.2 Testbed Configuration 146
6.3 Bluetooth Beacon Deployment challenges 147
6.4 Occupancy Trial Experiments 148
6.4.1 Preliminary Trial results and analysis 148
6.4.2 Lego Trial Task Design 153
6.4.3 Lego Trial results 156
6.4.4 Validation 165
6.5 Performance Specification and Analysis 171
6.6 Discussion 174
Chapter 7 A POTENTIAL USE OF POSITIONING DATA IN BUILDING SIMULATION 176
7.1 Introduction 176
7.2 Agent-Based Modelling and Simulation 177
7.3 EABSS Framework 178
7.4 Applying the EABSS Framework 179
7.4.1 Motivation for the study 179
7.4.2 Agent-Based Model Development 181
7.5 Implementation of the conceptual model 191
7.5.1 Assumptions and Simplifications 191

7.5.2 NGB Floor Plan and Route flow 193
7.5.3 The final simulation model 201
7.6 Experimentation 203
7.6.1 Model Validation using existing Lighting Policy against Estates' Data ... 206
7.6.2 Experiment 1: Impact of trajectory route choice in Occupant Model 212
7.6.3 Experiment 2: Random route choice vs probability-based route choice 215
7.6.4 Experiment 3: Impact of light switch off delay on energy consumption 222
7.7 Methodological Implications and Limitations 226
7.8 Potential Applications of Occupancy data 229
7.9 Discussion 231
Chapter 8 CONCLUSION 233
8.1 Summary of Research Results 233
8.1.1 Review of Objectives 233
8.1.2 Knowledge Contribution 236
8.2 Limitations 236
8.2.1 Motion Detection 237
8.2.2 Heading Estimate 238
8.2.3 Particle filter and Sensor fusion 238
8.2.4 Interoperability 238
8.3 Future Work 239
8.4 Conclusion 240
Appendix I 244
Appendix II 253
Reference 273

LIST OF FIGURES

Figure 1-1. Building blocks showing the Steps for Achieving the Objectives. 11
Figure 1-2 Thesis outline showing chapter interconnection with steps for achieving the aims and objectives. 12
Figure 2-1 Origin and axes of the Earth Centered Inertial Fame, $\boldsymbol{i}$ denoting the inertial frame. Source (Groves, 2013) 16
Figure 2-2 ECEF frame showing the axes fixed with respect to the Earth's surface. Source (Groves, 2013) 17
Figure 2-3 The axes of the local navigation frame aligned with the pole and z-axis pointing towards the centre of the Earth. Source (Titterton *et al.*, 2004) 18
Figure 2-4 The axes of the body frame in a motion known as the roll, pitch and yaw. Source (Groves, 2013) 19
Figure 2-5 Applying trigonometric identity showing the coordinates describing the position after rotation resolved through ϒ frame. 19
Figure 2-6 Euler angle rotations, source (Groves, 2013) 20
Figure 2-7 Euler angle rotation when resolving between coordinate frames for each of the successive rotation 21
Figure 2-8 An example of angular rotation and vector direction denoted by ω. 24
Figure 2-9 The position of the origin of frame α with respect to the reference β in frame ϒ axes showing the x, y and z coordinate components. 25
Figure 2-10 Basic schema of an INS. Source (Groves, 2013). 33
Figure 2-11 Basic Schematic diagram of the INS process, source (Groves, 2013) 34
Figure 2-12 Typical matrix showing association between doors and walls and rooms for map matching (Jing, 2015). 38
Figure 2-13 Indoor positionings mass market coverage and accuracy based on user requirement. Source (Mautz, 2012) 39
Figure 2-14 Approaches for RSS based positioning. Source (Davidson and Piché, 2017) 42

Figure 2-15 Tactile systems used in industry and surveying and their performance parameter. Source (Mautz, 2012) 49
Figure 2-16 A generalised pedestrian dead reckoning system listing possible technology and techniques fusion 54
Figure 4-1 Signal strength (dBm) plot between Wi-Fi 2.4 GHz and 5 GHz spectrum 74
Figure 4-2 Signal strength (dBm) plot between Wi-Fi 2.4 GHz and 5 GHz spectrum 75
Figure 4-3 Signal strength (dBm) plot between Wi-Fi 2.4 GHz and 5 GHz spectrum 75
Figure 4-4 Signal strength (dBm) plot between Wi-Fi 2.4 GHz and 5 GHz spectrum 76
Figure 4-5 Attenuation of BLE signal (dBm) varying with distance. The red lines show the mean at each point. 77
Figure 4-6. Representation of BLE signal attenuation (dBm) due to obstruction from building walls indoor. 78
Figure 4-7. Data Collection position when analysing *RSS* quality due to the angle of reception, LoS and obstruction from the user's clothes. 79
Figure 4-8. Effect of angle of reception and clothes on signal quality (dBm). 80
Figure 4-9. Data collection position when analysing signal quality in narrow corridors. 80
Figure 4-10. Observed signal strength (dBm) qualities in corridors from a BLE beacon. 81
Figure 4-11. Training point (TP) locations for fingerprint data collection from Wi-Fi and Bluetooth 83
Figure 4-12 Floor A map with BLE beacons in green and Wifi AP in red markers. 85
Figure 4-13 Floor B map with BLE beacons in green and Wifi AP in red markers. 85
Figure 4-14. Floor C map with Wifi AP in red markers. Floor C is not used for positioning trial. 86
Figure 4-15 Heatmap for some selected 2.4 GHz Wi-Fi transmission showing the signal coverage in Floor A. 89
Figure 4-16 Heatmap for some selected 5 GHz Wi-Fi transmission showing the signal coverage in Floor A. 90

Figure 4-17 Heatmap of some selected BLE beacons showing the coverage of the signal strength in Floor A.....90
Figure 4-18 Heatmap of some selected 2.4 GHz Wi-Fi transmission showing the signal coverage in Floor B.....91
Figure 4-19 Heatmap of some selected 5 GHz Wi-Fi transmission showing the signal coverage in Floor B.....92
Figure 4-20 Heatmap of some selected BLE beacon showing the coverage of the signal strength in Floor B.....92
Figure 4-21 Nearest Neighbour classification showing the positioning accuracy in Floor A. 97
Figure 4-22 Nearest Neighbour classification showing the positioning accuracy in Floor B.....97
Figure 4-23 Maximum likelihood classification showing the positioning accuracy in Floor A. 98
Figure 4-24 Maximum Likelihood classification showing the positioning accuracy in Floor B. 99
Figure 4-25 Probability Distribution Comparison showing positioning accuracy in Floor A 100
Figure 4-26 Probability Distribution Comparison showing positioning accuracy in Floor B.....100
Figure 5-1 Process flow diagram showing the connection of the different sensor components producing the final location output. 104
Figure 5-2 Accelerometer X-axis is showing successive bias for each of the M estimate. 107
Figure 5-3 Accelerometer Y-axis is showing successive bias for each of the M estimate. 107
Figure 5-4 Accelerometer Z-axis is showing successive bias for each of the M estimate. 108
Figure 5-5 Gyroscope X-axis is showing successive bias for each of the M estimate...109
Figure 5-6 Gyroscope Y-axis is showing successive bias for each of the M estimate...109

Figure 5-7 Gyroscope Z-axis is showing successive bias for each of the M estimate. ...110
Figure 5-8 Accelerometer data for each of the axis is shown in the top plot. The lower plot shows the normalised acceleration. The plot corresponds to a fast speed walking scenario. ...112
Figure 5-9 Accelerometer data for each of the axis is shown in the top plot. The lower plot shows the normalised acceleration. The plot corresponds to the medium speed walking scenario. ...113
Figure 5-10 Accelerometer data for each of the axes is shown in the top plot. The lower plot shows the normalised acceleration. The plot corresponds to a slow speed walking scenario. ...114
Figure 5-11 Gyro data for each of the axis during the fast walking scenario. ...114
Figure 5-12 Gyro data for each of the axis during medium speed walking scenario. ..115
Figure 5-13 Gyro data for each of the axis during slow speed walking scenario. ...115
Figure 5-14 Typical accelerometer sensor output for 9 seconds and 2 seconds, respectively during walking. ...118
Figure 5-15 Walking stance phase showing one complete cycle starting from initial contact to terminal stance (Dubin, 2013). ...118
Figure 5-16 Block diagram showing the step by step process of motion detection algorithm development. ...119
Figure 5-17. Illustration showing the peak and valley points for every 2 second and their corresponding average. ...121
Figure 5-18 Simplified diagram of the conversion of time series data from time domain to frequency domain (Smith, 2019) ...122
Figure 5-19 The amplitude plot at the top showing the different amplitude for each window of signal data after DFT conversion. ...123
Figure 5-20 Trial walk-1, circles showing wrongly detected motion in peak-valley average but corrected using the DFT as shown in the combined plot. ...125
Figure 5-21 Trial walk 2, circles, showing wrongly detected motion in DFT but corrected using peak-valley analysis in the combined plot. ...126

Figure 5-22 Trial walk 3, circles, showing wrongly detected motion in DFT but corrected using peak-valley analysis in the combined plot. 126
Figure 5-23 Accelerometer and corresponding amplitude plot from DFT showing the amplitude of the offset frequency during irregular motion such as jumping etc. instead of walking. 127
Figure 5-24 Distinguishable heading change obtained from a table top experiment on the right were the 135
Figure 5-25 Heading change computed from a walk in a square pattern around four corners of a room. Eight complete rotations were made during the trial. 135
Figure 5-26 Heading computed throughout approximately for six hours to check for any drift. 136
Figure 5-27 Heading evaluation trial walk results showing distinguishable heading changes during major turns with clearly identifiable heading change corresponding to the turns. 137
Figure 5-28 Wi-Fi and BLE observation and computation of missing epochs. 138
Figure 5-29 Location engine showing the different sensor integration. 139
Figure 5-30 Validation of the positioning system, showing the computed trajectory in red and blue trajectories from the robotic total station as ground truth. 142
Figure 5-31 Validation of the positioning system, showing the computed trajectory in red and blue trajectories from the robotic total station as ground truth. 142
Figure 6-1 Nottingham Geospatial Building (NGB), Floor A and Floor B, respectively. 146
Figure 6-2 Floor A Trials showing the particle filter trajectory from two test walk. 149
Figure 6-3 Floor A Trials showing the particle filter trajectory from two test walk. 149
Figure 6-4 Trials combining multiple floors showing the particle filter trajectory from a test walk from Floor A to Floor B 150
Figure 6-5 Trials combining multiple floors showing the particle filter trajectory from a test walk from Floor A to Floor B 150
Figure 6-6 Multiple trial plots showing the sequence of movements left to right over a continuous period. 152

Figure 6-7 Occupancy time series plot showing the occupancy corresponding to the plots in Figure 6.6 152
Figure 6-8 Sample of 8 Lego model picture built by the participants during the Lego trial. 155
Figure 6-9 Collation of a sequence of plots from a segment of a trial showing a typical particle filter process. 158
Figure 6-10 Plot showing trajectory output from a trial segment, the red line is processed blue line is an actual path. 159
Figure 6-11 Plot showing trajectory output from a trial segment, the red line is processed blue line is an actual path. 160
Figure 6-12 Plot showing trajectory output from a trial segment, the red line is processed blue line is an actual path. 160
Figure 6-13 Plot showing trajectory output from a trial segment, the red line is processed blue line is an actual path. 160
Figure 6-14 Plot showing trajectory output from a trial segment, the red line is processed blue line is an actual path. 161
Figure 6-15 Plot showing trajectory output from a trial segment, the red line is processed blue line is the actual path. 161
Figure 6-16 Plot showing trajectory output from a trial segment, the red line is processed blue line is the actual path. 162
Figure 6-17 Plot showing particle drift and trajectory output from a trial segment, the red line is processed blue line is an actual path. 163
Figure 6-18 Plot showing particle drift and trajectory output from a trial segment, the red line is processed blue line is an actual path. 164
Figure 6-19 Plot showing particle drift and trajectory output from a trial segment, the red line is processed blue line is an actual path. 165
Figure 6-20 Trial validation plot of Figure 6.10 showing time series of occupancy. 167
Figure 6-21 Trial validation plot of Figure 6.11 showing time series of occupancy. 167
Figure 6-22 Trial validation plot of 2nd Figure 6.14 showing time series of occupancy. 168

Figure 6-23 Trial validation plot of 2nd Figure 6.15 showing time series of occupancy. 168
Figure 6-24 Trial validation plot of Figure 6.17 showing time series of occupancy. 169
Figure 6-25 Trial validation plot of 2nd Figure 6.13 showing time series of occupancy. 169
Figure 6-26 Trial validation plot of 1st Figure 6.16 showing time series of occupancy.170
Figure 6-27 Trial validation plot of 2nd Figure 6.16 showing time series of occupancy. 170
Figure 7-1 Structure of the EABSS framework as depicted in (Siebers *et al.*, 2017) 178
Figure 7-2: Activity diagram showing possible interaction between agents and between the agent and the physical world within the simulation environment. 185
Figure 7-3: State chart showing the possible transition between various states in the office building.....187
Figure 7-4: State chart showing the light switch on and off stage. 187
Figure 7-5: UML Class diagram of Light and Office object.....189
Figure 7-6: UML sequence diagram showing interaction sequences between actors and between the physical entities. 190
Figure 7-7: The artificial Lab class of the simulation model environment. 191
Figure 7-8 Simulation examples from AnlyLogic (AnyLogic, 2018).....192
Figure 7-9: The floor plan of NGB and its partition into zones and rooms as seen during the simulation. 195
Figure 7-10: The possible route choices an occupant can make when moving within the two floors of the building.....196
Figure 7-11 Final Simulation model main screen, user, office and light model respectively. 203
Figure 7-12. Actual electricity consumption of floor A and floor B of NGB combined for weekdays and weekends, respectively. The central red line in the upper plots shows the mean electricity consumption. Top two corresponds to mean plot and the bottom corresponds to box plot 206

Figure 7-13. Screenshot showing the simulation main screen with agent movement during office hours on the left and the subsequent electricity consumption plots on the right. 207
Figure 7-14 NGB simulated power consumption during weekdays only (inset right, Figure 7.13) 208
Figure 7-15. NGB Estates' power consumption during weekdays only. (inset right, Figure 7.13) 208
Figure 7-16. Simulation energy data vs Estate's energy data consumption over 24 hours. (inset right, Figure 7.13) 208
Figure 7-17 Simulation result after 100 repetitions compared against Estate's data every 30 min over 24 hours. 209
Figure 7-18 Normalised plot of Figure 7.16 211
Figure 7-19 Box Plot showing the total energy consumption over 24 hours for 100 replications. 211
Figure 7-20 Graphical representation of transition between two rooms. 212
Figure 7-21 Image showing the main view of the simulation window comparing plots with and without trajectory 214
Figure 7-22 The difference between power consumption when using and not using trajectory route choice during agent movement is seen above. The blue is the extra energy usage when route choice is introduced. 214
Figure 7-23 Showing energy consumption data without using trajectory and using trajectory information 215
Figure 7-24 Showing the energy consumption between random and probability-based route choice 217
Figure 7-25 Snapshot of the agent attendance distribution over two days during the simulation run. 217
Figure 7-26 Building attendance plot with 100 replications over 24 hours showing both the mean and the box plot. 218
Figure 7-27 Box plot showing the difference in total energy consumption between different scenarios. 218

Figure 7-28 Paired confidence interval test calculation for 100 replications. 222
Figure 7-29 Energy consumption data for a 10-minute delay in automated lighting setting.....223
Figure 7-30 Energy consumption data for a 15-minute delay in automated lighting setting.....224
Figure 7-31 Energy consumption data for a 20-minute delay in automated lighting setting.....224
Figure 7-32 Energy consumption data for each of the automated lighting switch-off delay. 225

List of Tables

Table 4-1 Output type for Accelerometer and Gyro from the Android API 70
Table 4-2 Overall positioning error (m) showing their mean and median for each algorithm and combination. 95
Table 5-1 Allan Variance for each of the sensor axis 110
Table 5-2 Shows the confusion matrix from 17 Trials, which are used to compute the classification performance of the peak-valley motion detection algorithm. 129
Table 5-3 Performance measure for peak-valley technique 129
Table 5-4 Shows the confusion matrix from 17 Trials, which are used to compute the classification performance of the DFT based motion detection algorithm. 129
Table 5-5 Performance measure for DFT-based technique 129
Table 5-6 Shows the confusion matrix from 17 trials, which are used to compute the classification performance of the combined peak-valley and DFT based motion detection algorithm. 130
Table 5-7 Performance measure for the combined peak-valley and DFT technique 130
Table 6-1 Table shows the validation plot legends and the room numbers for respective occupancy corresponding to Figure 19. Room numbers do not correspond to actual rooms and assigned for ease of understanding. 166
Table 6-2 Lego Trial Result Statistics 173
Table 6-3 Lego Trial zone level accuracy chart corresponding to Figure 7.9 173
Table 7-1: The Scope of the Model and the elements available in the model environment with justification 184
Table 7-2: Agent population's behaviour stereotype in the simulation environment. 186
Table 7-3 State machine transition table of user agent shown in Figure 7.3. 188
Table 7-4: State machine transition table of light shown in Figure 7.4. 188
Table 7-5: List of possible routes and their associated probability when moving between zones from floor B to floor A. C1, C2, C3, C4 denotes corridors and S1, S2, S3 denotes stairs 197

Table 7-6: List of possible routes and their associated probability when moving between zones from floor A to floor B. C1, C2, C3, C4 denotes corridors and S1, S2, S3 denotes stairs 198
Table 7-7: List of possible routes and their associated probability when moving between zones in Floor A. C1, C2, C3, C4 denotes corridors and S1, S2, S3 denotes stairs. 200
Table 7-8 Showing the *paired – t* approach confidence interval test result..... 225

Glossary

AGU->Angular Gradient Update

ANN ->Artificial Neural Network

AHRS ->Attitude and Heading Reference System

AP->Access Points

AGPS->Assisted GPS

ABM->Agent-Based Modelling

ABSS->Agent-Based Social Simulation framework

BOM->Building Occupant Models

BLE->Bluetooth Low Energy

BEM->Building Energy Models

CTRS->Conventional Terrestrial Reference System

CHAIN ->Cardinal heading aided solution

DFT ->Discrete Fourier Transform

ECI->Earth Centred Inertial Frame

ECEF->Earth-Centred Earth-Fixed Frame

EABSS ->Engineering Agent-Based Social Simulation Framework

EKF ->Extended Kalman Filter

GPS->Global Positioning System

GNSS->Global Navigation Satellite System

GPR->Gaussian Process Regression

GATT->Generic Attribute Profile

GP->Gaussian Process

HMM->Hidden Markov Models

HVAC->Heating, Ventilation, And Cooling

IP->Indoor positioning

IMU->Inertial Measurement Unit

ITRF->International Terrestrial Reference Frame

IERS ->International Earth Rotation and Reference Systems Service

ITU->International Telecommunication Union

INS->Inertial Navigation System

LBS->Location based services

LSTM->Long Short-Term Memory module

LoS->Line of Sight

LEED ->Leadership in Energy and Environmental Design

MEMS ->Micro-Electro-Mechanical System

MARU ->Magnetic Angular Rate Updates

MAS ->Multi-Agent Simulation

PDR ->Pedestrian Dead Reckoning

PSD ->Power Spectral Density

PTZ ->Pan-Tilt-Zoom

PIR ->Passive Infrared Sensor

QSF ->Quasi-Static Field

RFID ->Radio Frequency Identification

RSS ->Received Signal Strength

SLE ->Stride length Estimation

SMC ->Sequential Monte Carlo

SVM ->Support Vector Machines

SOM ->Self-Organising Maps

SLAM->Simultaneous Localisation and Mapping

TOA ->Time of Arrival

TOF ->Time of Flight

TDOA ->Time Difference of Arrival

AOA ->Triangulation using Angle of Arrival

TWR ->Two-Way Ranging

TTFF ->Total Time to Fix

TP ->Training Points

UML ->Unified Modelling Language

UKF ->Unscented Kalman filter

UAV ->Unmanned Aerial Vehicle

UWB ->Ultra- Wideband

WLAN ->Wireless local area network

ZUPT ->Zero Velocity Update

Chapter 1

INTRODUCTION

1.1 Overview

Nowadays, indoor wireless positioning technologies (IP) and built-in smartphone sensors are used in a wide variety of applications related to Location-Based Services (LBS) such as indoor car parking assistance (Wang, 2018), museum tour guidance (Fetzer *et al.*, 2018), hospital staff performance tracking (Pinchin *et al.*, 2014) to name just a few. Since the introduction of the Global Positioning System (GPS) and the advent of other Global Navigation Satellite System (GNSS) services like Galileo, Beidou, etc, they have become the *de facto* standard for outdoor positioning with applications ranging from navigation and guidance solutions for aircraft and cars, to vehicle routing and unmanned aerial vehicles (UAV) like drones and other military technologies, etc. GNSS can be used in indoor places but only in very limited areas so is not very useful. In contrast, there are no similar widespread techniques that are available for indoor positioning in GNSS denied areas. Pseudolites and GNSS repeaters are potential indoor positioning solutions in buildings like shopping centres and airports where the roof gives access to the GNSS satellites signals by placing GNSS antennas. The signals are relayed by the GNSS antennas and amplified by the repeaters which may be used to develop indoor positioning solutions as proposed by (Niwa *et al.*, 2008; Jardak *et al.*, 2009; Ozsoy *et al.*, 2013; Kim *et al.*, 2014; Xu *et al.*, 2015). Extensive research has been devoted to exploring the topic based on a variety of technologies such as Wi-Fi, Bluetooth, Ultra-Wideband (UWB), inertial navigation based on dead reckoning and inertial sensor embedded handheld devices such as smartphones.

The evolution of the smartphone has seen many advances in mobile technology and has produced devices with more advanced connectivity features making it a permanent part of our daily lives (del Rosario *et al.*, 2015). Smartphones nowadays are equipped with comparatively advanced mobile computing capabilities, a GNSS

receiver, and smart sensing capabilities using a low-cost Inertial Measurement Unit (IMU) known as Micro-Electro-Mechanical System (MEMS) sensor technologies (e.g., accelerometer, gyroscope, and magnetometer) with some even having a magnetometer and barometer. Low-cost IMUs already integrated with smartphones open up an array of opportunities and an application platform for dynamic human activity inference (Saeedi *et al.*, 2015).

Unfortunately, none of these has successfully made it into a widely accepted standard for indoor positioning, although significant progress has been made. Nevertheless, research related to commercialisation and application of IP systems and techniques depending on the context of usage is being continuously explored. At the same time, to ensure predicted performance, stability and robustness of the positioning systems, extensive trials are necessary. All of these require trials involving non-expert participants in a challenging real-world environment to cover all possible scenarios of system failure and performance issues before rolling out the system commercially.

This thesis investigates the possible application of IP technology as a contribution to the development of Building Occupant Models (BOM). It has the potential to have a widespread impact on the development of other behavioural models related to building occupancies, such as the presence model, window opening, light switching, HVAC system, and appliance usage, as well as the use within simulation environments when it comes to modelling human motion in buildings. To contribute towards the development of a BOM, an IP system capable of detecting an individual's movement continuously with a certain level of accuracy and detail is necessary. As such a prototype IP system needs to be developed with a pedestrian dead reckoning capability, requiring step detection, step length estimation and change in heading orientation. It also demands the use of easy to access and cheap IP infrastructure, technology, and devices to be used by participants for positioning data collection.

1.2 Background

There are many sources of literature providing an extensive review of existing IP technology, their method of usage and possible application opportunities. Earlier work

can be found in (Mautz, 2012) who undertook a thorough evaluation of technology and techniques but more recent ones like (Brena *et al.*, 2017) provide an extensive evaluation of state-of-the-art IP technology and methods and classification in terms of sensor type and physical features of measurement. The paper provides a detailed comparison of the advantages and disadvantages of each positioning technology over one another, their current trends and future opportunities in indoor positioning research.

It is essential to compute a position update at every epoch step-by-step in order to fully understand building occupancy, using a technique known as 'dead reckoning'. Dead reckoning is the process of computing one's current position by using the previous position and updating that position every epoch based upon acceleration, step detection, and orientation. The use of IP technology and techniques in developing pedestrian dead reckoning (PDR) systems can be seen in (Bao *et al.*, 2014) where the authors developed a PDR-based IP solution using step counting and improved position estimation using a map matching enhanced particle filter. Renaudin and Combettes (2014) looked to address issues and challenges using inertial foot-mounted systems and how they can be further improved using signals of opportunity for estimating the navigation solution. Quasi-Static Field (QSF) updates, Magnetic Angular Rate Updates (MARU) and Angular Gradient Update (AGU) are frequently applied for mitigating low-cost inertial sensor errors. Similar work related to the use of the foot-mounted inertial system and extended Kalman filter can be found in the work of Zhou *et al* (2014). Use of embedded inertial navigation system (INS) for a real-time PDR solution can be seen in (Muhammad *et al.*, 2016). Improvement of the traditionally used Wi-Fi fingerprinting-based PDR solution with an Extended Kalman Filter (EKF) and adaptive step length estimation can be seen in (Han *et al.*, 2018). Exploiting signals of opportunity and machine learning techniques such as simultaneous localisation and mapping (SLAM) physical effort of surveying and updating radio maps can be significantly reduced. SLAM works with the help of robotic agents which has the potential to access unknown environments and also keep track of the agent's location providing real time update of the maps as seen in (Huang *et al.*, 2011; Faragher *et al.*,

2013). The use of the SLAM particle filter together with MEMS inertial unit is seen in Shi *et al.*, (2018), fusing with a novel approach of using a feature point map during map matching. A survey of current inertial and magnetic sensors and MEMS-based low cost integrated positioning solutions can be found in (Abdul Rahim, 2012; Gobana, 2018; Zheng-Chun *et al.*, 2018).

The use of smartphones for IP with inertial sensor capability can be seen in the early work of (Lukianto *et al.*, 2010) based on a PDR system using the Nokia N900 smartphone. The system attempts to use any available signals of opportunity such as wireless local area network (WLAN) and Bluetooth to support its INS on top of an efficient sensor fusion algorithm. Smartphone cameras can be used for a PDR solution as seen in (Werner *et al.*, 2011) where the main novelty of the solution focused on developing an image recognition system for position updates instead of relying on any positioning infrastructure. The placement and carrying position of the smartphone also has significant importance to ensure ubiquitous positioning capability, as seen in Ayub *et al* (2012). The use of hybrid indoor positioning solutions using step counting and map matching with a particle filter can be seen in (Liu *et al.*, 2012; Yim, 2013; Tian *et al.*, 2015). Use of a Kalman filter with Wi-Fi fused with smartphone inertial sensors and use of calibrated magnetometer and magnetic map matching can be found in (Tian *et al.*, 2014; Deng, Hu, *et al.*, 2015; Huang *et al.*, 2015). Generally smartphone sensors are of poor quality and suffer from sensor bias, drift and require calibration. The paper by Moder *et al* (2017) analyses motion sensors used in PDR and discusses how to calibrate sensor data, showing the benefits of using calibrated rather than raw sensor data for PDR related applications.

Two of the most essential requirements when developing a PDR solution are orientation and step detection. To date, much research has taken place when it comes to step detection. Step detection is a complex phenomenon since human motion is not uniform and depends on the situation. The step length varies depending on the movement pattern such as running or walking, and the velocity of the feet movement varies from person to person depending on height and pace. Previous work related to

the identification of steps based on adaptive step length estimation using low-cost MEMS inertial sensors is seen in the work of Shin *et al* (2007). A more recent work related to step detection and step length estimation can be found in Do-Xuan *et al* (2015). In a more recent work Wang *et al* (2019) looked into the identification of steps in a complex environment, unlike typical movement in straight lines or cardinal directions. The authors collected a large amount of inertial sensor data such as the accelerometer and gyroscope from smartphones and used it to train a network model. They then used a Long Short-Term Memory module (LSTM) and De-noising Auto encoders, which aim to filter the noise in raw inertial sensor data and feed it into the network model together with available features extracted before and compared the results with other stride length estimation (SLE) algorithms. The use of machine learning algorithms such as the artificial neural network (ANN) to learn stride patterns and estimate stride lengths and step detection is seen in the work of Kupke *et al* (2016). The different walking pace and holding position of the phone provides unique signal frequency characteristics from the smartphone accelerometer. Herrera *et al* (2017) explored the options as well as providing a comparison of the performances.

Orientation estimation is one of the vital requirements for PDR solutions to identify the direction of orientation known as “heading”. The authors Deng and Wang, *et al* (2015) proposed a heading estimation algorithm by identifying the rotation matrix and principle component analysis of the accelerometer data. They also developed a turn detection algorithm to enhance heading change detection. The use of indoor navigation by visitors in large buildings like museums is beneficial but needs a reliable PDR solution. The authors, Huang *et al* (2015) developed an IP and orientation tracking system using smartphone inertial sensors with an improved error-tolerant magnetic calibration. Use of information and complementary filter can be fused to get accurate heading information as seen in (Yang *et al.*, 2017). Smartphone-based positioning activity recognition is seen in (Miyamoto *et al.*, 2014).

All these research efforts highlight the immense scope of IP systems and their capability for providing more detailed positioning output. The positioning details

related to the movement profile of individuals can potentially be used to understand building occupancy better and contribute to the development of an improved BOM.

1.3 Research Details and Approach

This section provides details of the research scope and perspective of the project, the problem statement, existing gaps in knowledge and therefore the motivation behind the research. It also provides details of the aims and objectives of the project and the corresponding plan and procedure that were followed which in general specify specific steps to be taken to achieve the objectives, highlighting broad assumptions to detail in the method of data collection, analysis and interpretation in the process.

Industry partner: Satellite Applications Catapult

Base Research Group: Nottingham Geospatial Institute

Research Scope: The research approach considered the requirements of the industry partner and Horizon Centre for Doctoral Training (CDT) respectively and looked into a novel contribution of the IP system towards the development of an improved BOM for energy usage prediction. The performance of the positioning system was evaluated by conducting real-world occupancy trials using non-expert participants. The positioning data collected from the trial was then used as input in the model and the significance of its impact was analysed.

Research Gap: There was limited or no actual work which has investigated the contribution of the IP system when developing predictive models for building occupancy to analyse building performance. The fact that tracking of individual movement can provide a more realistic movement profile may prove to be a meaningful contribution towards the development of BOM. This will consequently help analyse building performance such as energy usage prediction better.

1.3.1 Problem Statement

Research in IP systems and the potential application of the generated positioning data set in a wide variety of social contexts is becoming ever more popular. The importance

of IP in providing LBS is fuelling research opportunities in many sectors. Despite this, there is no single compelling solution to IP and the emphasis is generally given to the use of hybrid solutions to optimise and complement each technique's shortcoming while enhancing overall accuracy. The generation of movement data from indoor tracking opens the possibility of modelling energy usage within commercial and residential spaces. Human interaction with building infrastructure such as window blinds, shading devices, lighting and electrical appliances affect the energy balance inside buildings, and these interactions are more likely to occur upon arrival after an exhausting journey. The interactions depend on the presence of individuals. Thus, the use of occupancy data in the simulation of building energy usage is understandably the most critical aspect. As such, the development of a dynamic model of building occupancy is of profound importance leading to automated lighting and heating solutions and a better understanding of energy usage.

This leads to research on simulation of sustainable environments inside buildings which comprises of energy usage modelling based on different interaction models and occupancy models similar to previous studies (Haldi *et al.*, 2008; Page *et al.*, 2008; Robinson *et al.*, 2012; Zhang *et al.*, 2013; Burak Gunay *et al.*, 2015; Gunay *et al.*, 2016) to name just a few. Previous research related to BOM shows occupancy detection has been limited to individual room level observation with intermediate absence and presence (Page *et al.*, 2008) or estimating a general occupancy count of rooms and corridors. A multitude of techniques and methods are used such as probabilistic or agent-based modelling approaches and occupancy data collection using ambient sensors, camera, Wi-Fi logs etc. The models miss out essential details of energy usage due to their activities while present, the place and time, which may or may not always be in their designated rooms instead of in different zones of the building in between their movement to and fro. Also, the location within the room has an impact on how often we interact with different building infrastructures and fails to consider the importance of incorporating corridors, stairways, kitchens and other areas during the transition between rooms. Thus, significantly underestimating energy usage during occupancy. Indoor positioning can help to not only provide a detailed movement

profile from tracking but also expose the different patterns of occupancy exhibited by different individuals. These patterns can be aggregated to identify different occupant types of buildings and how they vary across building occupant demographics.

The interdisciplinary nature of this PhD research focuses on how we can bring together existing IP elements and analyse their contribution to the development of BOM to understand energy consumption. It requires the development of an IP system which can be used to detect our intricate pattern of occupancy not limited to private office space but rather spanning the entire building including corridors, hallways, stairs, kitchens and other areas. As such, the research can be divided into three main broad sections.

1. The first part of the research investigated novel ways of how existing IP techniques can be used to detect the movement and location of individuals indoors. It focused on developing an IP system with PDR capability, which can be used to detect the movement profile of individuals within an acceptable level of accuracy.
2. The second part involved carrying out a limited scale real-world occupancy trial encompassing a large part of a test building involving multiple floors and then analysed the occupancy positioning data to compute route choice probability for input to the BOM.
3. The third part considered developing a BOM for predicting electricity usage and demonstrating how the positioning data can be used in the model and analysed its impact.

1.3.2 Research Questions

Based on the research problem statement, the following questions arose at the start of the research:

1. How can existing indoor positioning technology and techniques be used to implement a positioning system to detect and monitor building occupancy?

2. What are the limitations and constraints when developing such positioning systems and for the participants when using them?
3. How can positioning data be used as input to building occupant model?
4. To what extent does indoor positioning data impact the predictive capability of building occupant models?

1.3.3 Aim

- The aim of this research was to improve building occupant modelling with the help of indoor positioning.

1.3.4 Objectives

1. Develop an easy to use prototype IP system using smartphone inertial sensors, Wi-Fi and Bluetooth.
2. Validate the prototype positioning system and its functionalities, e.g.: motion detection and heading estimate using personal and real-world trials.
3. Demonstrate the use of collected occupancy data within building simulations.

1.3.5 Steps for Achieving Objectives

To achieve the aim and objectives, specific milestones needed to be achieved at each stage of the PhD. The list below shows the relevant steps taken to achieve them.

1. Review existing IP technology, techniques, and algorithms and provide an overview of BOM approaches.
2. Develop custom-built data logger for collecting Wi-Fi, Bluetooth and motion sensor (accelerometer, gyroscope) data for an Android supported smartphone. And using this logger understand different characteristics of Wi-Fi and Bluetooth received signal strength (RSS) in typical deployment conditions.
3. Develop a fingerprint radio map and carry out static positioning trials. Evaluate different positioning algorithms for accuracy comparison.
4. Analyse the smartphone motion sensors, accelerometer and gyroscope.
    a. Estimate bias and noise
    b. Investigate signal patterns at different walking speeds

5. Implement a step-like motion detection algorithm using an existing or novel technique. Carry out trials for validation and analyse performance.
6. Implement a heading estimation algorithm using an existing or novel technique. Carry out trials for validation.
7. Implement a particle filter engine and integrate the fingerprint radio map, motion detection and heading estimate in a sensor fusion framework.
8. Validate the IP system against ground truth and carry out preliminary occupancy trials.
9. Carry out real-world occupancy trial using non-expert participants covering multiple floors.
10. Implement a BOM for electricity usage prediction. Validate the model against real-world energy usage and run simulations for several case studies.
11. Demonstrate how to use positioning data in the BOM as a case study and analyse its impact.
12. Discuss other possible contributions of IP towards building occupant modelling and its limitations.

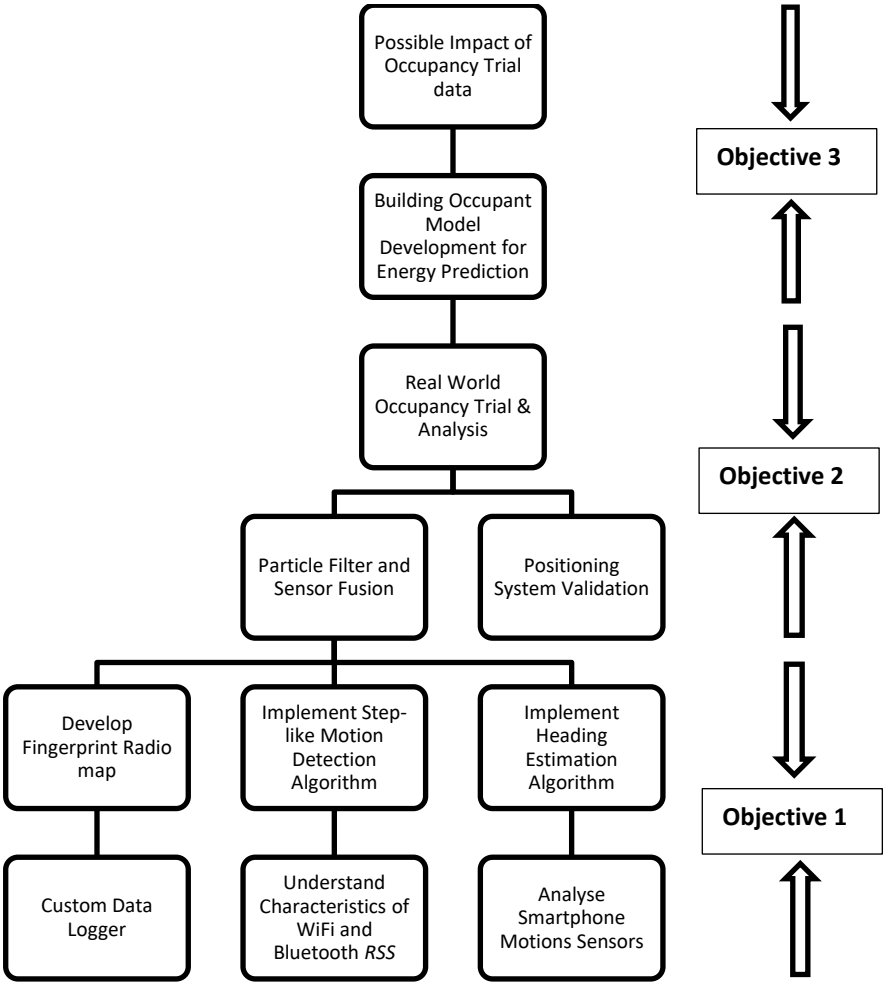


Figure 1-1. Building blocks showing the Steps for Achieving the Objectives.

1.4 Thesis Outline

This section provides a description of the outline of the thesis with a brief introduction to each of the chapters and how they are interlinked with the aims and objectives. Below, Figure 1.2 gives a diagrammatic skeleton of the thesis, showing the relevant connections.

Chapter 1 provides an introduction of the thesis with the problem statement, aims, objectives and the research approach that was taken.

Chapter 2 provides a detailed background of existing IP technology, techniques, and algorithms used in positioning and navigation systems.

Chapter 3 provides an overview of the current state of building occupancy and behavioural models, modelling techniques and technology and the opportunity that exists.

Chapter 4 provides the methods and measurement techniques adopted when developing the indoor positioning system.

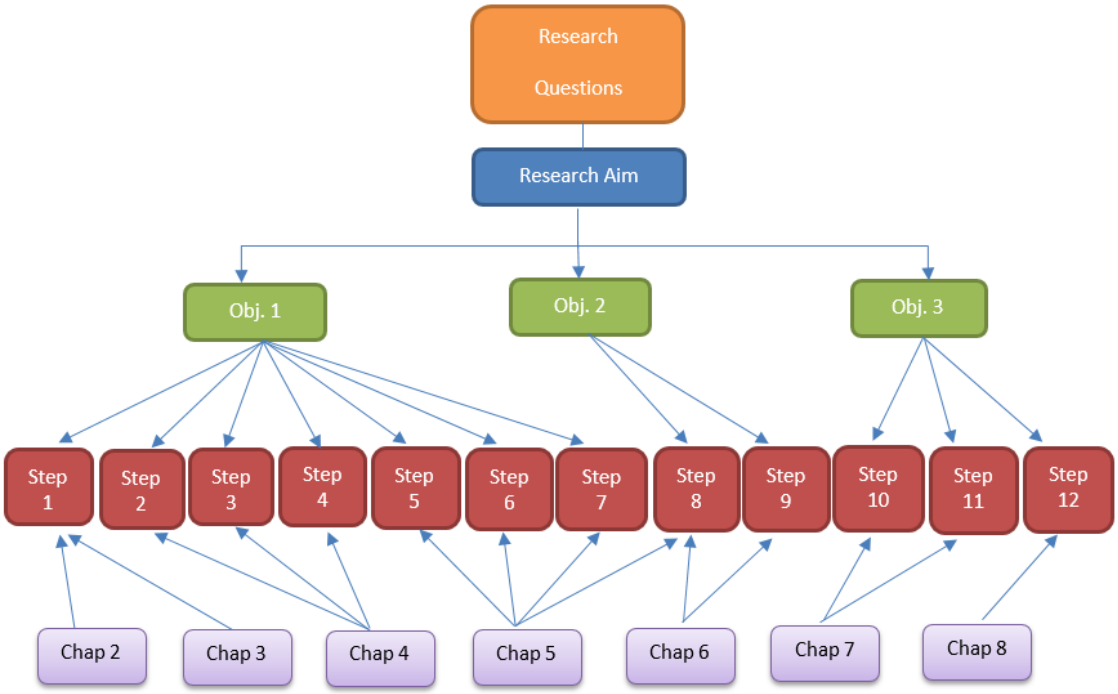


Figure 1-2 Thesis outline showing chapter interconnection with steps for achieving the aims and objectives.

Chapter 5 provides details of the different positioning algorithms used in developing the system and their integration into a multi-sensor positioning framework with trial results and validation.

Chapter 6 discusses extensive real-world trials over a long period and their results using non-expert participants and challenges faced. The trials were evaluated against a set of performance metric necessary for detecting building occupancy accurately. The positioning data from the trials were processed to compute route choice probabilities for input in the BOM.

Chapter 7 demonstrates how the positioning data collected from the trial in chapter 6 can be used in a BOM. For that purpose, an agent-based BOM has been developed for electricity usage prediction for building lighting. The model incorporates lighting and occupancy features mimicking one of the academic buildings at the University of Nottingham, and the predicted output is validated with real-world electricity usage data collected from the relevant authority. Further simulations were carried out, and the model output analysed for several electricity usage scenarios, including at least one with the positioning data serving as input in the form of route choice probability. Statistical significance for each of the simulation results and their impact are discussed. Electricity usage from building lighting is selected in this case since it is dependent on the occupancy of the individuals and positioning data has a direct relationship with occupancies such as length of occupancy, time of entry and exit and route choices involving rooms, corridors, and stairs.

Chapter 8 provides a series of conclusions according to the outcome of the tested IP system and observed impact from the BOM output. Limitations of the system and future work are also discussed.

Chapter 2

INDOOR POSITIONING OVERVIEW

Research work related to IP and navigation solution has received growing interest over the last decade with research focusing on a wide range of sensors and devices. Positioning is the process of knowing one's location at a known reference frame, navigation on the other hand provides complete guidance related to route choice such as Google Maps. In our case, we are more interested in the positioning solution. Due to the poor performance of GNSS-based positioning solution in indoor spaces, the opportunity for indoor location-based services using a multitude of sensor-based hardware is becoming popular and well received amongst users. IP-related research is playing a vital role by providing state-of-the-art solutions for location tracking, orientation detection and human activity recognition to name a few. Most of them use wireless communication devices such as Wi-Fi, Bluetooth, Radio Frequency Identification (RFID), UWB and motion sensors like an accelerometer, gyroscope and magnetometer, embedded in a typical IMU (Liu *et al.*, 2007). The problems faced when developing IP services are not that different when compared to services outdoors using GNSS. Each solution is dependent on the accuracy and robustness of the positioning solution deployed and the environmental context they are used in. Location tracking in an indoor environment is challenging for its temporal and spatial variation of wireless signals due to changing building layout, furniture placement and human activity. These features are unique and vary from building to building thus no single positioning solution can provide the same level of performance in every indoor environment and context using the same configuration. Thus they lack the same level of performance achieved using GNSS outdoors when it comes to high accuracy, high availability, high integrity and low user cost as discussed in (Mautz, 2012 and Brena *et al.*, 2017). In general, due to all these complexities, there is no single compelling solution for IP currently.

Nevertheless, research related to novel areas of application and services using IP is gaining popularity. Due to rapid advances in computing technology handheld devices

such as smartphones are now embedded with a wide array of sensors and wireless communication systems, such as Wi-Fi, Bluetooth, accelerometer, gyroscope, magnetometer, barometer, ambient light sensor and camera technology. These options provide the capability of developing a high accuracy ubiquitous positioning solution which is not dependent on any single positioning technique such as PDR, fingerprint radio maps or proximity detection but uses a fusion of the most appropriate techniques. As such it is crucial to deal with each problem individually and choose the most optimal solution for that specific context of application.

This chapter will discuss some of the widely studied IP tools and techniques and highlight research related to their applications in the real-world scenario such as human activity recognition and motion detection. It will provide the reader with a general understanding of the research field, setting the stage for the technical choices made in the later chapters and their relevance.

2.1 Coordinate System

To understand the physics of navigation, it is essential to understand the concept of coordinate systems and frames and how they are used to represent moving objects and describe the position, orientation and motion of these objects. These would typically include Cartesian position, velocity and acceleration, attitude representations and angular rotation. Generally, the position of an object is described using a set of three axes, x, y, z which must be non-coplanar and are mutually perpendicular relative to their origin O. To describe the motion, a coordinate system is also needed to explain the relative motion as discussed in (Groves, 2013). The origin and the axes together form the coordinate system and have six degrees of freedom. They are usually represented using the right-handed convention were the thumb represents the x-axis, the index finger points toward the y-axis and the middle finger representing the z-axis. This coordinate system can be used to describe both the object and reference frame. In navigation the object frame is typically the body in motion or whose position or orientation we want to describe against a reference frame such as Earth relative to which the transformation will be described. Of course, there can be more than two

coordinate frames involved but, typical navigation problems related to pedestrian navigation deals with two. There are some common reference frames; *Earth-Centred Inertial Frame, Earth-Centred Earth-Fixed Frame, Local Navigation Frame, Body Frame* whose coordinate systems' standard are widely adopted by the international community realised by the International Terrestrial Reference Frame (ITRF) coordinated by the International Earth Rotation and reference Systems Service (IERS).

2.1.1 Earth-Centred Inertial Frame

The system describes any coordinate frame that does not rotate or accelerate with the rest of the universe. In the Earth Centred Inertial Frame (ECI) the origin is the Earth's centre of mass, and the axes are mutually perpendicular to each with the Z-axis pointing towards the Earth's axis of rotation and the X and Y-axis lying along the equatorial plane as seen in Figure 2.1. Although this is not a valid inertial frame since the Earth's axes go through spin and rotation slowly as it orbits the sun, but since these effects are comparatively smaller than most of the measurement noise by the navigation sensors, the ECI frame can generally be treated as an inertial frame.

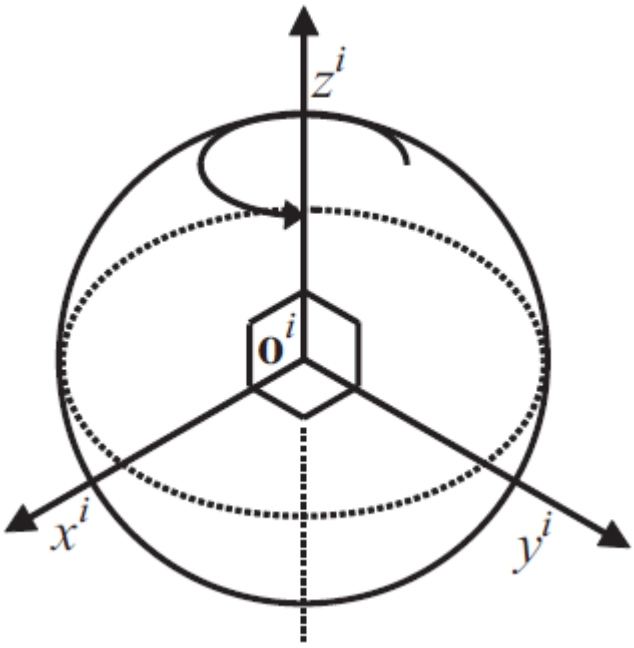


Figure 2-1 Origin and axes of the Earth Centered Inertial Fame, i denoting the inertial frame. Source (Groves, 2013)

2.1.2 Earth-Centred Earth-Fixed Frame

The Earth-Centred Earth-Fixed Frame (ECEF) denoted by *e* is similar to the ECI frame with its centre in the centre of mass of the Earth or the centre of the ellipsoidal model of the earth's surface. The only difference is that all the axes remains fixed with respect to the earth, as shown in Figure 2.2. Thus whatever small rotation is faced by the Earth during its orbit around the sun is taken into consideration when used as the reference frame. The ECEF system uses the IRP/CTP and IRM/CZM commonly known as the Conventional Terrestrial Reference System (CTRS). The ECEF frame can be used both as the reference frame and the resolving frame when realising the position relative to the Earth's surface.

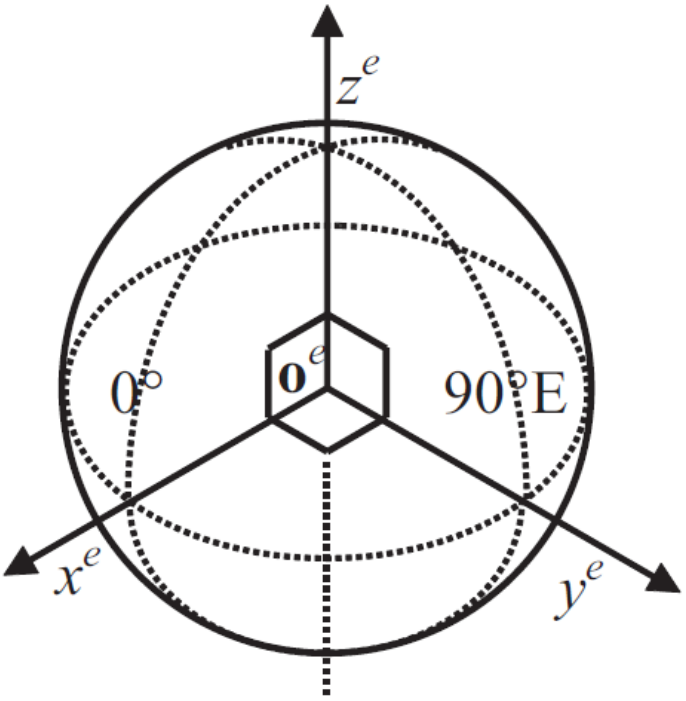


Figure 2-2 ECEF frame showing the axes fixed with respect to the Earth's surface. Source (Groves, 2013)

2.1.3 Local Navigation Frame

Local navigation frame or the geodetic or topocentric frame is the object described by the navigation solution, and it can be a part of the navigation system or the centre of mass of the host body. The axis *x, y, z* are always pointing towards the north, east, and

down i.e. gravity, respectively, as seen in Figure 2.3. The frame is used to identify the user's attitude relative to this north, east and down. Some convention uses the *down* axis instead of the *up* for the z-axis. The major problem with the local navigation frame is its singularity in the poles since the north and east are undefined there, hence alternative frame needs to be used for solution conversion at those points during navigation.

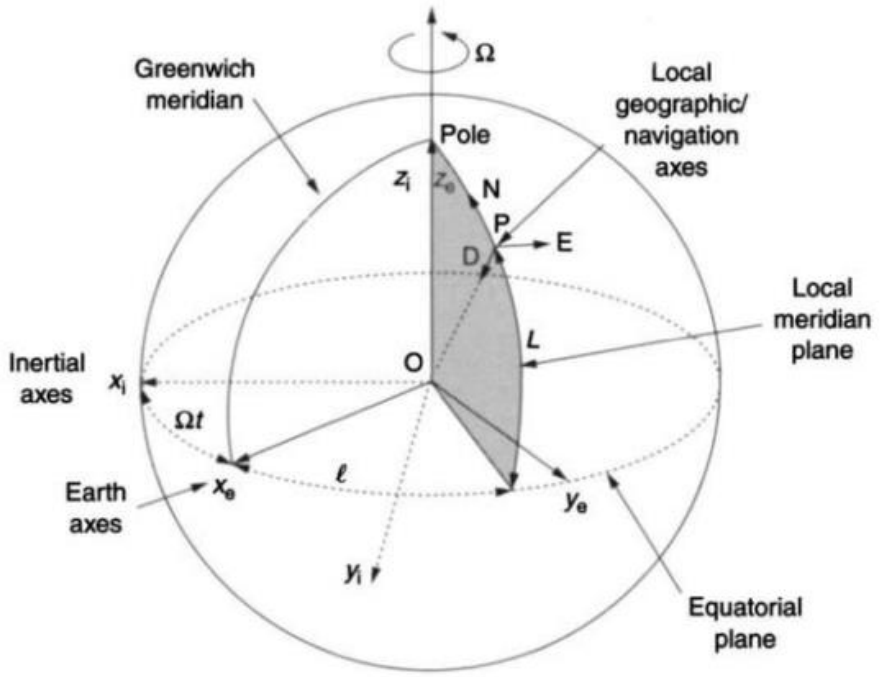


Figure 2-3 The axes of the local navigation frame aligned with the pole and z-axis pointing towards the centre of the Earth. Source (Titterton *et al.*, 2004)

2.1.4 Body Frame

Body frame is the main host body whose orientation we are trying to resolve and comprises the origin of the object described by the local navigation frame. The axes are always fixed with the body frame, with the convention shown in Figure 2.4. The X, Y and Z-axis are also known as the roll, pitch and yaw for angular motion respectively.

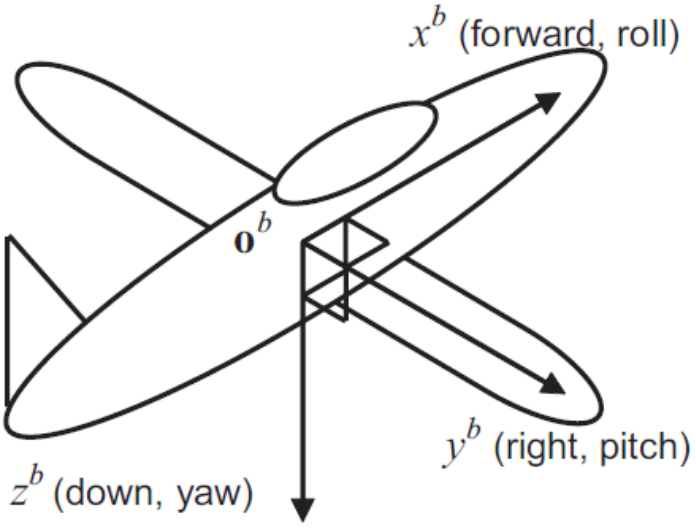


Figure 2-4 The axes of the body frame in a motion known as the roll, pitch and yaw. Source (Groves, 2013)

In general, different navigation solutions are measured and resolved in their reference frame. For comparing measurements from different systems, the results need to be converted to a common reference frame before performing operations. In this thesis, the local experimental environment is used as the local reference frame for comparing and resolving orientation and position from any inertial measurements obtained during the trials and experimental setup.

2.2 Attitude Representation

Attitude is generally described as a measurement of rotation of the axes. It can be seen in two ways, one is the rotation of one coordinate frame against another, e.g., object frame to a reference frame, and another is simply the rotation about the origin of the frame itself. In both the cases, the coordinates of the object going through a rotation ψ from α frame to β frame and can be described for a 2D case with rotation angle about Z-axis using the equation shown in Figure 2.5 below.

$$\begin{pmatrix} x^{\gamma}_{\beta\alpha} \\ y^{\gamma}_{\beta\alpha} \end{pmatrix} = \begin{pmatrix} \cos\psi & -\sin\psi \\ \sin\psi & \cos\psi \end{pmatrix} \begin{pmatrix} x^{\beta}_{\beta\alpha} \\ y^{\beta}_{\beta\alpha} \end{pmatrix}$$

Figure 2-5 Applying trigonometric identity showing the coordinates describing the position after rotation resolved through ϒ frame.

For 3D rotations, the transformation is more complex, and the order of rotations for axes transformation need to be maintained since they do not commute. These rotations are generally described by Euler Attitude, Coordinate Transformation Matrix and Quaternions and either of them can be used to describe rotations and transformation depending on the navigation solution. We will briefly cover them below and describe how they work.

2.2.1 Euler Attitude

Euler angles are a straightforward way to describe the attitude of a body frame with respect to the local navigation frame. The attitude computation is broken into three successive steps seen in Figure 2.6. The first rotation is along the Z-axis known as *Yaw*; second is the rotation along the Y-axis known as *pitch* and finally the third along the X-axis known as *roll*. Using these three successive rotations, we can define the orientation of the object frame α with respect to the reference frame β. The pitch and roll are sometimes known as *elevation* and *bank,* and the yaw referred to as 'heading' or 'Azimuth'.

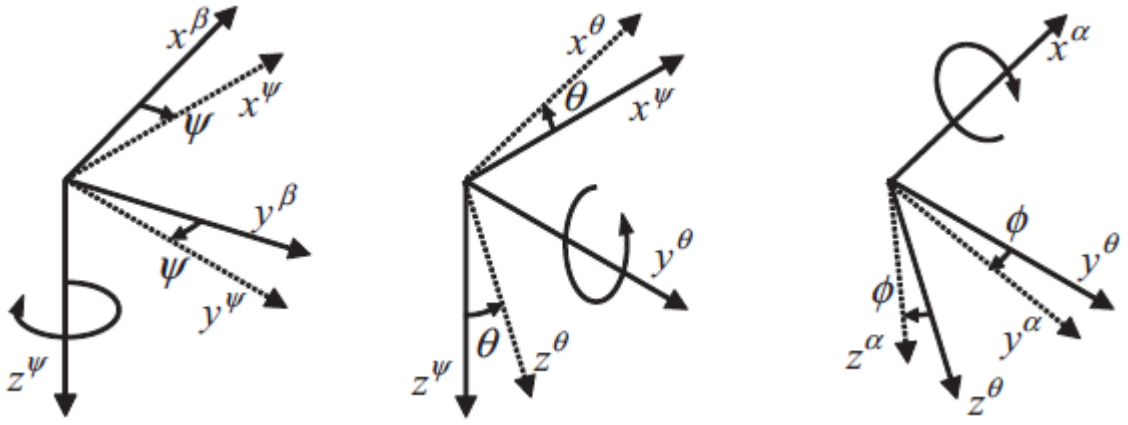


Figure 2-6 Euler angle rotations, source (Groves, 2013)

Euler angles can be used to transform vectors, X = (*x, y, z*) as well from one set of resolving axis β to another α. According to the following equations shown in Figure 2.7.

Yaw rotation *Pitch* rotation *Roll* rotation

$$x^{\psi} = x^{\beta}\cos\psi_{\beta\alpha} + y^{\beta}\sin\psi_{\beta\alpha} \qquad x^{\theta} = x^{\psi}\cos\theta_{\beta\alpha} - z^{\psi}\sin\theta_{\beta\alpha} \qquad x^{\alpha} = x^{\theta}$$
$$y^{\psi} = -x^{\beta}\sin\psi_{\beta\alpha} + y^{\beta}\cos\psi_{\beta\alpha} \qquad y^{\theta} = y^{\psi} \qquad y^{\alpha} = y^{\theta}\cos\phi_{\beta\alpha} + z^{\theta}\sin\phi_{\beta\alpha}$$
$$z^{\psi} = z^{\beta} \qquad z^{\theta} = x^{\psi}\sin\theta_{\beta\alpha} + z^{\psi}\cos\theta_{\beta\alpha} \qquad z^{\alpha} = -y^{\theta}\sin\phi_{\beta\alpha} + z^{\theta}\cos\phi_{\beta\alpha}$$

Figure 2-7 Euler angle rotation when resolving between coordinate frames for each of the successive rotation

The order of the rotation is critical when performing transformation. They are not commutative; hence, successive rotation cannot be added or reversed by changing the sign. A fundamental issue with Euler angles is its singularity at $\pm 90°$ pitch when both the *roll* and *yaw* become similar; hence, they are rarely used for attitude computation.

2.2.2 Coordinate Transformation Matrix

The coordinate transformation matrix is a *3 x 3* rotation matrix denoted by C_{α}^{β} . Any vector or matrix can be transformed from one set of resolving axis to another by pre-multiplying it with the correct set of coordinate transformation matrix according to the equation below.

$$X^{\beta} = C_{\alpha}^{\beta} X^{\alpha} \qquad (2\text{-}1)$$

The equation shows the transformation from α to β resolved around the β axis. Coordinate transformation matrices are easy to manipulate and to reverse a rotation merely the transpose of the matrix can be used when pre-multiplying. This is because rotations are not commutative and a coordinate transformation matrix is orthonormal as stated before. Successive rotations are performed by multiplying each coordinate transformation matrix in order according to the following equations.

$$C_{\alpha}^{\gamma} = C_{\beta}^{\gamma} C_{\alpha}^{\beta} \qquad (2\text{-}2)$$

$$C_{\alpha}^{\gamma} \neq C_{\beta}^{\gamma} C_{\alpha}^{\beta} \qquad (2\text{-}3)$$

$$C_{\alpha}^{\beta} C_{\beta}^{\alpha} = I_3 \quad (2\text{-}4)$$

To use coordinate transformation, Euler angles are converted to the *3 x 3* matrix by multiplying each of the Euler angles, roll, pitch and yaw according to the equation below.

$$C_{\beta}^{\alpha} = \begin{pmatrix} 1 & 0 & 0 \\ 0 & \cos \emptyset_{\beta\alpha} & \sin \emptyset_{\beta\alpha} \\ 0 & -\sin \emptyset_{\beta\alpha} & \cos \emptyset_{\beta\alpha} \end{pmatrix} \begin{pmatrix} \cos \theta_{\beta\alpha} & 0 & -\sin \theta_{\beta\alpha} \\ 0 & 1 & 0 \\ \sin \theta_{\beta\alpha} & 0 & \cos \theta_{\beta\alpha} \end{pmatrix} \begin{pmatrix} \cos \psi_{\beta\alpha} & \sin \psi_{\beta\alpha} & 0 \\ -\sin \psi_{\beta\alpha} & \cos \psi_{\beta\alpha} & 0 \\ 0 & 0 & 1 \end{pmatrix} \quad (2\text{-}5)$$

To obtain Euler angles once coordinate transformation is performed, the following equation can be used to get back roll, pitch and yaw.

$$\emptyset_{\beta\alpha} = arctan_2(C_{\beta 2,3}^{\alpha}, C_{\beta 3,3}^{\alpha}) \quad (2\text{-}6)$$

$$\theta_{\beta\alpha} = arcsin C_{\beta 1,3}^{\alpha} \quad (2\text{-}7)$$

$$\psi_{\beta\alpha} = arctan_2(C_{\beta 1,2}^{\alpha}, C_{\beta 1,1}^{\alpha}) \quad (2\text{-}8)$$

For small angle perturbation, the approximation changes to the following equation using the skew-symmetric matrix $[\psi_{\beta\alpha}\, \Lambda]$ of Euler angles.

$$C_{\beta}^{\alpha} = \begin{pmatrix} 1 & \psi_{\beta\alpha} & -\theta_{\beta\alpha} \\ -\psi_{\beta\alpha} & 1 & \emptyset_{\beta\alpha} \\ \theta_{\beta\alpha} & -\emptyset_{\beta\alpha} & 1 \end{pmatrix} = I_3 - [\psi_{\beta\alpha}\, \Lambda] \quad (2\text{-}9)$$

2.2.3 Quaternion Attitude

Another computationally efficient method is to use quaternion representation for rotations. Quaternions are hyper-complex numbers and represented with four

components $q = (q_0\ q_1\ q_2\ q_3)$ with q_0 being the magnitude of the rotation and the other three components are functions of both magnitude and rotation as shown in the equation below. It also avoids the singularity suffered by Euler angles.

$$q_{\beta}^{\alpha} = \begin{pmatrix} \cos \mu_{\beta\alpha}/2 \\ e_{\beta\alpha,1}^{\alpha/\beta} \sin \mu_{\beta\alpha}/2 \\ e_{\beta\alpha,2}^{\alpha/\beta} \sin \mu_{\beta\alpha}/2 \\ e_{\beta\alpha,3}^{\alpha/\beta} \sin \mu_{\beta\alpha}/2 \end{pmatrix} \quad (2\text{-}10)$$

Quaternions are more challenging to manipulate and needs to be carefully implemented in navigation equations to avoid errors. Further reading on quaternion mathematics can be found in the following report (Vectornav, 2008) and an in-depth understanding of quaternion kinematics can be found in the paper of (Solà, 2017).

2.3 Kinematics

Kinematics is concerned with the motion of the object in all the three coordinate frames of the body. The object frame α, whose motion is described, the reference frame β, used to describe the motion with respect to and the resolving frame ϒ, defining the set of axes on which the motion is described. The resolving frame can sometimes be the same as the reference frame or the object frame, but the object frame and reference frame have to be different; otherwise, there will be no motion during navigation as stated earlier. When we say kinematics in navigation, we are generally interested to know the Cartesian position, velocity, acceleration and angular rotation of the object in motion.

2.3.1 Angular Motion

Angular motion can be used to describe the rate of rotation of the vector $\omega_{\beta\alpha}^{\gamma}$ from α frame axis to β frame axis resolved against γ frame axis as described by Groves (Groves, 2013) illustrated in Figure 2.8 below.

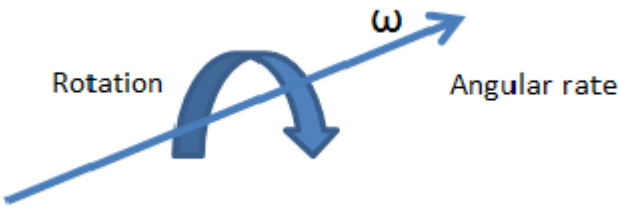


Figure 2-8 An example of angular rotation and vector direction denoted by ω.

The component of the angular rate vector along the resolving x, y and z-axes are denoted by $\omega_{\beta\alpha}^{\gamma} = (\, p_{\beta\alpha}^{\gamma}\,,\, q_{\beta\alpha}^{\gamma}\,,\, r_{\beta\alpha}^{\gamma})$.

Angular rates resolved in the same axes can be added given that the object frame and reference frame for each of angular rate are the same according to the equation $\omega_{\beta\alpha}^{\gamma} = \omega_{\beta\delta}^{\gamma}\,, + \omega_{\delta\alpha}^{\gamma}$. If there is a change in the resolving axes we can simply pre-multiply it with the appropriate coordinate transformation matrix and get the angular rate according to the equation $\omega_{\beta\alpha}^{\gamma} = C_{\gamma}^{\delta}\, \omega_{\beta\alpha}^{\gamma}$. If the angular rate of rotation is very small the skew symmetric matrix $[\, \omega_{\beta\alpha}^{\gamma}\, \Lambda]$ is also commonly used according to Equation 2.9.

2.3.2 Cartesian position

The Cartesian position, also known as the Euclidean position with respect to the relevant frame and the resolving axes can be seen in Figure 2.9 below.

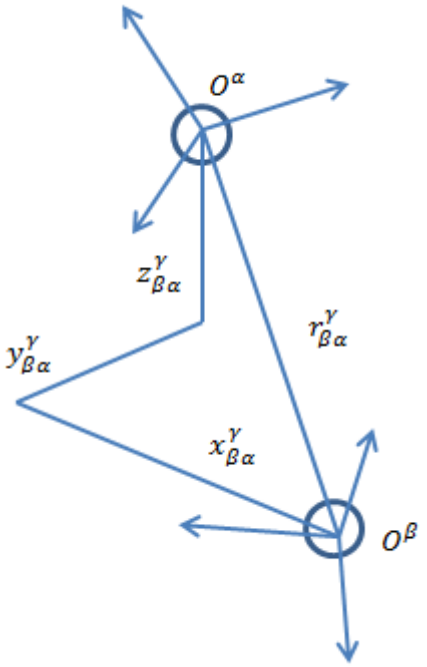


Figure 2-9 The position of the origin of frame α with respect to the reference β in frame ϒ axes showing the x, y and z coordinate components.

In Cartesian location, the object and the reference frame can be transposed simply by reversing the sign $\mathrm{r}^{\gamma}_{\beta\alpha} = -\mathrm{r}^{\gamma}_{\beta\alpha}$. Also with common resolving axes, the positions can be subtracted if they have a common reference frame $\mathrm{r}^{\gamma}_{\beta\alpha} = \mathrm{r}^{\gamma}_{\delta\alpha} - \mathrm{r}^{\gamma}_{\delta\beta}$ or added if the object frame and reference frame matches $\mathrm{r}^{\gamma}_{\beta\alpha} = \mathrm{r}^{\gamma}_{\beta\delta} + \mathrm{r}^{\gamma}_{\delta\alpha}$.

For the different resolving frame, the position can be computed by pre-multiplying with the relevant coordinate transformation matrix according to the equation below.

$$\mathrm{r}^{\gamma}_{\beta\alpha} = C^{\gamma}_{\delta}\, \mathrm{r}^{\delta}_{\beta\alpha} \qquad (2\text{-}11)$$

2.3.3 Velocity

Velocity is defined as the rate of change of position of the origin of the object frame with respect to the origin of the reference frame according to the equation below.

$$\mathrm{v}^{\gamma}_{\beta\alpha} = C^{\gamma}_{\beta}\, \dot{r}^{\beta}_{\beta\alpha} \qquad (2\text{-}12)$$

In general a velocity is registered if there is a motion by the object frame origin with respect to the reference frame origin and vice versa or if there is a rotation of the reference frame with respect to the object frame. It is important to note that if there is a rotation of the resolving axes ϒ with respect to the reference frame β it does not affect the velocity, thus $\mathrm{v}_{\beta\alpha}^{\gamma}$ will not be equal to the time derivative of $\mathrm{r}_{\beta\alpha}^{\gamma}$ in that case. Also, the velocities cannot be added if the reference frames are rotating against each other.

As in previous cases, velocities can be resolved in different axes by simply pre-multiplying by the relevant coordinate transformation matrix according to the equation below.

$$\mathrm{v}_{\beta\alpha}^{\gamma} = C_{\delta}^{\gamma}\, \mathrm{v}_{\beta\alpha}^{\delta} \qquad (2\text{-}13)$$

2.3.4 Acceleration

Acceleration is the second time derivative of the origin of the Cartesian position of object frame α with respect to the origin of the reference frame β about the axes of ϒ frame. It can be solved by pre-multiplying with a relevant coordinate transformation matrix s shown in the equation below. More details can be found in Groves' book (Groves, 2013).

$$\mathrm{a}_{\beta\alpha}^{\gamma} = C_{\beta}^{\gamma}\, \ddot{r}_{\beta\alpha}^{\beta} \qquad (2\text{-}14)$$

2.4 Filter Algorithms in Navigation System

Navigation filter algorithms are widely used in navigation and positioning solutions for optimal state estimation based on the measurement acquired from the IMU. These measurements can typically be velocity, position, acceleration, and they are generally time varying. One of the most common usages of the filter algorithm is GNSS integrated inertial navigation system where the Kalman filter is used to account for

missing measurements and other sensor noise to predict the next most optimal position in real time. A thorough evaluation of GPS with a low cost INS can be found in the work of Chris Hide (2003). Generally, navigation systems inherently have measurement errors such as hardware bias, random noise and environment-induced noise. Some of these errors are systematic and repeat every epoch, others are random hence non-repeatable. Both these errors can generally be modelled and optimised using filter algorithms discussed in (Groves, 2013). The initial condition and parameters of the system are generally embedded in a mathematical model known as the 'state model', and the measurements are collected from time to time, also known as the 'observation model'. The measurements are then analysed in a probabilistic or Bayesian estimator to predict the optimal solution in a prediction model. Different filter algorithms work differently and depending on the context of usage and the system; their performance varies as discussed in the filter algorithms chapter in (Quan *et al.*, 2015). In this section, we will only discuss two widely used navigation filter algorithm, the Kalman filter and Particle filter. Both are recursive Bayesian estimators and widely used in navigation and positioning solutions, the latter used mostly in nonlinear non-Gaussian systems for better performance but at an additional computational cost.

2.4.1 Kalman Filter

The Kalman filter, originally developed by R. E. Kalman (Kalman, 1960) has been widely used in navigation and tracking problems. The algorithm has been optimised and updated by later authors and used for real-time estimates of state change. The Kalman filter in its basic form is a stochastic linear system estimator operating recursively. The filter algorithm mainly has four main control elements:

1. System model
2. Measurement model
3. Measurement vector and error covariance
4. State vector and error covariance

As mentioned (Groves, 2013) the state vector consists of the system parameters which the algorithm estimates every epoch, namely, position, velocity, attitude, sensor noise and bias. The number of the state varies and can be both time-dependent and constant. The state vector also has error covariance, which represents the uncertainties the algorithm must consider when estimating.

The system model, sometimes known as the 'process model' describes the system and its parameters, clearly describing how the system and their associated equations change with time.

The measurement model represents all the related sensor measurements in the navigation system and describes how the model changes with time when compared to the actual state of the system and not the estimated one.

The measurement vector holds all the required measurements necessary for the state vector to estimate, and it also has the error covariance matrix to account for the uncertainty. The Kalman filter algorithm steps are listed below (Groves, 2013):

1. Calculate the transition Matrix Φ_{k-1}
2. Calculate the system noise covariance matrix Q_{k-1}
3. Propagate the state vector estimate from $\widehat{X_{k-1}^{+}}$ and $\widehat{X_{k-1}^{-}}$
4. Propagate the error covariance matrix from P_{k-1}^{+} to P_{k-1}^{-}
5. Calculate the measurement matrix, H_k
6. Calculate the measurement noise covariance matrix, R_k
7. Calculate the Kalman gain K_k
8. Formulate the measurement, Z_k
9. Update the state vector estimate from $\widehat{X_k^{-}}$ to $\widehat{X_k^{+}}$
10. Update the error covariance matrix from $P_{k-1}^{-}$to P_{k-1}^{+}

More details of the derivation of the state equation updates and their explanations can be found in (Thacker *et al.*, 1998) and (Faragher, 2012).

2.4.2 Closed Loop Kalman Filter

The basic Kalman filter assumes the system is linear even though it is not in most cases of the navigation system. To improve the results without using the modified version of the filter and to account for the loss of precision of the higher order derivative, the Closed-Loop implementation in an error state Kalman filter is used. In this case, the errors after the end of the estimation are fed back to the state at regular intervals to ensure the system is aware of the new errors by nullifying the state equations to zero. Thus, the state values will never grow too large with time, and the higher order precision loss is avoided due to linearisation.

2.4.3 Extended Kalman Filter

Even with closed loop correction, sometimes it is not possible to compensate for the accumulation of the higher order state values as describe in Groves' book (Groves, 2013). Also, the general Kalman filter does not always provide an optimal solution due to the linearity and Gaussian assumption of the system. It is especially true in ranging measurements for GNSS which are highly non-linear and in applications such as total state INS/GNSS integrations where the absolute position, velocity and attitude are estimated instead of the errors. As such a linear approximation and closed loop corrections will not work since there is no way to feedback the error to the Kalman states after each iteration. The EKF is a nonlinear version of the original filter which works by replacing the system matrix, F, and measurement matrix, H in the propagation and update equation with nonlinear functions from the state vector. It develops local linearisation of the equations similar to Taylor expansion and creates a sub-optimal solution as described in (Lettieri, 2007).

2.4.4 Unscented Kalman Filter

Another variation of the Kalman filter is the unscented Kalman filter (UKF) which can also account for highly nonlinear systems. Unlike EKF, instead of replacing the system function, f and measurement function, h, the filter uses a set of sample points or nonlinear equations. The UKF transforms the n-element state vector $\hat{X}$ and its covariance matrix P into 2n state vectors known as 'sigma points' as described in

(Groves, 2013; Quan *et al.*, 2015) . The UKF also assumes the noise in the system to be Gaussian just like the EKF and can be expressed by its mean and covariance only. As a result, with the carefully chosen sigma points, it is much easier to approximate the Gaussian distribution in the system instead of a generalised local linearisation. In terms of performance, the UKF has shown the superior result with more stability but with the same computational cost. (Lettieri, 2007). Literature related to the use of Kalman filter for real-time navigation combining multiple sensor-integrated inertial solutions can be seen in the work of (Ganti *et al.*, 2014; Deng, Hu, *et al.*, 2015).

2.4.5 Particle Filter

The family of Monte Carlo methods was first described in 1954 by Hammerly and Morton's work in (Hammersley *et al.*, 1954), ever since a lot of work had been done in developing algorithms that use the principles of Monte Carlo simulation and applications in a wide-ranging field encompassing mathematics, engineering, physics, economics, finance etc. The Sequential Monte Carlo (SMC) method typically involves working with stochastic processes such as Hidden Markov Models (HMM) requiring random sampling. A particle filter is a SMC method of non-linear filter that incorporates Bayesian statistical inference. Particle filtering methodology, basically a Markov process follows a genetic type mutation-selection sampling approach, with a set of particles to represent the posterior distribution of some stochastic process given some noisy observations. Several upgrades of the algorithm exist as discussed in (Doucet *et al.*, 2012), but in general, particles are initialised with weights based on specific criterion and application context. Then based on the model prediction, an update is made of the state. It also involves re-sampling of the particle distribution based on the fitness of the particles after every epoch or if most of the particles are found to be impoverished. Particle filters are widely used in position estimation because of their ability to compensate for the uncertainties in the non-linear system were a traditional Kalman filter would fail.

Particle filter has a lot of similarity to the Kalman filter in its operation as described by Groves (Groves, 2013). The particle filter mainly has three phases, system propagation,

measurement update and resampling with the first two similar to the Kalman filter. The system propagation phase involves initialisation of each of the particles with system parameters and system noise to account for uncertainty. Then the transition function is specified for the propagation of the particles. In the measurement phase, the particle measurement is acquired and using the measurement probability distribution function, the probabilities of the particles, also known as weights, are updated to get the absolute likelihood. It is important to note, during the system propagation only the state of the particles is changed, the weight is always updated in the measurement phase, which involves normalisation of the particle weight distribution. The most crucial phase is the resampling process since this stops the degeneracy of the particles. It is because after only a couple of iterations, the particles will start to suffer from reduced weight, and this will lead to increasing computational cost as described in (Lettieri, 2007). One way to solve this is to increase the number of particles, but this approach has limitations, another is to replace the particles with a reduced weight with more fit particles, thus replenishing the stock and propagating the particles toward an optimal solution. This replacement is done in the resampling phase using sequential resampling using either of the four standard resampling schemes, multinomial resampling, stratified resampling, systematic resampling and residual resampling. More details of the schemes and their performance comparison can be found in (Lettieri, 2007).

Resampling can be done after each iteration, at a specific interval or after a certain threshold is reached and helps the filter to be more responsive to changes in the system's environment making it more stable. Some examples of particle filter used in positioning solutions can be seen in (Kaji *et al.*, 2012b; Pinchin *et al.*, 2012; Chateau *et al.*, 2014; Jing, 2015; Tian *et al.*, 2015). The papers highlight the use of particle filter with inertial measurements and traditional dead reckoning technique together with map matching in a multi-sensor fusion positioning solution. The paper by Tian et al. looks explicitly to minimise sensor drift error and regular correction using commercial smartphones. Pinchin et al. look to minimise heading error using cardinal heading information. Chateau et al. provide a comparative analysis between different

positioning algorithms with the particle filter approach using smartphones. The use of Gaussian mixture model in combination with particle filter can be seen in Kaji et al.

2.5 Inertial Navigation and Dead Reckoning

Inertial navigation system (INS) is a dead reckoning technique used to estimate position, velocity and attitude of the object using the measurement from an IMU, as shown in Figure 2.10. Application of INS is wide-ranging, covering civil aviation industry, military, ships, guided missile systems, UAVs, pedestrian navigation and automotive navigation. As stated, the INS system is mainly dependent on the IMU unit and the navigation processor which typically comprises of a 3-axis accelerometer and gyroscope but may have other sensors wafer-fabricated in the chip. The quality of the sensors varies depending on the grade of the sensors, such as marine/aviation grade, tactical grade, industrial grade and consumer grade (VectorNav, 2008). Most of the low cost, cheap, mass-produced ones are consumer grade known as 'MEMS' for short and come mostly in strap down format nowadays. Also, handheld mobile devices and smartphones are integrated with a wide array of inertial sensors and can also perform the role of IMU. Of course, their performance may vary (Dabove *et al.*, 2015) and are generally of more inferior quality in comparison. Nevertheless, the potential for using them is significant in navigation and geospatial computing (R. Chen *et al.*, 2014).

INS is an iterative process described in (Groves, 2013) that makes use of the result from the previous iteration. As such initialisation is necessary for attitude, velocity and position. Position and velocity need to be provided at the start.

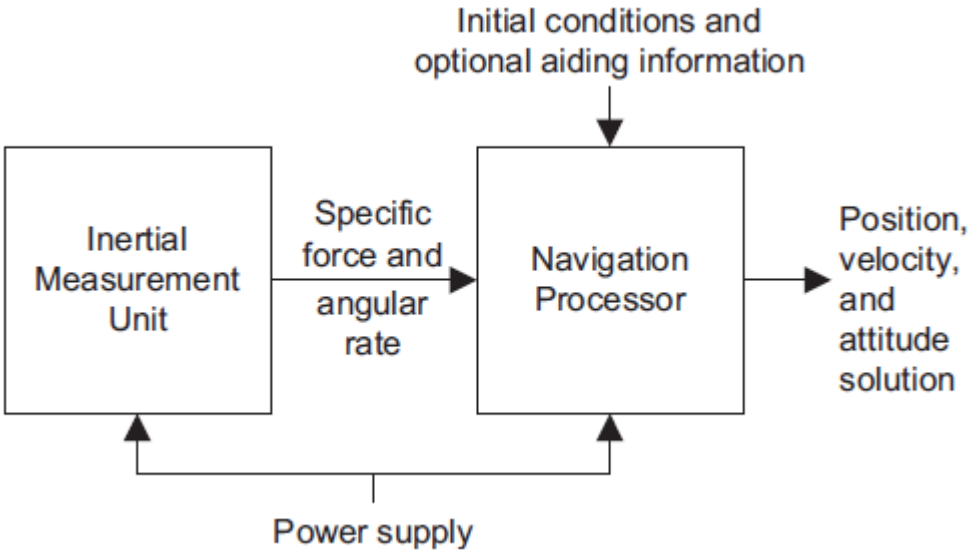


Figure 2-10 Basic schema of an INS. Source (Groves, 2013)**.**

These can be reference points or local coordinates, providing a reliable starting position. Other navigation systems can also aid the initialisation such as GNSS measurements. Attitude initialisation can be done using self-alignment/coarse alignment when stationary and may use the magnetic compass. The accelerometer can also be used for initialisation using a technique called levelling process; the idea is to measure the true direction of gravity when stationary using the accelerometer to correct the errors in the gyro and determine the heading using the corrected roll and pitch with gyro-compassing. It may require a reference system such as the magnetic north in the ECEF frame for absolute heading or initialising with zero in the starting direction for a relative heading estimate. The schematic diagram of the inertial navigation process can be seen in Figure 2.11.

Once initialisation is complete, we can compute the velocity at time *t* from the specific-force measurement in the resolving axes in ECEF frame, given we know the velocity v_{pb} at time t_0 according to Equation 2.15.

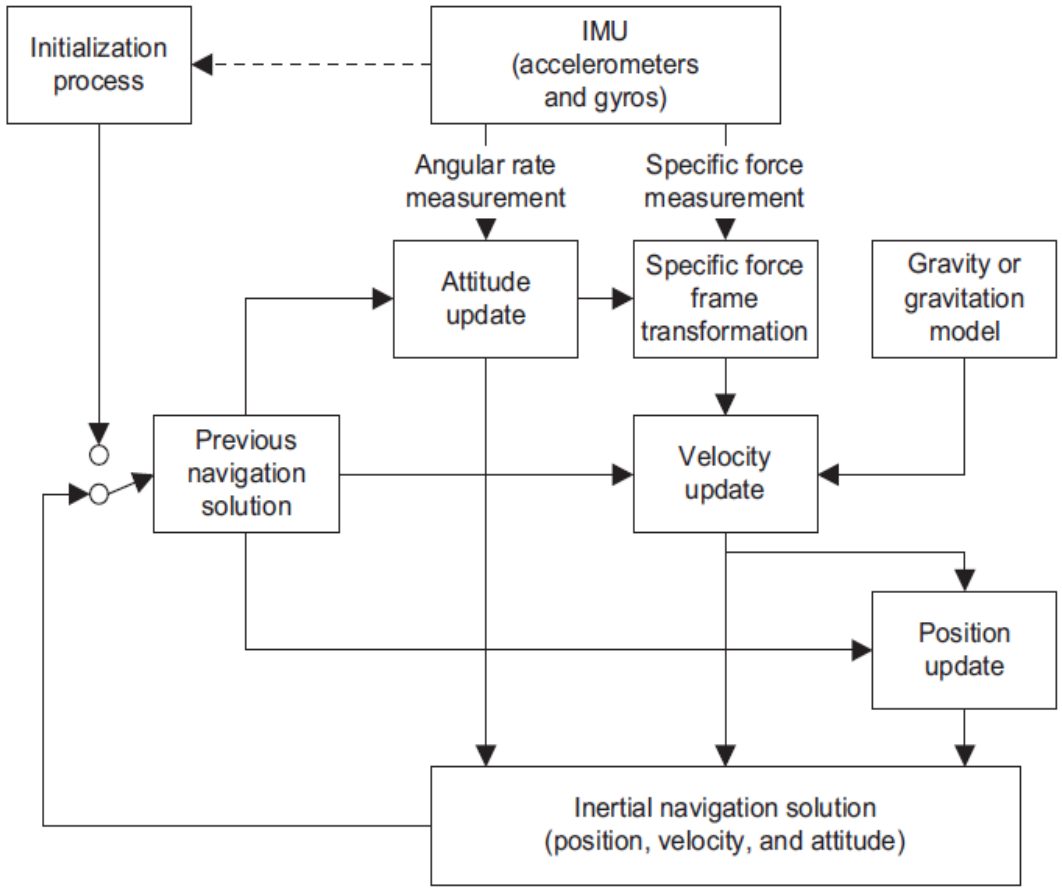


Figure 2-11 Basic Schematic diagram of the INS process, source (Groves, 2013)

$$v_{pb}(t) = v_{pb}(t_0) + \int_{t_0}^{t} a_{pb}\ (t')dt' \qquad (2\text{-}15)$$

Then to compute the position we need to integrate the specific force acceleration twice or integrate the velocity previously computed and estimate the new position r_{pb} at time *t,* given we know the position at the time t_0 according to the following equation.

$$r_{pb}(t) = r_{pb}(t_0) + \int_{t_0}^{t} v_{pb}\ (t')dt' \qquad (2\text{-}16)$$

Finally, to compute the heading ψ_{pb} at time t and given we know the value at an earlier time t_0 the following equation can be used.

$$\psi_{pb}(t) = \psi_{pb}(t_0) + \int_{t_0}^{t} \omega_{pb,\ z}\ (t')dt' \qquad (2\text{-}17)$$

Of course, all real-life motion is in three dimensions, and the parameters need to be modified to account for the six degrees freedom in the IMU sensors. More details are available in (Titterton *et al.*, 2004; Groves, 2013) to understand the derivation of the navigation equation for each of the different reference frame.

2.5.1 Pedestrian Dead Reckoning

Pedestrian dead reckoning (PDR) is one of the most critical elements of inertial navigation and covers both indoor and outdoor navigation. PDR is very challenging because of the complexity of human motion and environmental constraints it needs to take into account when estimating a position solution (Groves *et al.*, 2013; Wang *et al.*, 2018). At the same time handling of the sensors by an individual also contributes to the accuracy of the positioning output, for example, whether it is mounted on the shoe, attached to the body, or handheld. Generally, MEMS sensors are small and light and typically used in shoe-mounted IMU or strapped around the body, such as arms or the waist. As described in (Groves, 2013) PDR solution requires a combination of INS solution, step detection, step length estimation and heading and provides the position update for every epoch of the individual's movement step by step. Typically step detection and step counting would look for zero velocity updates (ZUPT) when shoe-mounted IMUs are used. Shoe-mounted IMUs generally have low cost sensors and extensive work in mitigating heading drift for such low cost sensors can be found in (Abdul Rahim, 2012). For other handheld devices such as smartphones, built-in motion sensor data such as an accelerometer is analysed for clearly distinguishable peaks or template matching (Brajdic *et al.*, 2013; Chandel *et al.*, 2014; N.-H. Ho *et al.*, 2016; Abadleh, 2018; Nguyen-Huu *et al.*, 2018). Step length varies depending on the physical characteristics of the person but in general it is linearly correlated to the step frequency, accelerometer measurement variance and the environment and can be trained with machine learning models (Dabove *et al.*, 2015; N. H. Ho *et al.*, 2016; Park *et al.*, 2017). So, either a motion model needs to be developed or a fixed step length

with random noise may be used, providing accuracy to 10% of the distance travelled but may deteriorate significantly if the environment is very complicated. The motion sensors in smartphones can also be used for classification of different kinds of motion mode and phone placement positions. As discussed in (Incel, 2015; Wang *et al.*, 2018) useful for obtaining highly accurate PDR solutions in a different context of navigation. Thorough performance evaluation of smartphone inertial sensors and their measurement for determining motion can be found in (Mourcou *et al.*, 2015).

The heading is also an essential component of the PDR solution and provides the direction of motion. For most of the low-cost consumer-grade IMU sensors, an attitude and heading reference system (AHRS) is implemented primarily where velocity and position updates are not required, such as UAVs. AHRS works with the same principle just like an INS; initialisation of the attitude using the acceleration to measure the direction of gravity and computing the roll and pitch during *levelling* (Yadav *et al.*, 2014; Valenti *et al.*, 2015). This corrected roll and pitch are then used to correct the gyro roll and pitch in a complimentary or smoothing filter (OlliW, 2016). A magnetometer is also used sometimes to further correct the gyro computed heading in a smoothing filter and use the corrected roll and pitch to get the magnetic heading (Yadav *et al.*, 2014). Magnetometers are prone to interference from ferrous materials, especially in an indoor environment and may provide an erroneous solution as such; it is advisable to implement a mechanism to reject measurement if the magnetic disturbance is detected. Typically AHRS provides heading accuracy within 1.2 degrees and may be affected by a factor of 2 during sharp turns or high-speed manoeuvres as specified in (Groves, 2013).

There is much work related to PDR encompassing navigation, motion detection and orientation determination as seen in (G. Chen *et al.*, 2015; Li *et al.*, 2015; Lee *et al.*, 2017) where the authors discussed dead reckoning combined with sensor fusion of Bluetooth, Wi-Fi and Map assisted localization methods. Work on shoe-mounted pedestrian navigation and constraints can be found in the work of Abdulrahim *et al.* (2011). Also, research related to smartphone-based PDR solutions, motion detection

and heading estimation are widely explored and many advances have been made as seen in the following papers (Kang *et al.*, 2012; Deng, Wang, *et al.*, 2015; Incel, 2015; Deng *et al.*, 2016).

2.6 Map Matching

Map matching is a part of the environmental feature matching, as explained in (Groves, 2013). It is widely used in positioning algorithms to aid the movement of objects or particles so that we get a well-controlled projection of movements within the area at each epoch. Typical applications of map matching would be related to digital road maps, road link identifications, road positioning, rail map matching and pedestrian map matching. For the pedestrian, the applicable constraints are less. As a result, a more flexible approach is required. A pedestrian can be both stationary and moving. Movement near doors needs to check for potential door crossings, or if drifting in the wrong direction and through a wall, the direction needs to be realigned with the correct direction. It also requires the positioning solution to be sufficiently accurate for the map matching to provide reliable position fix. Particle filter solutions with a sufficiently wide distribution of dead reckoning hypothesis help provide more than one alternative solution. These solutions are verified iteratively, and unlikely ones are removed until we are left with the most likely choice for a position fix. Even then this may not be able to provide the right position fix all the time as such a database with predefined permitted routes within the building may be created to make a judgement in such cases of ambiguity and shift the positioning output to the nearest permitted route.

In this research, NGB floor plan designs were provided in CAD format. These CAD files were used to record the coordinate points and applying geometric transformation were converted into matrices of polygons with characteristics of the floor, doors, walls and their association with adjacent walls and rooms. Rooms are identified as polygons with the walls and doors accordingly represented as coordinates. All the rooms and doors are given an ID with wall boundaries. Typical floor plan matrices used in this research can be seen in Figure 2.12 below.

(a) Room polygon-wall relationship

Polygon No.	Wall position	Door No.
1	$\begin{bmatrix} x^1_{w1} & y^1_{w1} \\ x^1_{w2} & y^1_{w2} \\ \vdots & \vdots \\ x^1_{wn} & y^1_{wn} \end{bmatrix}$	$[1]$
2	$\begin{bmatrix} x^2_{w1} & y^2_{w1} \\ x^2_{w2} & y^2_{w2} \\ \vdots & \vdots \\ x^2_{wn} & y^2_{wn} \end{bmatrix}$	$[2, \quad 4]$
$\vdots$	$\vdots$	$\vdots$
m	$\begin{bmatrix} x^m_{w1} & y^m_{w1} \\ x^m_{w2} & y^m_{w2} \\ \vdots & \vdots \\ x^m_{wn} & y^m_{wn} \end{bmatrix}$	$[k]$

(b) Door-room relationship

Door No.	Door position	Linked Rooms
1	$[x_1, y_1]$	$[1, 11]$
2	$\begin{bmatrix} x_2 & y_2 \\ x_4 & y_4 \end{bmatrix}$	$[2, 11]$
$\vdots$	$\vdots$	$\vdots$
k	$[x_k, y_k]$	$[m]$

Figure 2-12 Typical matrix showing association between doors and walls and rooms for map matching (Jing, 2015).

2.7 Indoor Positioning Technology and Techniques

Determining an IP solution is complicated because of its varying context of application and user-dependent performance requirement. Different technology, including hybrid systems, may combine multiple sensors with an appropriate measurement principle and algorithms for determining the positioning solution (Mautz, 2012). As seen in Figure 2.13 below, application areas may come with inherent constraints related to technology capability, deployment issues and options for modifications such as added functionality. Some of the most critical performance parameters that are generally looked for in an IP solution are not limited to accuracy, area coverage, latency, availability, robustness, data accessibility and security but most importantly cost. All these parameters need to be addressed when choosing a positioning technology and matched with the user requirements. To make things more complicated, these

parameters are not readily determinable beforehand since they are in turn dependent on environmental factors, assumptions and the application domain. Thus it is challenging to determine the best possible solution objectively and generally requires an iterative trial and error process (Mautz, 2012; Basiri *et al.*, 2014, 2015).

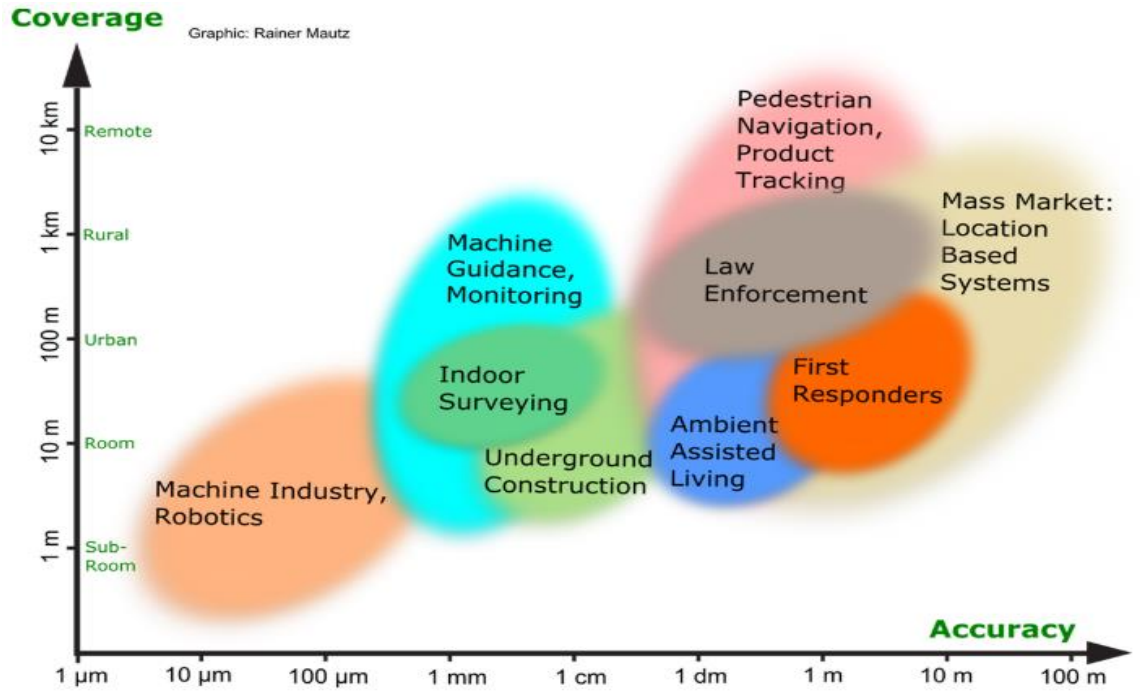


Figure 2-13 Indoor positionings mass market coverage and accuracy based on user requirement. Source (Mautz, 2012)

2.7.1 Measurement Techniques

Some of the universal positioning measurement principles and methods are (but not limited to) trilateration/multilateration techniques such as Time of Arrival (TOA)/Time of Flight (TOF), Time Difference Of Arrival (TDOA), Triangulation Using Angle of Arrival (AOA), Fingerprinting/Scene Analysis, Proximity and Path Loss Model.

(i) Trilateration/Triangulation

Trilateration is concerned with using the distance measurement from three or more base station/transmitters and the geometrical property to determine position. Typically positioning using range measurements are done using this technique whereas triangulation is mainly concerned with determining position using angular

measurement. Both require direct Line of Sight (LoS) for short-range communication devices such as UWB, Bluetooth and RFID.

(ii) Time of Arrival (ToA)

The distance from the transmitter to the receiver is always directly proportional to the propagation time and can be used as a positioning signature. For ToA positioning, signal measurements are taken from at least three different reference points, the one-way propagation time is measured, and the distance between them is calculated (Liu *et al.*, 2007). Then using geometry, the intersection point of the circles can be solved for the position. ToA method suffers from two problems, the transmitter and receiver must be precisely synchronised and transmitted and receiving the timestamp must be labelled to discern the distance the signal has travelled. ToA is particularly challenging to apply in indoor environments where the signal suffers from multi-path conditions and difficulty in ensuring continuous LoS from at least three reference points during navigation (Mautz, 2012).

(iii) Time difference of arrival (TDoA)

The idea of TDoA is to determine the relative position of the mobile transmitter by analysing the time difference of signal arrival in the receiver, rather than the actual arrival time in ToA. TDoA measurements eliminate the possibility of the receiver's clock bias since any time offset of a non-synchronous receiver's clock is eliminated by subtraction. With two transmitters at known locations, a receiver can be located onto a hyperboloid. For 3D locations, at least four transmitter measurements can be used by the intersection of three hyperboloids. Precise synchronisation of all transmitters is mandatory otherwise it will result in positioning error. GNSS positioning with low-cost receivers benefits from the automatic cancellation of the hardware drift using this approach (Liu *et al.*, 2007; Mautz, 2012).

(iv) The angle of arrival (AoA)

AoA information can be obtained by using directionally sensitive antennas placed within the transmitter. AoA technique does not require time synchronisation and

measures the angle of incidence during the reception. If the absolute orientation of antennas is challenging to manage, multiple antennas may be used as compensation. The position is then computed by solving for the intersection of the lines and commonly used in positioning using cameras which have direction antennas embedded in their chip for each pixel detected. AoA technique is difficult because of the specific configuration of hardware requirements and costs (Liu *et al.*, 2007; Mautz, 2012).

(v)Fingerprinting/Scene Analysis

Fingerprinting or scene analysis is the approach of collecting and storing radio signal parameters such as received signal strength (RSS) from a short-range communication device such as Wi-Fi or Bluetooth. Generally, the collecting points would divide the location of interest into cells or grids in the form of a grid map. During the navigation phase, the collected RSS is then compared to the stored fingerprint database using pattern matching algorithms to compute the location (Dahlgren *et al.*, 2014). Creation of the fingerprint database can be tedious and time consuming and as such has also seen significant research for improvement in the data collection phase using crowdsourcing, collaborative data collection, probabilistic methods and motion sensors in PDR as seen in (Bolliger *et al.*, 2009; Bisio *et al.*, 2013, 2016; Chen *et al.*, 2013; Luo *et al.*, 2013; Zhang *et al.*, 2015; Jing *et al.*, 2016; Hu *et al.*, 2018).

RSS based fingerprint localisation can be divided into three categories, as shown in Figure 2.14 below. The deterministic approach will typically use the Euclidean distance for pattern matching with the fingerprint radio map using Nearest Neighbour or K-nearest Neighbour or Weighted K-nearest Neighbour. The probabilistic method looks into the distribution of the signal strength such as Naïve Bayes, Bhattacharya distance, or partitioning the coverage area using fuzzy partitioning (Le Dortz *et al.*, 2012; Pritt, 2013; H. Zhou *et al.*, 2014). The machine learning approach is also discussed such as ANN, Support Vector Machines (SVM) and Decision Trees.

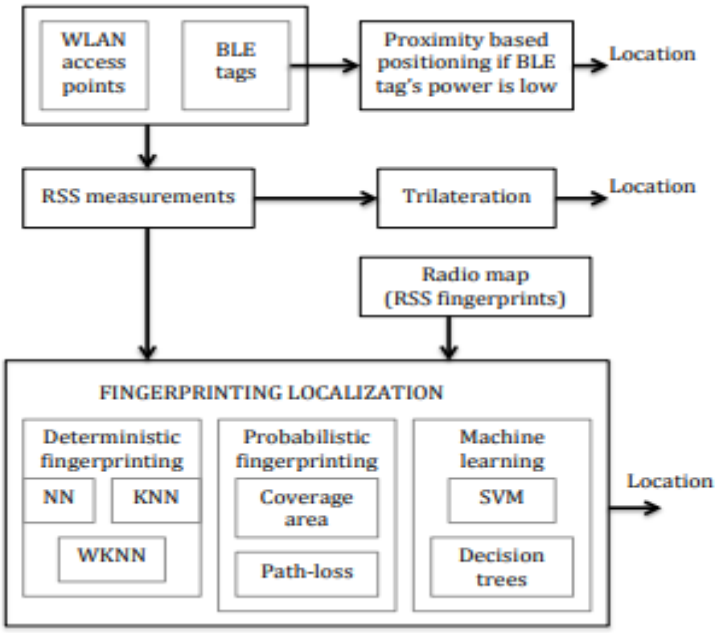


Figure 2-14 Approaches for RSS based positioning. Source (Davidson and Piché, 2017)

Machine learning models require extensive training of the model before comparing and may be computationally expensive in some cases (Liu *et al.*, 2007; Sánchez-Rodríguez *et al.*, 2015; Davidson and Piché, 2017).

(vi)Proximity

Proximity location tags provide relative location information using reference points. Generally, the proximity-based method requires densely covered, strategically positioned transmitters or sensors and a typically non-overlapping area of coverage. Bluetooth and RFID are perfect examples of devices used in proximity-based positioning, as seen in (Kim et al., 2015). To extract maximum accuracy, it is essential to understand the physical environment related to the topology, geometry and range of the tags. Proximity location estimation is based on the location of the detected tags and in most of the cases, more than one tag is detected. In such a case, location can be chosen based on the signal strength of the tag with an overlapping area of confidence. In terms of deployment, it is relatively straight forward and less complicated compared to other methods (Liu *et al.*, 2007; Dahlgren *et al.*, 2014).

(vii)Path Loss Model

Wireless signal attenuation can be used to estimate distance and position using RSS value. Signal strength attenuation can be modelled using the following equation ideally in free space (Kwok-Wai Cheung *et al.*, 1998; Faria, 2005).

$$P_R \propto P_T \frac{G_T G_R}{4\pi d^p} \quad (2\text{-}18)$$

P_R is the received signal strength in decibels; P_T is the transmitted power from the transmitter, G_T and G_R are the antenna gain for the receiver and transmitter and *P* is the path loss factor and is affected by no LoS and environmental factors.

Indoor path loss can be more appropriately explained using the basic International Telecommunication Union (ITU) model (Itu-R, 2017), as shown below.

$$L_{total} = 20log_{10}f - 28 + N\ log_{10}\frac{d}{d_o} + L_f(n) \quad (2\text{-}19)$$

Where N is the distance power loss coefficient, L_f is the floor penetration factor d_o is the reference distance. The value of N varies according to the location such as office, residential, commercial, corridors etc. and are tabulated in (Itu-R, 2017). The Motley-Keenan propagation model also considers the attenuation due to wall and corridors in indoor space by modifying the above equation to include the wall penetration factor W_f

$$L_{total} = L(d_o) + N\ log_{10}\frac{d}{d_o} + L_f(n) + W_f(n) \quad (2\text{-}20)$$

Even with all these parameters included it is challenging to model the signal coverage of any environment with the RSS value given the random nature and environmental factors affecting the signal propagation as discussed in the papers (Kaemarungsi *et al.*, 2012; Fet *et al.*, 2013; Zhu *et al.*, 2013). As such, much assumption needs to be considered when using any of the path loss models.

2.7.2 Positioning Technology

The last decade has seen a growing interest and progress in research related to IP and hybrid navigation solutions. These advances have fuelled much interest in inertial sensors, and wireless short-range communication technologies that can provide positioning solutions with most of them readily available on devices we use daily. To develop a positioning system, one must create its dedicated network infrastructure or use an existing one. The first option gives the user more control in determining the different specification required for the desired quality of the positioning solution. The later minimises infrastructure setup and surveying cost. We will briefly explore some of the standard positioning technology and provide the reader with a general understanding of the astonishingly growing array of wireless positioning options.

(i)Inertial Measurement Unit

Inertial sensors comprise accelerometers and gyros. An accelerometer measures specific force experienced due to gravity and motion and a gyro measures the angular rate of motion, both without an external reference. An IMU combines 3-axis accelerometer and gyro to produce three-dimensional measurement and navigation solutions. An IMU forms the core measurement unit of an INS, and most of the modern INS designs are a strap-down version focusing mostly on MEMS technology (Groves, 2013). In general, there are no agreed definitions of high, medium, and low-grade IMU, although the accuracy and performance of the inertial sensors depend on the quality of the IMU sensors. Higher grades are more expensive and larger compared to low-grade ones.

The highest grades of inertial sensors are generally used in military ships, submarines, and ballistic missiles. A marine-grade INS can be as expensive as $1 million with navigation drift of less than 1.8 km per day. Aviation-grade or navigation-grade, INS is used in commercial and military aircraft worldwide. They cost around $100,000 with a maximum horizontal position drift of approximately 1.5 km per hour of operation. An intermediate-grade IMU, comparatively inferior in performance, is used in smaller aircraft and helicopters and costs between $20,000 and $50,000 (Groves, 2013).

Tactical-grade IMU generally provides a drift-free inertial navigation solution for a few minutes, but their drift error can be mitigated by integrating with other positioning systems, such as GNSS/INS integration. These systems typically cost between $2,000 and $30,000 and are used in guided weapons and UAVs (Groves, 2013).

The lowest grade of inertial sensors is known as a consumer or automotive grade. They are generally sold on their own, without calibration and are not accurate enough for inertial navigation, even when integrated with other navigation systems, but can be used in an AHRS, for PDR using step detection, and for context detection. Accelerometers cost around a dollar while gyro prices start at about $10. Companies working with inertial sensors have now started to develop a bespoke IMU unit combining multiple accelerometers and gyros from multiple manufacturers of different accuracy (Groves, 2013). This research has used inertial sensors embedded within modern smartphones, which are typical of consumer grade.

(ii)Wi-Fi

WLAN or Wi-Fi operates in both the 2.4 GHz and 5 GHz band of the IEEE 802.11 family of standards, the spectrum of frequency varying between countries of operation (Groves, 2013). Wi-Fi infrastructure is common nowadays and can be found in both residential and commercial buildings and even in open streets. Theoretically their signal coverage is up to 100m, but generally, due to attenuation, it comes down to within tens of meters.

Wi-Fi-based positioning typically utilises either the pattern matching or proximity-based method and requires the collection of RSS from access points (AP) at specific locations creating a radio map database or location reference tag. Typically, the accuracy varies between 1- 5 m and depends on several factors; the number of APs, location topology, measurement method and pattern matching algorithm. Some of the commercial systems using WLAN positioning are Ekahau and Aeroscout MobileView. Wi-Fi signals are prone to multipath and attenuation from the physical environment, especially in an indoor environment due to spatiotemporal variation. Also, different Wi-Fi chip makers have different standard of RSS measurement and thus resulting in

variation in measurement due to non-standardisation. Complete scanning of Wi-Fi APs usually takes around 5 seconds, so for stationary positioning, this latency might be acceptable but during real-time dynamic motion we are likely to face a large positioning error of around 5 to 10 m or even more if used on its own. More details of signal attenuation property, modulation and bandwidth can be found in (Liu *et al.*, 2007; Groves, 2013; Brena *et al.*, 2017). Nowadays, Wi-Fi sensors are readily available in every smartphone and provide ubiquity in terms of ready-to-access positioning capability. Wi-Fi is widely used in collaborative positioning as seen in (Luo *et al.*, 2011; Jing, 2015; Zhang *et al.*, 2015). The use of Wi-Fi in the multi-sensor fusion positioning solution can be seen in the following papers where authors have discussed different approaches when developing indoor positioning solutions, with Wi-Fi measurements forming the core of their positioning framework (Lassabe *et al.*, 2009; Syed *et al.*, 2011; Kaemarungsi *et al.*, 2012; Kaji *et al.*, 2012a; Le Dortz *et al.*, 2012; Moghtadaiee *et al.*, 2012; Hong *et al.*, 2014; G. Chen *et al.*, 2015; Z. Chen *et al.*, 2015; Zhu *et al.*, 2015; Ma *et al.*, 2015; Jing *et al.*, 2016) .

(iii)Bluetooth Low Energy

Bluetooth low energy (BLE) is a smart feature of Bluetooth 4.0 and was released to improve short-range communication for devices that do not require a large amount of data transfer. The main objective is to facilitate efficient connectivity between devices for monitoring and control applications where a low amount of data transfer is necessary: such as sending sensor values or control commands. The new BLE comes with a completely new software stack and does not even require pairing between devices like its predecessor, Bluetooth classic, and can easily transmit data using the broadcast mode during the passive scanning mode (Dahlgren *et al.*, 2014).

BLE is now becoming a common sight in every smartphone and other devices such as laptops and tablets and widely used in IP solutions (Feldmann *et al.*, no date; Chawathe, 2009; Jianyong *et al.*, 2014; Oksar, 2014; Faragher *et al.*, 2015; Li *et al.*, 2015). The use of BLE with Wi-Fi in a hybrid positioning solution can be seen in (Baniukevic *et al.*, 2011, 2013). The use of BLE embedded in smartphones, with PDR

and fingerprinting can be seen in (Rodas *et al.*, 2008; Hay *et al.*, 2009; Gurrin, 2013; Rajkiran *et al.*, 2015; Kriz *et al.*, 2016; Zhuang *et al.*, 2016). It is also similar to RFID since its range can now be effectively configured to zero by varying the power level using state of the art BLE beacons from Kontakt.io and indoo.rs (indoo.rs, 2010; kontakt.io, 2013) with a user-friendly dashboard and admin panel. The battery life is also prolonged depending on the configured power level and can transmit bursts of signal continuously in a short period. It is ideal for proximity-based positioning providing room-level accuracy at a significantly lower deployment cost compared to RFIDs. Nokia's benchmark IP solution is an example where angular positioning using multiple high direction ceiling-mounted HAIP BLE signals are used, providing an estimated accuracy between 0.3 m to 1m (Groves, 2013).

(iv)Radio Frequency Identification (RFID)

Radiofrequency or RFID uses similar methods to barcodes but without any direct LoS. Typical usage would be in libraries, building access, tracking and public transport ticket systems (Groves, 2013). RFID works with electromagnetic transmission to an RF-compatible integrated circuit and is now being seen as a means of enhancing data handling processes. An RFID system has several necessary components, including several RFID readers, RFID tags, and the communication between them. The RFID reader can read the data emitted from RFID tags. RFID readers and tags use a defined RF and protocol to transmit and receive data. RFID tags are categorised as either passive or active.

Passive RFID tags operate without a battery. They are mainly used to replace the traditional barcode technology and are much lighter, smaller in volume, and less expensive than active tags. They reflect the RF signal transmitted to them from a reader and add information by modulating the reflected signal. However, their ranges are minimal. The typical reading range is 1-2 m, and the cost of the readers is relatively high. Passive RFID systems usually make use of four frequency bands: LF (125 kHz), HF (13.56 MHz), UHF (433, 868-915 MHz), and microwave frequency (2.45 GHz, 5.8 GHz) (Liu *et al.*, 2007).

(v)Ultrawideband (UWB)

UWB signals operate with ultra-short pulses of less than one ns and at least 500 MHz on the frequency domain. UWB, unlike conventional RFID systems operating on single bands of the radio spectrum, transmits the signal over multiple bands of frequencies simultaneously between 3.1 to 10.6 GHz. UWB transmitted signal length is much shorter compared to conventional RFID and consumes less power than conventional RF tags. UWB needs to operate across a broad area of the radio spectrum since it does not have a dedicated spectrum, thus having to share spectrum with other users. As a result, the power spectral density (PSD) must be very low for UWB. UWB transmission spectrum varies among countries, and some even have detect-and-avoid (DAA) technology which minimises UWB transmission in spectrum already used by other narrowband spectrum users. The most crucial feature of UWB is its multipath resolution capability. Since they transmit over a broad spectrum, the short duration pulses can be easily filtered, differentiating between multipath signals and correct signals.

Penetration power of UWB signals is excellent, and they pass easily through walls, equipment and clothing. However, metallic and liquid materials cause UWB signal interference. Use of multiple UWB receivers and strategic placement could overcome this disadvantage. UWB ranging techniques include ToA, TDoA and Two-Way Ranging (TWR). Since the UWB PSD is very low, the range depends on the bandwidth-to-data-rate ratio typically of the order of 10^{5} for a range of 1 km. UWB ranging is performed by known data sequences, thus maximising the bandwidth-to-data ratio allowing exact timing measurements to be made. These ensure accurate determination of the TOA and the precise TOF of a burst transmission from a short-pulse transmitter to a corresponding receiver (Liu *et al.*, 2007).

Some of the key applications of UWB are asset tracking and navigation and tracking of military and emergency personnel without the requirement of any dedicated base stations inside (Groves, 2013).

(vi)Tactile Sensors

Tactile sensors are devices measuring or acquiring positioning information through physical interaction with its environment or area of contact. They are generally used for surveying or in industrial applications. They are very accurate, providing positioning measurements between 0.1 mm to 0.01mm. Some of the conventional tactile systems used in surveying are laser trackers, total stations like Leica Geosystems or 3D Disto, laser scanners, iGPS as discussed in (Mautz, 2012). Tactile systems are costly to acquire and has a limited range typically within a room. The performance parameters of some of these systems used in surveying and geodesy are shown in Figure 2.15 below.

Device	Typical Accuracy (m)	Measuring Range (m) or Area (m^2)	Measuring Principle	Application	Typical Hardware Costs	Market Maturity
measuring arm	15 µm + 10 ppm	3 m	polygonal chain	object inspection	> 30.000 €	product
CMM	2 µm + 0.4 ppm	10 m × 3 m	mechanical, interferometry	automotive, inspection	size depend.	product
laser tracker	10 µm + 5 ppm	80 m	distance & angular meas.	automotive, aerospace	> 110.000 €	product
totalstation	2 mm + 5 ppm	> 2000 m	distance & angular meas.	surveying, multipurpose	10.000 €	product
laser scanner	3 mm + 5 ppm	< 1000 m	distance & angular meas.	3D modeling	50.000 €	product
3D Disto	2 mm	50 m	distance & angular meas.	setting out, plumbing	8.000 €	product
laser radar	15 µm + 5 ppm	120 m	distance & angular meas	aerospace, industry	250.000 €	product
iGPS	0.2 mm	1200 m^2	TDoA, resection	industry, metrology	> 60.000 €	product

Figure 2-15 Tactile systems used in industry and surveying and their performance parameter. Source (Mautz, 2012)

(vii) Other Positioning Technology

There are many other technologies that can be used for positioning and navigation. Non- wireless technology would typically investigate camera technology, image analysis and sound. GNSS based systems investigate pseudolites, which are mainly used in GNSS-denied areas to enhance their area coverage. Pseudolites are also known as 'pseudo satellites' since they transmit pseudo code signals similar to GNSS in L1 or L2 frequency band. GNSS repeaters also work on similar principles but instead of having their signal transmission amplifies the weak original unmodified satellite signal

and retransmits them in indoor. It can be achieved by placing a GNSS antenna outdoor typically on the rooftop which would pass the original signal via cable and then using the repeaters which would transmit the signals wirelessly inside the room. They are mainly used to track the satellite in GNSS-denied areas. Assisted GPS (AGPS) is another technology used mainly outdoors but also in an indoor environment to locate mobile phones or devices with access to internet services. AGPS comes with its data link of satellite ephemeris almanac, differential corrections and timing information and thus can reduce the GNSS cold start time or Total Time to Fix (TTFF) significantly with the information. Other systems are Zigbee, radio, ultrasound, infrared, optical and magnetic. Details of these positioning systems can be found in (Mautz, 2012; Groves, 2013) Due to the limitations of this thesis we will not discuss each of the methods individually and also may be limited to the ones listed above. The reader is requested to read them on their own for further understanding.

2.8 Discussion on Application

Research on the use of Wi-Fi and BLE in an IP system has mostly been related to the improvement of their stand-alone position computation, radio map fingerprint generation or integration with INS for PDR solution to improve overall positioning capability. Example of Wi-Fi-based positioning can be seen in the work of (Le Dortz *et al.*, 2012; Pritt, 2013) where the authors have suggested using probability distribution comparisons and maximum-likelihood classification techniques respectively as pattern matching algorithms when comparing with a fingerprint database for position computation as an alternative to Nearest Neighbour (Euclidean distance) discussed in (Groves, 2013). Both the methods perform better comparatively but are computationally demanding, (Ma *et al.*, 2015) proposed several improvements when matching with the fingerprint database. They suggested an improved Euclidean Distance Positioning by incorporating the standard deviation to take the Wi-Fi fluctuation into consideration. An improved joint probability-based positioning by using the log of the probability weights and a weighted fusion. Positioning using variance as well as Euclidean distance, computing positioning from K possible fingerprint. The authors in (Faragher *et al.*, 2015) explored BLE fingerprinting as an

alternative to Wi-Fi and looked into the different advertisement channels, power level and advertisement rate. The result shows positioning accuracy changes depending on the density of the deployment with a cumulative positioning error of less than 2.5 m for high-density deployment and less than 5m for sparse deployment 95% of the time. The research showed significant improvement for BLE-based positioning over Wi-Fi, even when using a relatively sparse deployment of beacons. Fargher et al. in (Faragher *et al.*, 2014) provides a thorough analysis of the accuracy of Bluetooth fingerprint positioning and compares with the Wi-Fi fingerprinting. The authors mention BLE communicates in the 2.4 GHz domain similar to Wi-Fi with 40 channels, each having a bandwidth of 2 MHz however, only three channels 37, 38 and 39 are used for advertisement. BLE pseudo-randomly moves between these channels and transmits signal data from each channel. Unfortunately, it is not possible to identify which channel is transmitting the signal when recording the RSS value. It becomes more problematic when there is fast fading due to deep multipath, and we do not know which channel is broadcasting which RSS value. They investigate the effects using a ray tracing simulator in a 3D map by reconstructing signals with a single source of reflection for both Wi-Fi and Bluetooth. They conclude that multipath effects can be significantly reduced by smoothing the variance over a batch of data over a minimum window size while ensuring that we get RSS readings from all three channels. Then they test this mitigation technique by comparing with a Wi-Fi fingerprint against a ground truth. The use of BLE and Wi-Fi together in a hybrid configuration can be seen in the work of (Baniukevic *et al.*, 2011, 2013) were the authors used Bluetooth as hotspots for proximity detection which can be used to improve Wi-Fi-based positioning. Bluetooth receivers were placed between connected doors and hallways such that proximity analysis can be done when someone is passing through. At the same time, it was ensured they never overlap. The idea was to complement Wi-Fi search by partitioning the floor space into smaller zones of connected pathways. So, when a person is moving from one zone to the other, the Bluetooth AP will serve as a reference point to invoke the relevant part of the fingerprint map for Wi-Fi search.

Use of Bluetooth in the PDR solution can be seen in (Rodas *et al.*, 2008) using a particle filter solution. Various *RSSI* sampling periods (T_s: 0.1, 0.5, 1.5, 3) were experimented with and results showed the probability of not detecting the mobile device is higher when the sampling period is highest. It is because the number of beacons detected with a higher sampling period is much smaller. The authors compare static positioning results between the multilateration and particle filter algorithm with the later showing significant improvement. Further experiments were carried out to verify the accuracy when in motion using computer simulations. Some of the important features of errors encountered took place when the object in motion changes its dynamics. If speed is considered a feature of the particles then during moments of increment, the particles with higher weight were found to have a lesser speed and after some iterations, they will lose weight with respect to the ones with higher speed thus reducing accuracy. However, when the simplified model is used where the speed of the particles is not considered, changes in the mobile devices' speed can cause bigger errors. Another example of BLE used for PDR solution can be seen in (Li *et al.*, 2015). The authors use the smartphone's inertial sensors to develop a step detection algorithm using multi-threshold peak detection and dynamic step length estimation based on the variance and periodicity of the acceleration. Heading is estimated using magnetometer and gyro in a Kalman filter, to compensate for the accumulated error with the phone in the hand. At first, the BLE position output is combined with improved map matching to get the PDR solution and then fused with an extended Kalman filter. The experimental setup was done along the corridor of a single floor and required walking at a normal pace between 1.5 m/s to 1.8 m/s with a fixed number of walking steps (316). They tested four different positioning algorithms and found the maximum error varying between 44m and 5 m respectively. They also verified the accuracy of the positioning system with a different number of beacons (20, 15, 10) respectively when fused with the EKF, with beacons deployed every 10m along the corridor. The maximum error was around 5 m for all the scenarios, but the mean error reduced from around 4m to 2m due to improved filtering. The use of the foot-mounted inertial system for PDR solutions using EKF and using particle filter for map matching constraints can be seen

in (Pinchin *et al.*, 2012). The authors propose a cardinal heading-aided solution (CHAIN) which can be used to improve the heading of the particles when enforcing mapping constraints which can be difficult to do with the EKF alone for a PDR solution. In another paper (Tian *et al.*, 2013) the authors combine short-range proximity access control system (SRP) like RFID or NFC with indoor map matching and particle filter to develop a smartphone-based hybrid PDR solution. They propose a novel lost track recovery (LTR) method, common for the particle cloud when turning corners. The method reassigns the position to the nearest known turning point when particle weights are all zero or missed turns due to various reasons like overestimated step length, blocked wall etc. Improvement of Wi-Fi-based positioning can be seen in (Jin *et al.*, 2014) where uncertainty due variation of Wi-Fi *RSS* is corrected using an IMU-assisted nearest neighbour solution when selecting reference points for position computation. Similar work can be seen in (G. Chen *et al.*, 2015) where a PDR solution using Wi-Fi fingerprint fused with UKF and step counting for a smartphone-based 3D navigation solution is proposed. The authors suggested an improved K-means clustering to reduce fingerprint retrieval during position computation. Step counting was achieved using autocorrelation of accelerometer data, and heading was computed using the gyro and accelerometer fused in the UKF. Improvement of W-fi fingerprinting database creation using collaborative data collection with foot-mounted IMU can be seen in (Jing *et al.*, 2016). Improvement of particle filter-based position estimation can be seen in (Zhu *et al.*, 2015) . The authors propose a novel particle filter approach based on a Rao Blackwellized particle filter (RBPF). The authors partition the map into multiple sub-maps and propose multiple filters for local maps and a global filter for estimating the global position. This significantly reduces computation load and reduces overall positioning error to 1.2m. The use of UWB in collaborative and seamless positioning in combination with particle filter and Kalman with Wi-Fi or BLE can be seen in the work of (Jing, 2015; Peltola *et al.*, 2017). UWB is used as an anchor for aiding positioning using ranging measurement (P2P), and the effects of network geometry and size for collaborative positioning are also examined. Results show UWB can help bring down positioning errors to around 1.4m, 95% of the time. As seen

earlier, most of the PDR solutions proposed using a smartphone requires a specific carrying position. The paper (Yu *et al.*, 2019) proposes a Wi-Fi-based PDR solution with an unconstrained phone carrying position (handheld, pocket, swinging, phone call) using two UKFs, one for position estimation and another for heading estimation. Step detection is carried out using acceleration peak detection with thresholding and opting for a linear step length estimation model using step frequency and acceleration statistics. The experiment was carried out in a single floor consisting of corridors and multiple rooms with participants walking along a predefined path to test the accuracy. Comparison was also done between UKF with EKF and KF and with PDR and Wi-Fi positioning alone. Results show an improvement in positioning accuracy for the proposed UKF methodology with a mean positioning error of 0.76m.

Figure 2.16 shows a simplified generalised flow chart of a possible PDR solution with options for multiple positioning data source integration and sensor fusion.

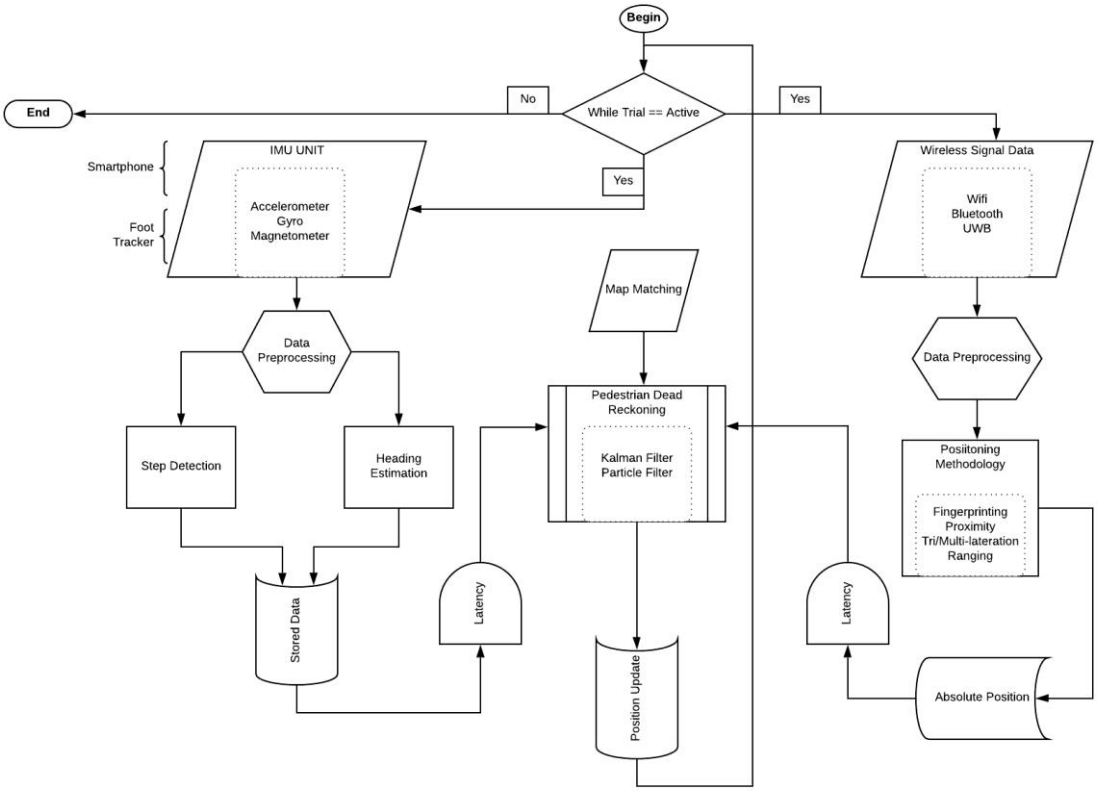


Figure 2-16 A generalised pedestrian dead reckoning system listing possible technology and techniques fusion

This section provided some selected applications of the different positioning technology and techniques and how they are integrated with hybrid positioning solutions. It also highlights the different context and scenario of the experimental setup (number of floors and layout) and constraints enforced when carrying out trials which are key to making decisions related to the choice of technology and techniques in this PhD for occupancy detection.

2.9 Choice of Technology and Discussion

This chapter provided the reader with an overview of most of the existing indoor positioning solutions covering a wide array of positioning technology and measurement methodologies. The positioning algorithms and techniques are described thoroughly, citing their usage and applications in existing literature where appropriate. Based on this overview it can be understood that there is no single compelling solution to any IP problems, but due to the advent of smartphones and other handheld devices coming with their own positioning capability the opportunities are endless. Existing indoor positioning methods typically used with smartphones can be seen in (Davidson and Piche, 2017). The challenge is in choosing the right technology based on the context of the application and requires careful consideration of the environmental factors and trial setup involving human participation.

For this research, positioning information needs to be collected for the understanding of building occupancy as such requires the use of IP technologies that are easy to deploy, capable of providing the required level of accuracy and cost-effective. Also, the data collection device needs to be user-friendly and readily available to the users. Based on these understanding Wi-Fi and BLE seem to be the most feasible choices since Wi-Fi is already deployed as a communication medium and BLE is very good for proximity solutions and cost effective as well for deploying all over the building. In terms of measurement methodology, the fingerprinting approach will be most appropriate since positioning data to understand occupancy will require continuous data collection over a long time with much unconstrained movement. Trilateration/triangulation techniques will not be the right choice because of the noisy

characteristics of the Wi-Fi/BLE signal and will always require good LoS to achieve a satisfactory result which may not always be possible especially with Wi-Fi. Fingerprinting will also be suitable since we will have an established radio maps with the RSS signature to compare with and can be manipulated later on depending on the quality of the Wi-Fi and BLE, *RSS* value collected during the trial. With regards to state estimation, particle filters will be more stable for nonlinear Bayesian tracking compared to any Kalman Filter configuration given the unconstrained movement expected from participants during real-life occupancy. With regards to data collection, the smartphone would be the most optimal choice compared to a foot tracker since it will be easy to carry and has all the required inertial sensors to develop a potentially optimal indoor PDR solution.

Chapter 3

BUILDING OCCUPANT MODELLING OVERVIEW

3.1 Background

The urbanisation of the world is occurring at an unprecedented scale and is being affected by various local and global factors. Quality of life, environment, and policy related to the regulation of energy supply will be severely affected if sustainable urban growth is not ensured. Building energy models (BEM) has historically been the mode of understanding and analysing energy performances of municipalities and neighbourhoods for building designers and energy policymakers (Reinhart *et al.*, 2016). This increasing demand for more energy-efficient buildings has created a challenge for the construction industry to ensure the building energy performance predicted during the design stage is sustained once the building is in use and has led to extensive analysis of occupancy and energy usage in multipurpose commercial buildings such as academic buildings (Ward *et al.*, 2008; S Douglas, 2014; Gul *et al.*, 2015; Pappi *et al.*, 2015). Unfortunately, current statistics provide evidence to suggest that buildings are not performing as well as expected (Menezes *et al.*, 2012). The reason for this gap in performance is due to various discrepancies related to design and model assumptions, management of power sources, occupancy behaviour and quality of building materials. Initiatives such as Post Occupancy Evaluation (POE), Post-Occupancy Review of Buildings and their Engineering (PROBE) and CarbonBuzz aim to illustrate the extent of this so-called 'performance gap' (Preiser, 1995). Typically, POE takes place after twelve months of building occupancy, and in all the cases prediction tends to be unrealistically low while actual energy performance is usually unnecessarily high. Many of the causal factors relate to the use of unrealistic input parameters in the model regarding occupancy behaviour, energy facilities management and usage patterns and are further associated with the lack of feedback to designers once a building has been constructed and occupied. Results from a case study using the PROBE suggested the measured electricity demands are approximately 60–70% higher than predicted in

schools and offices, and over 85% higher than predicted in university campuses (Menezes *et al.*, 2012). Thus, to understand how better to manage resources in an urban environment, it is imperative that we develop sophisticated predictive models related to behaviours of building occupants and their actions.

3.2 Probabilistic Modelling approaches

A lot of research work has taken place focusing on developing occupancy/occupant presence models, behavioural models, and multi-agent simulation (MAS) platforms. These platforms incorporate occupant presence, activities and behavioural models during the simulation. The critical part of the simulation is to address the stochastic or random nature of each of these behaviours and predict how it impacts different activities of our daily life overall and has a significant impact on predicting resources used inside buildings such as energy and water. There is a growing community of researchers developing different behavioural models which are stochastic. To understand the impact of these models, it is important to interface them together with some building performance tool like Energy Plus (U.S. Department of Energy, 2016) or use state of the art simulation tool like Anylogic (AnyLogic, 2018), Design Builders (DesignBuilder, 2020), etc. The University of Nottingham Built Environment Department has worked on a building simulations platform to predict energy usage of buildings using simulation tools like Design Builders and Energy Plus. Over the last few years, significant progress has been made to develop this in-house custom built Multi-Agent Simulation Platform (Chapman *et al.*, 2014). This MAS platform coded in C++ (Chapman *et al.*, 2018), integrates different occupant behavioural (Reinhart, 2004; Haldi *et al.*, 2009, 2010) and occupant presence models (Page *et al.*, 2008) which are being researched with considerable progress. The simulation platform can be coupled with building simulation tools; more specifically, Energy Plus which allows third-party integration with other platforms aiding the simulation. The platform interfaces with Energy Plus which provides the environmental parameters necessary as input and the models provide the consequences of performing certain activities as output in each time step of a simulation. The platform is still evolving, and some of the sub-models incorporated in the platform are listed below.

- Activity model: This model (Page, 2007) (Haldi *et al.*, 2008) predicts the probability that any one of the ten potential activities will be performed in each time step when the simulation configuration runs in a residential setting. These activities include sleeping, passive, audio/visual, IT, cooking, cleaning, metabolic, washing appliance use, personal washing and absence from the building. In non-residential setting, the activity performed is limited to IT and absence from the building.
- Window action: This model discussed in (Haldi *et al.*, 2009) predicts the probability of interaction with windows i.e. opening and closing.
- Lighting: This model discussed in (Reinhart, 2004) predicts the switching of lights on/off by taking the input of illuminance from Energy Plus and calculates the probability of turning on/off the lights when an occupant arrives or is present.
- External shading actions models discussed in (Haldi *et al.*, 2010) proposes an algorithm to define the probability of lowering or raising of the shading devices depending on different indoor parameters.
- Metabolic Gains: This model (Chapman *et al.*, 2014) calculates the metabolic gains of agents while performing different activities and actions which Energy Plus takes in as input to predict energy usage during simulation in each time step.
- Occupancy: This is one of the most essential models acting as input to all the other models for their occurrences. The platform states two methods for detecting occupancy. For residential buildings, it can be identified for the activity models; otherwise, for commercial spaces, it is using the presence model in (Page *et al.*, 2008).

The MAS platform by Robinson is a build-up of a series of extensive research conducted by (Page, 2007; Page *et al.*, 2007; Robinson *et al.*, 2011, 2012) related to the approaches in modelling occupants' presence and behaviour. The uniqueness of the models is that it generates a time series of presence and absence using data collected from surveys acquired over 8 years from Solar Energy and Building Physics Laboratory

(EPFL). It also models behaviours related to personal activity and environmental activity such as the use of windows and blinds (Haldi *et al.*, 2008) that have proven themselves to be realistic on both hourly and daily time scales. These models are then integrated into an urban energy modelling tool CitySim (Haldi *et al.*, 2011), and simulations are run for hypothetical scenarios of occupancy and their impact on energy demands and usage.

Occupant lifestyle patterns and behaviour have a significant impact on energy demand and also account for the stochastic nature of occupancy; presence and absence. Building type is also a factor and determines observed behavioural differences in the residential and commercial setting. Climate is a significant factor as well since it dictates the way occupants make use of building energy utilities such as heating, ventilation, and cooling (HVAC) systems as seen in (Yousefi *et al.*, 2017). In another paper by (Kashif *et al.*, 2013), the authors simulated the dynamics of occupant activities to understand power management in energy-smart homes. Surveys and questionnaires were used to collect routines of daily activities of occupants in residential homes such as using lighting, washing machine, TV, oven, cooker, and fridge. The time duration for each activity also varies and has a causal relationship with each other. The behaviours are then modelled using the Brahms environment (NASA, 2008). During the simulation, these behavioural set points are manipulated, which in turn compute the thermal comfort of the environment ideal for occupants at any different setting. Thermal comfort is vital for human beings and is also an essential factor in achieving energy efficiency and economic sustainability, as discussed in (Vazquez *et al.*, 2010). The study, part of the ThinkHome project discussed by the authors, is a MAS and knowledge base (KB) covering usage profiles of individuals' activities, including occupancy. These usage profiles are used to learn behavioural patterns using artificial intelligence such as self-organising maps (SOM) and ANN and simulate usage profiles to understand sustainable energy consumption. Further study related to the coupling of building simulations with stochastic occupant behavioural models can be found in (Parys *et al.*, 2011).

One of the most important inputs for building occupant models is the occupancy or presence model, which acts as input for all other behavioural models. As seen in (Wang *et al.*, 2005) where the authors carried out experiments in a singly occupied office room to model occupants' presence and absence by incorporating random arrivals and departures followed by intermediate periods of absence and presence. The model was to some extent, stochastic in nature, but it still failed to reproduce the intricate pattern of occupancy. The authors themselves acknowledge that "presence cannot be reproduced by an exponential distribution with a homogeneous coefficient, and times of arrival, of departure, as well as absences during lunch breaks, are not normally distributed". This assumes all weekdays are similar, and weekends and long absences are completely ignored. The occupancy model proposed by (Page *et al.*, 2008) uses a profile of probability of presence instead of a fixed profile in a 2x2 state Markov Chain and produces a time series of presence and absence exponentially distributed using a time-dependent coefficient including long absences and random arrivals and departures. A problem with this model is that it considers only two states of occupancy: either present in your office or absent from the entire building. Also, tests show that long absence is underestimated as well as the configuration of the mobility parameter. To address these issues, the authors in (Wang *et al.*, 2011) suggest a higher order inhomogeneous Markov chain involving multiple states of transition including the generic arrival and departure time and long absences and breaks etc. and any number of occupants. The authors also highlight the complexity of Pages' model in terms of defining the probability time series of a presence vector during the simulation and calibrating the mobility parameter from data collected over long periods of time. Activity during long vacations or absences over a week also have a significant impact on energy usage and may often lead to underestimations. The authors of (Stoppel *et al.*, 2014) combined all these factors and applied them to an existing Leadership in Energy and Environmental Design (LEED) certified military dormitory. The comparison is done with corresponding values from the energy model's original prediction and real energy data, showing improvement in the combined model prediction. Other papers predicting and simulating occupancy in single-person offices based on their daily

activity can be found in (Wang *et al.*, 2005). Another approach to predicting energy usage is to predict the number of occupants in a building by tuning the physical and behavioural parameters of occupants (Manna *et al.*, 2013). Using multiple Markov models at different time lags, real-time occupancy forecasting for single person offices is done. The prediction is then validated using real data collected from multiple buildings using PIR sensors. Also estimating the number of occupants with regards to the time of the day is very important given that some of the HVAC systems operate throughout the day and night at fixed schedules, even though the rooms can be empty at times. This estimation, done in (Ai *et al.*, 2014) using an autoregressive hidden Markov model, can potentially contribute to the efficiency of the control policy of the building's HVAC system by reducing energy consumption. Sometimes capturing the context of occupancy and related events in the Markov model at each state can lead to improved performance as seen in (Adamopoulou *et al.*, 2016). Comparison between probabilistic and non-probabilistic methods for detecting building occupancy and occupant modelling and their performance evaluation can be seen in (Mahdavi *et al.*, 2015).

3.3 Environmental Sensors

Determining occupancy using environmental sensors, indoor positioning, and camera technology has also gained a lot of exposure and research interest. Advanced camera technologies such as programmable pan-tilt-zoom (PTZ) are used to detect occupancy, even in low light and understand occupancy patterns, activity behaviour using image processing and machine learning approaches such as SVM (Shih, 2014). Ambient sensors, as well as CO_2 and related sensors, can be used to capture the occupancy status of buildings. Environmental signatures such as light, humidity, CO_2, and temperature are important indicators of occupancy in buildings. Statistical modelling and using machine learning algorithms such as decision trees, ANNs, SVMs, and Random Forest can be used to determine occupancy level. The occupancy data can then be used to learn patterns of occupancy and develop occupancy models (Candanedo *et al.*, 2016; Zuraimi *et al.*, 2017). A combination of environmental sensors and camera technology is also quite popular for detecting occupancy in buildings

(Dong *et al.*, 2010). In (Yang *et al.*, 2014), the authors suggested a systematic approach to modelling occupancy in buildings using 12 ambient sensor variables and then comparing the prediction performance using six machine learning algorithms. The developed occupancy model is then used in a building simulation to estimate energy use and occupancy in an office testbed building for three months. The results are also compared to models developed earlier in Design-Builder and Energy Plus for HVAC control system and shows. It is found that CO_2 and light variables have important contributions to the final modelling outcome. It is observed that the overall accuracy generally increases as the number of sensors increases. Since occupant behaviour plays an important role in determining occupancy and energy consumption in buildings, the authors (Diao *et al.*, 2017) decided to identify behavioural patterns of occupants in residential buildings. They used clustering technique and ANN to classify occupants' behavioural patterns. In total, ten distinct patterns were identified and subsequently used as input to simulate building energy usage. In another paper by (Sun *et al.*, 2017), the authors identified specific behavioural attributes of occupancy that correlate to energy-saving measures in buildings. The authors identified five attributes and used them to simulate energy-saving possibilities using Energy Plus for multiple climate conditions and buildings as a case study. Similar work related to occupancy behaviour, activity and a critical review of existing models and their implementation can be found in (Buso *et al.*, 2015; Hong *et al.*, 2018).

3.4 Localisation Sensor and Technology

Use of localisation sensors and IP technology can be seen to explore the area of occupancy detection. Wi-Fi technology, widely available at home and in offices seems to be a feasible choice for getting the signature of logged in and nearby detected users. The log data of detected devices can then be used to determine occupancy using statistical modelling. In (Depatla *et al.*, 2015), the authors developed a mathematical model to compute occupancy based on the *RSS*. Radio signals suffer from a spatiotemporal variation due to multipath and scattering effect and attenuation from the LoS. These characteristics can provide an important signature of human behaviour related to the occupancy pattern. The authors observed the effect of LoS

and the scattering effect on the human body and developed a mathematical model where the parameter can be tuned to compute the number of occupants in the building. Wi-Fi signals can also be used to estimate the number of occupants based on the location of the APs and connected devices of individuals by using data mining techniques as seen in (Wang *et al.*, 2017). Their study shows the temporal variation of the occupancy pattern identified, which, according to the authors seem to provide more detailed information on building usage compared to the traditional methods of detecting occupancy discussed before. With their model, the authors claim to reduce the predicted energy consumption by 26.1% after validation with real data. BLE can also be used to detect occupancy in buildings. Bluetooth with its customisable range and low cost can be a very effective solution for occupancy detection. Individuals with smartphones can be detected in each room and using the configured range the location of the individual can be identified providing detailed occupancy information as seen in (Corna *et al.*, 2015).

3.5 Alternative Modelling Approaches

There are other nonconventional approaches to building occupancy modelling and energy usage prediction, as described by (Oliveira-Lima *et al.*, 2016). The authors mentioned the use of car parks to determine the number of occupants as a separate additional data source and in the process minimising the cost involved in deploying sensors for detecting occupancy.

Due to the capability of capturing occupants' dynamic behaviour related to energy consumption, an agent-based modelling (ABM) approach is also explored as a viable alternative methodology. (Zhang *et al.*, 2013) used such an ABM approach for modelling building occupants as agents and investigated different electricity management policies and regulations and building appliance usage to understand their impact on energy consumption and conservation in office spaces in an academic building. In another paper (Pan *et al.*, 2007), a multi-agent building occupant simulation is used to understand human social behaviour, especially in times of emergencies.

At times the sensor data for occupancy estimation can be complicated due to the uncertainty in the occupancy pattern and deployment cost. (Liao *et al.*, 2010) suggested fusing the sensor data with an agent-based occupant model for validation and improving predictive capability by extracting reduced order graphical models from the Monte Carlo simulation of the model. In another paper (Papadopoulos *et al.*, 2016), the authors emphasise the importance of BPS and integration with ABM using trained regression surrogate models. Research related to thermal comfort and controls of HVAC and diverse factors of a single office such as open plan, corridors, stairs also involves the use of the building occupant and behavioural model (Bourgeois, no date; Duarte *et al.*, 2013; Dobbs *et al.*, 2014).

Due to the availability of positioning and environmental sensors and camera technology, a massive amount of occupancy data is being generated, thus taking a data-driven approach to building occupant modelling. The authors in (Wei *et al.*, 2018) extensively evaluated the current trend in data-driven approaches and thoroughly review different classification algorithms and their performance when predicting building energy consumption.

3.6 Conclusion

This chapter provided a short review of the current state of occupant modelling and different approaches to developing such models. Currently, there is a surge in interest related to BOM and energy prediction, growing significantly over the last few years as seen from this review. Occupant modelling is dependent on a lot of factors, including occupancy pattern, interactions, and behaviour, thermal comfort and clothing. All of these are time-varying and dependent on occupant attitude and behaviour. Social scientists have been scrutinising the attributes of occupant behaviour for decades now as described in (Hong *et al.*, 2016), but identifying these patterns is complex. The modelling also suffers from challenges due to the oversimplification of the input parameters and may require significant calibration. As a result, they cannot be generalised for other building types and context. As rightly said by Hong et al. (2016), “the stochastic nature of the occupant is distilled into homogeneous and deterministic

inputs, often ignoring the diversity and inter-dependency of various behavioural and seemingly stochastic actions. Model inputs are typically model specific, often selected based on the intent of the study and suffer from user input assumptions. The incorporation of qualitative models can significantly improve the predictability of behaviour".

To develop more realistic and accurate occupant models for BPS, IP technology can play a very constructive role and can be used to identify route choices and the movement of occupants throughout large commercial buildings with greater detail and develop movement profiles of individual occupants with an acceptable level of accuracy. This movement profile of individuals can be used to improve the model by adding more detail to the simulation of energy usage prediction. Research related to occupant modelling in buildings is multidisciplinary incorporating social and behaviour science, building science, sensing and control technologies, computing science, and data science. One of the critical challenges associated with occupancy data collection is the lack of methods for unbiased, standardised data collection and appropriate addressing of privacy issues. Uncertainties during occupancy data collection occur due to situational awareness, as participants' behaviour is influenced by increased awareness about being in an experimental trial. This makes data collection challenging. IP technologies, which are ubiquitous and do not interfere with an occupant's usual daily activity during trials, has the potential to overcome this bias. In this thesis, indoor positioning techniques using smartphone phones will be applied to demonstrate the feasibility of collecting unbiased real-life occupancy data from non-expert participants and how that data can potentially be used in a BOM for predicting energy usage. The use of non-expert participants is critical to ensure we get ecologically valid trial results which are not influenced by the researcher in any way thus ensuring a real-world trial experience with no preconceived idea of how to maintain an ideal experimental condition.

Chapter 4

INDOOR POSITIONING USING BLE and Wi-Fi

4.1 Introduction

Wi-Fi and BLE are two well established and relatively mature positioning technologies in the scientific community, working with positioning solutions and location tracking. Previous studies have already demonstrated the technical performance, potentials and limitations of positioning solutions based on these technologies to some extent. They have also seen commercial applications related to indoor localisation services or context-aware applications based on smartphones. Both are relatively cheap and easy to deploy in buildings as wireless infrastructure, especially in large commercial ones and potentially be highly feasible for monitoring building occupancy.

As discussed earlier, WLAN or IEEE 802.11 protocols commonly known by its trademark Wi-Fi is one of the most widely deployed wireless infrastructures in both the residential and commercial environment. Wi-Fi operates in both in 2.4 GHz and 5 GHz radio frequency band, the latter relatively new due to too much interference from other radio devices in the 2.4 GHz spectrum. Wi-Fi with its long-range provides a more readily available technology for research related to indoor localisation. Bluetooth, on the other hand, was more common for short-range data transfer between mobile phones. That changed since 2010, when a completely new Bluetooth technology, referred to as Bluetooth Low Energy (BLE) or ”Bluetooth smart” was released promising low power consumption, changed radio frequency properties and an entirely new software stack for connectivity and data transfer (Dahlgren *et al.*, 2014). It also opened the possibility of research using BLE for IP solutions due to its low cost, versatile range and power consumption.

In this chapter, we will begin by discussing the functionalities provided by the Android platform for developing an IP system specific to our requirements and describe the custom-built android data logger development for collecting Wi-Fi, BLE, accelerometer and gyro data. We will then discuss *RSS* propagation characteristics shown by Wi-Fi APs

and BLE beacons when deployed in indoor space, due to furniture, architectural features like walls, corridors, pillars and occupant movement. We will then discuss the methodology adopted when developing the radio fingerprint database using Gaussian Process Regression (GPR) and compare static positioning accuracy between different existing IP classification algorithms. The experiment will cover several test points throughout the building, covering multiple floors. The discussion will focus on the outcome of these experiments and how these results might impact the development of the positioning system for occupancy detection in the next chapter.

4.2 Android Data Logger

A bespoke data logger was developed using the Android platform to collect positioning data and related motion specific measurements. The Android platform currently provides access to scan results from BLE and Wi-Fi devices in range, and motion sensor measurements from the accelerometer and gyro. Of course, a smartphone needs to be embedded with these sensors and wireless communication technologies to provide connectivity and capture the required data. Most of the smartphones are now coming with in-built Wi-Fi, and BLE and most of them come with accelerometer and gyro plus other environmental sensors such as light, temperature and pressure with some exceptions.

4.2.1 Android Wi-Fi API

Wi-Fi scanning can be done in the Android platform using the *WifiManager* API in the following three steps.

- Register the *WifiManager* in a broadcast listener to broadcast scan results when establishing a connection and to request a scan.
- Request a scan using *WifiManager.startScan()* to initiate scanning of available Wi-Fi APs. The method scans all the 12 Wi-Fi channels for each AP and returns scan results if they are available with details of the device ID, signal strength *RSSI,* network status, frequency band and a host of other relevant information. The scan process does not require establishing a peer-to-peer connection for sniffing nearby APs.

- Then using the *WifiManager.getScanResults()* method, we can retrieve the scan results and process the data as required.

Though there is some inconsistency with the result; the scan result undergoes some latency since it completes the scanning of all the channels, for all the available APs in the range and only then returns the results. Meaning there is a delay in receiving the results even though the scanning rate can be pre-set. In our data logger, it is configured for every second. Also, since it provides the most recently updated scan results, it might be that some results from the previous scan are included in the current scan due to them not being in the updated list in the last scan. The described latency above is a hardware issue with no software solution and can have a detrimental effect on the positioning accuracy since ideally; all measurements need to be correlated with time to reflect any change of state.

4.2.2 Android BLE API

As of Android 4.3 (API level 18) support for Bluetooth low energy is provided with appropriate API providing a host of functionalities to allow passive scanning and discovering of nearby active BLE enabled devices. These features help to provide proximity-based services as well as transfer with a small amount of data using the Generic Attribute Profile (GATT) by establishing a connection if required. BLE scanning can be done in the following steps

- Verify the device supports BLE and not the classic Bluetooth. Access the *Bluetooth adapter* for the device and get the *BluetoothManager* to establish a connection for the scan.
- Using the *BluetoothManager* enable Bluetooth of the device is disabled.
- Then use the startLeScan*()* and *BluetoothAdapter.LeScanCallback* gets scan results from nearby active devices.

BLE scan is not continuous and automatically stops after a single scan. As a result, a synchronised timer needs to be implemented as well to continue the scan after a certain period. In this case, the BLE scan was configured for every second. Scan results

would fetch the device ID, *RSSI*, time stamp and a range of other features. BLE scan is different from Wi-Fi in a way it does not wait to fetch scan results from all available active devices. BLE probes the environment at the configured rate and returns record of all devices the moment it finds them. So, it can be such that in a specific moment it could find only one device and in another, it could find more than one. If it finds none of the results for those time stamps it will be empty as such will not be stored in the result array. The time signature of detection is generally in milliseconds since it may detect multiple devices at the different windows of time gaps.

4.2.3 Android Motion Sensor

The Android platform provides a lot of built-in sensors and sensor-related outputs that allow the capture of user motion and motion-related characteristics such as acceleration, rotation, tilt, swing, significant motion, step counter and step detector. Some are solely dependent on hardware; others require software integration for output. Not all of them provide accurate results and may require further calibration for consistently reliable output, especially for indoor positioning solutions. In this research, we have used sensor output from the accelerometer and gyro, both of which are hardware-based providing inertial data of the user in motion. For both the accelerometer and gyro, the Android sensor API provides the following output.

Table 4-1 Output type for Accelerometer and Gyro from the Android API

Accelerometer	*TYPE_ACCELEROMETER*	*TYPE_ACCELEROMETER_UNCALIBRATED*	*TYPE_LINEAR_ACCELERATION*
Gyro	*TYPE_GYROSCOPE*	*TYPE_GYROSCOPE_UNCALIBRATED*	

In our research, we collected the data from *TYPE_ACCELEROMETER,* which includes the gravitational acceleration ($9.81 m/s^2$) in measurements unlike the TYPE_LINEAR_ACCELERATION and *TYPE_GYROSCOPE* for rotation. Both the methods provide calibrated motion data for all the three axes by the Android API. The sensor value is retrieved using the *SensorManager* to specify the sensor type which then calls the SensorEventCallback() method to retrieve the sensor value for every change in measurement and also the time stamp in a nanosecond for each of the three axes of

the smartphone. In this research, the sampling rate was configured at 50 Hz, and the output provided nearly consistent measurement data at the configured rate with almost negligible latency. Latency from these measurements if any, can be attributed to a hardware failure or crash and is always a cause for concern.

4.2.4 Discussion

One of the main issues with collecting radio and motion data related to positioning from the smartphone is time synchronisation. Each of the sensor and radio outputs operates independently of each other with their time stamp. Even though all of them start together, the time stamp for each record has the potential to vary, however small they are. This is especially true for motion sensors compared to Wi-Fi and BLE since the motion sensor output rate is very stable with almost negligible latency whereas Wi-Fi and BLE are dependent on the scan results from the APs and beacons deployed and logs the record when they become available. As a result, a global timestamp variable is kept and initialised at the beginning to synchronise each sensor output when recording the data in the log. Even then there can potentially be a small time mismatch, but we can potentially overlook them since they get compensated due to the very high sampling rate of the motion sensors; 50Hz compared to both Wi-Fi and BLE which are in the order of milliseconds with a scanning interval of a second.

The data logger has the discussed functionality encapsulated as a service so that the app can run in the background continuously as the user goes on doing their tasks during the trial. Data is recorded in the internal memory of the Android device continuously when the app is started until it is stopped explicitly by the user using the stop button. Since the app in this project is developed for research data collection, minimum effort is given on the user interface, and the focus was on the integrity of the data collection.

It is important to note that the Android platform continuously updates its API level and by the time this research is concluded some methods might be deprecated for the newer API levels with improved methods providing a similar kind of output. Of course,

Android will continue to provide support for the deprecated methods in older and legacy API.

4.3 Wi-Fi and Bluetooth *RSS* characteristics

Before we start developing the radio fingerprint database, it is essential to observe the *RSS* characteristics of Wi-Fi and BLE in the building when deployed. There are two signal frequencies currently used by Wi-Fi networks in most of the countries (Poole, 2006; rabbit.com, 2007):

- 2.4 GHz - Comprises 14 channels, each with a bandwidth of approximately 20 to 22 MHz operating in the Industrial, Scientific, and Medical frequency bands with designated radio frequency bands also known as ISM band. 802.11b/g networks operate in the 2.4 GHz band. A lot of other devices also operate in this frequency band and as such there can be much interference from other radio signals such as Bluetooth.
- 5 GHz - Comprises 13 channels, each with a bandwidth of approximately 20 MHz operating in the Unlicensed National Information Infrastructure radio frequency band also known as the U-NII band. U-NII band is used by IEEE 802.11a networks operating in the 5 GHz band.

Higher frequency signals have higher attenuation passing through obstacles than do lower frequency signals. This is because of some of the energy of the electromagnetic field transfers into the material of the obstacle (walls and furniture), which reduces the strength of the signal.

Bluetooth low energy also operates in the 2.4 GHz frequency range and is widely used for proximity detection apart from data transfer and has been added to the Android platform service since API level 18. The service has been integrated with other Android proximity sensors and provides support for services such as heart rate monitors and fitness devices etc. Traditional Bluetooth operates with 79 channels for a scan, but the new BLE operates with 40 channels with three dedicated channels for the advertisement of packets. Both BLE and Wi-Fi support passive scanning and logs the

signature of the discovered devices without establishing a connection and thus does not require any authorisation from the end user.

The difference between the *RSS* characteristics of 2.4 GHz and 5 GHz frequency band for Wi-Fi was observed from Wi-Fi time series logs from four different Wi-Fi APs at four different location site indoor. Theoretically, the 5 GHz signal is more prone to absorption compared to 2.4 GHz signal when there are exposed obstacles such as furniture and walls. As a result, the range of 5 GHz is less compared to 2.4 GHz. During data collection the smartphone was placed on a tripod and data was collected for a few minutes at each test point. The reason for collecting from four different test point was to observe any significant behavioural changes of Wi-Fi signal strength when exposed to indoor obstacles and barriers at different locations of the building from different Aps in a live office building with people walking past and doing their daily task. The plots in Figure 4.1, 4.2, 4.3 and 4.4 show sharp spikes for both the spectrum but the 5 GHz signal seems to be fluctuating more showing higher signal attenuation compared to the 2.4 GHz. The number of records for 5 GHz is also slightly higher compared to 2.4 GHz; (5GHz – 1254, 2.4 GHz - 858) in Figure 4.1, (5 GHz – 953, 2.4 GHz - 661), in Figure 4.3 and (5GHz – 810, 2.4 GHz - 779) in Figure 4.4 except for (5GHz – 828, 2.4 GHz - 938) in Figure 4.2. This can be due to the higher data transmission rate of 5 GHz over 2.4 GHz. It needs to be noted that the fluctuation for 5 GHz in Figure 4.1 and 4.3 is higher compared to Figure 4.2 and 4.4 probably due to increased exposure to walls, furniture or human movement during data collection. Also most of the spikes for 5 GHz signal points toward stronger signal strength whereas for 2.4 GHz it's always towards the weaker end and dropping.

Both Wi-Fi and BLE undergoes severe fluctuations, and due to the stochastic nature of the signal propagation it is complicated to identify the exact cause at any specific moment, but generally, they can be classified as large-scale and small-scale propagation. Large-scale propagation occurs due to path loss typically due to the dissipation of power over a distance; shadowing occurs from absorption of signals in building infrastructure, reflection and scattering. The level of absorption is also

dependent on the type of surface of the object. In general, the plots showed the *RSS* characteristics for both 5 GHz, and 2.4 GHz is more or less similar in all the four test points irrespective of the location of the Wi-Fi AP.

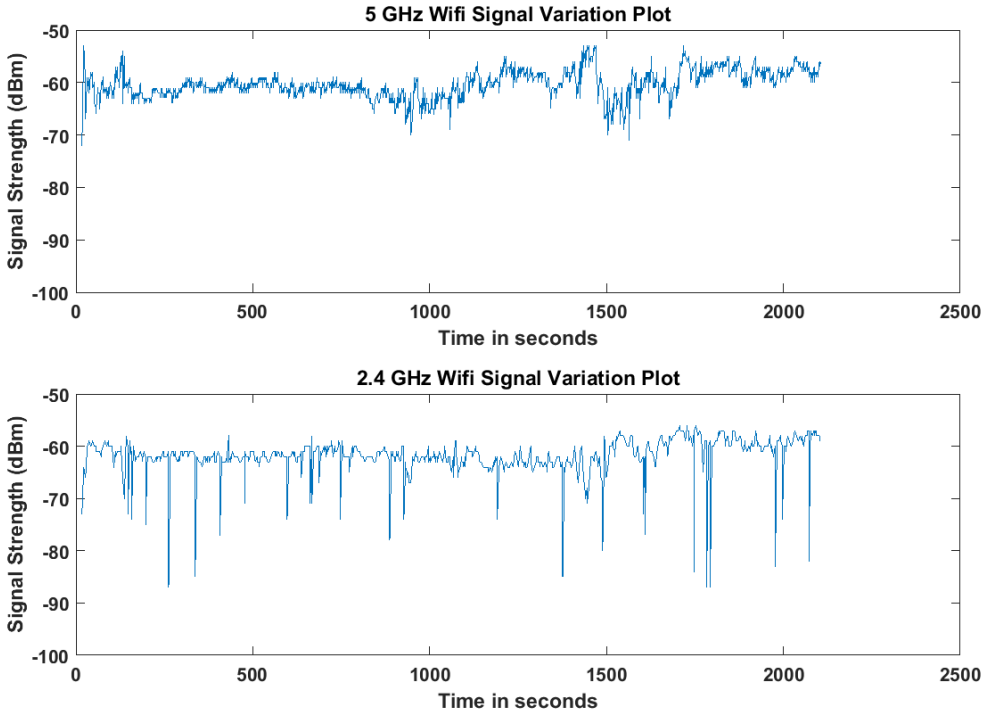


Figure 4-1 Signal strength (dBm) plot between Wi-Fi 2.4 GHz and 5 GHz spectrum

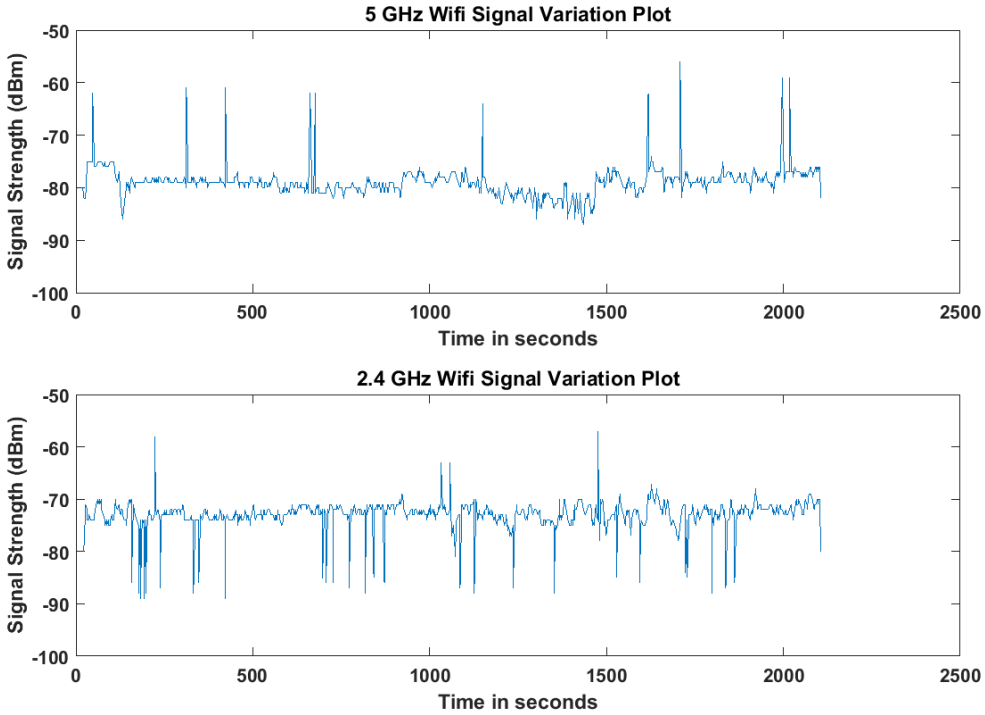


Figure 4-2 Signal strength (dBm) plot between Wi-Fi 2.4 GHz and 5 GHz spectrum

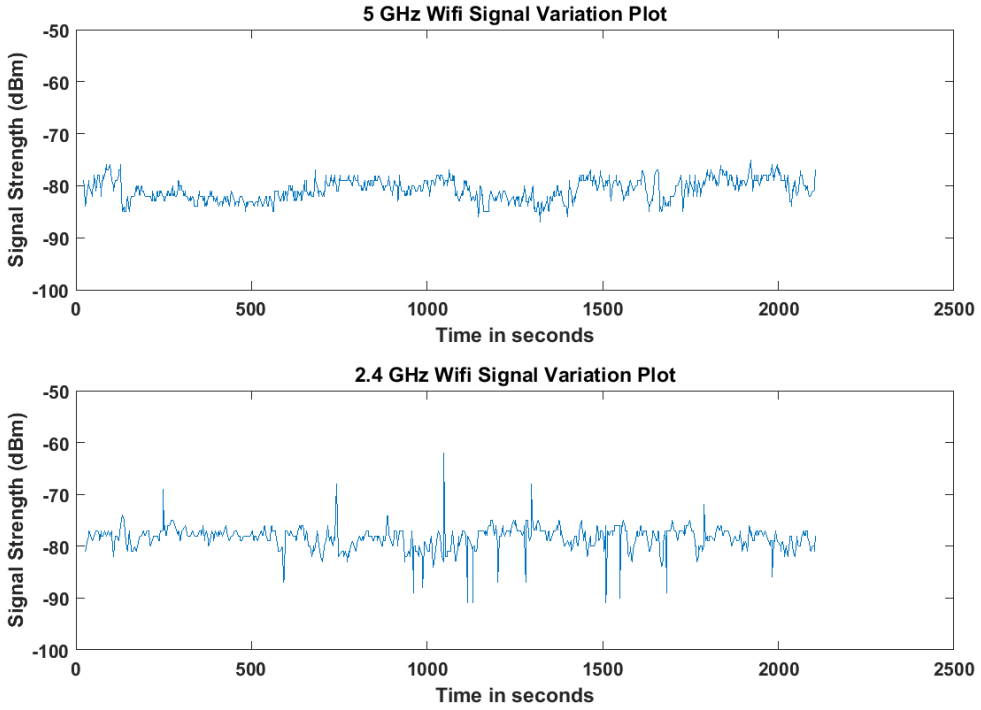


Figure 4-3 Signal strength (dBm) plot between Wi-Fi 2.4 GHz and 5 GHz spectrum

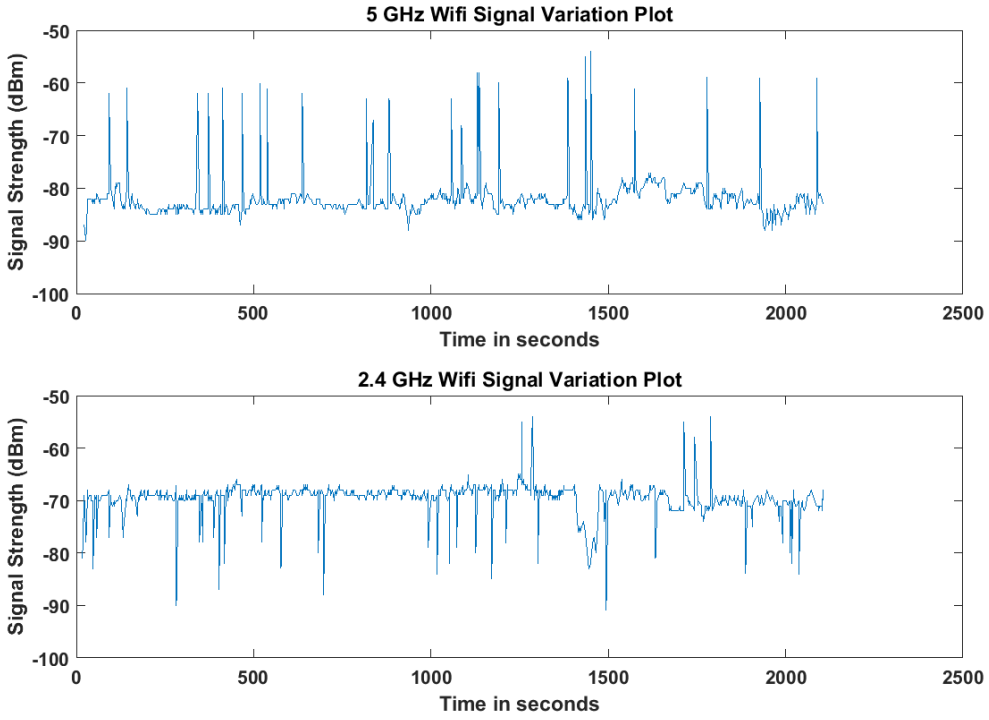


Figure 4-4 Signal strength (dBm) plot between Wi-Fi 2.4 GHz and 5 GHz spectrum

Another experiment was carried out to observe the attenuation of BLE *RSS* with distance. Data was collected in indoor using the smartphone placed on a tripod at a gap of 1m for 8 m. The plot in Figure 4.5 shows the result for the BLE signal varying over the distance between 1m and 8 m. The gradient of the red line showing the mean of the *RSS,* decreases as the distance increases. The *RSS* dropped by almost 20 dBm at 8m from the BLE beacon. The blue points highlighting the spread of the *RSS* at each point shows a lot of variation.

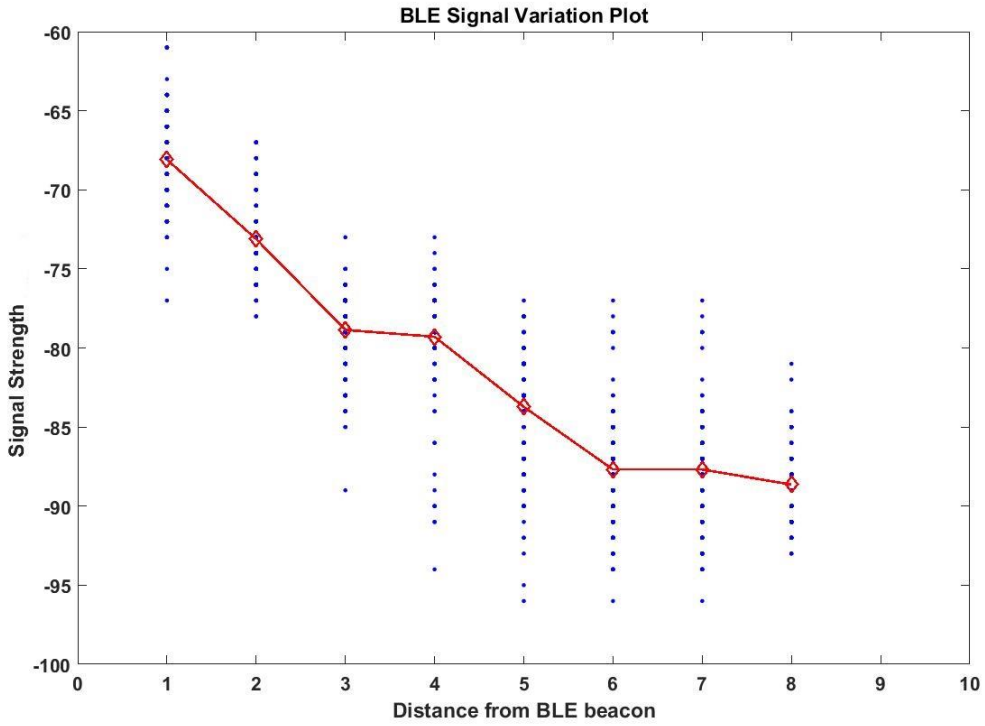


Figure 4-5 Attenuation of BLE signal (dBm) varying with distance. The red lines show the mean at each point.

The effect of obstruction from walls on the *RSS* can be seen in Figure 4.6 with red lines showing signal quality in (dBm) with no obstruction and blue lines showing the degradation of signal quality (dBm) from the impact of walls. The illustration is not a time series plot but only the recorded *RSS* data. At first, data was collected using the smartphone placed on a tripod with the BLE beacon directly placed in front and then again from the other side of the wall. As expected the signal strength became weaker when placed behind the wall having a minimum difference of 10 dBm with a maximum difference of around 25 dBm, as observed in the plot. It is important to note that data was collected for the same amount of time for both the scenarios but the number of RSS records without the wall is less showing latency in the reception of RSS data even without any direct obstruction. This is an important observation since during the positioning trial; there can be similar kinds of outages or delays which need to be compensated in the positioning solution.

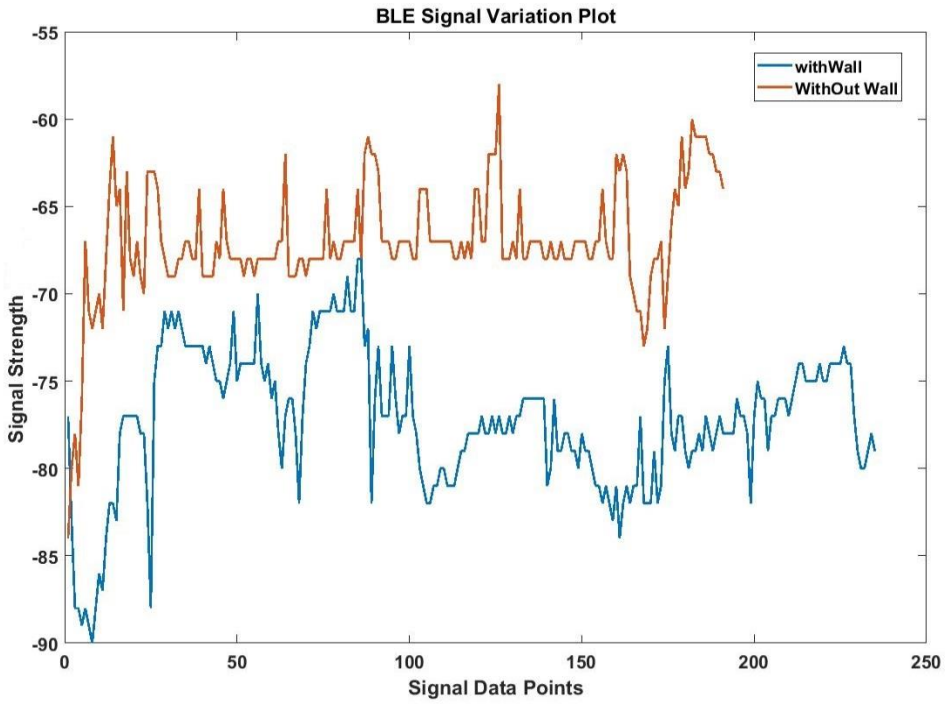


Figure 4-6. Representation of BLE signal attenuation (dBm) due to obstruction from building walls indoor.

The propagation of the signal from BLE beacons may also be affected by the angle of reception and LoS and also obstruction from the user's clothes. An experiment was carried out to observe such effects using the smartphone data logger indoor. Data was collected at 'left', 'right' and 'centre' of a pillar from a single BLE beacon as seen in Figure 4.7. The blue points mark the *RSS* with the smartphone in hand and the green points mark the signals with the phone in the pocket. For each scenario signal was collected at the left, right and centre of the BLE beacon respectively, as seen in Figure 4 7. At first, data is collected at the three positions with the smartphone on the hand and then when kept inside the pocket. It is difficult to conclude any specific pattern of signal variation for each position (left, right and centre) but it is evident from Figure 4.8 that the mean signal strength recorded at 'left', 'right' and 'centre' position varies. We can also see the changes when the smartphone is in the pocket at the same locations. This variation has the potential to impact the position estimation, especially when comparing against fingerprint radio map and may very likely produce significant errors.

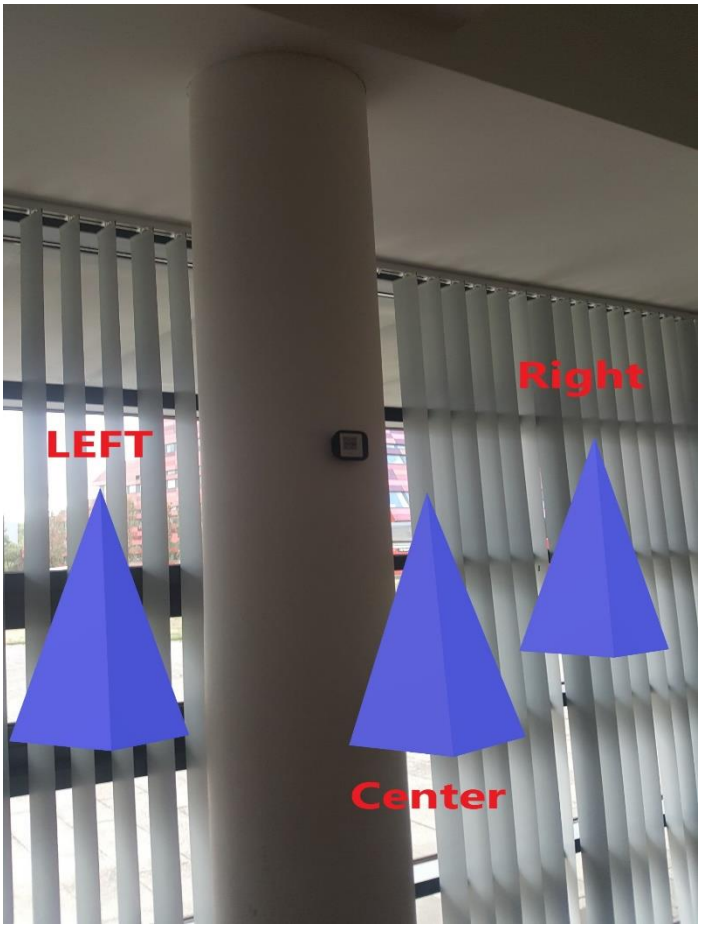


Figure 4-7. Data Collection position when analysing *RSS* quality due to the angle of reception, LoS and obstruction from the user's clothes.

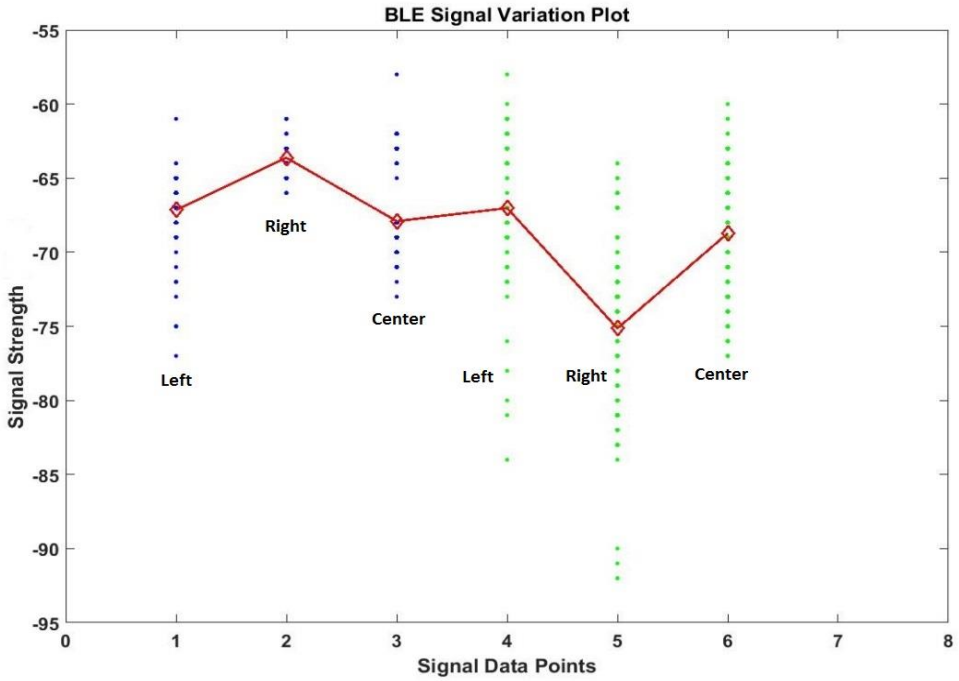


Figure 4-8. Effect of angle of reception and clothes on signal quality (dBm).

Radio signal suffers severely from multipath, absorption and shadowing in narrow indoor spaces and corridors seem to show the maximum impact. The experiment was carried out in the corridor of NGB with data collected at locations shown in Figure 4.9.

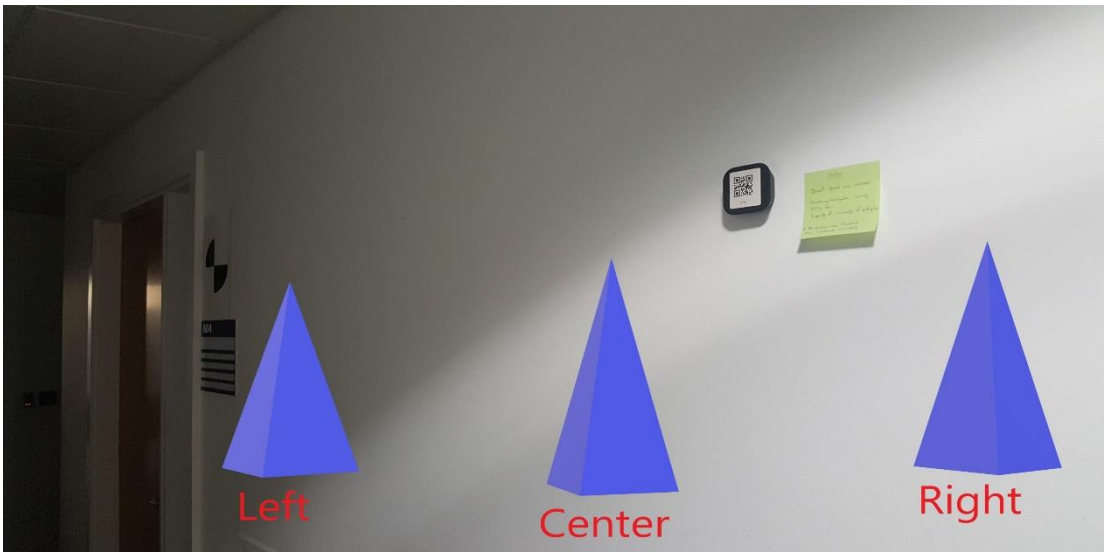


Figure 4-9. Data collection position when analysing signal quality in narrow corridors.

The resulting plot in Figure 4.10 which is again not a time series but merely the plot of the recorded signal strength, shows a significant variation in the quality of the received signal at the 'left', 'right' and 'centre' of the BLE beacon location. Surprisingly the 'centre' position seems to be affected by maximum attenuation even though it has direct LoS. A plausible explanation can be the design and shape of the beacon antenna seems to provide better signal propagation sideways comparatively. Also the placement of the beacon on the wall seems to limit the signal strength quality towards certain directions. Perhaps information of antenna design for the Kontakt BLE beacons may provide a clearer understanding which can be part of future work. Thus, even though the 'left' and the 'right' positions do not show severe degradation of the signal quality, the 'centre' position seems to be severely affected. Also, the number of recorded observations suffer from the signal outage and latency at the 'centre' showing a significant lack of *RSS* data for the same amount of collection time as seen from the plot below.

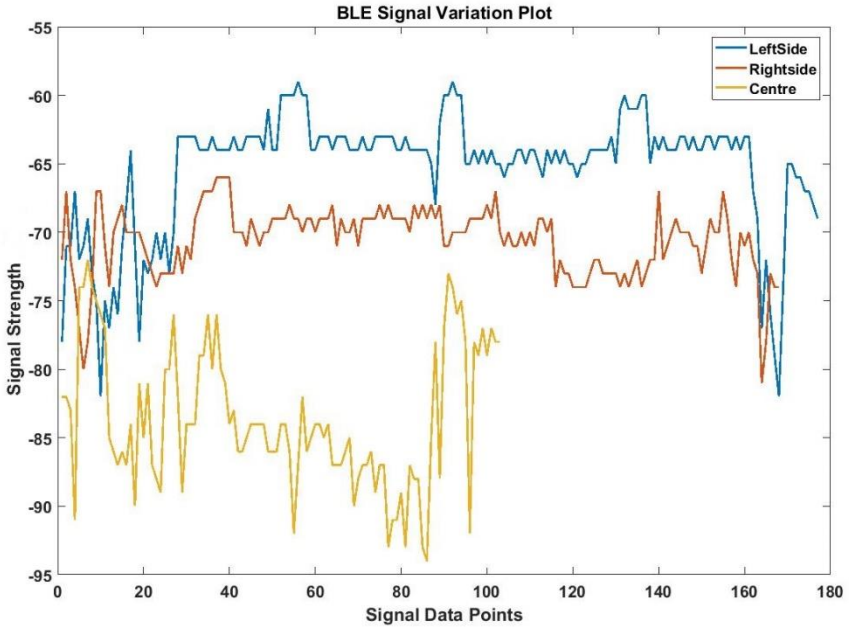


Figure 4-10. Observed signal strength (dBm) qualities in corridors from a BLE beacon.

In this section, we showed some analysis of the *RSS* characteristics on a limited scale related to Wi-Fi signals and BLE beacons deployed. In general, the characteristics

observed from the plots above show how data collection for occupancy detection might be affected during the occupancy trial and how it may impact the quality of the fingerprint database to be developed. Further analysis of the signal statistics can be found in (Ma *et al.*, 2015) (Moghtadaiee *et al.*, 2012).

4.4 Radio Fingerprint Mapping and Analysis

Based on the understanding of positioning techniques discussed earlier in chapter 2, the concept of fingerprinting is chosen as a methodology for indoor positioning in this PhD for undertaking surveys and experiments. The objective is to evaluate the accuracy of position estimation when using both Wi-Fi and Bluetooth radio fingerprint maps together to compute positions. Recall that radio map development using the fingerprinting technique is a widely used and popular method (Zhou *et al.*, 2011; Ochiai *et al.*, 2014; Faragher *et al.*, 2015; Yiu *et al.*, 2017) used in IP research. Data collection for the fingerprint database can be physically exhaustive and time-consuming and as such has also seen significant research for improvement in the data collection phase using crowdsourcing, collaborative data collection, probabilistic methods and using motion sensors in PDR as seen in (Bolliger *et al.*, 2009; Bisio *et al.*, 2013, 2016; Chen *et al.*, 2013; Luo *et al.*, 2013; Jing *et al.*, 2016). Typically fingerprinting based positioning has two phases; the offline or calibration phase when the fingerprint database is developed and online or navigation phase when trials are carried out to evaluate the fingerprint database quality.

4.4.1 Offline Phase

The method employs the concept of creating radio maps of floors in the offline phase to train the radio map. This requires creating an array of training points generally in a grid structure of cells associated with the floor map to be used for testing. At each training point (TP) RSS values from Wi-Fi and Bluetooth are collected for some time and stored in the radio map corresponding to that TP. RSS values form Wi-Fi and Bluetooth undergo many fluctuations, typically due to multipath, shadowing and

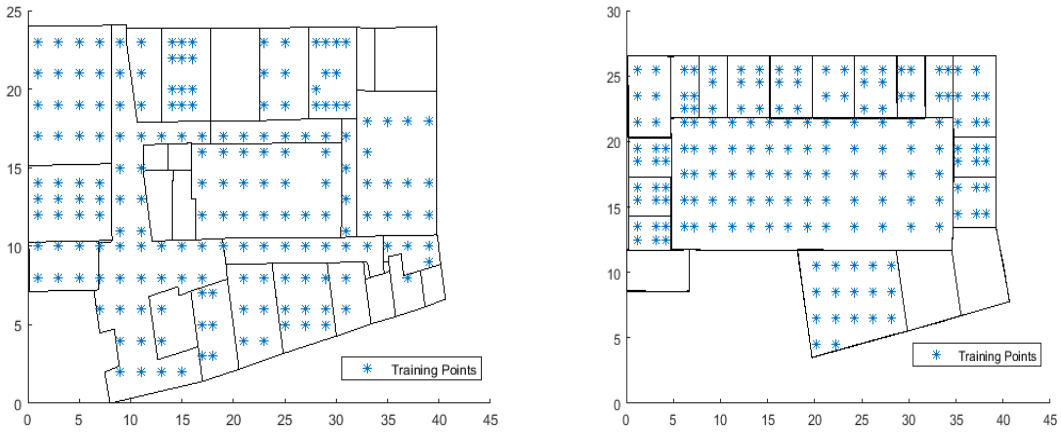


Figure 4-11. Training point (TP) locations for fingerprint data collection from Wi-Fi and Bluetooth.

interference from obstacles and moving objects. As such, it is sometimes preferable to collect the signals facing each of the cardinal directions to account for any noise to obtain a smoothed estimate of the mean signal strength and other statistics associated with that TP. The TP location for our test site Nottingham Geospatial Building (NGB) can be seen below in Figure 4.11.

4.4.2 Online Phase

In the online phase experiment, the actual position estimation is computed. Generally, an individual will be carrying a mobile node equipped with a Wi-Fi or BLE sensor and try to determine its position based on the comparison with the fingerprint database of the created radio map. The mobile node collects measurements of the same kind of attributes stored in the online phase and compares them against the values that are stored in the database. Typically, the RSS parameter is used as an attribute, the mobile node collects RSS values from all the APs or beacons within its range and compares them to each of the fingerprints of the TP that are stored in the database. The position estimate to be returned will be the one that is associated with the fingerprint having the best match; generally the one with the minimum difference.

4.4.3 Training Point Data Collection

Data is collected at the TPs as shown in Figure 4.11 using the custom-built data logger, collecting Bluetooth and Wi-Fi received signal strength (*RSS*), device ID, frequency and

time stamp respectively. The left plot shows TPs for Floor A and the plot in the right-hand side shows TPs for Floor B. Data collection is done facing at each cardinal direction for around 5 minutes at each TP to account for any noise or disturbance from the surroundings. The TPs were initially marked with tapes throughout the floors before starting the data collection since not all rooms are always accessible. There are in total eight Wi-Fi APs in the building transmitting at both 2.4 GHz and 5 GHz. Data is logged for each of the two frequencies separately, and all the APs were used during the data collection process. In Floor A there are 15 BLE beacons, and in Floor B there are 10 BLE beacons, in total Floor A had 181 TP's and Floor B had 165 TPs.

The reason for placing such a high number of TPs is because the fingerprint database will be the only valid source of position signature when estimating positions for both static instances and during motion using a particle filter. Due to the stochastic nature of the radio signals and their vulnerability to external interference, we decided to get a uniform coverage of the signal strength throughout the floors. In total, almost 40 hours were spent collecting data throughout the two floors spread over weeks due to restrictions at certain hours of the day and accessibility issues in some rooms. The placement of the Wi-Fi APs and BLE beacons can be seen in Figures 4.12, 4.13 and 4.14 below. The power and range of the BLE beacons were modified using the Kontakt admin panel (kontakt.io, 2013) depending on the location and also to ensure minimum overlapping with other beacon signals. This approach did not always prove useful since after completing the data collection it was found that there are many ways signals leak through walls and doors and have different propagation behaviours in large open areas compared to rooms and corridors. Wi-Fi APs were pre-positioned on all the three floors, marked in red but for our research and trials we only used Floor A and Floor B as such BLE beacons marked in green were deployed in the respective two floors only as shown below.



Figure 4-12 Floor A map with BLE beacons in green and Wifi AP in red markers.

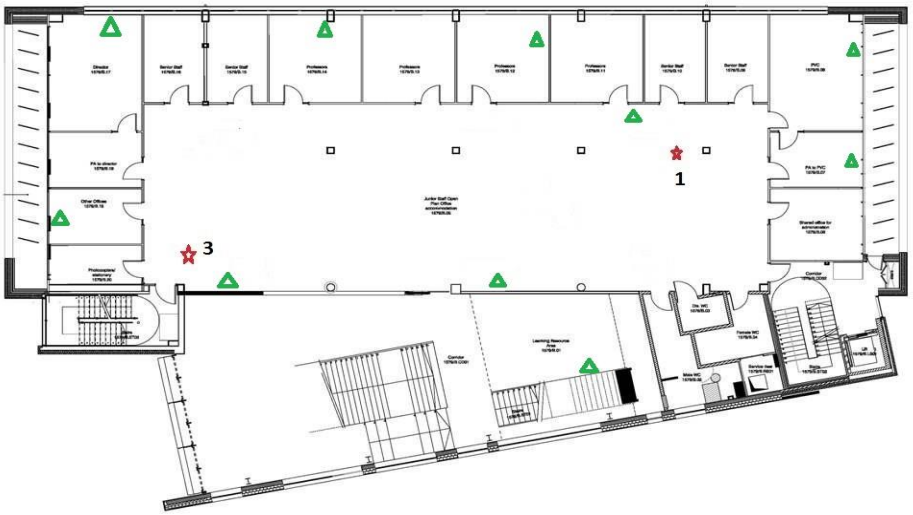


Figure 4-13 Floor B map with BLE beacons in green and Wifi AP in red markers.

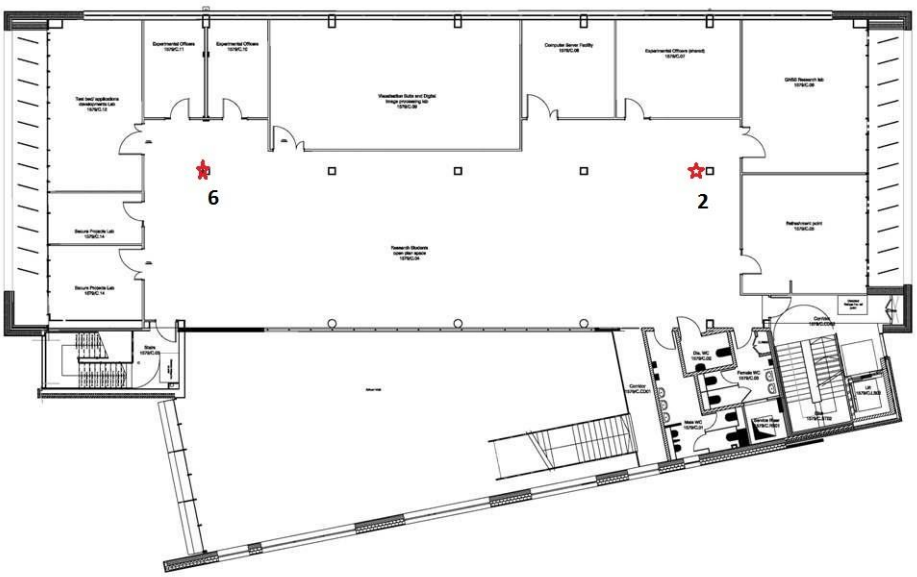


Figure 4-14. Floor C map with Wifi AP in red markers. Floor C is not used for positioning trial.

4.4.4 Gaussian Process Regression Fingerprint Database

In general, supervised learning can be divided into regression and classification problems. Whereas the outputs for classification are discrete class labels, regression is concerned with the prediction of continuous quantities (Rasmussen *et al.*, 2006). GPR is used to build a denser resolution database using the TP data, which can predict finer continuous *RSS* values at a resolution of 0.5 mm x 0.5m. Since the variation of the signal strength (*RSS*) over the floor space is not linear, a GPR is performed with TPs as an input function for supervised learning of the pattern of *RSS* values and perform interpolation or extrapolation of the RSS data for denser fingerprints. Gaussian process regression is a supervised machine learning approach which takes into account the relationship between the distance from the Wi-Fi APs or BLE beacons, the current location and input values (*RSS*) and the covariance and mean function (covariance function is also known as *Kernel*) and helps to model a predictive function with a Gaussian noise distribution.

$$y = f(x) + \epsilon \quad (4\text{-}1)$$

$$\varepsilon \sim N(0, \sigma^2) \quad (4\text{-}2)$$

The assumption here is that the RSS values follow a Gaussian pattern and thus can be modelled better using a Gaussian regression rather than interpolating using a linear model. A Gaussian process (GP) is a collection of random variables specified by their mean function $m(x)$ and covariance function $k(x, x')$.

$$m(x) = \mathbb{E}[f(x)] \quad (4\text{-}3)$$

$$k(x, x') = \mathbb{E}[\big(f(x) - m(x)\big)(f(x') - m(x'))] \quad (4\text{-}4)$$

$$f(x) = gp(m(x), k(x, x')) \quad (4\text{-}5)$$

The above mean and covariance equations are further expanded to get the predictive GPR $f(x)$ for prediction in a noisy environment according to the equations below.

$$\overline{f_*} \triangleq \mathbb{E}[f_*(X, y, X_*)] \quad (4\text{-}6)$$

$$cov(f_*) = K(X_*, X_*) - K(X_*, X)[K(X, X) + \sigma_n^2 I]^{-1} K(X, X_*) \quad (4\text{-}7)$$

The main idea in GP regression is determining the right hyper-parameters and maximising the marginal log likelihood from the selected mean and covariance function. The marginal log likelihood is derived from integrating the marginal likelihood, which is the integral of the product of likelihood and the prior according to the following equation.

$$p(y|X) = \int p(y|f, X)p(f|X)\, df \qquad (4\text{-}8)$$

In our research we used a GPML library (GPML Library, 2018) to perform the regression., the GP function takes the following arguments: a hyper-parameter, an inference method, a mean function, a covariance function, a likelihood function, training inputs, training targets, and possibly test cases. The library default *squared exponential* covariance function is used according to Equation 4.9.

$$k_y\left(x_p, x_q\right) = \sigma_f^2 \exp\left(-\frac{1}{2l^2}\left(x_p - x_q\right)^2\right) + \sigma_n^2 \delta_{pq} \qquad (4\text{-}9)$$

The covariance function has the characteristic parameters; scale length (l) and signal standard deviation σ, which need to be trained for optimised learning and prediction. These parameters are known as hyperparameters. Hyperparameters are free parameters for each of the GP functions; mean, covariance and likelihood and need to be specified during initialisation some of which may be empty. The number of hyperparameters also varies depending on the type of function chosen for the mean, covariance and likelihood. Some common hyper parameters are characteristics scale length, signal standard deviation, standard deviation of noise; more details of hyperparameters can be found in (Rasmussen *et al.*, 2006; GPML Library, 2018). The likelihood function also needs to be specified in our case we used the default *likeGauss* function. The training inputs and targets are the coordinate of the floor space in 2D and the signal strength (*RSS*) value respectively. The TP for each of the Wi-Fi AP's; both 2.4 GHz and 5 GHz and the BLE beacons for each of the floors were passed in the GPML function to produce the 0.5m x 0.5m resolution GP fingerprint database. The heat map for a few of the Wi-Fi APs and Beacons are shown below for each of the floors. The heat maps are scaled to ensure a common scale for comparison of penetration power between the Wi-Fi 2.4 GHz and 5 GHz and BLE beacons between different floors.

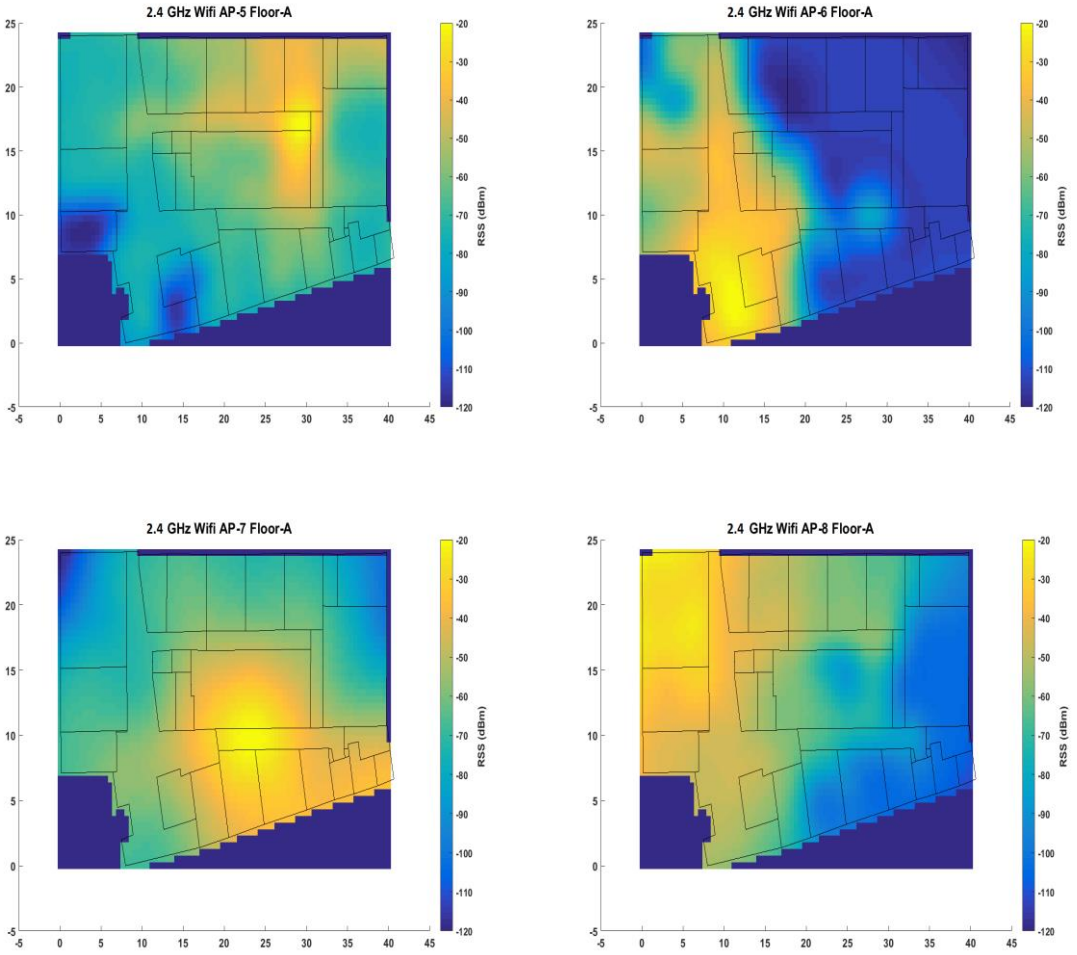
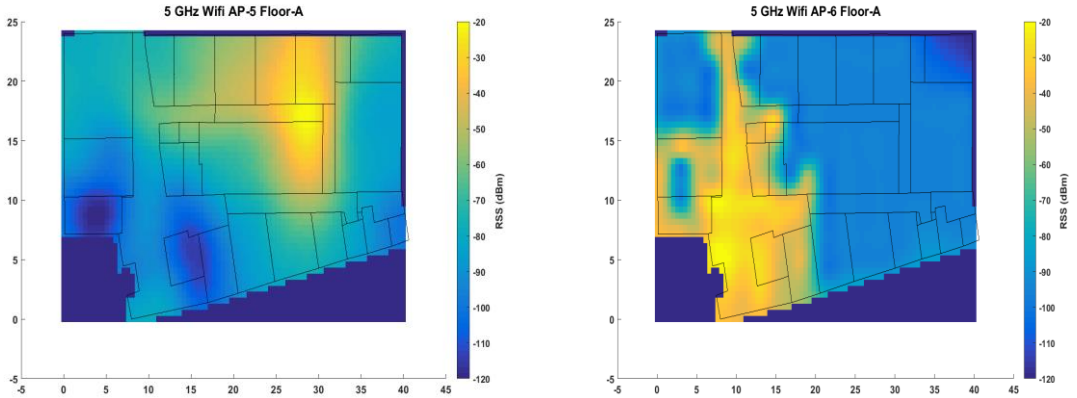


Figure 4-15 Heatmap for some selected 2.4 GHz Wi-Fi transmission showing the signal coverage in Floor A



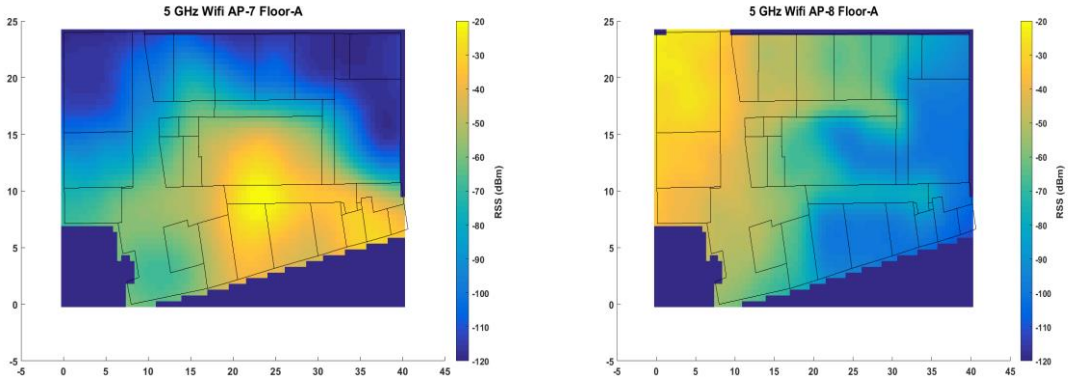


Figure 4-16 Heatmap for some selected 5 GHz Wi-Fi transmission showing the signal coverage in Floor A

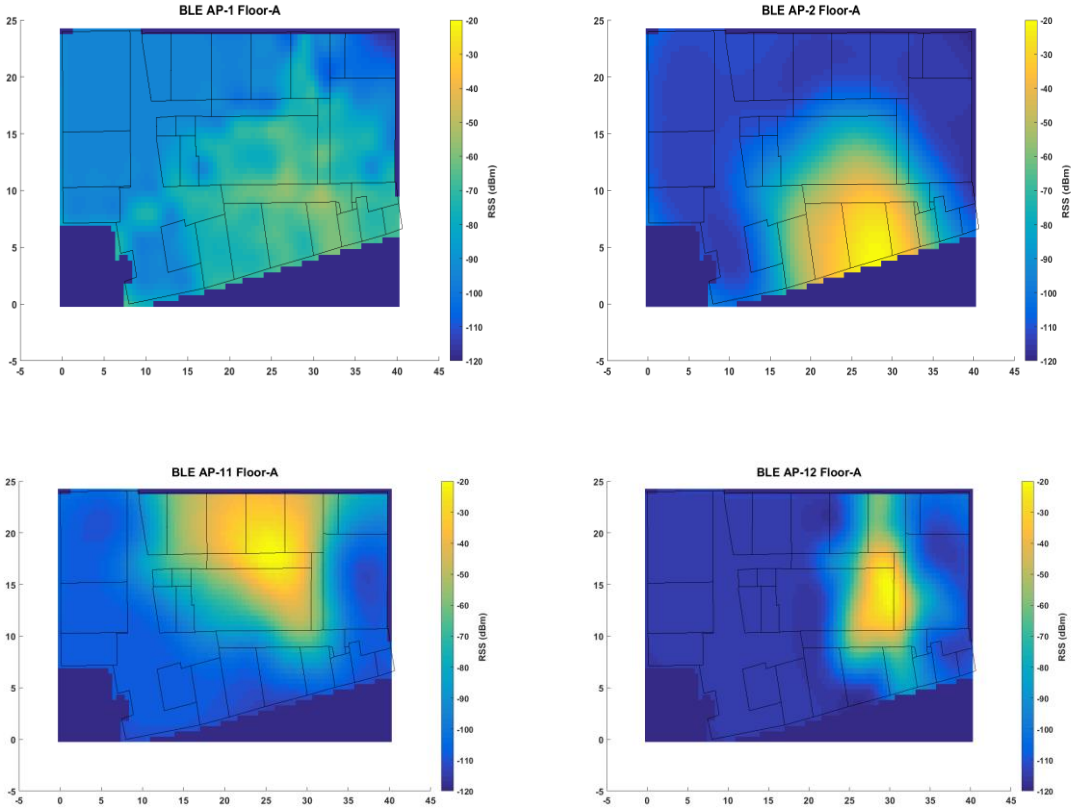


Figure 4-17 Heatmap of some selected BLE beacons showing the coverage of the signal strength in Floor A

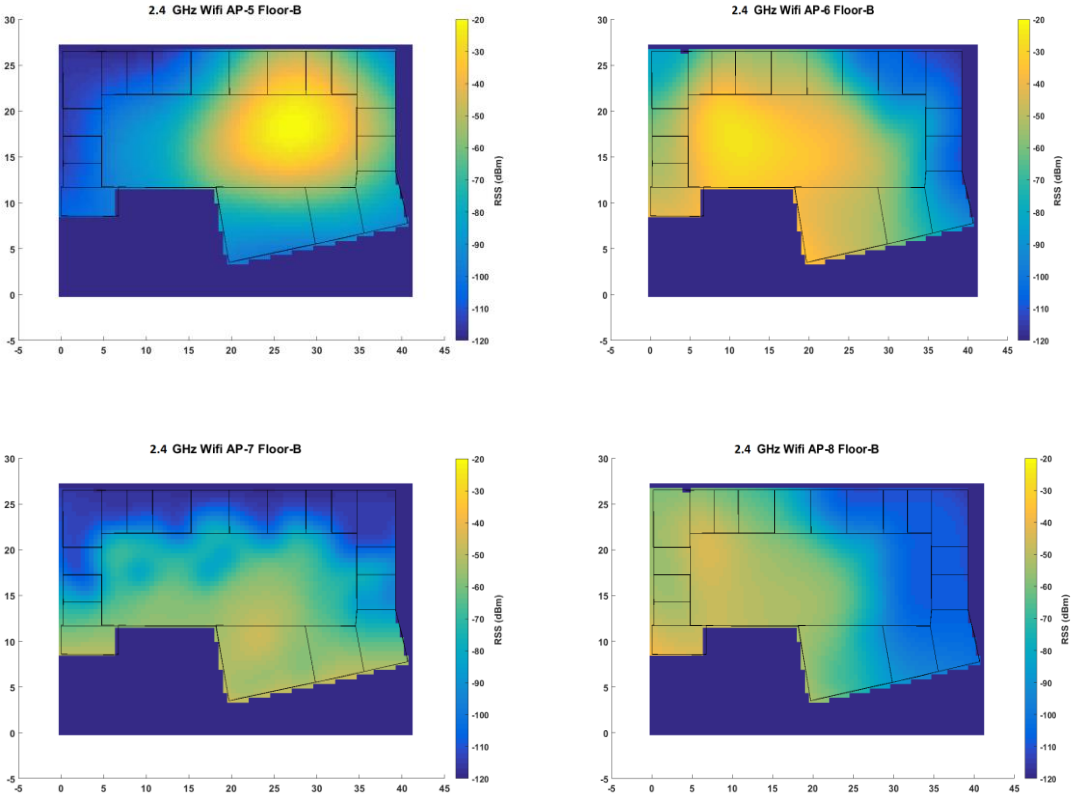
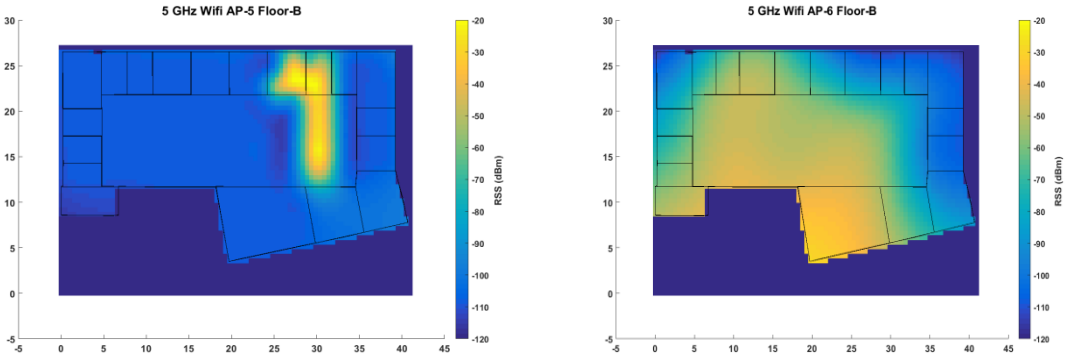


Figure 4-18 Heatmap of some selected 2.4 GHz Wi-Fi transmission showing the signal coverage in Floor B



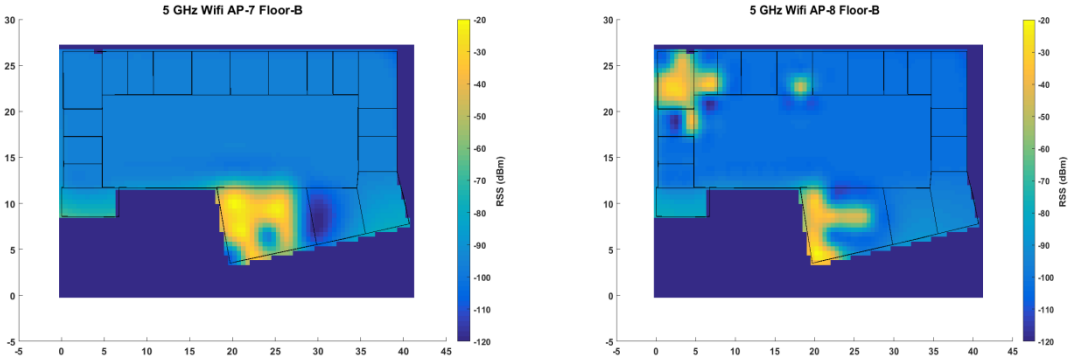


Figure 4-19 Heatmap of some selected 5 GHz Wi-Fi transmission showing the signal coverage in Floor B

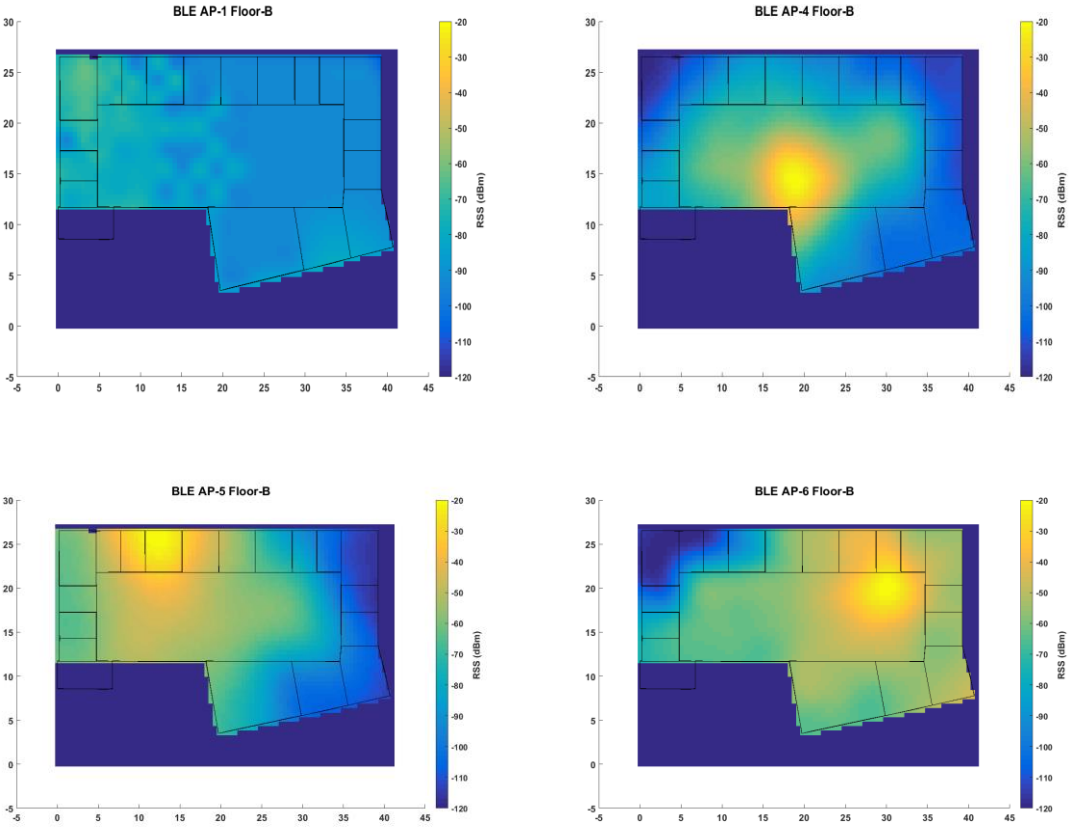


Figure 4-20 Heatmap of some selected BLE beacon showing the coverage of the signal strength in Floor B

4.5 Positioning algorithm comparison

Identifying the most appropriate position from signal strength requires some pattern matching algorithm or test statistic as discussed in (Groves, 2013). Following the

development of the GP fingerprint database, the performance of the database is evaluated with three pattern matching classification algorithms commonly used to match with the fingerprint database for position estimation.

The most common is using the Euclidean distance to compare the measured signal strength $S_j\ (X_m\ ,\ Y_m)$ in the calibration phase with the observed $S_d\ (X_n\ ,\ Y_n)$ signal strength during navigation according to the formula of Nearest Neighbour classification.

$$D_S = \sqrt{\frac{1}{m} \sum_{j=1}^{m} [S_j - S_d]^2} \qquad (4\text{-}10)$$

The problem is that it does not use all the information available, namely the standard deviations of the signal strength since they undergo temporal variations due to moving bodies and door openings. Maximum likelihood classification considers this standard deviation. Thus, the probability of obtaining the navigation fingerprint F' at a location whose calibration fingerprint, F is given by the following equation (Pritt, 2013)

$$p(F'|F) = \frac{1}{\prod S_i \, 2\pi^{n/2}} \, e^{\frac{1}{2}\sum(\frac{\bar{x}_{i'} - \bar{x}_i}{S_i})^2} \qquad (4\text{-}11)$$

Another way is to compare the signal strength probability distribution using the Bhattacharya Coefficient, which is a standard measure of the overlap between two distributions, calibration (C) and navigation (*N*) (Le Dortz *et al.*, 2012) and then compute the Bhattacharya distance function for each of the fingerprint locations for all the APs or BLE beacons according to the following equation. An implementation is available in Matlab Central (Cao, 2008).

$$BC(C, N) = \sum_{i=1}^{m} C(x)N(y) \qquad (4\text{-}12)$$

$$D_B = \ln(BC(C, N)) \quad (4\text{-}13)$$

For each of the algorithms, we compare the signal strength from the three strongest APs or BLE beacons and compute the similarity map when comparing with the radio fingerprint database. We then look for the position with the minimum difference ΔRSS. The number of positions found from the map can be more than one and can have a very small difference from their neighbours. As a result, to avoid ambiguity or miss out more probable positions, we use the weighted k- Nearest Neighbour to compute the final position (Ma *et al.*, 2015). In weighted k-NN positioning, the first k positions are selected with the smallest ΔRSS, which are used to compute the weights. As a result, more weight is given to fingerprints with smaller ΔRSS.

$$(\tilde{x}, \tilde{y}) = \frac{\sum_{k=1}^{N} W_k \, (X_k, Y_k)}{\sum_{K=1}^{N} W_k} \quad (4\text{-}14)$$

Data were collected in the NGB at specific test points; 14 in Floor A and 13 in Floor B using the smartphone data logger placed on a tripod. The position was computed for Wi-Fi and BLE separately and then combining both to get the aggregate position. The experiment was carried out for both the floors to verify we get a relatively similar accuracy since the number of beacons deployed and their layout is different for the two floors.

The overall positioning error for all the test points combined for each of the algorithms can be seen in Table 4.2. The table shows the performance of Wi-Fi and BLE on their own and when combining them. Comparing the positioning accuracy between the nearest neighbour and maximum likelihood algorithm the aggregate of Wi-Fi/BLE gave a mean error of 3.7 m compared to 2.2 m respectively for Floor A. In Floor B the mean error was 4.2 m compared to a nearly similar value of 4m. The probability distribution comparison using the Bhattacharya distance function the aggregate of Wi-Fi/BLE gave a mean error of 4.7 m and 2.99 m for Floor A and Floor B, respectively. The median gave a better representation of the errors since it helps to avoid possible outliers. This is evident in the table as the median error for all the algorithms reduced significantly. We also checked the individual performance of BLE and Wi-Fi only positioning. The

general conclusion is maximum likelihood classification and probability distribution comparison gave better accuracy in comparison to the nearest neighbour algorithm for the combined Wi-Fi/BLE aggregate method. In this research, we used the combined aggregate output of Wi-Fi/BLE when estimating static positions of occupants in the online phase.

To obtain an understanding of the accuracy for each test point, individual error bar plots are shown in Figure 4.21, 4.22, 4.23, 4.24, 4.25 and 4.26 for each of the positioning algorithm mentioned above. It is impossible to identify the exact cause of why the accuracy varied for different test points, but the difference can be attributed to the spatiotemporal variation of *RSS* during the signal data collection due to multipath, attenuation from furniture, walls and human movement inside the building.

Table 4-2 Overall positioning error (m) showing their mean and median for each algorithm and combination.

		Mean Wi-Fi/BLE Aggregate (m)	Mean BLE (m)	Mean Wi-Fi (m)	Median Wi-Fi/BLE Aggregate(m)	Median BLE (m)	Median Wi-Fi (m)
Floor B	Nearest Neighbour	4.2	4.5	3.2	4.0	4.2	3.2
	Maximum Likelihood	4.0	5.5	4.3	4.2	5.8	4.3
	Probability Distribution Comparison	2.99	4.1	3.0	2.5	4.0	2.44
Floor A	Nearest Neighbour	3.7	4.2	7.5	3.6	3.9	5.2
	Maximum	2.2	2.7	3.9	1.63	2.4	3.2

	Likelihood						
	Probability Distribution Comparison	4.7	3.2	6.2	2.7	2.5	3.9

When we compare the results for the nearest neighbour algorithm in Figure 4.21, Wi-Fi/BLE combined and BLE alone showed better performance for the first 9 test points compared to Wi-Fi alone in Floor A. Wi-Fi errors rose significantly for test points 10 to 13, possibly due to poor Wi-Fi signal reception. The results for Floor B shown in Figure 4.22 switched completely with Wi-Fi alone performing much better. This can be due to reduced variation of the *RSS* from the deployed BLE beacons in the open plan area, creating overlapping areas of similar signal strength and contributing to an increased positioning error at each test point. Another reason is Floor B is more densely populated and has a large open plan layout. As such there is an increased activity of occupants unlike in Floor A which is mostly quiet. These can be a contributing factor for an increased positioning error in Floor B for BLE beacons.

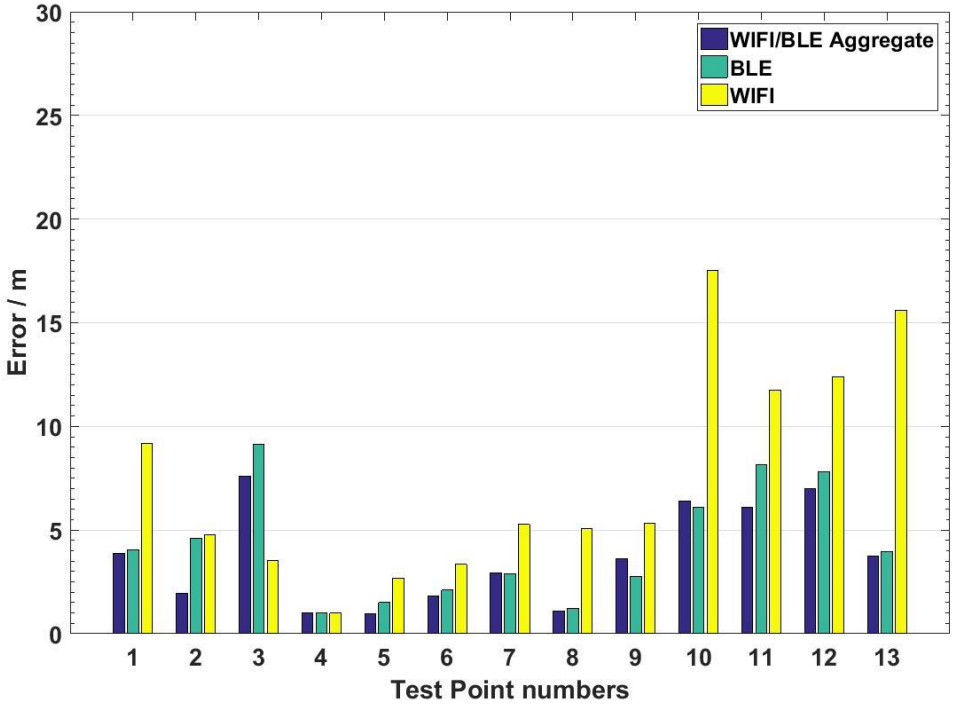


Figure 4-21 Nearest Neighbour classification showing the positioning accuracy in Floor A.

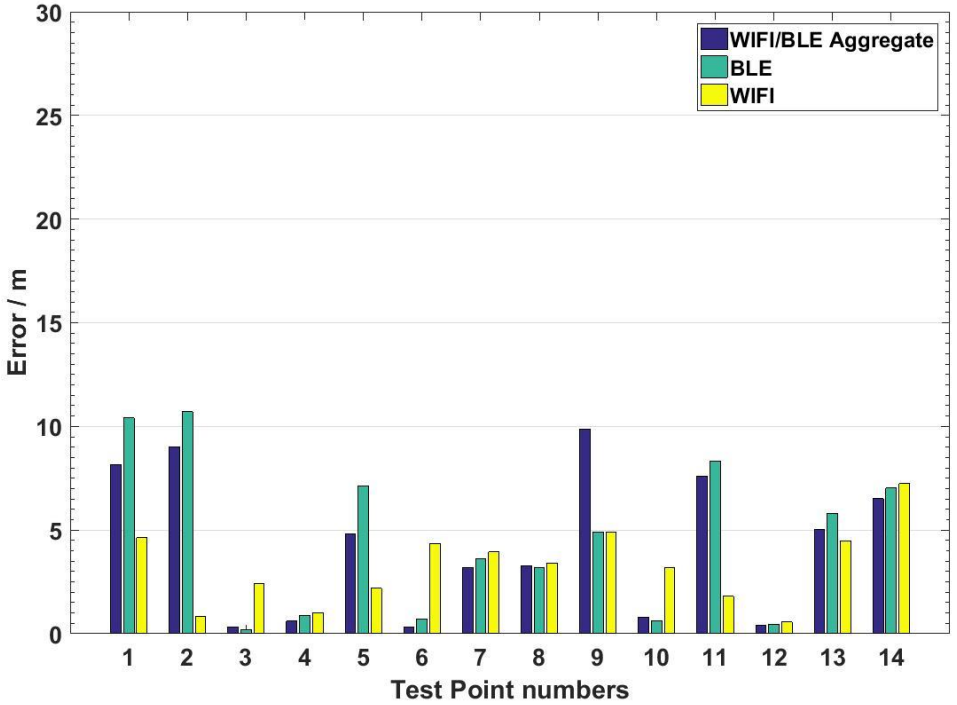


Figure 4-22 Nearest Neighbour classification showing the positioning accuracy in Floor B.

The result for the maximum likelihood classification algorithm seen in Figure 4.23 and Figure 4.24 shows a similar overall accuracy for both the floors with Wi-Fi/BLE combined giving better accuracy for most of the test points. Accuracy of Wi-Fi and BLE alone varied between each test point with errors going up to 11m and as low as less than a meter, but BLE gave better accuracy in comparison as seen in the plots.

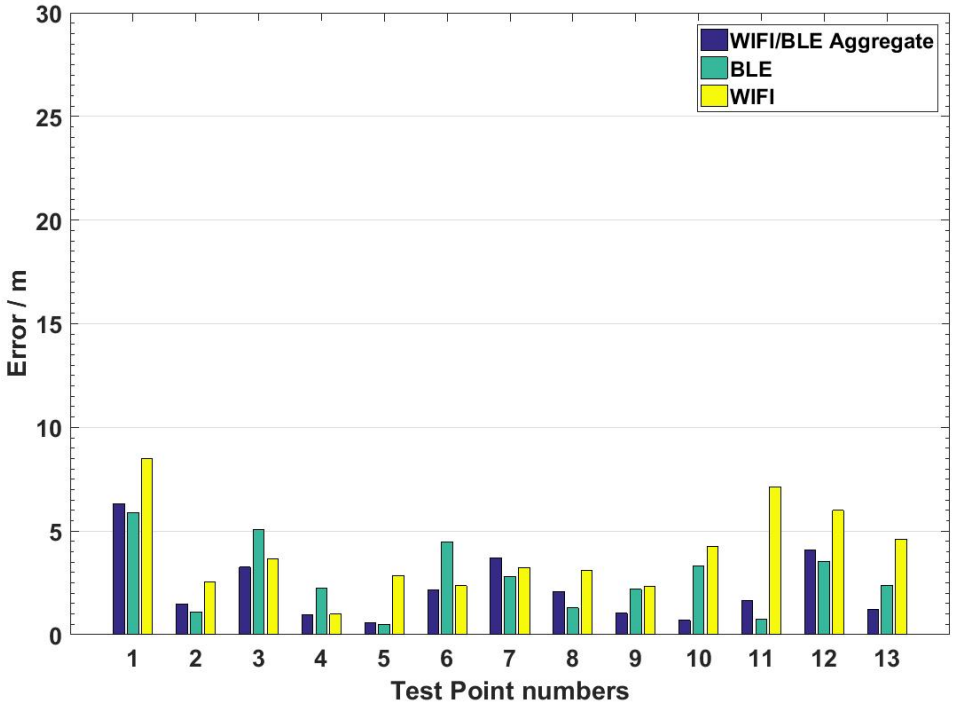


Figure 4-23 Maximum likelihood classification showing the positioning accuracy in Floor A.

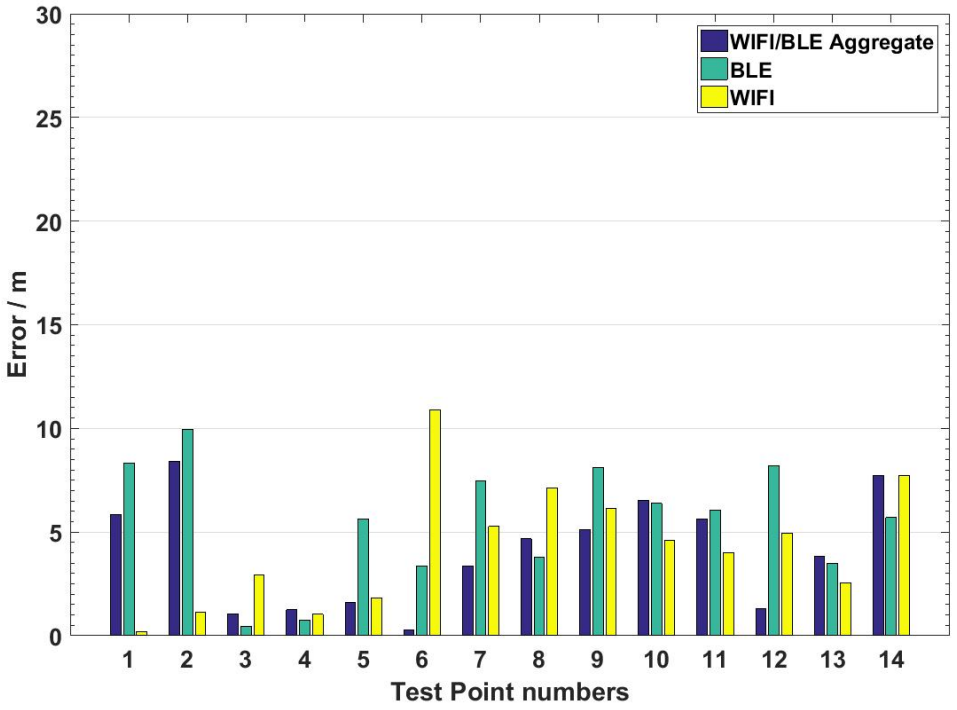


Figure 4-24 Maximum Likelihood classification showing the positioning accuracy in Floor B.

The Probability Distribution Comparison method results can be seen in Figure 4.25 and 4.26 below for Floor A and Floor B. Floor A shows a table result for all the methods with Wi-Fi/BLE combined, showing better accuracy for all the 12 test points. Test point 13 had high error value of nearly 26m for Wi-Fi alone, which subsequently skewed the Wi-Fi/BLE combined result even though BLE alone had a very low error of around 2m. This probably happened due to noisy signal reception or multipath during the data collection phase. Floor B plot saw varying accuracy across the test points with Wi-Fi/BLE combined performing better at some points and Wi-Fi or BLE alone at other. In general, Wi-Fi/BLE combined seem to control the error within 5m most of the time with some test points giving meter-level accuracy.

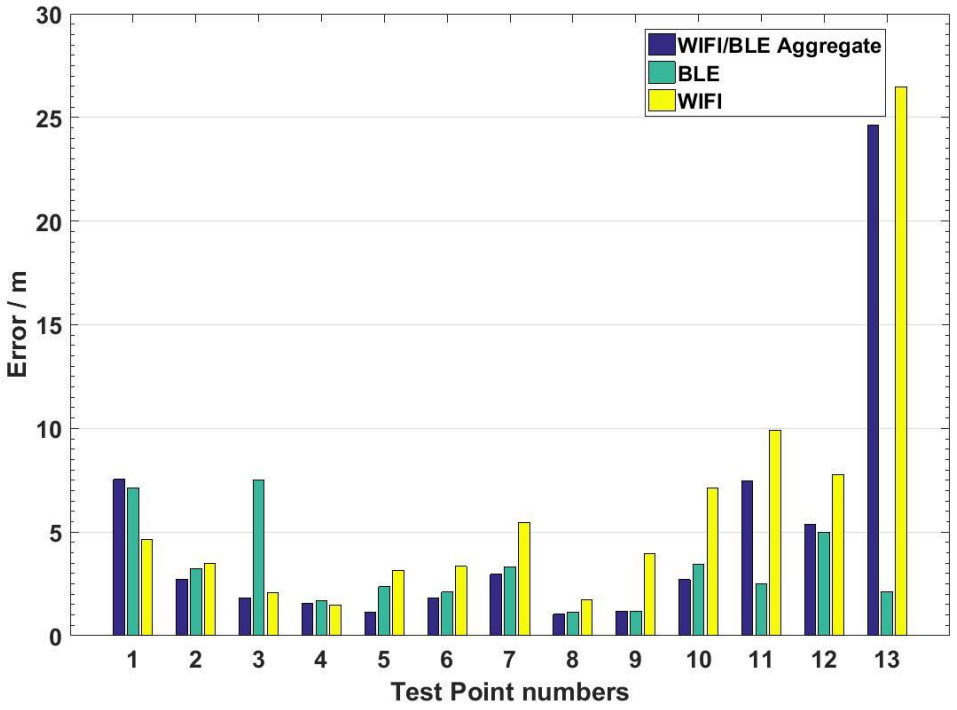


Figure 4-25 Probability Distribution Comparison showing positioning accuracy in Floor A

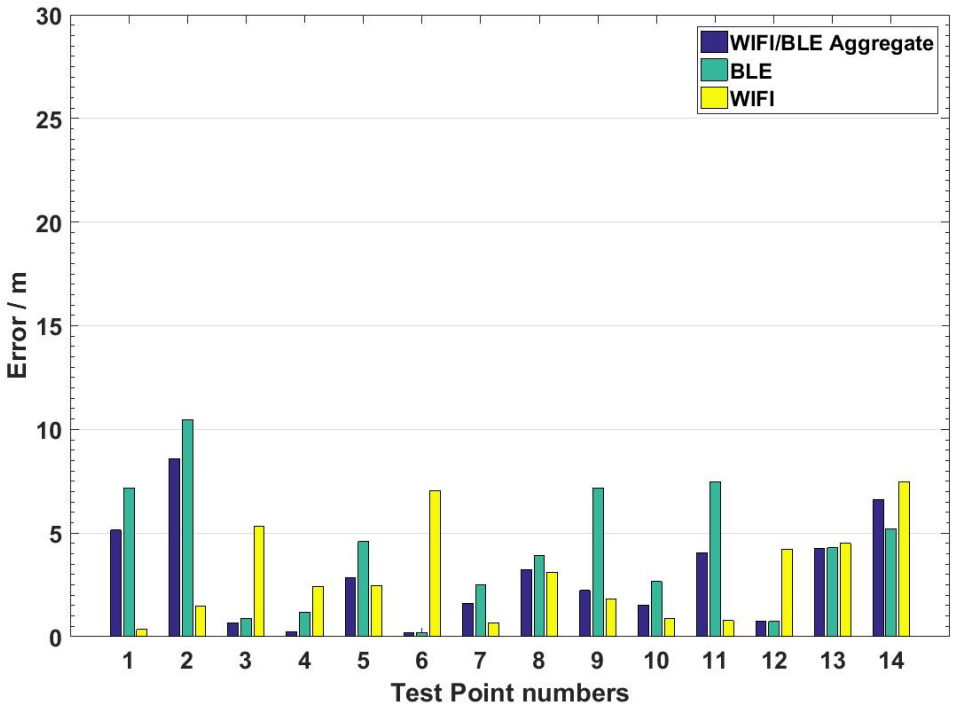


Figure 4-26 Probability Distribution Comparison showing positioning accuracy in Floor B

4.6 Discussion

In this chapter, we have shown some of the typical *RSS* characteristics of Wi-Fi and BLE while deployed in the Nottingham Geospatial Building for the development of the positioning framework. The received signal characteristics were studied in different scenarios and situations which are likely to repeat during occupancy positioning trials later. The impact of different radio signal frequencies for Wi-Fi on signal strength quality and how they vary with time has been illustrated using *RSS* plots at multiple locations from different APs to observe any inconsistency. Based on these observations it can be concluded that 5 GHz bandwidth is highly prone to attenuation from any obstruction such as furniture and walls as seen in the heat map in Figure 4.19 compared to Figure 4.18 but shows more considerable variability when compared to 2.4 GHz as seen in Figure 4.16 and 4.15. BLE signals, on the other hand, showed essential characteristics related to the position of data collection and the environment. Ideally, the range of BLE beacons are configured to partition the floors into zones according to Figure 4.12 and 4.13 but is likely to experience overlapping areas of signal strength. This overlap will worsen the quality of the signal due to interference together with multipath and will likely cause ambiguity when choosing the most reliable beacons during position computation. These factors may affect the continuous reception of *RSS* data, which is of paramount importance and might suffer from occasional outages, which then needs to be compensated by the Wi-Fi or estimation from earlier BLE *RSS* data.

We have shown the development process of the radio fingerprint database using GPR. The heat maps for Wi-Fi in Floor B showed a stark contrast between 5 GHz and 2.4 GHz compared to Floor A. This is likely to impact the choice of signal strength data from specific frequency when computing positions in Floor B and shows that even though a 5 GHz frequency provides more variability it may not be suitable at specific conditions and we may need to fall back to 2.4 GHz. As such, we will continue to use both 2.4 GHz, and 5 GHz, radio fingerprint database, where appropriate.

The quality of the fingerprint database was tested using static trials by comparing three different existing indoor positioning algorithms and evaluating their performance using the collected data. The mean and median positioning errors for both maximum likelihood and probability distribution comparison method showed better performance compared to the nearest neighbour method for both the floors. When looking at the errors for individual test points, the results show much variation with maximum error going over 20 m at times and generally hovering around 5m.

If we look back at the thesis objectives and steps for achieving them in Chapter 1, the development in this chapter satisfies step two and three towards fulfilling the first objective of developing a prototype indoor positioning system for detecting building occupancy. The positioning results from fingerprinting alone, shows they are not reliable enough to detect building occupancy at room level accuracy at all times consistently. These results will further degrade when in motion due to spatiotemporal variation of the participant's body. These analyses are particularly important since they help to understand the limitations and accuracy of the fingerprinting based position. The radio fingerprint database developed in this chapter will serve as the foundation of the positioning framework, and the location engine will be developed further in the next chapter into a fully functional pedestrian dead reckoning system using a particle filter for state estimation; combining map matching, step detection and heading estimate using smartphone's inertial sensors.

Chapter 5

LOCATION ENGINE ALGORITHMS

5.1 Introduction

We have seen in the last chapter the deployment of the BLE beacons in the Nottingham Geospatial Building and the subsequent development of the radio map using the fingerprint technique for both Wi-Fi and BLE. The small amount of static testing done using the fingerprint technique shows that the achieved accuracy is insufficient on its own and requires support from other measurement techniques or technologies. Improving occupancy modelling; the principal aim of this PhD as discussed in chapter 1, requires the development of an indoor positioning solution in the first place, capable of detecting an individual's movement through rooms, corridors and stairways. The detection needs to be of enough accuracy so that we can get a clear picture of their journey and warrants the development of a pedestrian dead reckoning system to detect building occupancy. This chapter will present research work done to achieve precisely that; a prototype multi-sensor PDR system.

This chapter will describe in detail the state-of-the-art algorithms implemented and functioning as the main components of the proposed positioning system; motion detection, heading estimate and the sensor fusion with particle filter engine. Each of the following sections discusses the algorithms chosen in detail, the implementation techniques and the results of experimental trials with objective performance analysis followed by the validation of the positioning system against ground truth obtained from a laser-guided robotic total station. The main objective of developing this positioning system has been to detect building occupancy with the help of a ubiquitous device such as a smartphone and using carefully selected state-of-the-art positioning and navigation algorithms. The block diagram in Figure 5.1 below shows the connecting components of the different elements of the positioning system and provides the reader with a high-level understanding of how the positioning system operates.

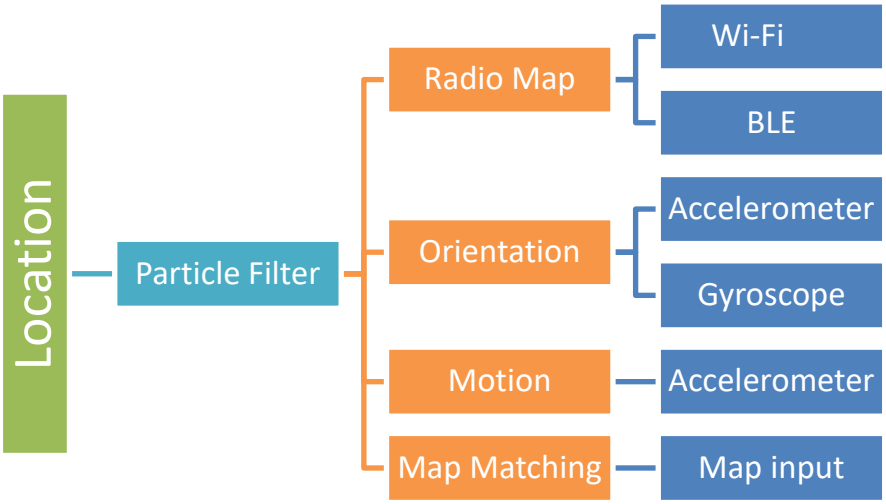


Figure 5-1 Process flow diagram showing the connection of the different sensor components producing the final location output.

5.2 Smartphone Motion Sensors

Collecting and utilising information about user motion is becoming widespread and is partly motivated by the possible applications in the health sector, sports, and context-aware services from the navigation. Several opportunities can arise from the availability of such information to flexibly adapt the services to different circumstances. For example, motion detection can be applied to detect symptoms of Parkinson's disease analysing data collected from a smartphone-based system for multiple vital sign monitoring, switching between different navigation modes in smartphone navigations recognising the change in motion type from stationary to walking or driving.

As such the growing popularity of smartphone applications has resulted in considerable research directed towards the recognition and monitoring of dynamic activity patterns using the low-cost inertial sensors and evaluation of the motion sensors' performance. This potentially will likely revolutionise a large number of existing business sectors and ultimately significantly impact our everyday lives as rightly pointed out in (Lane *et al.*, 2010).

It is essential to understand the physics of these motion sensors to develop accurate and performance-wise capable smartphone applications. A lot of research has looked into the evaluation of different smartphone sensor performance compared to the gold standard performance described as "an industrial robotic arm with an actual standard use inertial motion unit in clinical measurement, an Xsens product" as seen in (Mourcou *et al.*, 2015). Most of the motion sensors like the accelerometer and gyroscope suffer from bias and noise, and their accuracy degrades considerably with time due to drift. This is especially true for low-cost MEMS device in smartphones. These performance issues can potentially be understood using the widely accepted concept of Allan Variance to estimate the performance of the motion sensors as seen in (El-Sheimy *et al.*, 2008). The authors in (Kos *et al.*, 2016a) did an excellent job in providing a thorough analysis of smartphone inertial sensor performance and compared against different phone models.

5.2.1 Experimental Setup

In this PhD, LG Nexus 5 smartphone is used for collecting inertial data from accelerometer and gyroscope, and the Allan Variance concept is used to check the bias and noise variance of the sensors. Sensor bias is the average sensor output when there is zero sensor input.

Sensor bias is defined according to the following Equation 5.1.

$$S_{bias} = \frac{1}{N}\sum_{n=0}^{N-1} X[n] \qquad (5\text{-}1)$$

X[n] is the sensor signal data vector, N is the block of sensor data typically relevant to sensor frequency f_s. For a continuous data set the bias estimate is modified according to Equation 5.2 to account for successive bias *m* and stored in y[m]:

$$y[m] = \frac{1}{N}\sum_{n=0}^{N-1} X[n + m.N] \qquad (5\text{-}2)$$

This total number of successive bias (M) estimates from Y[m] is used to compute the Allan variance using Equation 5.3 seen below.

$$\sigma_A^2[N] \approx \frac{1}{2(M-1)} \sum_{m=0}^{M-1} (Y[m] - Y[m-1])^2 \qquad (5\text{-}3)$$

The approximation error of bias estimate for the device can be found from Equation 5.4 using the value of M defined at the beginning.

$$\delta_A = \frac{1}{\sqrt{2(M-1)}} \qquad (5\text{-}4)$$

In this experiment, we kept the smartphone placed on a table for an extended period without any external interference or motion. Throughout most of the data collection process, the smartphone is kept untouched except when switching the data logger on/off. The frequency of data collection is configured at 50 Hz, and the total number of accelerometer and gyro record collected equals 3250 measurements. We chose N equal to 50 measurement points and M, which is the number of successive bias estimates, was computed to be 65 for each sample period of N data points. The relative approximation measurement error δ_A for our device is 0.088388. The bias estimate plots are shown below for accelerometer and gyroscope.

5.2.2 Results

The successive bias estimate for blocks of M measurement for each of the accelerometer axes (X, Y and Z) can be seen in Figure 5.2, 5.3 and 5.4. The bias for X and Y-axis shows fluctuations close to zero with X-axis hovering between -0.015 and -0.017 g and Y-axis 0.022 and 0.0235 g. The Z-axis illustrates the gravitational acceleration bias fluctuating roughly between 1.001 and 1.004 g, which is very close to 1 g or 9.8 m/s^2. In short, the accelerometer biases for the phone is very much within the tolerable range and shows the sensor is in good condition. The sharp change at the beginning of each of the plot is due to the phone being placed on the table after switching on the data logger.

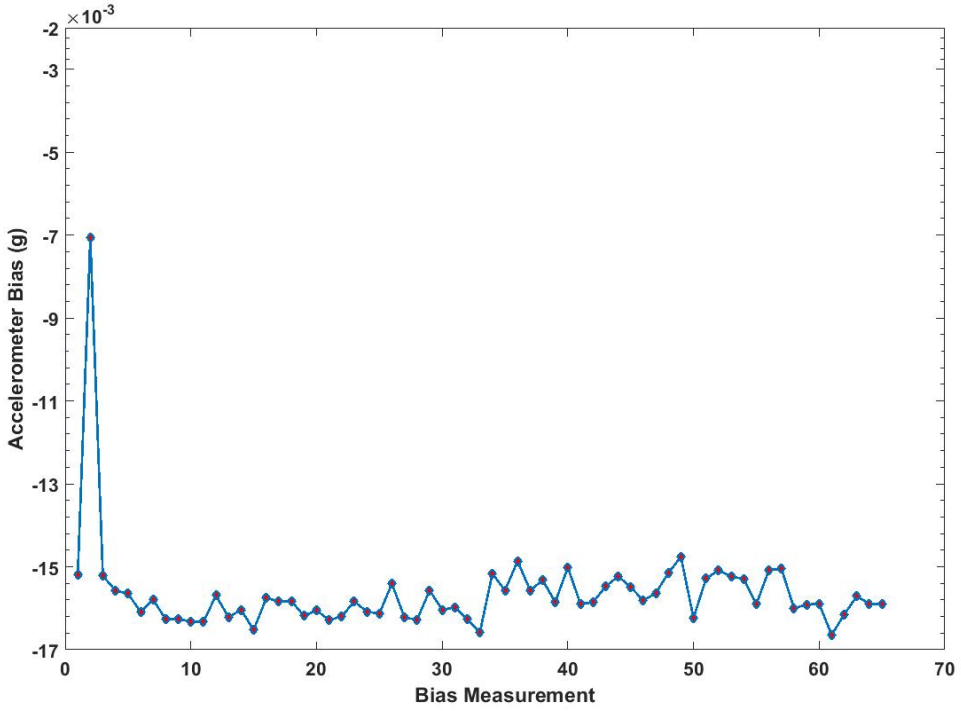


Figure 5-2 Accelerometer X-axis is showing successive bias for each of the M estimate.

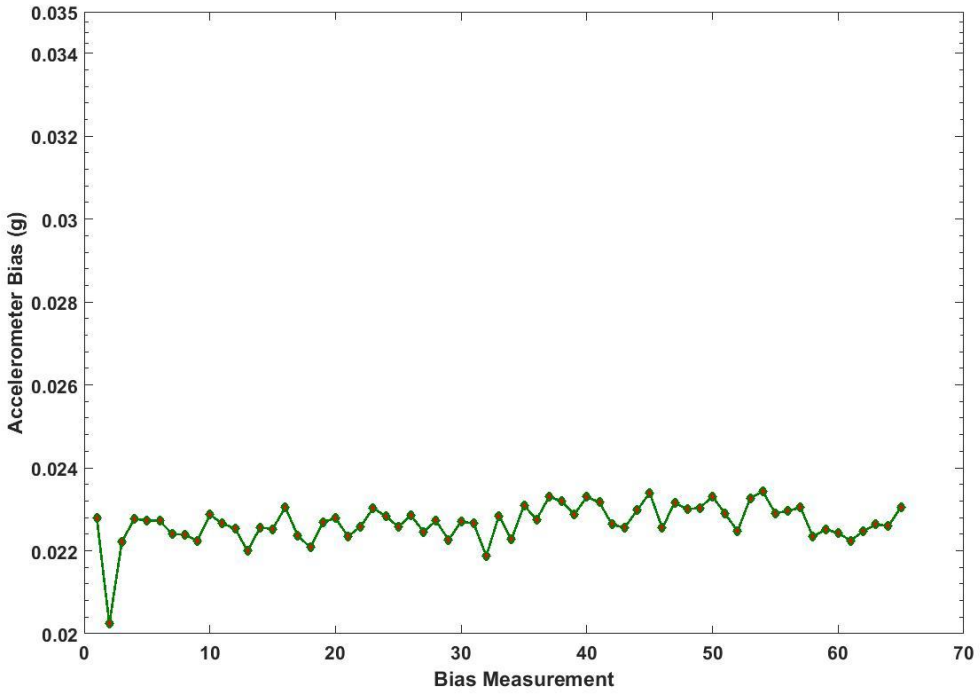


Figure 5-3 Accelerometer Y-axis is showing successive bias for each of the M estimate.

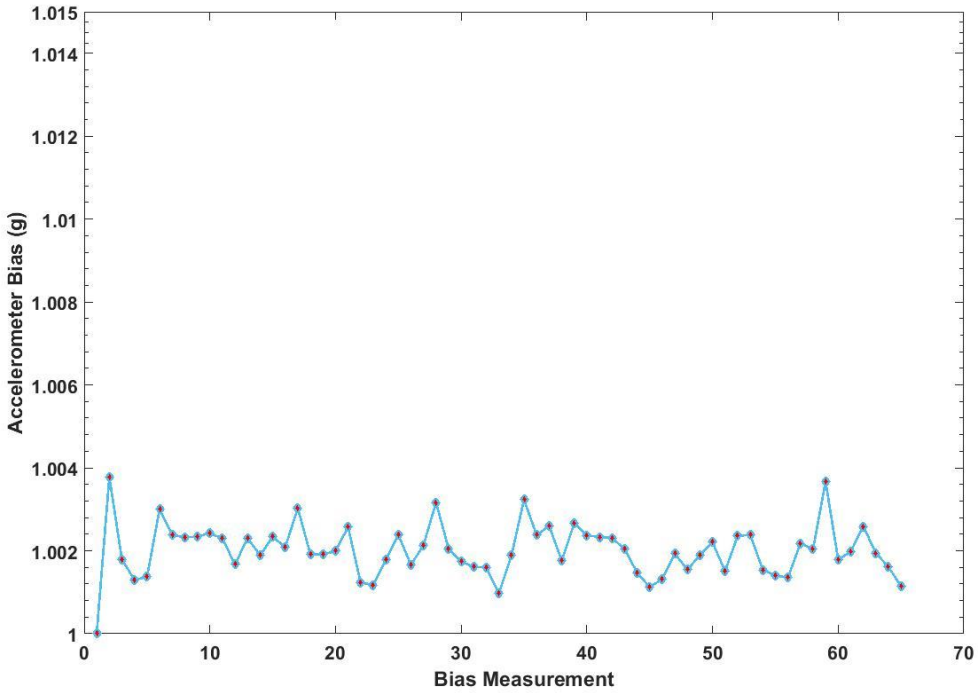


Figure 5-4 Accelerometer Z-axis is showing successive bias for each of the M estimate.

A similar experiment is carried out for gyro, and the successive M bias estimate is computed, and the result is seen in Figure 5.5, 5.6 and 5.7 below. It can be seen from the fluctuations the magnitude of the gyro bias is negligible for all the three axes in general (X, Y and Z) showing almost negligible drift for Y and Z-axis with a slight occurrence for X-axis.

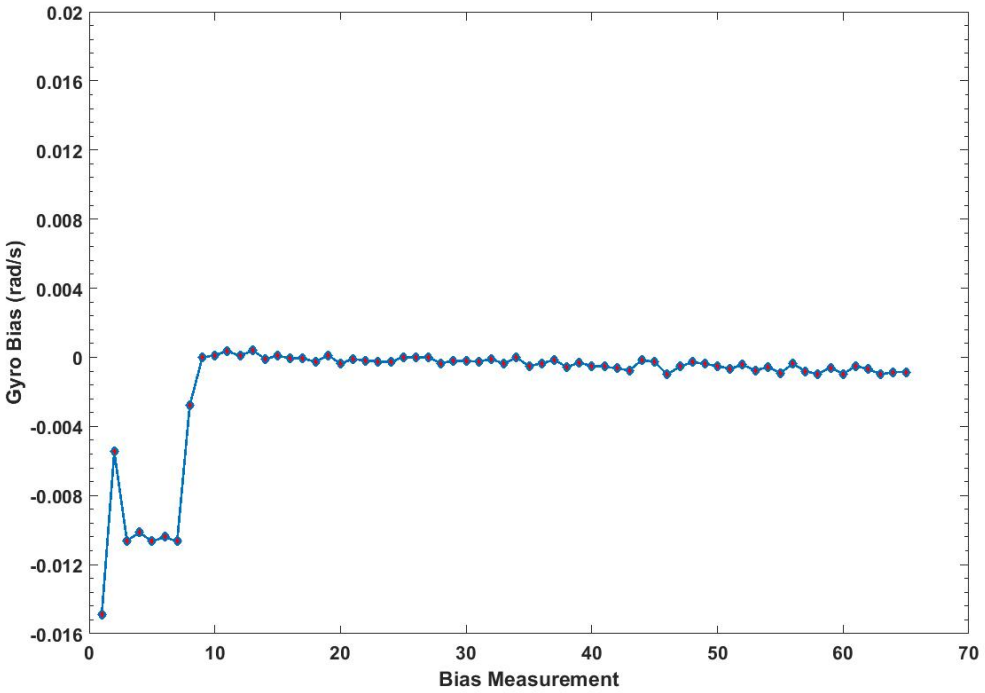


Figure 5-5 Gyroscope X-axis is showing successive bias for each of the M estimate.

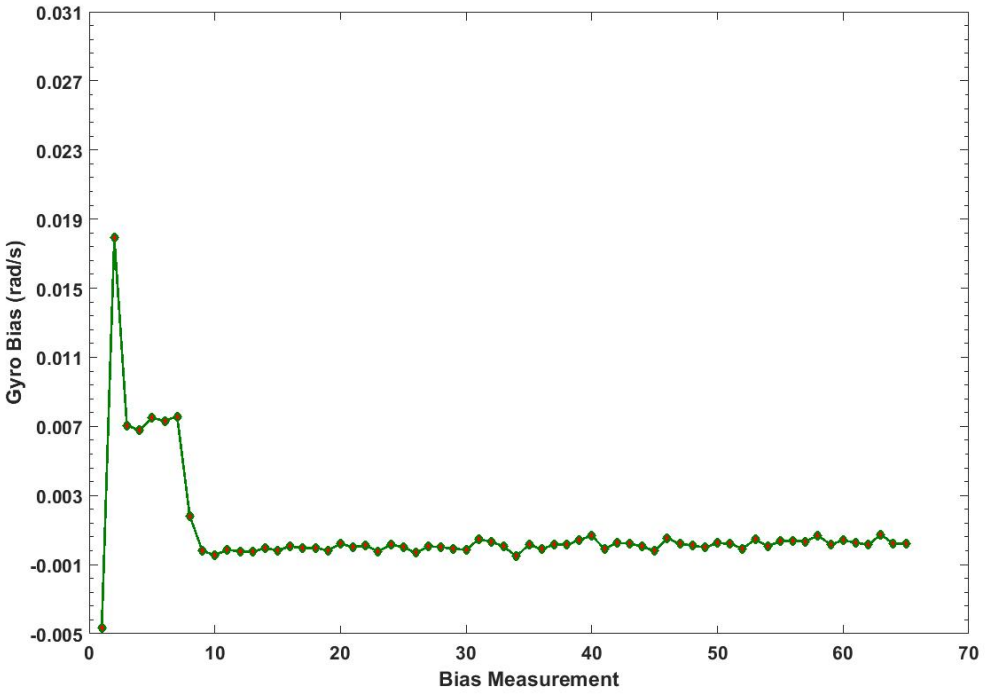


Figure 5-6 Gyroscope Y-axis is showing successive bias for each of the M estimate.

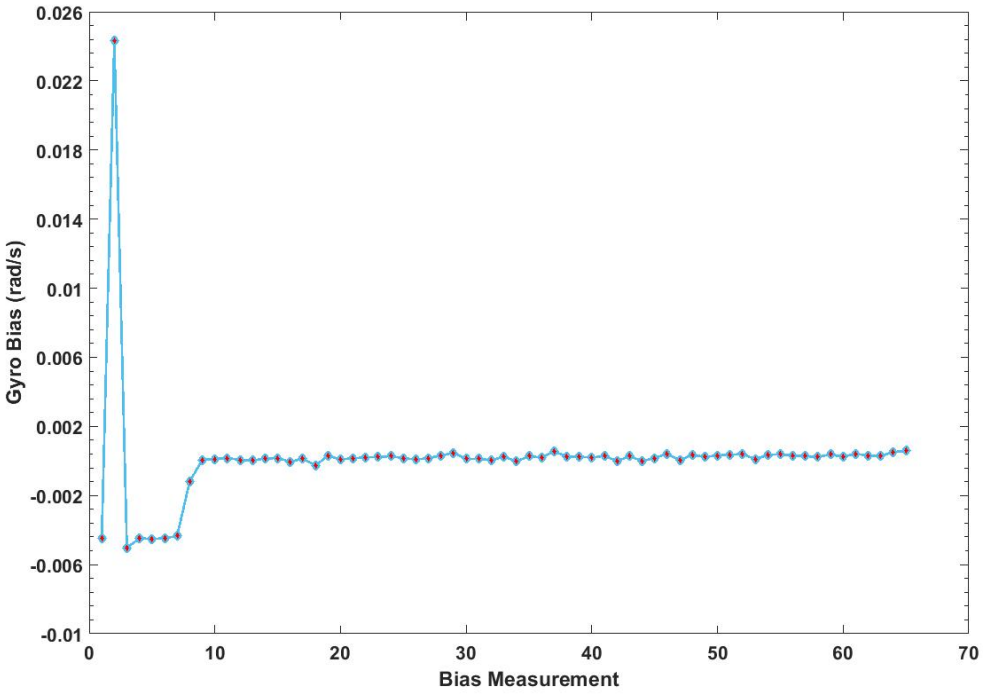


Figure 5-7 Gyroscope Z-axis is showing successive bias for each of the M estimate.

The Allan variance result computed from the successive bias M estimate for both accelerometer and gyro are seen below in Table 5.1. Allan variance computes the stability of the sensor's output and helps to observe any unconventional or deteriorating performance when there is no external interference. The bias estimate and Allan variance noise for the smartphone used show a stable output from the sensors with excellent sensitivity as seen from the measurement plots of real world trials from Figure 5.8 to 5.13.

Table 5-1 Allan Variance for each of the sensor axis

Sensor	**X axis**	**Y-axis**	**Z axis**
Accelerometer	1.1642e-06	1.6870e-07	3.6941e-07
Gyro	1.486e-06	5.2674e-06	1.3338e-05

We then test the accelerometer and gyro for different walking speeds; slow, medium and fast pace and see how the pattern varies and if there is any visible drift during motion. The plots below show the variation for each kind of motion respectively, for each of the axes and when normalised. Throughout the experiment, the phone is kept in the pocket with the data logger running in the background and recording. During initialisation, the phone is held in the hand when switching on the data logger, and this period corresponds to the irregular peaks at the beginning for each of the plots below. The phone is then placed inside the pocket, and we remain stationary for some time before starting to walk. At the end of the walk, we again remain stationary for some time before the phone is taken from the pocket and the data logger switched off. This period again corresponds to the irregular peaks at the end of the experiment.

The acceleration value for each of the three axes during the trial walk at a fast pace can be seen in the first plot of Figure 5.8 below. Apart from the irregular peaks at the beginning and end the corresponding motion peaks can be seen in the middle. We can see the data is quite compact with a small window of records during motion, clustered very close to each other with very sharp changes. This is due to coverage of the trial distance at a short period when walking at a fast pace. Depending on the placement of the phone in the pocket it would seem the Y-axis of the phone is facing downward towards gravity with oscillating value centred on the 10 m/s^2 mark. The other two axes, X and Z, show oscillation centred around zero consistently. The norm of the three axes in the second plot right below shows oscillation centred around gravity with a maximum acceleration of 30 m/s^2, an average of 20 m/s^2 and as low as 5 m/s^2.

Similar plot can be seen in Figure 5.9 with a medium pace for the individual axes. Both the individual axes and the normalised plot show a higher number of records during motion compared to Figure 5.8 due to more time being taken to cover the trial distance. The change in acceleration is less sharp compared to Figure 5.8 with more gaps in between. Also, the maximum acceleration for the normalised plot has come down to 25 m/s^2 with an average between 15 and 20 m/s^2 as seen in the plot.

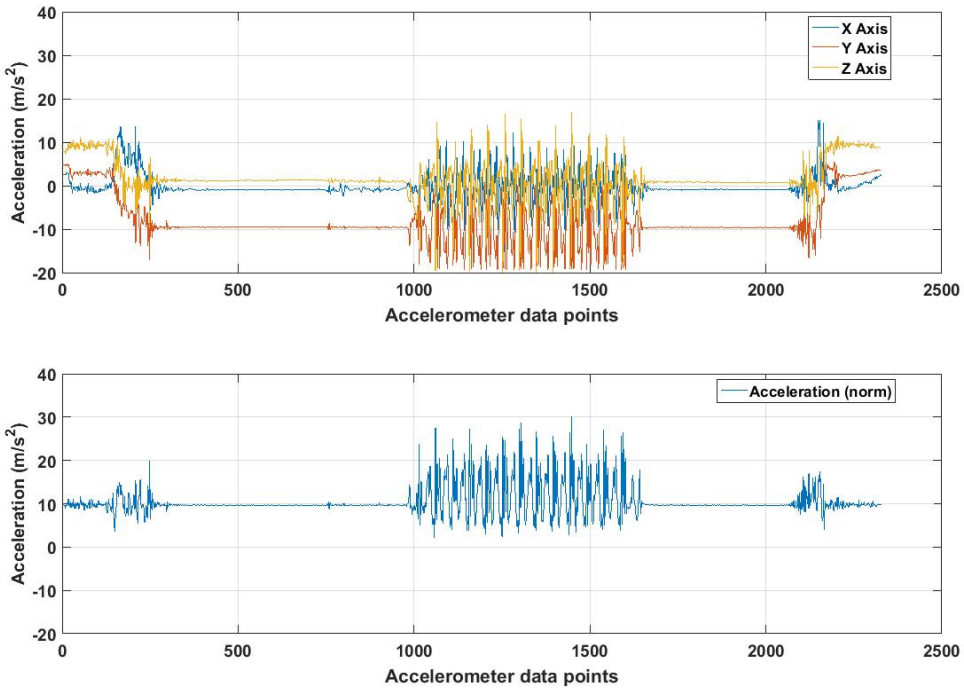


Figure 5-8 Accelerometer data for each of the axis is shown in the top plot. The lower plot shows the normalised acceleration. The plot corresponds to a fast speed walking scenario.

The illustration in Figure 5.10 shows the plot for slow-paced walking. Both the individual axes plots and the normalised plot shows large number of several records during motion due to more time now being taken to cover the same trial distance. Also, the maximum acceleration has gone down below 15m/s^2 for the normalised plot with a fewer sharp jumps. The changes in acceleration during the walk are more prominent since the gap between successive peaks is visible showing when each step is taken.

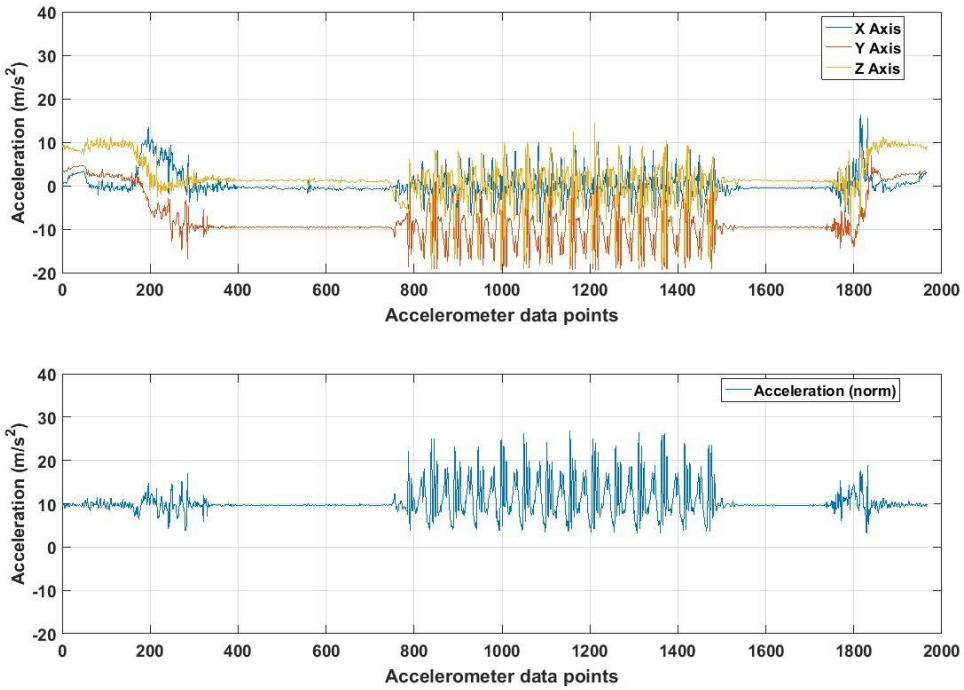


Figure 5-9 Accelerometer data for each of the axis is shown in the top plot. The lower plot shows the normalised acceleration. The plot corresponds to the medium speed walking scenario.

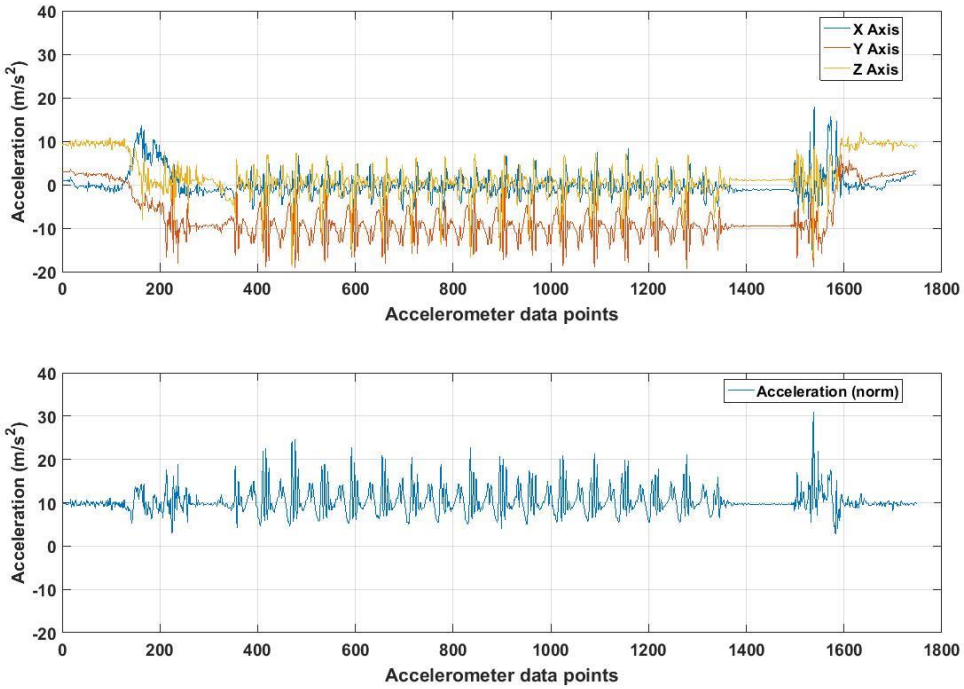


Figure 5-10 Accelerometer data for each of the axes is shown in the top plot. The lower plot shows the normalised acceleration. The plot corresponds to a slow speed walking scenario.

Gyro signal is also collected at the same time during each of the trials for different walking paces. Like the acceleration data, the plots in Figure 5.11, 5.12 and 5.13 below show similar characteristics when it comes to the increasing window of motion records as the pace of walking decreases. The changes in gyro readings are sharper during the fast pace but as the speed slows down the change in gyro reading becomes more prominent and distinguishable, highlighting the gyro rotation with the feet movement for each step taken.

The objective for doing this walk trial is to observe the changes in acceleration and gyro readings at various walking paces likely to be encountered during real-life occupancy. The sensor readings are also stable with no visible drift when kept in the pocket during motion, thus making the smartphone suitable to carry out future experiments and trials related to occupancy detection.

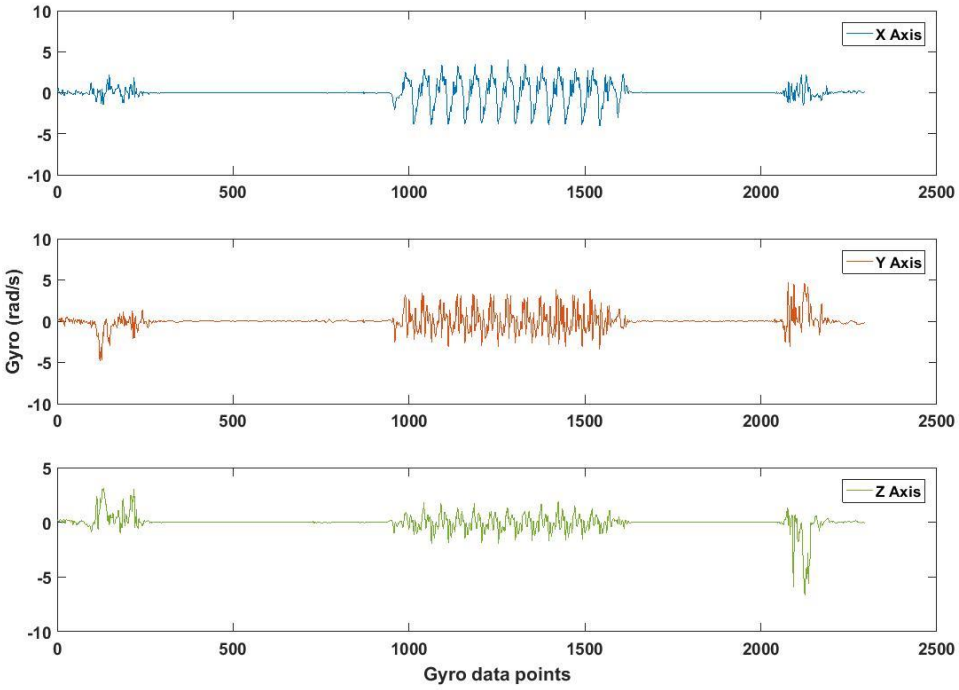


Figure 5-11 Gyro data for each of the axis during the fast walking scenario.

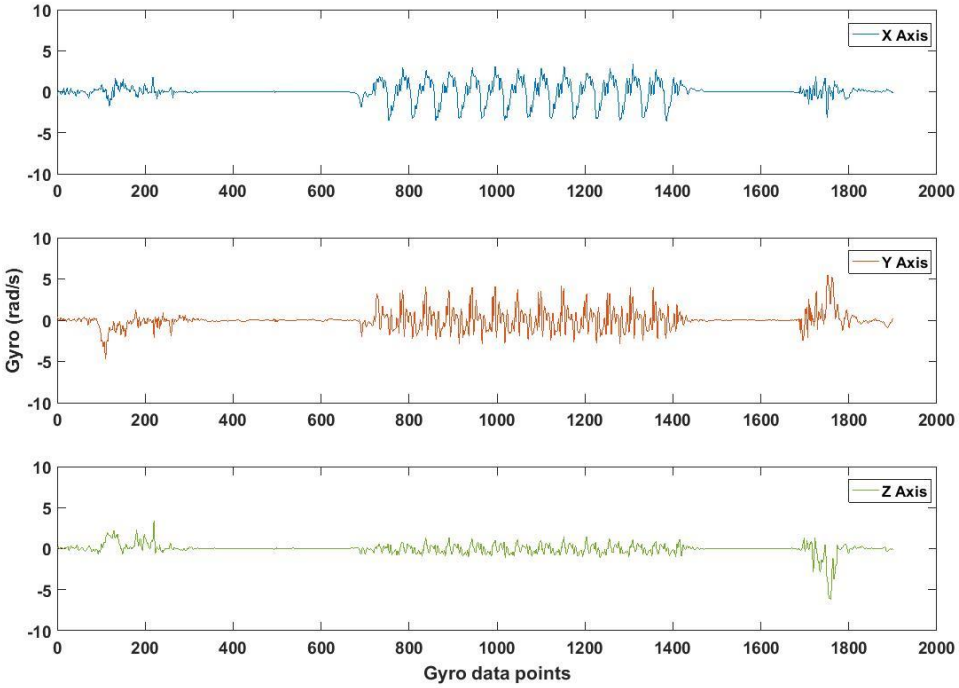


Figure 5-12 Gyro data for each of the axis during medium speed walking scenario.

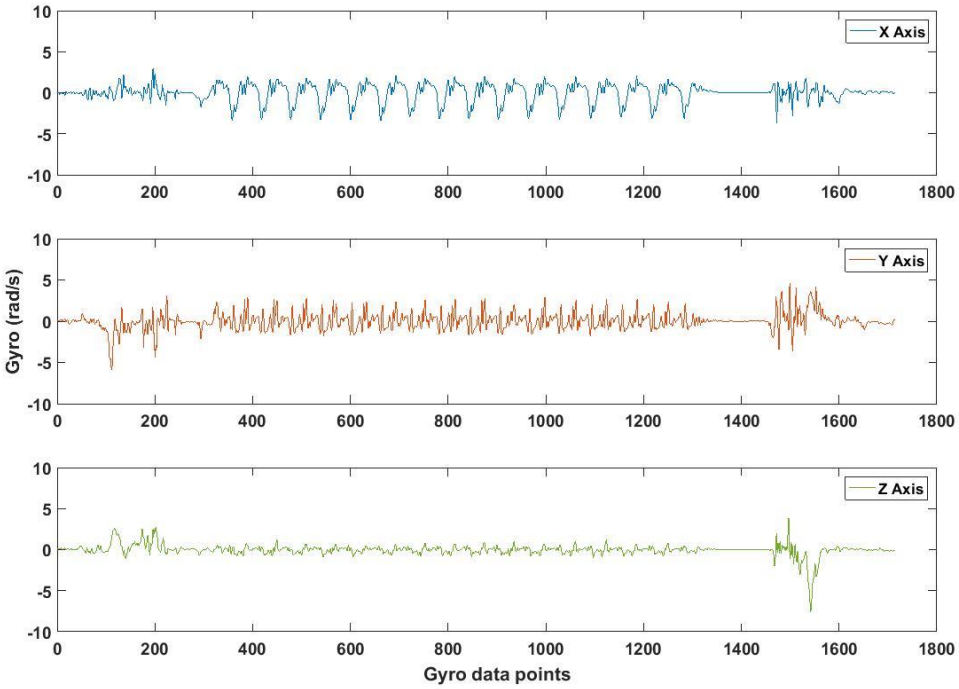


Figure 5-13 Gyro data for each of the axis during slow speed walking scenario.

5.3 Motion Detection

5.3.1 Background

Human steps can be analysed using accelerometer data, which can be easily retrieved from built-in sensors in most modern smartphones. Generally, smartphones have a poor quality of sensor, which makes the output very noisy and unlikely to give results of high quality on their own when used in an unaided INS. When working with foot-mounted IMU (Groves, 2013; Ilyas *et al.*, 2016), we can detect zero peak acceleration or zero crossings to identify a potential step. These zero crossings are just periods of low acceleration detected during the moment of heel strike of the feet, and then we apply a ZUPT in the filter. During building occupancy detection, foot mounted IMU can be cumbersome to wear for the participants and might impact their natural feet movement consequently affecting their overall motion pattern when compared to real-life occupancy.

In this research, it has been decided to use the smartphone's IMU for step detection with the phone kept in the user's pocket to ensure a real-world occupancy environment during trials. Unfortunately, in this condition correctly identifying a step becomes very complicated and subsequently unreliable because the phone will always be in motion both during each walking stance and when the foot is on the ground due to hip movement. Thus, compared to a foot-mounted IMU, it is almost impossible to detect reliable zero crossings from the acceleration data with the phone in the pocket. In this section accelerometer data from the smartphone is analysed to detect motion only for input to the particle filter engine and no attempt for a full INS is being made using ZUPTs.

To understand the pattern of acceleration during human motion, a test walk is carried out with the smartphone in the pocket and data collected using the developed Android data logger. Data is collected from all the three axes of the accelerometer and then normalised. The subsequent plot of the normalised acceleration for nine seconds and two seconds can be seen in Fig. 5.14. From the first plot, it can be observed that the signal from the accelerometer is a sinusoidal wave with repeated patterns over time

due to a periodic pattern of our feet movement during walking seen in Figure 5.15. The second plot of Figure 5.14 is a zoom in of the first plot showing peaks and valley with multiple local maxima and minima marked in a circle. Typically, during a step, the acceleration varies from person to person depending on walking speed. Previous work on step detection using smartphones show the use of different techniques such as peak-valley analysis as seen in (Lee *et al.*, 2015; Abadleh *et al.*, 2017; Nguyen-Huu *et al.*, 2018) where the authors have mostly worked towards accurate identification of maximum acceleration peaks or removing noise due to local maxima and minima. Improvement of peak detection shows the use of different movement patterns and multiple thresholds to detect steps (Li *et al.*, 2015). In general peak-valley analysis of accelerometer data has proven to be very challenging because of uncertainty from random body movement due to change in postures and turns. Alternative methods look into machine learning approaches such as using a decision tree, ANN and SVM (Kupke *et al.*, 2016; Park *et al.*, 2017; Wang *et al.*, 2018). The use of spectral analysis of accelerometer data based on frequency and time domain using Fourier Transform is seen in (Brajdic *et al.*, 2013). The process requires splitting the signal data into successive time windows of appropriate size DFT_{win} and then label each as walking if the DFT amplitude is higher than some threshold DFT_{thresh} at typical walking frequencies. Other methods, such as autocorrelation are also discussed, and the authors carried out a detailed performance analysis between different existing techniques, including machine learning techniques.

One of the most significant disadvantages of most of these algorithms is that they are likely to be triggered by any motion with a similar periodicity to walking, increasing chances of fake step detection. Machine learning techniques are complex to implement and require a large amount of data to train the models beforehand. Alternatively, to reduce computational load template matching technique can be used with a predefined reference walk template created offline and cross-correlating with the online signal pattern. The problem with this is, the reference template cannot be generalised for all kind of users. This will require multiple reference template to be

defined and matched to provide a robust and reliable result since people's height and walking pattern varies and may produce an erroneous result.

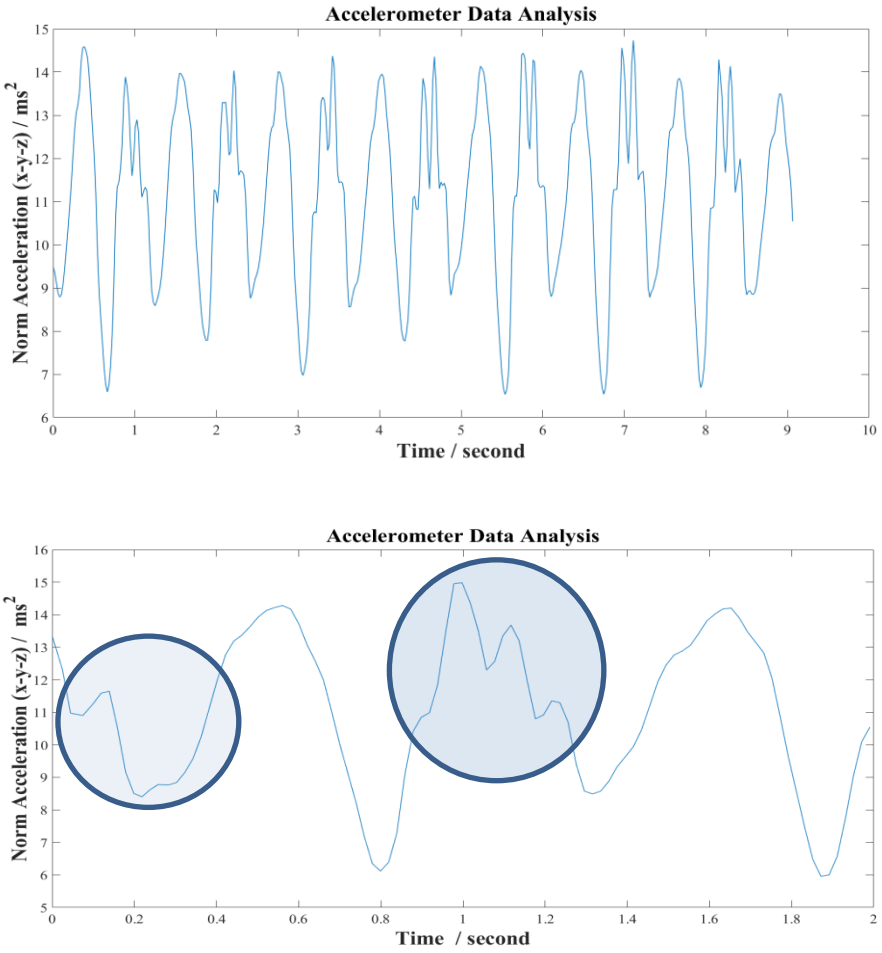


Figure 5-14 Typical accelerometer sensor output for 9 seconds and 2 seconds, respectively during walking.

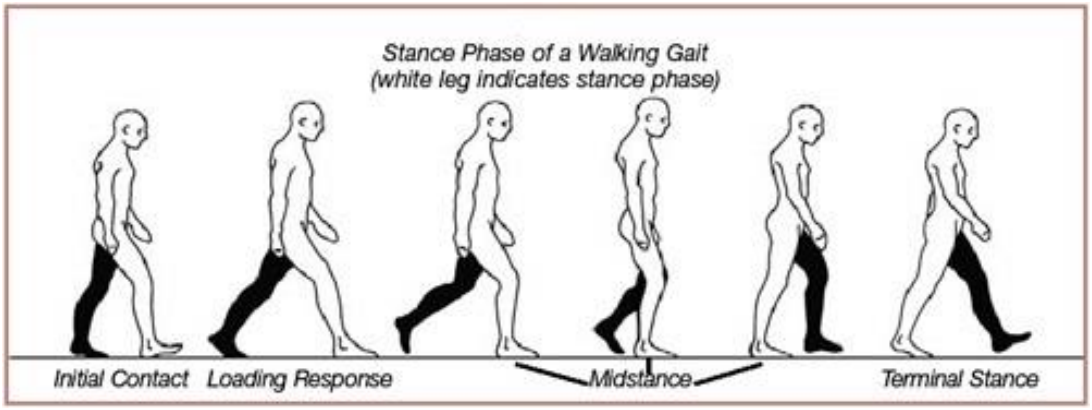


Figure 5-15 Walking stance phase showing one complete cycle starting from initial contact to terminal stance (Dubin, 2013)**.**

An illustration of a typical walking gait cycle is seen in Figure 5.15. Empirical results show that it takes a minimum 1 sec to complete one walking cycle, i.e. two steps using both feet, starting from initial contact to terminal stance shown in the picture. Due to time constraints and the scope of this research, only the walking mode is taken into consideration when detecting motion discarding running or jogging. Since it is complicated to correctly identify distinguishable zero crossings or acceleration peaks with the phone in the pocket, we try to detect step-like motion for a short window of time i.e. every two seconds. In this chapter, two different methods of identifying motion have been discussed, and a more straightforward implementation technique is followed compared to the literature discussed earlier; peak-valley analysis of the normalised accelerometer data and frequency amplitude thresholding using Discrete Fourier transform (DFT) analysis of every two seconds of accelerometer data. The reason for their choice is simply because of the ease of implementation, and that previous research results show these techniques work well with reasonable accuracy. The peak-valley analysis is used as a complementary check with the DFT results, and a combined algorithm is developed for step-like motion detection. The methodology of motion detection trial is discussed briefly in the next section before we move on to the main algorithm development phase, describing the algorithms and discuss the results.

5.3.2 Motion Detection Methodology

During the pre-processing stage, the normalised raw accelerometer data is passed through a sliding-window moving average filter for noise removal and smoothing. The following block diagram in Fig. 5.16 shows the steps for developing the motion detection algorithm.

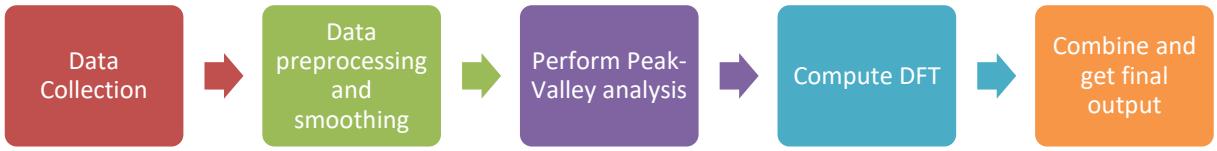


Figure 5-16 Block diagram showing the step by step process of motion detection algorithm development.

5.3.1 Peak-Valley motion detection

In a peak-valley analysis, every two seconds of acceleration data is analysed for peak acceleration and their immediate adjacent valley corresponding to minimum acceleration. We compute the step average of the peak and valley acceleration values for those two seconds of data similar to (Lee *et al.*, 2015) for robustness and ensure the average of the two should be above a certain threshold to imply motion. The authors suggest step average can be used to detect the short-term changes in the statistics of acceleration, such as the variation in motion mode. This helps to identify a more reliable step average peak-valley threshold corresponding to walk-like motion instead of relying only on individual peak detection, which can be false or noisy. It can be seen in Figure 5.17 that the green points mark the peak acceleration, and the black points mark the corresponding adjacent valley acceleration for every 2 seconds of data. The purple point is the average of the two extremities. During motion, there can be multiple peaks and valleys in the two-second window, but we take only the maximum peak and their adjacent valley data. It can be seen, during the regular walking motion, the average of the peak-valley is always above a certain threshold; in this case, the experimental threshold is above gravity, ***g,*** or roughly $10 m/s^2$. At the same time, it can also be seen that there are some false peaks due to the smartphone in hand at the beginning or feet movement not implying actual walk but rather change in body postures in static scenarios. This will create the false impression of a step-like motion being taken and will likely overestimate and end up with an erroneous position. The paper (Lee *et al.*, 2015) suggests using this technique with a periodic update of the peak and valley to compensate for irregular movement based on the average time interval between adjacent peaks and valleys with an adaptive threshold to identify steps, motion mode and pose. The algorithm is quite complicated, and the conditions in which the trials were carried out were very much in a controlled environment where the number of steps was clearly defined and prominent unlike in a real-world environment where participants will be freely navigating without any constraint. In our research, as stated earlier, we are more interested in identifying

step-like motion and not actual steps, hence the step average of peak-valley will be sufficient to identify walk-like motion as seen in the Figure 5.17.

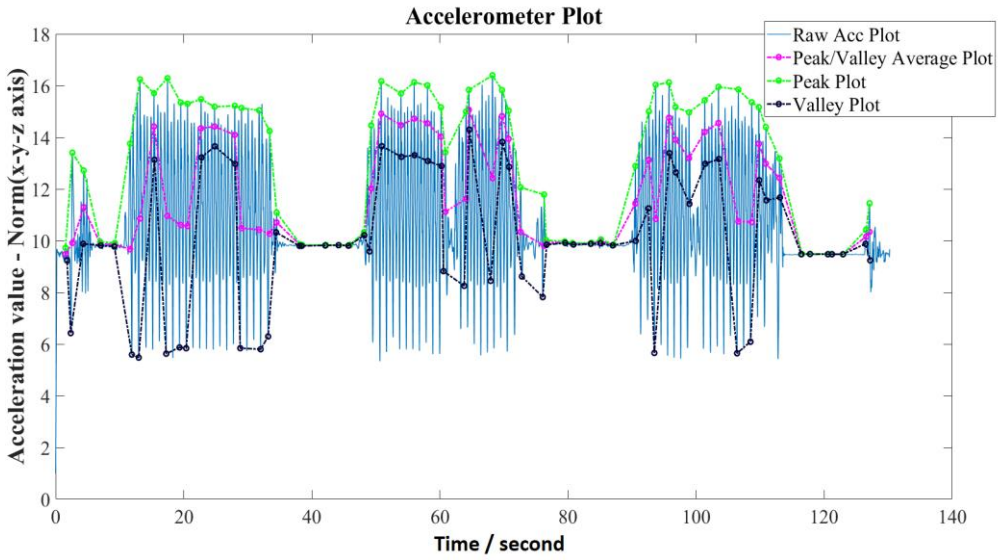


Figure 5-17. Illustration showing the peak and valley points for every 2 second and their corresponding average.

5.3.2 Discrete Fourier Transform based motion detection

A DFT based motion detection splits the acceleration signal into the successive window of data and computes the spectral energy amplitude based on the frequency of the data. The amplitudes are then checked against a specific threshold to identify step-like motion. Compared to peak-valley detection, which suffers from local minima and maxima and makes it challenging to identify peaks corresponding to actual steps, DFT based method is not affected by these characteristics. We have implemented a simple threshold matching algorithm that takes in two seconds of the accelerometer data as input in the time domain and performs a DFT process. The output is in the frequency domain producing the amplitude output of the sine and cosine waves. A discrete Fourier transform changes an N point long input signal in the time domain into two N/2 +1 length output signal in the frequency domain as seen in Figure 5.18.

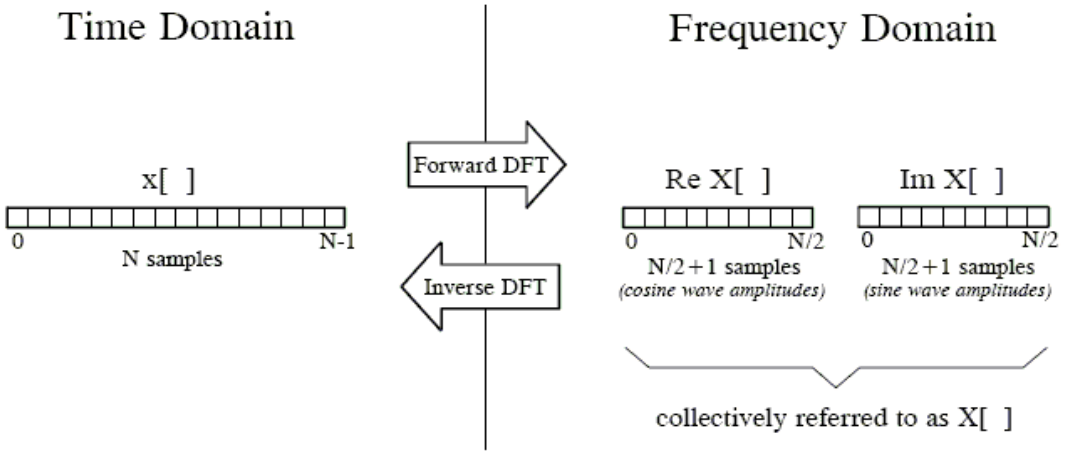


Figure 5-18 Simplified diagram of the conversion of time series data from time domain to frequency domain (Smith, 2019)

The information contained in the time domain is the same as in the frequency domain but just in a different form. The input signal in $X[f]$ is decomposed into two parts; one real Re $X[f]$ containing the amplitude from cosine waves another imaginary Im $X[f]$ containing amplitude from sine waves.

The since and cosine amplitude waves in a DFT are known as *Basis* functions and generated from the equation shown below, where *k* is the frequency number running from *i = 0* to *N-1,* e.g. a 32 point DFT produces discrete 17 sine and 17 cosine waves for its Basis function.

$$\mathrm{CK}\,[\mathrm{i}] \;=\; \cos(2\pi * \mathrm{k} * {}^{\mathrm{i}}/_{\mathrm{N}}) \qquad (5\text{-}5)$$

$$SK\,[i] \;=\; \sin(2\pi * k * {}^{i}/_{N}) \qquad (5\text{-}6)$$

The mathematical details of how the DFT calculates the amplitude is not part of the research but rather the analysis of the amplitude to find patterns, satisfying a predefined threshold that can be used to identify walk-like motion. A typical DFT amplitude plot of a sample data from a test walk can be seen in Figure. 5.19. The illustration shows the computed amplitude of the spectral energy and their phase for a

successive window of the acceleration data. The test walk is carried out with the smartphone in the pocket with the data logger continuously collecting acceleration data corresponding to the user movement.

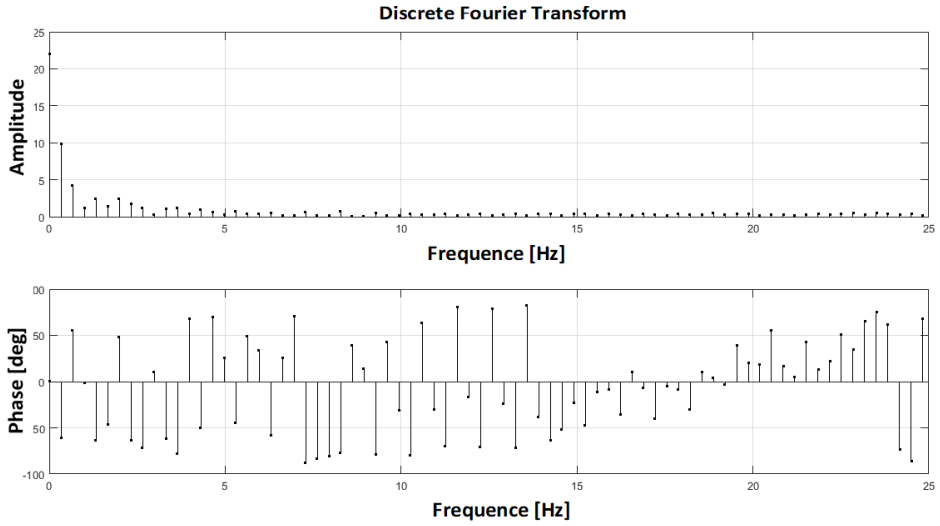


Figure 5-19 The amplitude plot at the top showing the different amplitude for each window of signal data after DFT conversion.

In this case, the accelerometer sampling rate was 50 Hz or every 0.02 second; thus, every 2 seconds of data is worth 100 samples in the walk template. The DFT output will have 50 amplitude peaks in the frequency domain plus one offset peak. The idea is to look for the dominant frequencies; in this case, the top 5 dominant frequencies are checked against a threshold typical of a walk like motion.

5.3.3 Combined DFT and Peak-Valley motion detection

To minimise the effect of falsely detected motion, a novel algorithm has been developed in this work that combines results from both the techniques during detection of step-like motion. Results from the DFT method are compared with that of peak-valley analysis for every two seconds of accelerometer data. The DFT method is used to detect identifiable step-like motion that agrees with the DFT threshold for the dominant frequencies and the upper limit threshold. The step average peak-valley analysis result is used to identify the lower limit threshold in motion, which is below a specific average. In a real-life walk scenario based on experimental evaluation, the

average peak-valley value will never be equal to or less than the gravity g even though the individual peaks and valley may be well above or below g. The idea is to correct by checking for average peak-valley results which are below gravity g acceleration but wrongly detected as motion using the DFT method, thus providing a filtering layer to minimise error. Also, there is an upper limit threshold which puts a bar on the maximum acceleration a person can achieve when walking based on empirical observation. The corresponding DFT amplitude filter is used to verify the upper limit threshold is never crossed to ensure the algorithm detects only regular walk like motion and filter out fake ones related to feet movement such as jumping and running. It is important to note that since the algorithm investigates every two seconds of accelerometer data to detect step-like motion, in this work, it implies the individual is in motion for both the seconds according to the implemented motion detection engine.

(i)Algorithm steps

1) Smooth the normalised raw accelerometer data using a moving average filter
2) Compute the DFT amplitude for 2 seconds of the actual walk
3) Analyse the top 5 dominant frequency peaks and define a threshold α_{DFT} (experimental threshold) for the amplitude
4) Check if the number of peaks above α_{DFT} is greater than or equal to 2 (the experimental threshold for a minimum number of peaks required to qualify for a step like motion) and the amplitude at zero frequency is less than 25 (experimental upper limit) to filter out fake motions
5) If true a step-like motion is detected according to the DFT method
6) Find the peak and valley from the same two seconds of accelerometer data and compute the mean acceleration μ_{Pkv}
7) Check if DFT motion is detected and mean μ_{Pkv} is below a threshold α_{Pkv} (experimental threshold 9.75)
8) If true, update the step-like motion detection to false otherwise keep the DFT value

9) Repeat from step 3 for every 2 seconds of accelerometer data till the end

5.3.4 Testing the combined DFT and Peak-Valley method

Some of the typical walking trial results can be seen in the following figures. A brief analysis of the plots (at variable walking pace) show peak-valley analysis in black along with the actual accelerometer plot, the DFT plot in red and the combined analysis plot in green. Fig. 5.20 shows the circled points where peak-valley analysis suggests a step-like motion is being taken, but the DFT technique correctly identifies them as no-step. In Fig. 5.21 and Fig. 5.22 the DFT has wrongly identified a step-like motion, but the peak-valley analysis corrects it as shown in the circled area.

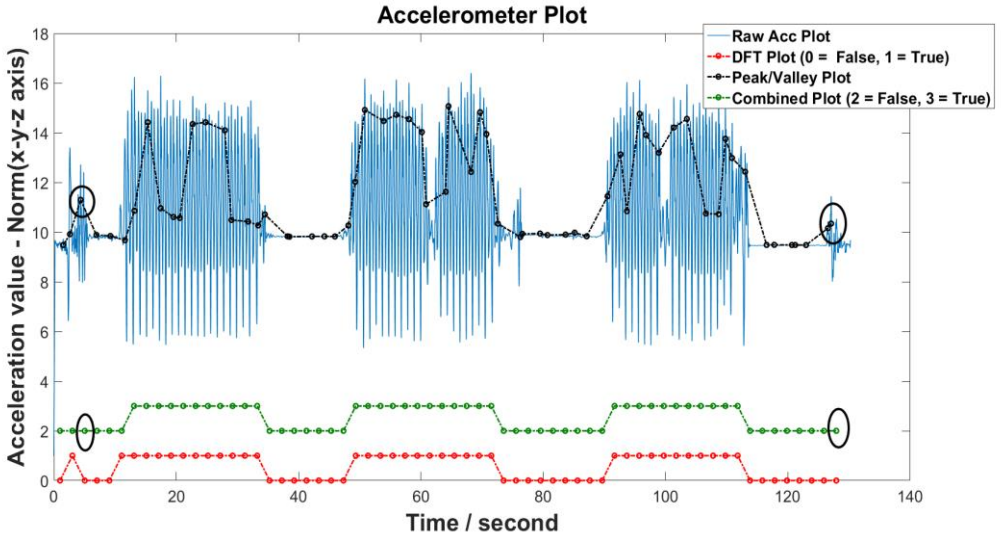


Figure 5-20 Trial walk-1, circles showing wrongly detected motion in peak-valley average but corrected using the DFT as shown in the combined plot.

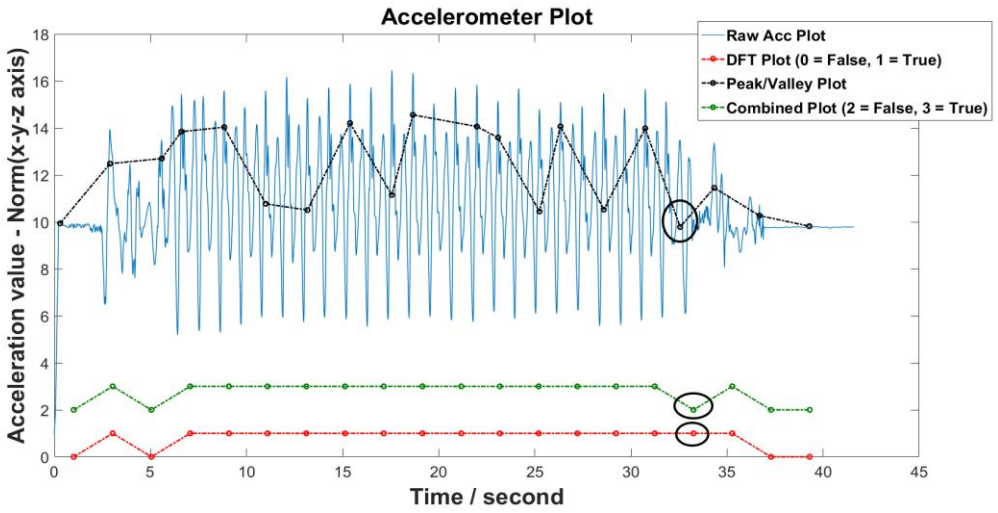


Figure 5-21 Trial walk 2, circles, showing wrongly detected motion in DFT but corrected using peak-valley analysis in the combined plot.

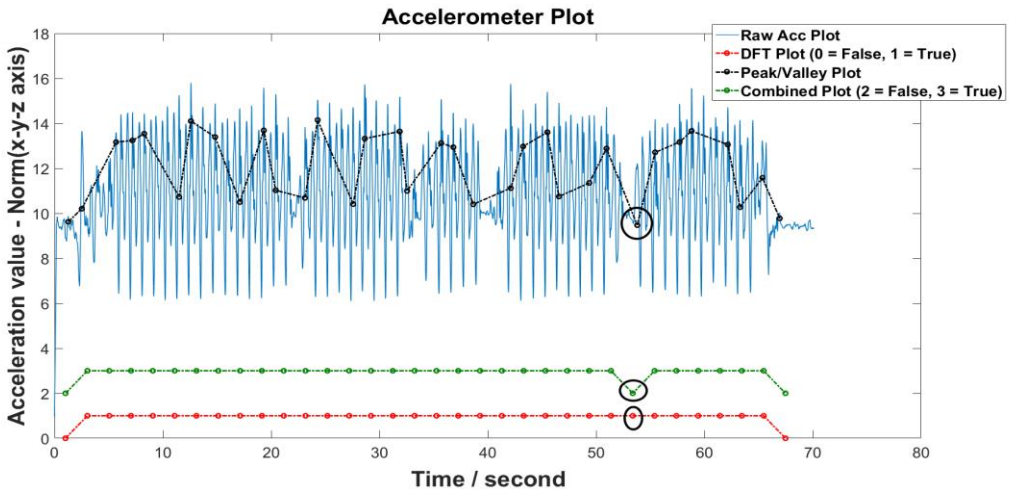


Figure 5-22 Trial walk 3, circles, showing wrongly detected motion in DFT but corrected using peak-valley analysis in the combined plot.

A further experiment was done to validate the algorithm's upper limit when irregular feet motion such as jumping or postures are made. The two plots in Figure 5.23 show data corresponding to irregular feet movement and a 2-second chunk of the corresponding DFT plot. The offset frequency amplitude marked in red is higher than the defined threshold of 25. Thus, this motion will not be labelled as a step-like walk in the DFT match. This was to ensure we do not inadvertently classify non-walking motion with a high amplitude as an actual walking motion.

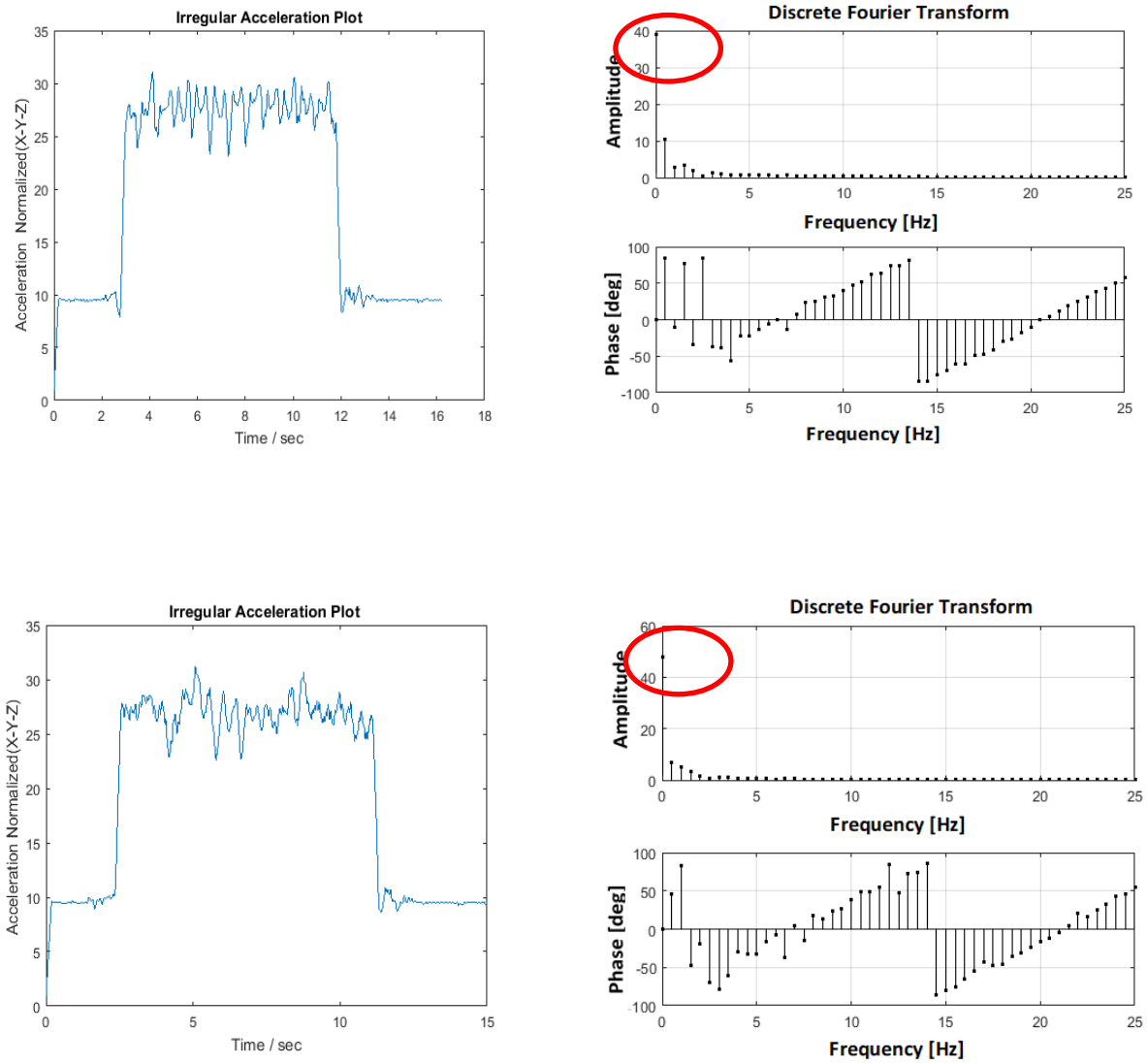


Figure 5-23 Accelerometer and corresponding amplitude plot from DFT showing the amplitude of the offset frequency during irregular motion such as jumping etc. instead of walking.

The performance of the motion detection algorithm is evaluated with a 2 X 2 confusion matrix from seventeen walk trials covering different parts of the building. The walking pattern consisted of different walking speeds and turned around corners making sure the walking stances are as natural as possible. For each trial, motion detection outcome for every epoch of two seconds is recorded and a confusion matrix showing the true positive (TP), true negative (TN), false positive (FP) and false negative (FN) is tabulated by summing up the results as shown in Table 5.2. We then compute the accuracy, recall and precision for the motion classification performance. Since we are

combining two separate techniques; peak-valley and DFT in our algorithm, we analyse the performance of the individual techniques at first and then compare the results with the combined one for improvements. Accuracy is the measure of correct identification of the fraction of all our predictions. Recall measures the proportion of actual positive predictions being correctly identified. Precision is the measure of what proportion of positive predictions made by the algorithm are correct. Equations 5.7, 5.8, and 5.9 for calculating each one of them respectively can be seen below.

$$\text{Accuracy} = \frac{TP + TN}{TP + TN + FP + FN} \quad (5\text{-}7)$$

$$\text{Recall} = \frac{TP}{TP + FN} \quad (5\text{-}8)$$

$$\text{Precision} = \frac{TP}{TP + FP} \quad (5\text{-}9)$$

The confusion matrix for the peak-valley technique can be seen in Table 5.2 below and the corresponding performance measure in Table 5.3. The algorithm on it shows an overall accuracy of 86% with a precision of 77% and a recall of 100%. It is not surprising for the recall to be 100% since any real motion is picked up from the accelerometer data having the step average above threshold α_{Pkv} specified in the algorithm earlier. The precision is quite low, at 77% due to a higher percentage of false motion being classified as positive. This is understandable since we are not setting a dynamic threshold for α_{Pkv}. As a result, any signal above the defined threshold α_{Pkv} is labelled positive, and that is precisely why we decided to have the DFT acting as a high pass filter.

Table 5-2 Shows the confusion matrix from 17 Trials, which are used to compute the classification performance of the peak-valley motion detection algorithm.

	Positive	Negative
True	47%	39%
False	14%	0%

Table 5-3 Performance measure for peak-valley technique

Recall	Precision	Accuracy
100%	77%	86%

The DFT technique performance is shown in Table 5.4 and 5.5 gave an overall accuracy of 92% with a recall of 95% and a precision of 88%. The result in comparison to peak-valley method shows better performance in both accuracy and precision metric. The recall value is a bit less in comparison since not all motion is classified as positive defined by the threshold of $\alpha_{DFT.}$

Table 5-4 Shows the confusion matrix from 17 Trials, which are used to compute the classification performance of the DFT based motion detection algorithm.

	Positive	Negative
True	45%	47%
False	6%	2%

Table 5-5 Performance measure for DFT-based technique

Recall	Precision	Accuracy
95%	88%	92%

The performance of the combined peak-valley and DFT method shown below in Table 5.6 and 5.7 gives a similar accuracy to the DFT method of 92%, but the precision improves and goes up to 90%. This is mainly because the peak-valley technique acts as a low pass filter by correctly identifying false motion below the threshold $\alpha_{Pkv,}$ which may be identified as positive by the DFT. Again the recall is a bit less 94% compared to both the previous method due to a slightly higher percentage of the FN as seen in Table 5.6.

Table 5-6 Shows the confusion matrix from 17 trials, which are used to compute the classification performance of the combined peak-valley and DFT based motion detection algorithm.

	Positive	Negative
True	44%	48%
False	5%	3%

Table 5-7 Performance measure for the combined peak-valley and DFT technique

Recall	Precision	Accuracy
94%	90%	92%

Since both the algorithms are based on some defined threshold, there is always a chance that both the method outputs incorrect prediction when combined during complicated motion manoeuvre. In general, the proposed combined method gives a slightly better performance compared to each one of them on their own. The implementation technique is straightforward yet highly effective when detecting step-like motion as seen from their performance analysis and both the peak-valley and DFT technique complements and corrects each other's output to provide a reliable step-like motion detection solution.

5.4 Heading Estimation

Recall from Chapter 2 that the MEMS inertial sensors (3D accelerometers and 3D gyroscopes) have become widely available because of a low cost and smaller size.

Measurements from inertial sensors like the accelerometer and gyro are obtained at high sampling rates and can be integrated to obtain position and orientation information. These estimates are accurate on a short timescale but suffer from integration drift over longer time scales, as discussed in this paper (Harle, 2013). Also, as discussed earlier, for collecting occupancy data, it is not convenient to wear a foot-mounted INS over a long period. As such, an IMU from the smartphone is the most practical choice instead of a foot tracker; though the sensors can be of even more inferior quality and would suffer from the same drift issue. A significant amount of research has been done to understand the application of mobile phones in PDR solutions (Kang *et al.*, 2012; Deng, Wang, *et al.*, 2015; Kos *et al.*, 2016a, 2016b; Kok *et al.*, 2017) and they discuss the performance of the positioning solution and evaluate related issues such as bias and noise in mobile phone sensors.

Orientation computation using IMU is not something new, and there are numerous papers (Deng, Wang, *et al.*, 2015; Kos *et al.*, 2016b; Solin *et al.*, 2017) that discuss the implementation. Typically heading can be computed using a fusion of gyro and magnetometer measurements if the initial orientation of the device is known or if the earth's magnetic north is used as a reference. A magnetometer is also known to complement the accelerometer when providing sensor heading ideally when there is no magnetic material present nearby. Unfortunately, it is well known that magnetometers suffer from distortion when indoors due to various reasons, most importantly due to the presence of a ferrous or magnetic substance in the building structure or furniture and positioning such as when mounted (Kok *et al.*, 2017). As such heading estimate using a magnetometer and gyro often gives unreliable results. Thus accelerometer can be used as an alternative or in combination with a magnetometer or gyro to improve accuracy (Yadav *et al.*, 2014) by providing corrections to the gyro measurement in a sensor fusion. This sensor fusion may use any but not limited to the following algorithms for accurate estimation of the heading primarily focusing on the use of low-cost IMU; Madgwick AHRS filter (OlliW, 2016), Mahony AHRS filter (OlliW, 2016), Complimentary filter(Jouybari *et al.*, 2017), Kalman filter (Michel *et al.*, 2015), Compensation of Magnetic Disturbances (Roetenberg *et al.*,

2005). The Kalman filter is excellent for providing a stable and accurate estimation of orientation, but they can be very complex to implement and challenging to understand, as stated in the paper by *Jouybari et al.* above. Similarly, in the case of using a magnetometer-based orientation filter, much calibration and bias estimation are required to nullify the effect of any possible magnetic perturbation from ferrous substances nearby, thus making the algorithm quite complicated. The Madgebwick filter, Mahony filter and complementary filter are all comparatively simple and easy to implement. The Mahony filter corrects gyro drifts based on the accelerometer data by computing the error in the estimated direction of gravity every epoch and applying the feedback to the gyro measurement with two gains K_p and K_i known as proportional and integral adjustable gains which help to reduce gyro drift. The Madgwick filter uses a gradient descent approach based on the rate of divergence of the quaternion vectors and their derivative at each epoch. The complementary filter is ideal for foot mounted devices and does not have any gyro drift compensation, and only one adjustable gain is used. A comparison for all the algorithms discussed can be found in the following papers (Michel *et al.*, 2015; Jouybari *et al.*, 2017). When it comes to the Madgwick filter, its performance is similar, with a focus on pedestrian navigation when compared to the Mahony filter with a focus on aerial navigation. Also, the Mahony filter is shown to be better for heading estimation compared to the complimentary filter. Based on all these factors and ease of implementation Mahony filter is chosen for heading estimation in this research.

Current smartphones are generally equipped with a tri-axial accelerometer, gyro, and magnetometer. To estimate heading just by using the accelerometer and gyro, it is vital to have a heading direction reference for initialisation. Since it will be inconvenient for participants to start every time facing a specific direction we try to compute relative heading by merely using the gyro and accelerometer in the Mahony filter (Mahony *et al.*, 2008; OlliW, 2016). The mean accelerometer data is used during the initialisation period of coarse alignment known as *levelling* to compute the error between the attitude and a known measured direction of gravity and the rate of change of quaternion. This means the participant needs to be stationary for a while

during the initialisation state. We then use the gyro and accelerometer reading at every epoch and use quaternion computation to estimate the relative heading from the gyro data. In our case, since the particle filter will be used and the particles are initialised with random heading (0-360◦ uniform distribution), it is not necessary to compute absolute heading. An accurate heading-change estimate is enough to guide the particles to propagate in the right direction.

When using the Mahony filter to compute heading, accelerometer data is collected at each epoch and applied to correct the estimated direction of gravity. During trial data collection, the phone is always kept in the user's trouser pocket with the data logger running in the background. This helps to ensure the measured direction of gravity never deviate too much due to tilting of the phone over time and will remain stable. The corrected direction of gravity is applied to the corresponding gyro data with the filter gain. Filter gain is the rate of convergence toward the measurement error, in this case, in the gyro measurement. The compensation of gyro bias in traditional Kalman filter is done in an additional state, but according to Mahony et al. (Mahony *et al.*, 2008), this can be quickly done in simple orientation filters through the integral feedback of the error in the rate of change of orientation calculated. Thus, the gyro bias drift is automatically compensated when the rate of change of quaternion is computed and subsequent integration to yield quaternion for that epoch. The heading is then obtained by computing the yaw from the quaternion vector. The algorithm below provides a step by step guide for computing the heading using Mahony filter. To get a clear idea of quaternion mathematics, the reader is referred to the following paper (Solà, 2017).

(i)Mahony Filter Algorithm Steps

1 Preprocess gyro and accelerometer data

2 Initialise quaternion

$$q = [q^1, q^2, q^3, q^4]$$

3 Normalise accelerometer measurement

$$acc = acc/norm(acc)$$

4 Estimate direction of gravity

$$v = \begin{bmatrix} 2(q(2) * q(4) - q(1)q(3)) \\ 2(q(1)q(2) + q(3)q(4)) \\ q(1)^2 - q(2)^2 - q(3)^2 + q(4)^2 \end{bmatrix}$$

5 Compute error from the cross product between estimated direction and measured direction

$$e = cross(acc, v)$$

6 Apply error feedback to correct gyro measurement using filter gain $\triangle$

$$gyro = gyro + \triangle * e$$

7 Compute rate of change of quaternion using the corrected gyro measurement

8 Integrate to yield new quaternion and normalize

9 Compute yaw to get heading

5.4.1 Heading Estimation - Experimental Results

In the trial, an LG Nexus 5 smartphone was used which has a 3-axis accelerometer and a gyroscope integrated. The data collection rate was kept at 50Hz. To analyse the stability of the gyro and the accelerometer, the smartphone was kept on a table for almost 6 hours with two 90◦ rotations. This was done to check if there are any significant drift over a long period. The resulting plot can be seen in Figure 5.26

We then experimented with checking the heading change computation from the phone by keeping it on a table and rotating it, as shown in Figure 5.24. This was mainly a preliminary analysis of heading estimation before performing actual walk trials.

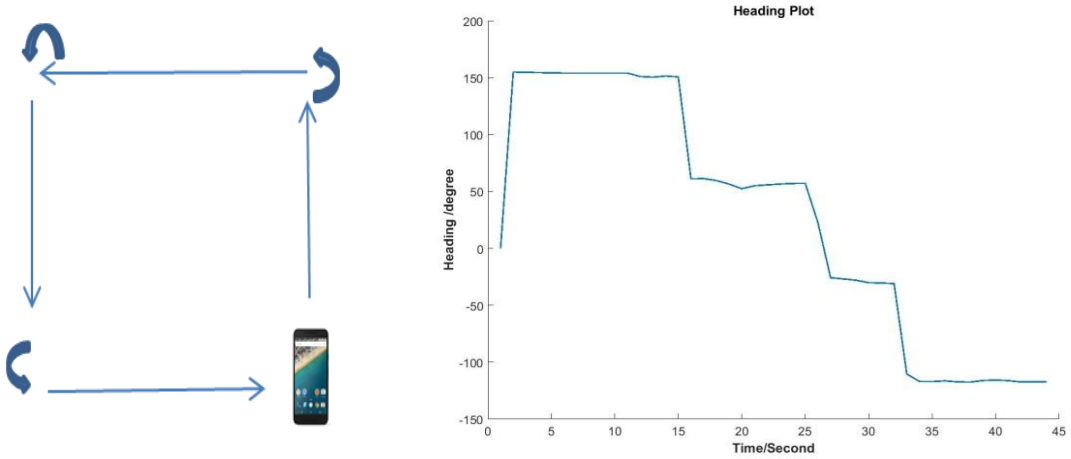


Figure 5-24 Distinguishable heading change obtained from a table top experiment on the right were the phone was rotated from time to time, as shown in the left plot.

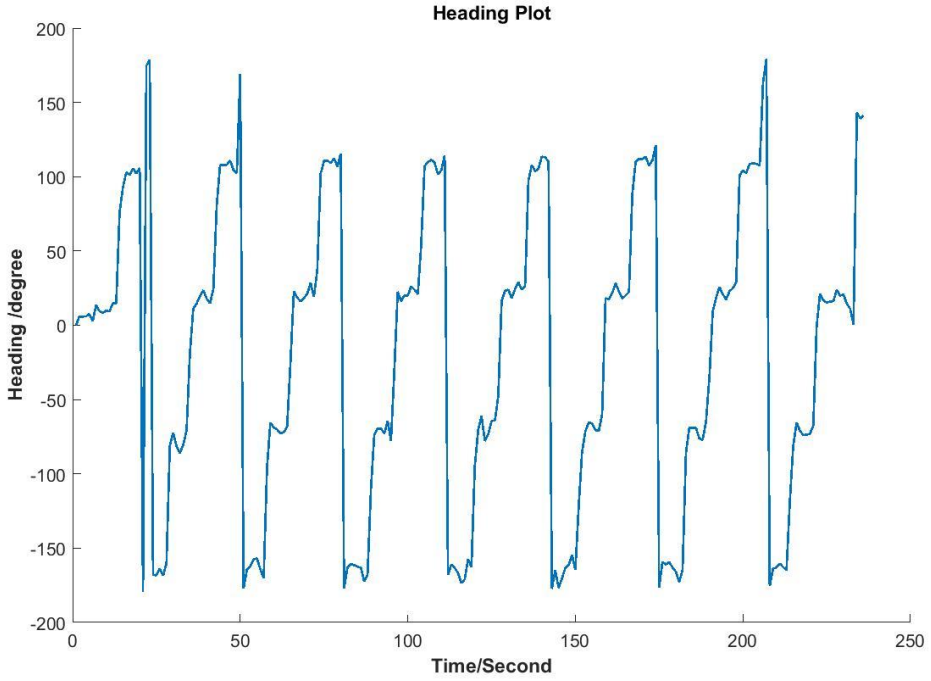


Figure 5-25 Heading change computed from a walk in a square pattern around four corners of a room. Eight complete rotations were made during the trial.

To evaluate the accuracy and stability of the heading estimate walk trials were carried out, as shown in Figure 5.26 and Figure 5.27. The results show a stable heading

estimate and distinguishable change is heading during each turn. The phone was always kept in the pocket, and a regular walking pace was maintained throughout.

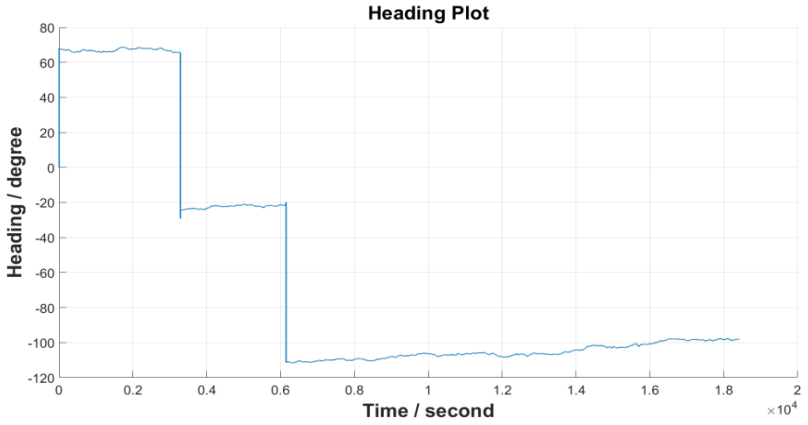
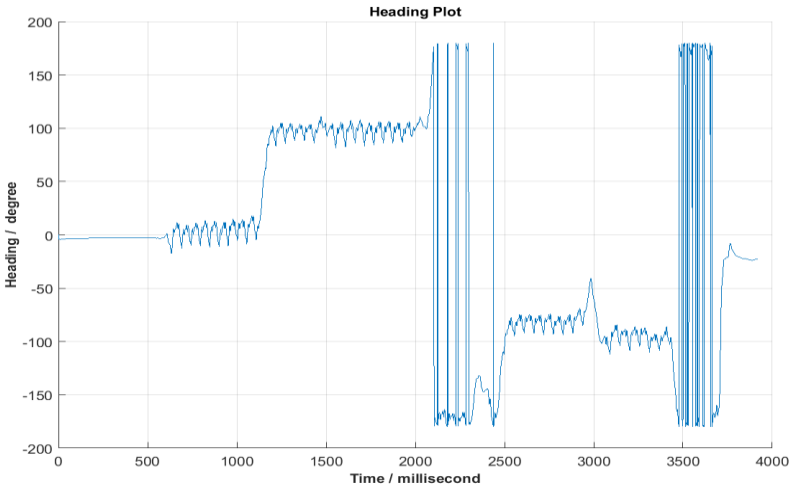


Figure 5-26 Heading computed throughout approximately for six hours to check for any drift.



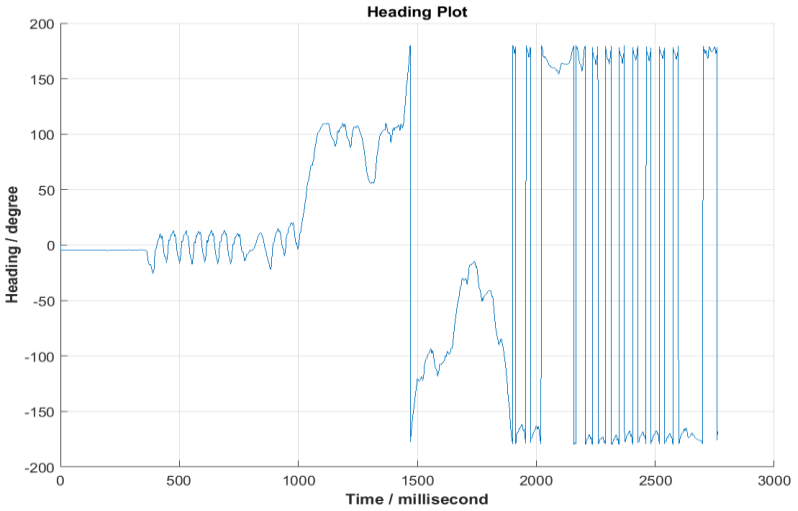


Figure 5-27 Heading evaluation trial walk results showing distinguishable heading changes during major turns with clearly identifiable heading change corresponding to the turns.

5.5 Particle Filter Engine

A standard implementation of the particle filter engine was developed with the particles having features of heading information and importance weight. Heading is initialised with random input uniformly distributed from 0-360◦. Then during the predict stage updated heading information is provided to the particles at each epoch. Importance weight is given to the particles from the Wi-Fi/BLE observation computed by comparing with the fingerprint database. The particles are propagated forward based on the trigger from step-like motion detection and step length is configured at 1.3m (empirically observed human walk velocity) depending on few constraints and added noise to account for uncertainty of motion. The particle filter engine is activated only when the user is in motion and integrated with map matching and floor detection for dynamic radio map switching. The transition between floors was identified based on stair detection using BLE markers placed at regular gaps to detect entry and exit. A multinomial resampling process is implemented to ensure regular monitoring of particle fitness and replacement with stronger ones to avoid impoverishment and engine failure and filter restart. The filter algorithm steps are listed below for a clearer understanding.

The sensor fusion diagram can be seen in Figure 5.29. Since data is post-processed in this positioning system, at each epoch when radio observations became available the Wi-Fi and BLE GP fingerprint database are looked up respectively, compared with their recorded mean RSSI and a difference map is computed for each. The sampling rate of the Wi-Fi was every four seconds and BLE was every two seconds and the missing observations between the epochs were computed according to Figure 5.28. The difference map of the Wi-Fi and BLE is normalised to get probability maps, and their joint probability is computed to get the aggregate observation map. This aggregate observation is used at each epoch to compute a static position when stationary and alternatively when in a motion passed to the particle filter engine to update the weights of the particles, dependent on the occurrence of a step event. Here an epoch corresponds to a second. In our filter engine, 4000 particles were used, and their weights were taken directly from the computed Wi-Fi and BLE aggregate map as discussed in Chapter 3 fingerprinting section.

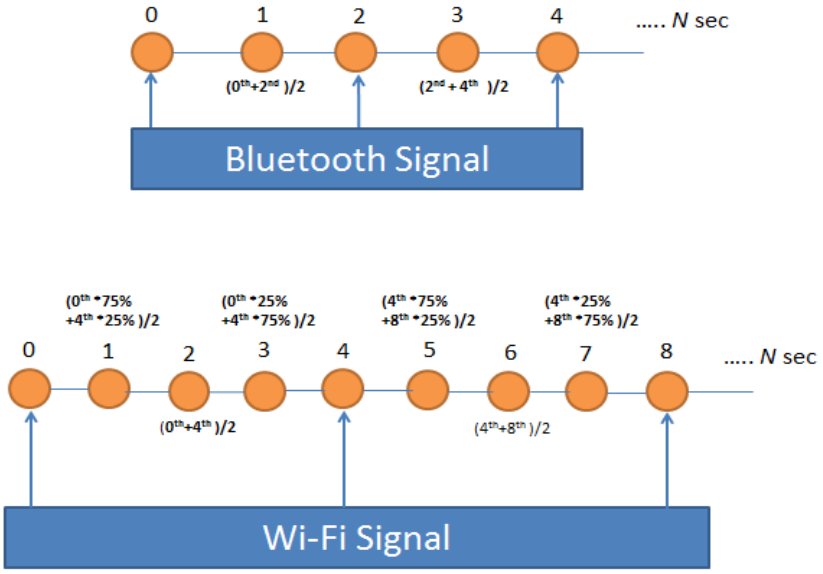


Figure 5-28 Wi-Fi and BLE observation and computation of missing epochs.

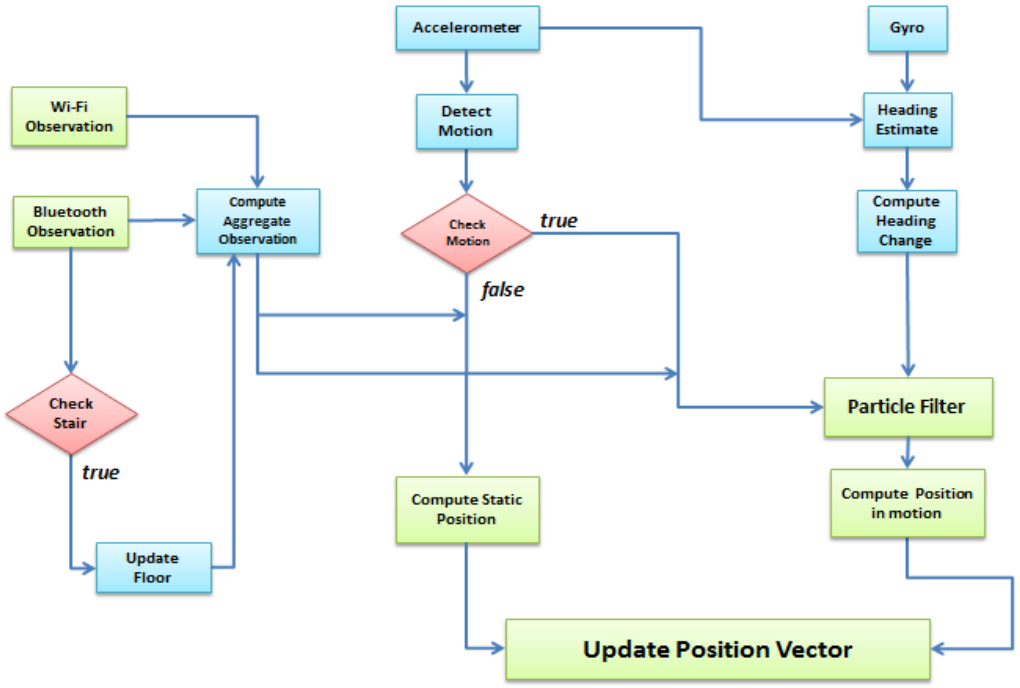


Figure 5-29 Location engine showing the different sensor integration.

(i)Particle Filter Algorithm Steps

1 Initialise particles with random heading uniformly distributed from 0-360◦ and with some uncertainty around the initial starting position. The initial starting position is taken from the last known stationary position already computed.

2 For each epoch check if the step-like motion is detected.

3 Check stair detection, if true, record stair number and repeat step 2 else go to step 4.

4 Prediction state: If step-like motion detection is true propagate particles forward based on heading and step length. Step length can vary depending on person's height, weight, and context. Also, step length can vary significantly if a door is encountered or if the person stops for a few seconds; this situation is taken into account as well to simulate a realistic scenario as much as possible. All the values are based on experimental observation.

a. Default= 1.3m
b. Door encountered = 0.3m
c. Sudden pause = 0.8 m for next 3 seconds

5 Check for heading change (threshold 10◦) and update the particle cloud heading together with some heading noise. Random noise is added +/- 0.3 m to account for uncertainty in step length. Then the new position coordinate for each particle is predicted using the updated heading and step length.

6 Update State: Use map matching to constrain particle movement within walls and corridors by checking if a particle crosses a wall. If a particle crosses a wall without a door within 0.5 m vicinities, it is given a zero weight. Then each particle is given weight from the RSSI difference map directly. Then the particles are normalised so that

$$\sum W_{Pt} = 1$$

7 Re-sampling: After the update step, the effective particle size with non-zero weights is taken, and multinomial re-sampling method is employed to re-sample the particles based on their weights. A particle trajectory history was kept, and this is also resampled. This ensures the characteristics such as heading, position and weight of the fittest and longest surviving particles are copied to the old ones according to the equation

$$Pt_{new} = Pt_{old} + \epsilon.$$

If the effective number of particles with non-zero weights become zero, we reinitialise the particle distribution to the previously computed Wi-Fi/BLE position with the random heading distribution of 0 - 360◦. Finally, compute the effective median position from the particle history and repeat from step 2.

The position vector is then updated with the newly computed position from the particle filter. In epochs when stairs are detected, the position matrix is kept null but labelled separately with the stair number to facilitate floor transition and stair identification.

5.6 Location-Engine Validation

Trials were carried out in Floor B of the testbed configuration shown in Figure 4.13 to verify the positioning system developed against ground truth obtained from a robotic total station. During the trial, the total station was given the coordinate system of the navigation frame and the starting point for each trial and used to compute the position of the participant. The researcher then walked along the tracks marked with tapes on the floor, holding the reflector prism all the time. During the trial, the phone was kept in the pocket with the data logger running in the background. The series of plots in Figure. 5.30 and 5.31 shows results from the trials with the computed trajectory in red from the location engine against the trajectory from the robotic total station. The positioning output from the particle filter suffers from significant drift, mainly due to the fluctuation of weights from the BLE and Wi-Fi observations. The variation of the radio signal seems to be high and gets skewed at times from dominant BLE beacons nearby, thus pulling the trajectory towards them. It can be seen from the BLE beacon deployment of Floor-B in Figure. 4.13, the two beacons in the left side of the open plan room would skew the positioning output whenever the signal strength from the right one is weak or not as strong as expected. Also, any movement in the top left will be pulled down, and bottom right would be pulled up due to the dominance of any individual beacons nearby as evident from some of the plots. The location of the BLE beacons deployed seems to play a significant factor in the skewness and drift of the filter. If the BLE beacons were placed at a more regular interval more densely, it may be that the weights of the particles would have varied more uniformly with a change in position every epoch. In general, the accuracy of the positioning output shows accuracy within 5m during motion from observation, but this can have a significant impact on occupancy detection when detecting movement in smaller rooms and corridors.

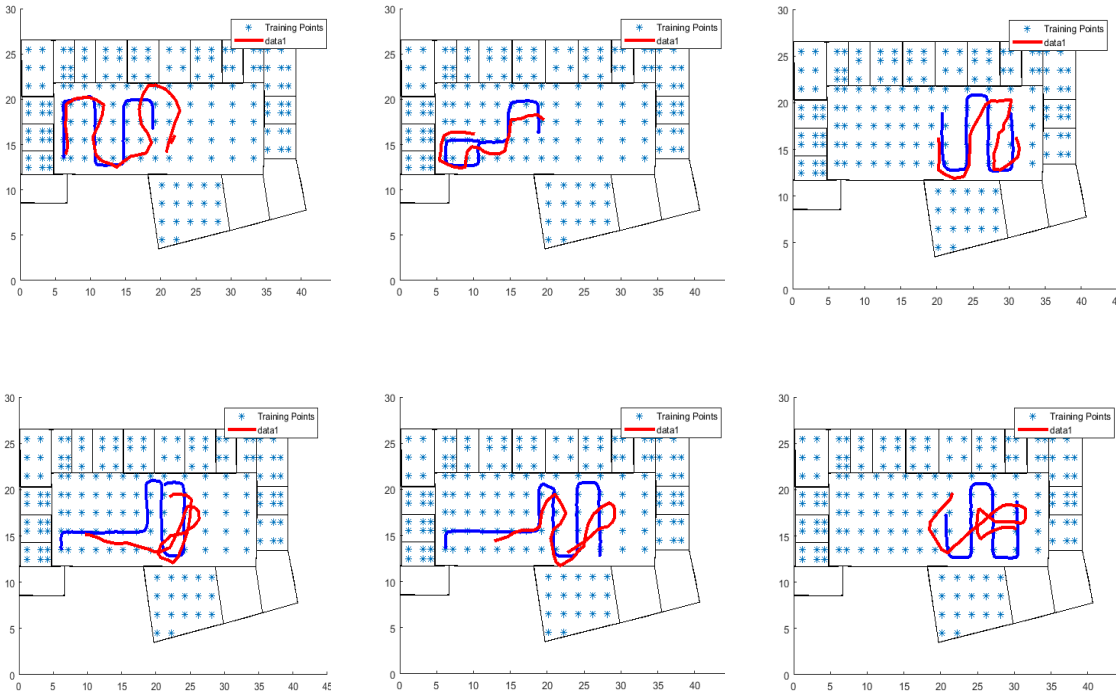


Figure 5-30 Validation of the positioning system, showing the computed trajectory in red and blue trajectories from the robotic total station as ground truth.

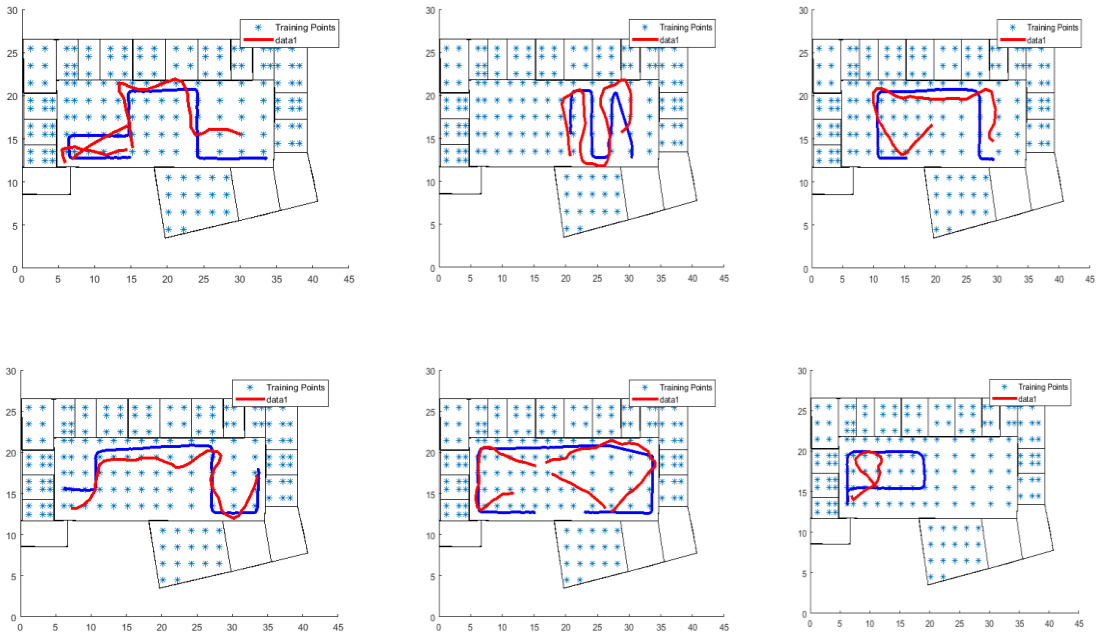


Figure 5-31 Validation of the positioning system, showing the computed trajectory in red and blue trajectories from the robotic total station as ground truth.

5.7 Discussion

This chapter discusses in detail the implementation of different components of the positioning system; heading estimation, motion detection and Particle Filter Engine and their integration with Wi-Fi/BLE radio map observation into a fully functional pedestrian dead reckoning system. The chapter provides the reader with detailed information on the implementation of each algorithm and techniques followed. Each component is tested and validated, and their performance analyses done using an objective manner were appropriate.

After analysing the experimental results of the heading estimate, it can be concluded that the Mahony filter provided a satisfactory result when it comes to accurately identify heading changes during turns. It was relatively simple to implement compared to the other techniques discussed and performed well with the sensor fusion technique proposed for the positioning system in this work. Of course, any one of the other techniques could have been used if it provided the heading accuracy and performance required for building occupancy detection, which Mahony filter successfully achieved. The continuous measurements acquired were almost drifted free, and the heading estimate computed during walk trials were stable over long periods.

Motion detection algorithm also produced a robust performance, required for a reliable step-like motion detection solution. The state-of-the-art techniques were simple to implement yet efficient and effective. Detecting actual steps based on the smartphone's accelerometer data when in the pocket is complicated and requires the implementation of complex algorithms discussed earlier. We decided to investigate the novel approach of motion detection by combining two motion detection techniques; peak-valley and DFT and did a complimentary check on each other acting as a high pass and low pass filter. The motion was constrained to walking since participants are not ideally expected to run around in office buildings. Also, the placement of the phone was limited to the pocket only during data collection.

The state estimation from particle filter suffers from poor weight allocation due to fluctuating signal quality of the Wi-Fi APs and BLE beacons, evident from plots in Figure 5.30 and 5.31. The drift in the trajectory can be attributed to the unpredictable radio signal strength (RSS) from Wi-Fi and especially Bluetooth beacons. Apart from typical attenuation and multipath the signal quality is degraded further due to the extra layer clothing from keeping the smartphone in the pocket and it would seem the placement of Bluetooth beacons seem to affect the quality of signal reception in the smartphone significantly. The asymmetric placement of the beacons seems to develop overlapping signal distribution over the area, causing skewness in the movement of the particles at each epoch. In terms of positioning accuracy obtained, the results were within 1m to 5m as seen from most of the plot. The computed position would generally follow the trajectory obtained from the robotic total station except in cases when they suffer from drift. When it comes to occupancy monitoring this level of accuracy is sufficient enough for zone level and room level detection but it needs to be seen how it performs when required to correctly detect occupancy of a person in narrow areas like corridors or small rooms during motion, but that can be verified once we carry out the multi-user multi-floor occupancy trial with non-expert participants in the next chapter.

In general, the positioning system developed in this chapter is functioning correctly; producing reliable positioning output required for occupancy detection and can be used for extensive trial with non-expert participants covering different parts of the building. This chapter highlights the successful completion of Step 5, 6 and 7 towards achieving the first objective of the thesis and also Step 8, completing half of the second objective as outlined in the thesis plan in Chapter 1. In the next chapter, the positioning system developed will be put to the test in the form of extensive real-world trials to verify its capability in detecting building occupancy; the core aim of this thesis.

Chapter 6

MULTI-USER POSITIONING TRIAL

6.1 Introduction

Detecting building occupancy at an individual level requires a robust and user-friendly indoor positioning system to be deployed and tested under real-world conditions. It is of paramount importance that the trial conditions and testbed scenario can reproduce a similar pattern of occupancy likely to be experienced by any building occupant. Only then will we be able to observe the limitations of the positioning system when exposed to such complex navigational conditions and identify areas of possible improvement. We have seen that the capability of the indoor positioning system developed in the last chapter has been validated using a robotic total station to ensure it is in working condition. The validation involved a series of trials across multiple tape marked routes in an open plan office room of the NGB. The positioning system now needs to be rigorously tested, covering tracks involving multiple floors and stairways of the building by a non-expert user to verify its capability and limitations. The performance of the positioning system will also impact the quality of the positioning data to be collected and consequently affect its contribution to the improvement of building occupant modelling.

In this chapter, we will discuss the results from multi-user trials carried out with the positioning system developed for detecting occupancy in buildings. The outcome should also verify the positioning system's capability of detecting building occupancy in the generic term against a set of performance specification essential for the developing occupancy model and building performance simulation.

The first part of the trial is carried out by the researcher himself to evaluate the stability and performance of the positioning system involving trajectory routes combining multiple floors in the Nottingham Geospatial Building (NGB).

In the second part, a comprehensive and large-scale trial is designed in the form of spatially distributed Lego building tasks where the Lego bricks are spatially distributed across the two floors of NGB. The non-expert participants (22) are provided with instruction sheets defining the objectives and time limitations. The participants are not provided with any guidance, and the researcher would simply shadow the participant's movement and note down their occupancy rooms and times with a stopwatch as they go about their way. Since the participants are free to choose any route they prefer, it is not possible to validate the positioning output against any ground truth to enable a quantifiable comparison between the real and the estimated trajectories. As such, this note is used to validate the output from the positioning system in terms of occupancy of different rooms and corridors during the trial.

The main objective of the Lego trial is to recreate a natural everyday occupancy scenario where participants move around the building, completing everyday tasks without any hindrance and analyse the performance of the smartphone-based positioning system. The positioning system is analysed by comparing the determined sequence of places visited versus manual observations, timing, number of filter failures / restarts, partially correct trajectories (due to limitations of the particle filter and inferior weighting from Wi-Fi/BLE signal strength) or failures due to wrong heading estimation, step counting, data logger initialisation and missing stair detection etc.

6.2 Testbed Configuration



Figure 6-1 Nottingham Geospatial Building (NGB), Floor A and Floor B, respectively.

The Nottingham Geospatial Building is at the Jubilee Campus, University of Nottingham. It is a three-story state-of-the-art building housing academics, PhD students and researchers. The trials are carried out covering the first two floors of the building. In total there were 8, Wi-Fi APs marked red in Figure 6.1 transmitting in both 2.4 GHz and 5 GHz frequencies. Floor A had 15 and Floor B had 10 BLE beacons deployed, marked in green according to Figure 6.1. The range and power of the beacons were configured according to the required area of coverage to ensure there is enough variability of the radio signal across the floor. BLE beacons were also used to detect the transition between floors. The Kontakt BLE beacons range can be configured from their admin panel, and they are tuned to the minimum to ensure detection only when passing by. NGB had three stairs, and the appropriate numbers of beacons were placed on each stair to detect an individual's entire journey time through the stairway. The beacons for each stair also act as a label, thus providing the stair information as well. This helps to identify the transition from one floor to the other, and the stair information helps to locate the entry and exit when transiting between floors. The custom built Android-specific data logger developed earlier could log Wi-Fi, Bluetooth, accelerometer and gyro data together with system time information in separate files. The data collection rate of the accelerometer and gyro was configured at 50Hz and Wi-Fi and Bluetooth was configured at every second for the trials.

6.3 Bluetooth Beacon Deployment challenges

Since Wi-Fi APs are already installed within the building, there is very little that could be done to place them in the building for optimal performance effectively, but the deployment of Bluetooth beacons is a challenge and significant for reliable positioning performance. One of the pitfalls is placing the beacons too low or high up on the walls. In the former case, building occupants may take them down out of curiosity or even steal them. In the latter, the signal reception may be insufficient or might overlap with the other beacons. Since beacons send out Bluetooth signals, they are easily obstructed by any physical barrier so it is essential to minimise interference from certain materials such as metal or poorly shielded cabling.

It is also essential to make sure they stick to their place and do not fall off. Strong adhesive tape or blue tack should be used when placing the beacons on the walls. If the beacons do not stick well enough to their walls and keep falling off, it will undoubtedly trigger a complete failure of the positioning system since we are using pre-built radio fingerprint map for both Wi-Fi and BLE and they are time-consuming and exhaustive to build.

Throughout the trial, we faced similar situations at the beginning, and when we were lucky, the fallen beacons would be returned by other occupants. In the worst case, the beacons lying on the floor would be thrown away by the cleaning staff, messing up the whole positioning system. To manage beacons effectively, we used the Kontakt Beacon management system (kontakt.io, 2013) where we could configure the beacon power and range and play with other settings as required. All the beacons in use were registered and could be managed effectively from the admin panel. One of the good aspects of Kontakt beacons is their battery health monitoring, which can easily be tracked and pre-emptive action can be taken when the battery is nearing the end for any beacons.

All these issues contribute to the performance of a reliable positioning system and are one of the main reason for weak signal variability of our beacons throughout the floor and poor reception at places with overlapping radio signals in the fingerprint map which triggers allocation of unpredictable weights to the particle filter during participant movement.

6.4 Occupancy Trial Experiments

6.4.1 Preliminary Trial results and analysis

Initially, before starting the main trials with non-expert participants, some preliminary trials were conducted to ensure the positioning system is functioning correctly and capable of providing positioning solutions covering multiple floors of the building. The trials were carried out by the researcher himself, keeping the movement as natural as possible, starting from both sitting and standing positions. The smartphone is kept in

the trouser pocket during the trials with the Android data logger running in the background and recording data continuously. All the trials were done in a walking state only. The red trajectory on each plot is the aggregate position (median) from the particle filter, and the yellow ones are the position of the particle at the end of the trial. The blue colours highlight the maximum spread of the particle distribution and their historical positioning coordinate before being replaced by more fit particles during the resampling process of filter state estimation. The trial plots on different floors can be seen in Figure 6.2 and Figure 6.3.

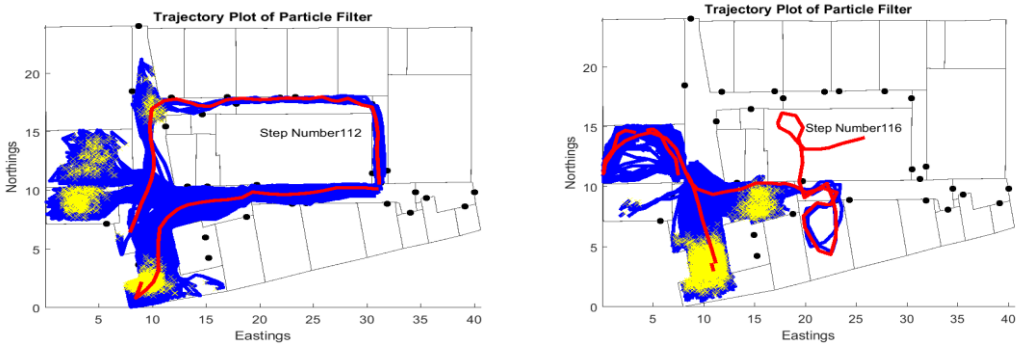


Figure 6-2 Floor A Trials showing the particle filter trajectory from two test walk.

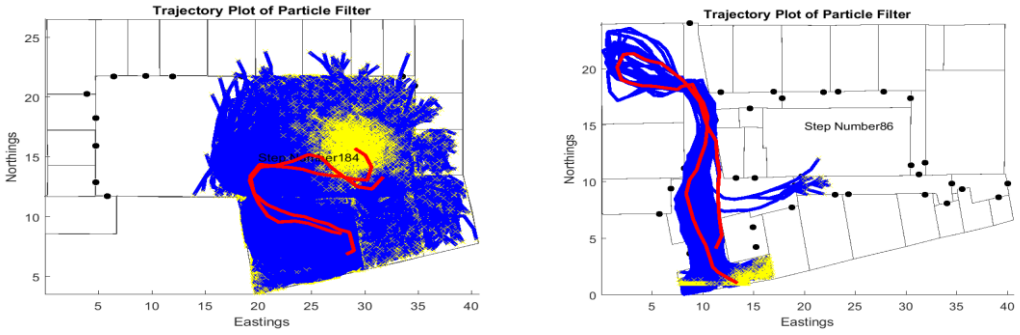


Figure 6-3 Floor A Trials showing the particle filter trajectory from two test walk.

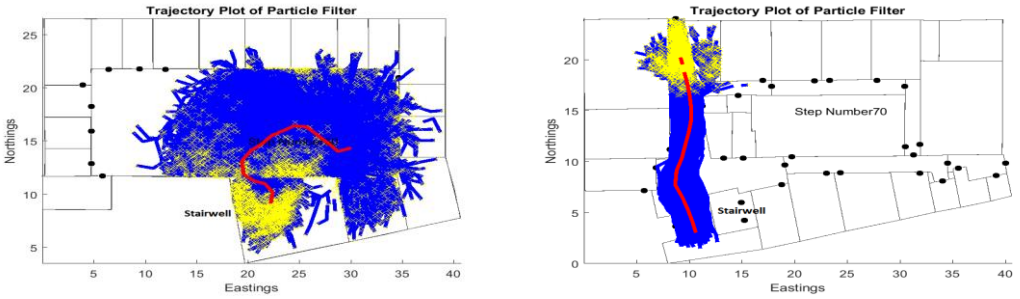


Figure 6-4 Trials combining multiple floors showing the particle filter trajectory from a test walk from Floor A to Floor B

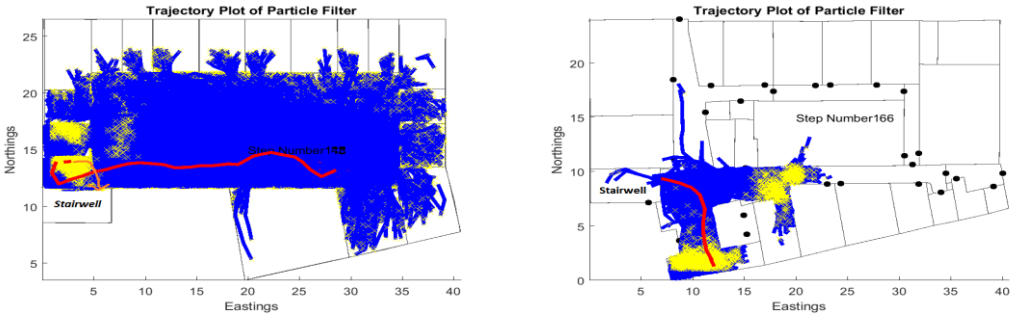
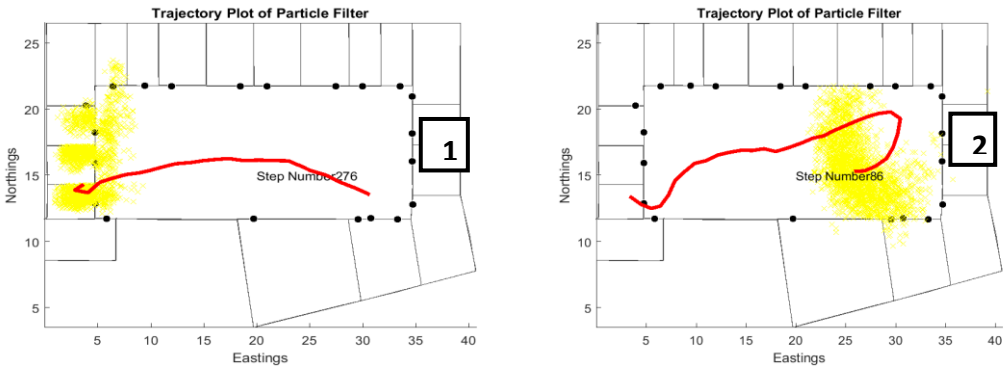


Figure 6-5 Trials combining multiple floors showing the particle filter trajectory from a test walk from Floor A to Floor B

In general, the results showed relatively good performance in terms of accurately identifying occupancy information, i.e. transition between rooms and corridors. The plot in Figure 6.4 and Figure 6.5 shows trajectories involving multiple floors and stair detection. It can be seen in Figure. 6.4, the trajectory halting in front of the stairway in Floor B and then reappearing in Floor A and then continuing. A similar trial can be seen in Figure 6.5 where stairs were detected, and the transition between floors occurred. It should be noticed that the trajectory on the left plot of Figure 6.5 should have turned a bit further after the turn and ended in front of the stair. Similarly, the plot on the right, the particles are clustered at more than one position. This happened mainly because of the particles receiving good weights from the fingerprint difference maps due to less variability and an overlapping coverage area from the BLE beacons. To ensure relatively unique signal coverage more BLE beacons could have been placed at regular intervals or important junctions. Wi-Fi has almost no impact since it has an extensive coverage area with relatively poor variability of signal strength within short distances. The map constraint helped aid the positioning significantly, especially along the narrow corridors and smaller rooms with walls. The blue part of the map shows the historical coverage of the particle distribution. The representation of the historical particle coverage is important because the more significant the area of the blue zone, the higher the uncertainty within the particle distribution when it comes to providing a reliable position update. This would significantly degrade the reliability and

consistency of the computed aggregate position at each epoch of state transition due to higher uncertainty.

To analyse occupancy detection, another trial was carried out for almost an hour involving both stationary state and movement. The plot in Figure 6.6 shows the sequence of movement when in motion only. Stationary periods involved sitting on the desk for an extended period or talking while standing in between each trajectory to mimic a realistic occupancy scenario; evident from the occupancy plot in Figure 6.7 but excluded from the trajectory plot. The corresponding occupancy plot can be seen in Figure 6.7 with the entire time series of occupancy with room numbers marked. Floor changes are detected with a short transition between the stairs. In the figure, rooms are numbered randomly and do not represent actual physical room numbers. Stairs were labelled with a negative number for ease of visual illustration only. The plot marked one on Figure 6.6, shows the aggregate median position in red almost near the wall of the next room due to the particle weight distribution from the map. The plot marked three shows the trajectory going inside the room instead of turning toward the stairs, marked in blue. This was also mainly due to most of the particles drifting inside the room due to good area coverage from beacons inside, resulting in erroneous positioning at the end. The later sequence shows the trajectory transiting to floor B through the stair as seen in plot four, then entering one of the rooms and then returning to the starting point in floor B seen in plot five and six respectively.



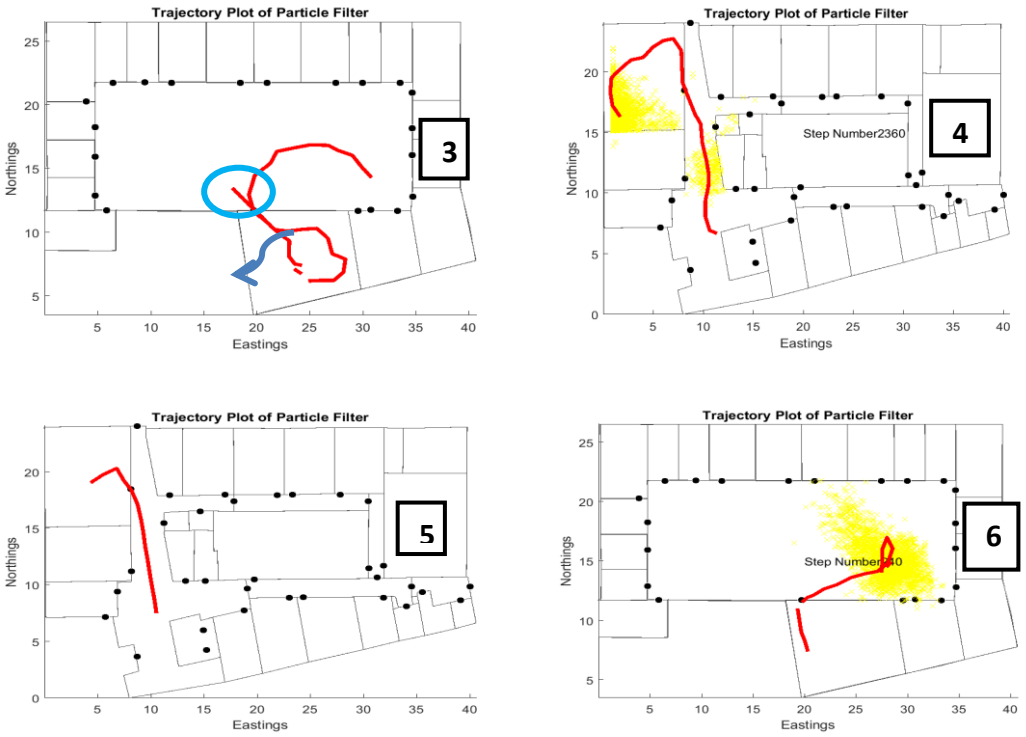


Figure 6-6 Multiple trial plots showing the sequence of movements left to right over a continuous period.

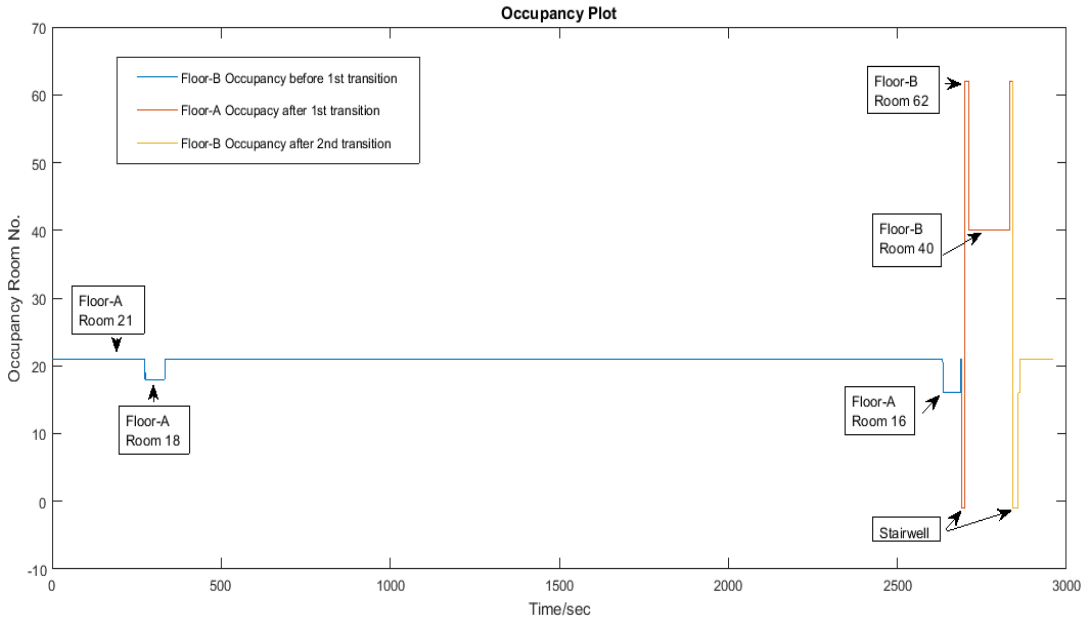


Figure 6-7 Occupancy time series plot showing the occupancy corresponding to the plots in Figure 6.6

6.4.2 Lego Trial Task Design

(i) Trial Objectives

To understand the performance of the positioning system a real-life occupancy trial is developed in the form of a Lego building task with Lego bricks, resources and model pictures spatially distributed across the NGB floors in different rooms and corridors. Non-expert participants who have no previous idea of using the positioning system were recruited with their consent and asked to complete the trials within a specified time. The main objective of the Lego trials was to observe the robustness and accuracy of the positioning system within the metrics of accurate identification of occupancy of rooms and corridors during the transition from one zone to another. At the same time, due to the availability of multiple stairways and corridors, route preferences will also be identified, which will be useful when modelling building occupancy and energy consumption in Chapter 7. There were in total 22 participants from the Nottingham Geospatial Building agreeing to participate in a total of 50 trials covering floor A and floor B. There is no statistical significance attached with the above numbers although more participants and trials are always preferred. In this case it was all that could be managed within the limited time scale of the PhD. Each participant took part in more than one trial; most of the time having a different route or a different starting location point.

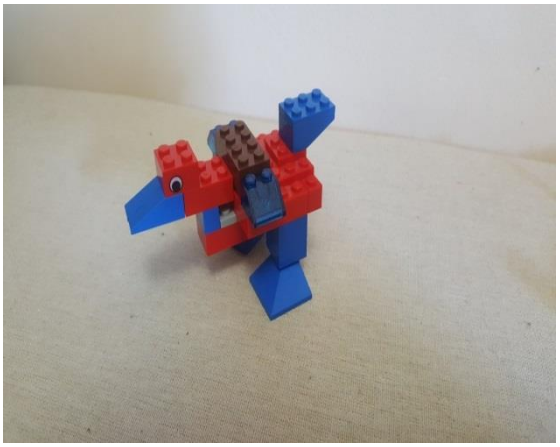
(ii) Task Description

Lego building is used to simulate daily activity during occupancy and participants were asked to move between rooms and corridors within the Nottingham Geospatial Building (NGB) to collect materials and resources for the toy brick (Lego) building task. The participants were initially provided with the floor maps and instruction sheet. They had to complete as many Lego models as they can within 20 minutes from an existing list of 8 Lego pictures; sample shown in Figure 6.8 below. The researcher started and stopped the data logger app during the task and shadows them while recording their time and location and creating a journey log in the process. The recorded data from

the smartphone is used to compute the participant's position, and subsequently, movement trajectory and the journey log is used to compare and validate the tracking algorithm.

The participants had complete control over route choices to reach their destination and were not advised or distracted by the researcher during the task. The instruction was changed for different participants by changing the location of the resources to be collected and their starting location. A sample instruction list is provided below.





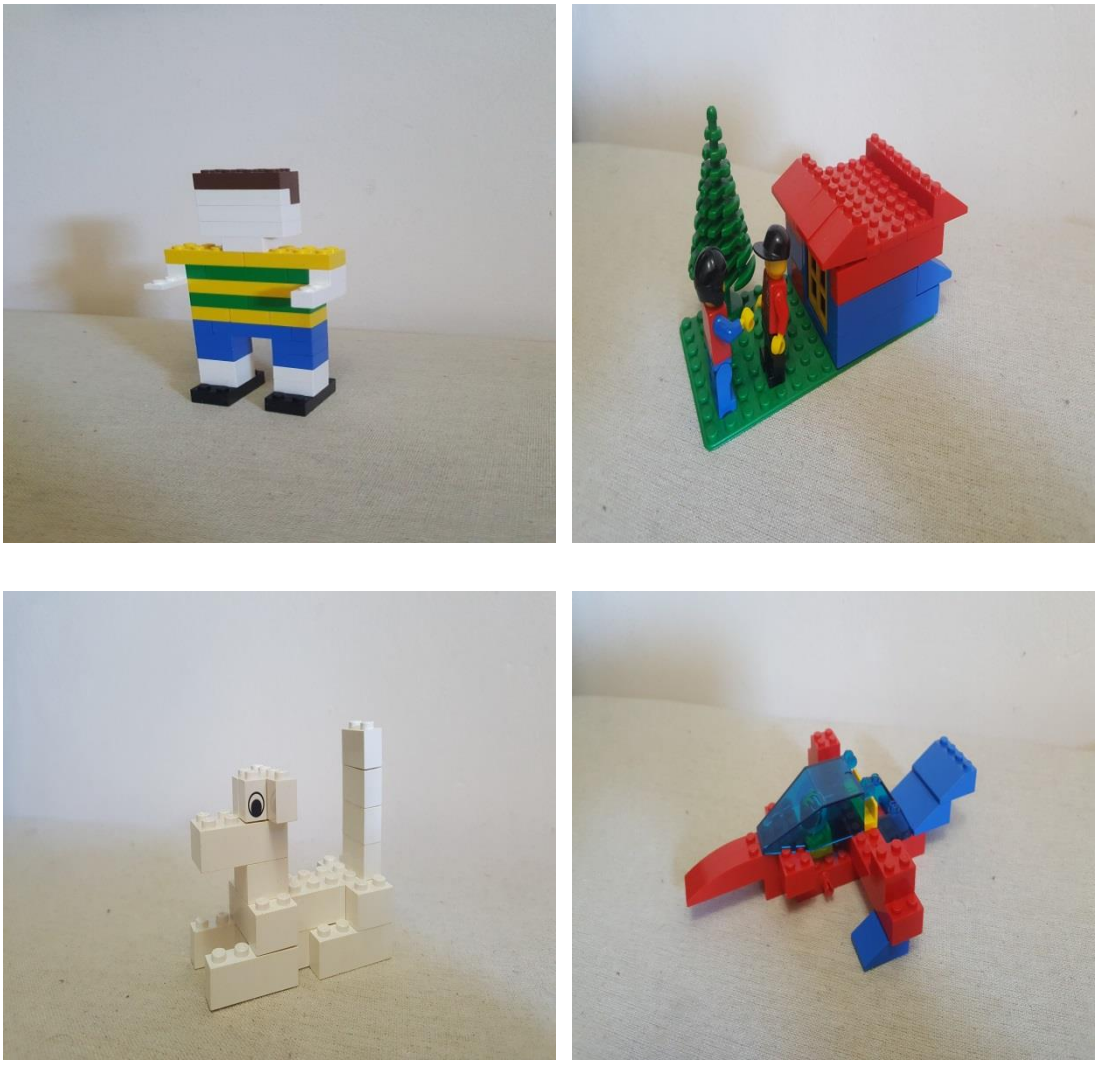



Figure 6-8 Sample of 8 Lego model picture built by the participants during the Lego trial.

(iii)Sample instructions for Lego building game

1 You will start from a desk in room B05, floor-B (to be shown by the researcher). Keep the phone in your trouser pocket and wait for approximately 20 seconds for initialisation after the data logger is started by the researcher.

2 Go to Corridor 4 and Corridor 2 (marked on the floor map) and find the Lego model pictures on the floor. There will be a total of eight pictures.

3 Keep the Lego pictures with you as well as all another sheet.

4 Take the Lego pictures in the room A20 floor- A. The Lego bricks are also kept in room A20, marked in the map. You can check the Lego pictures decide which model you want to build and gather the Lego bag. You can then go and build Lego models in room A19, Floor A. You can only take one Lego picture for building at a time. If you finish or decide to change your mind and build another one, you can check the remaining Lego model pictures in room A20 and collect appropriate Lego structures as many times as you want, but you can build the models only in room A19.

5 You will have to complete as many models as you can within 20 minutes.

6 When finished, the researcher would ask you to stop, and he will stop the data logger app for you.

6.4.3 Lego Trial results

In this section resulting plots from segments of different trials are presented, mainly highlighting different positioning errors encountered and how they impact the accuracy of the overall occupancy detection. Each trial lasted approximately 20 minutes and participants were told to follow the instruction sequentially. The instructions were varied by changing the starting location of the participants or moving the resources to different places so that we can observe occupancy across a variety of locations and routes within the building. During the trial, the smartphone was kept in the trouser pocket all the time with the data logger running in the background and continuously recording a radio signal and motion sensor data. The data is retrieved from the phone after the trial and post-processed using the implemented positioning algorithm to compute the resulting position and plotted in the corresponding NGB map as seen in the illustrations below.

The red trajectory on each plot is based on the aggregate position (median) from the particle filter, and the yellow clusters are the position of the particles at the end of each epoch. The blue lines are hand drawn (not to scale) to highlight the actual trajectory being taken based on manual observation for validation.

An illustration of the trajectory from a typical particle filter process is shown epoch by epoch following a left to the right sequence in Figure 6.9. The black markers state the weighted Wi-Fi/BLE aggregate position computed from the radio fingerprint matching technique at each epoch. You can see how the particle filter processed trajectory in red develops and how it shifts its position depending on the density of the particle cluster. The density of the particle cluster, in turn, drifts based on the weights they are getting from the fingerprint similarity map. This significantly affects the accuracy of the trajectory since the signal variability of the similarity map seems to be quite low as such sometimes much epoch is required to pull back the particle cloud to the correct path as seen in the sequence of plots. The final output can be seen in the second plot of Figure 6.10, showing the occupancy error in the computed trajectory compared to the actual route taken shown in blue lines.

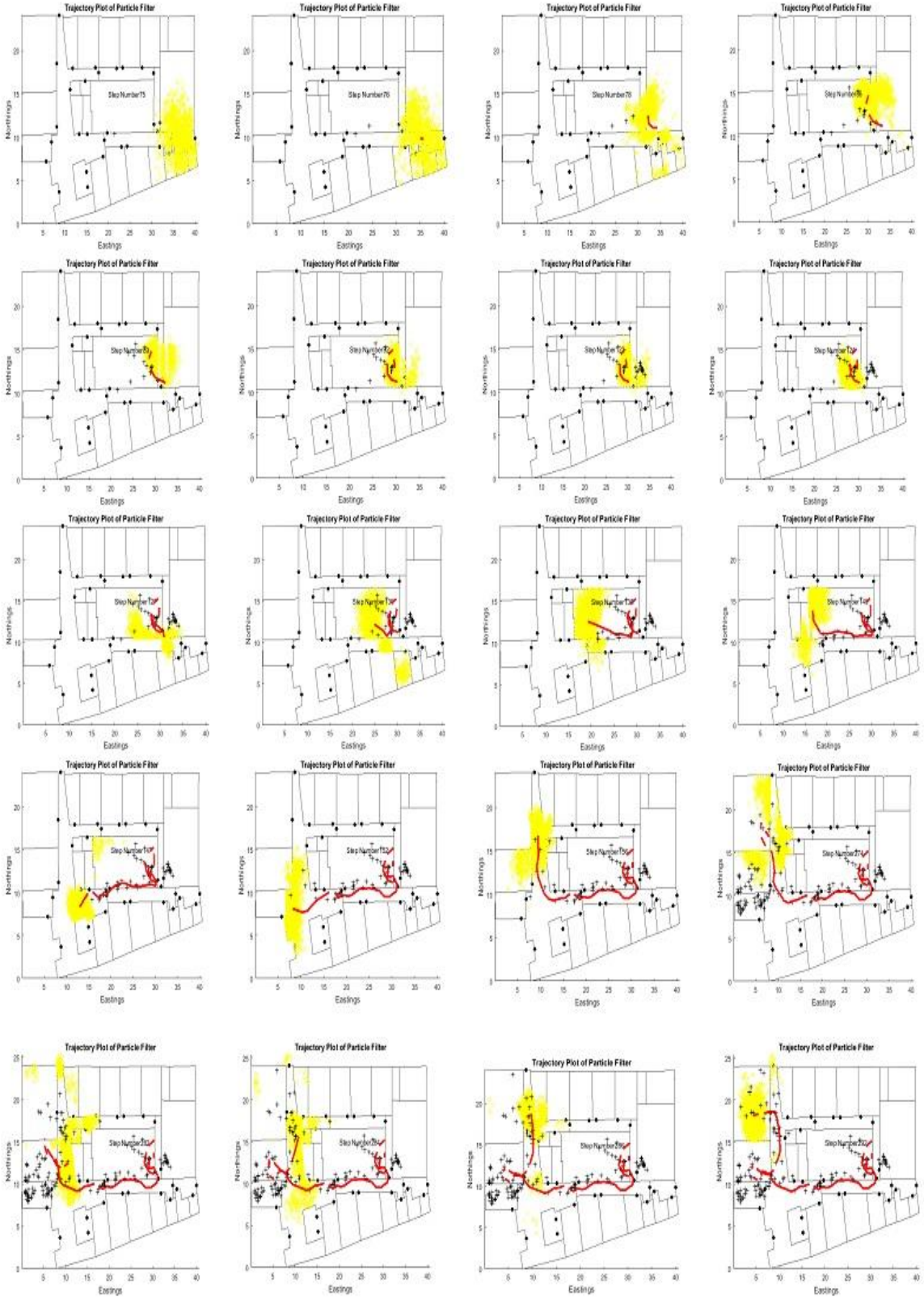


Figure 6-9 Collation of a sequence of plots from a segment of a trial showing a typical particle filter process.

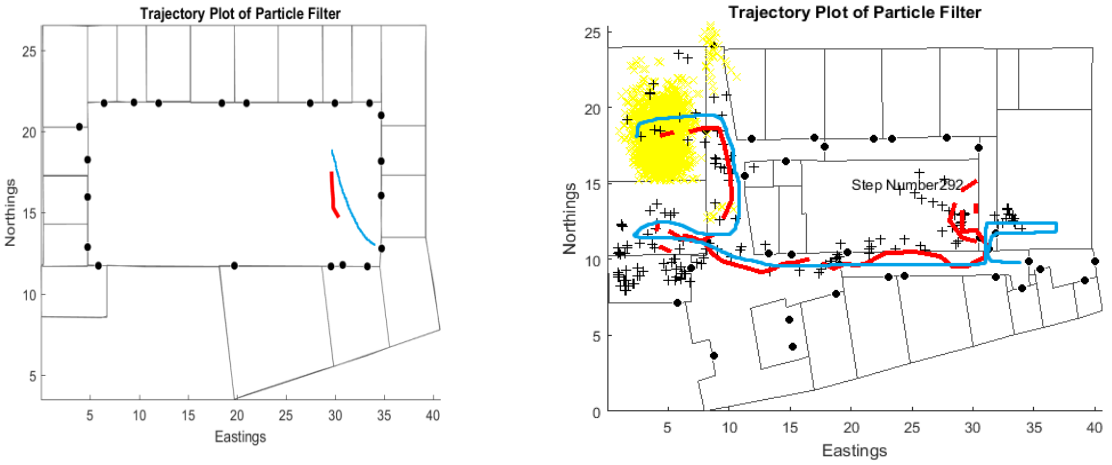


Figure 6-10 Plot showing trajectory output from a trial segment, the red line is processed blue line is an actual path.

The three plots in Figure 6.10, 6.11 and 6.12 illustrate examples of erroneous trajectory outputs from the positioning system. The error zone marked in green circles in the second plot of Figure 6.11 shows the particles stuck in a room and that they could not circumvent their way out when according to the observation the trajectory was moving toward the left shown in blue lines. Similarly, the first plot in Figure 6.12 shows the trajectory starting from inside the garage room and moving inside before coming out and entering the adjacent storeroom. This is entirely inaccurate as shown by the actual path taken in blue. The second plot shows the trajectory falling short of entering the room and thus representing an erroneous occupancy when compared to the blue lines. The plots in Figure 6.13 show a similar kind of error in the second plot after getting stuck in one of the rooms and after receiving zero weights from the similarity map for some time restarted causing a particle filter reset from the next nearest position update from the Wi-Fi/BLE radio fingerprint matching technique.

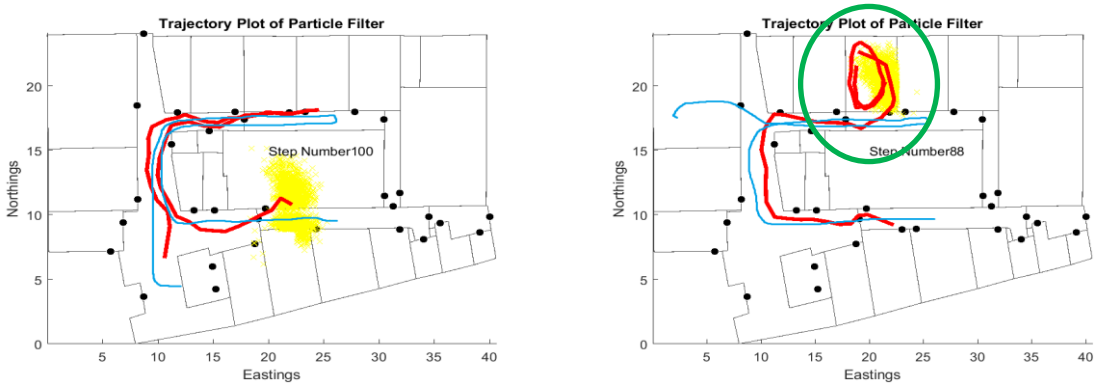


Figure 6-11 Plot showing trajectory output from a trial segment, the red line is processed blue line is an actual path.

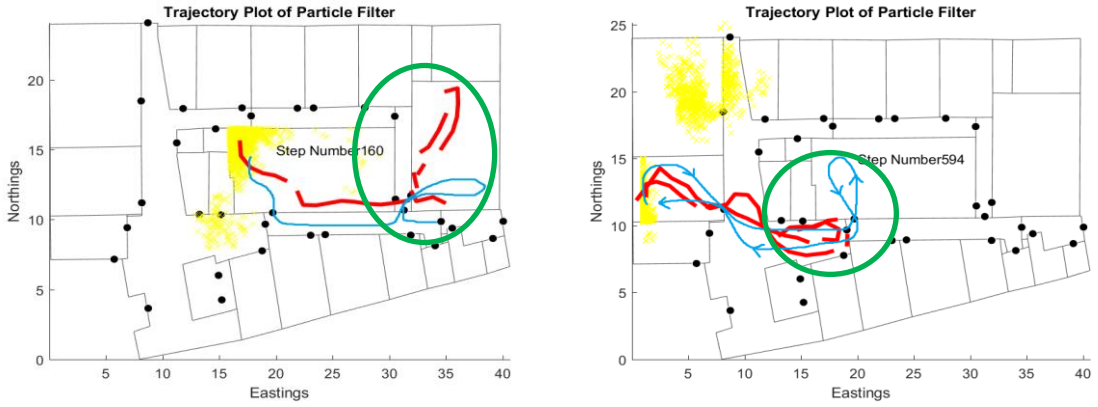


Figure 6-12 Plot showing trajectory output from a trial segment, the red line is processed blue line is an actual path.

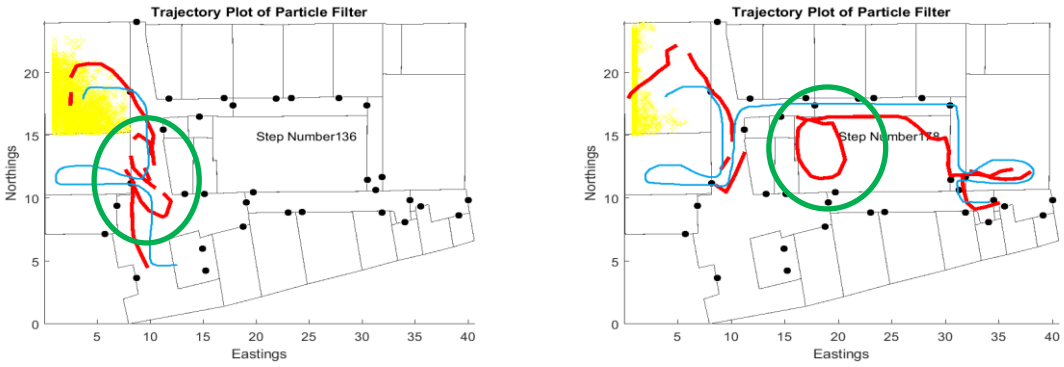


Figure 6-13 Plot showing trajectory output from a trial segment, the red line is processed blue line is an actual path.

The plots in Figure 6.14, 6.15 and 6.16 illustrate a few sample trajectories of correctly detected occupancy in room or zone level accuracy when compared to the actual route taken, highlighted in blue. Even though there are significant drifts in the movement of the particles evident from the first plot of Figure 6.14, the location engine could process the occupancy trajectory satisfactorily.

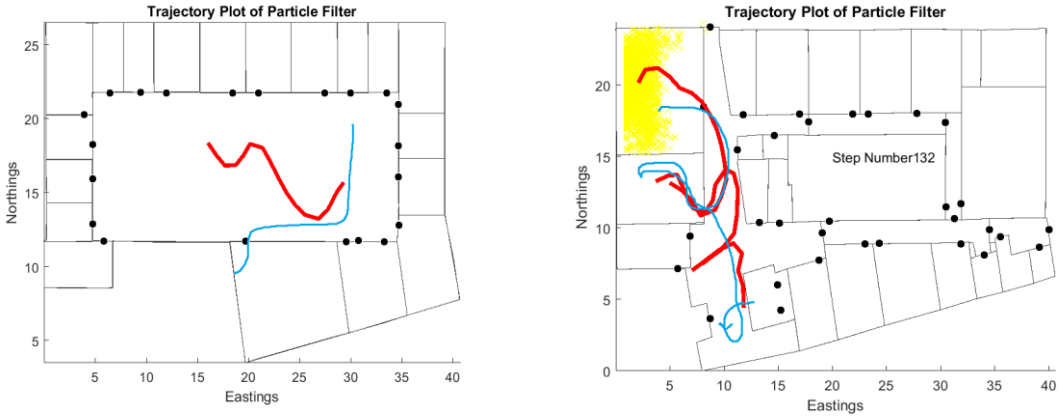


Figure 6-14 Plot showing trajectory output from a trial segment, the red line is processed blue line is an actual path.

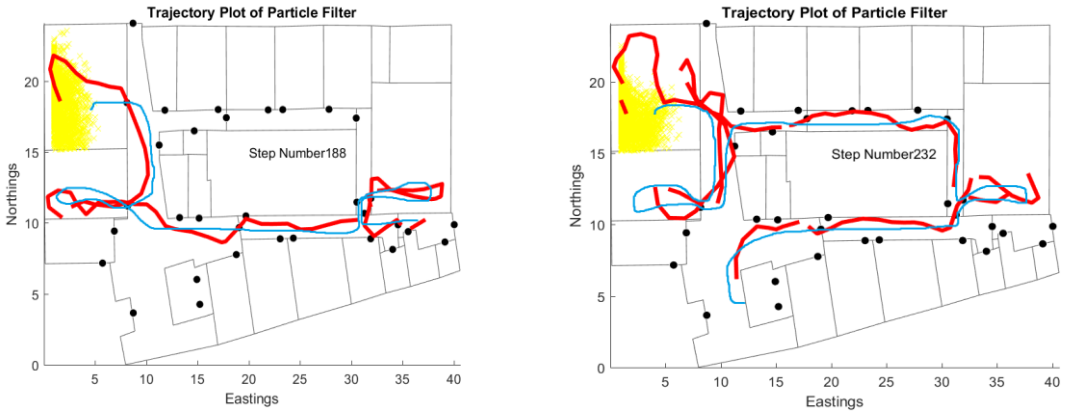


Figure 6-15 Plot showing trajectory output from a trial segment, the red line is processed blue line is the actual path.

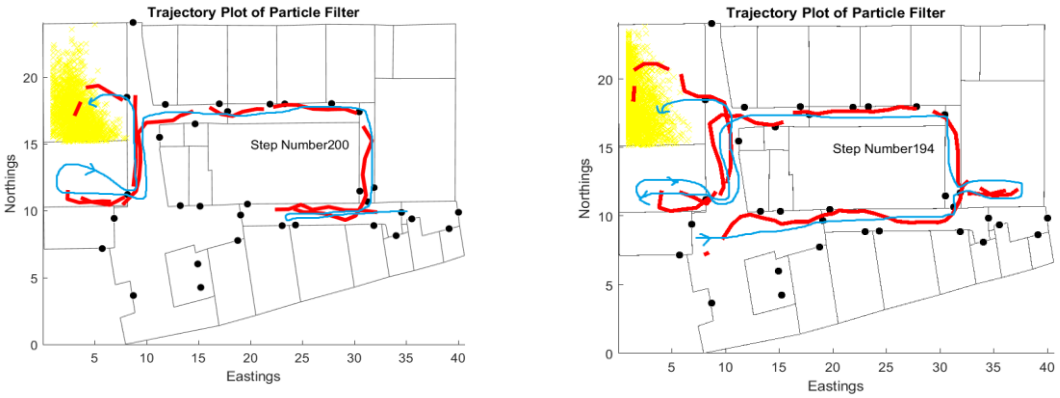
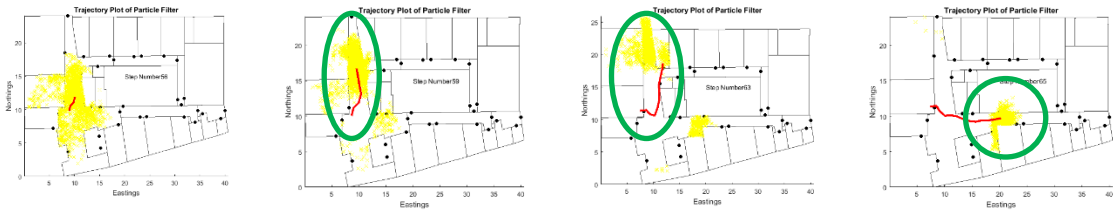


Figure 6-16 Plot showing trajectory output from a trial segment, the red line is processed blue line is the actual path.

To get an understanding of the level of drift affecting position computation from the particle distribution, we need to look at Figure 6.17 below. The plot shows the sequence of trajectory developing epoch by epoch and how the trajectory shifts its direction. The significant drift of the particles as they propagate in different direction 0-360^{o} after initialisation is seen in the sequence of plots marked in green. The particles split in two different clusters at the beginning, and the majority keep on drifting in the wrong direction for quite some time. They are seen altering their path only after the majority of the particles got reweighted correctly during the resampling process of the particle filter. This is again due to the reduced variability of radio signals from BLE beacons and Wi-Fi APs and has the potential to produce completely wrong trajectory output in scenarios having a shorter path.



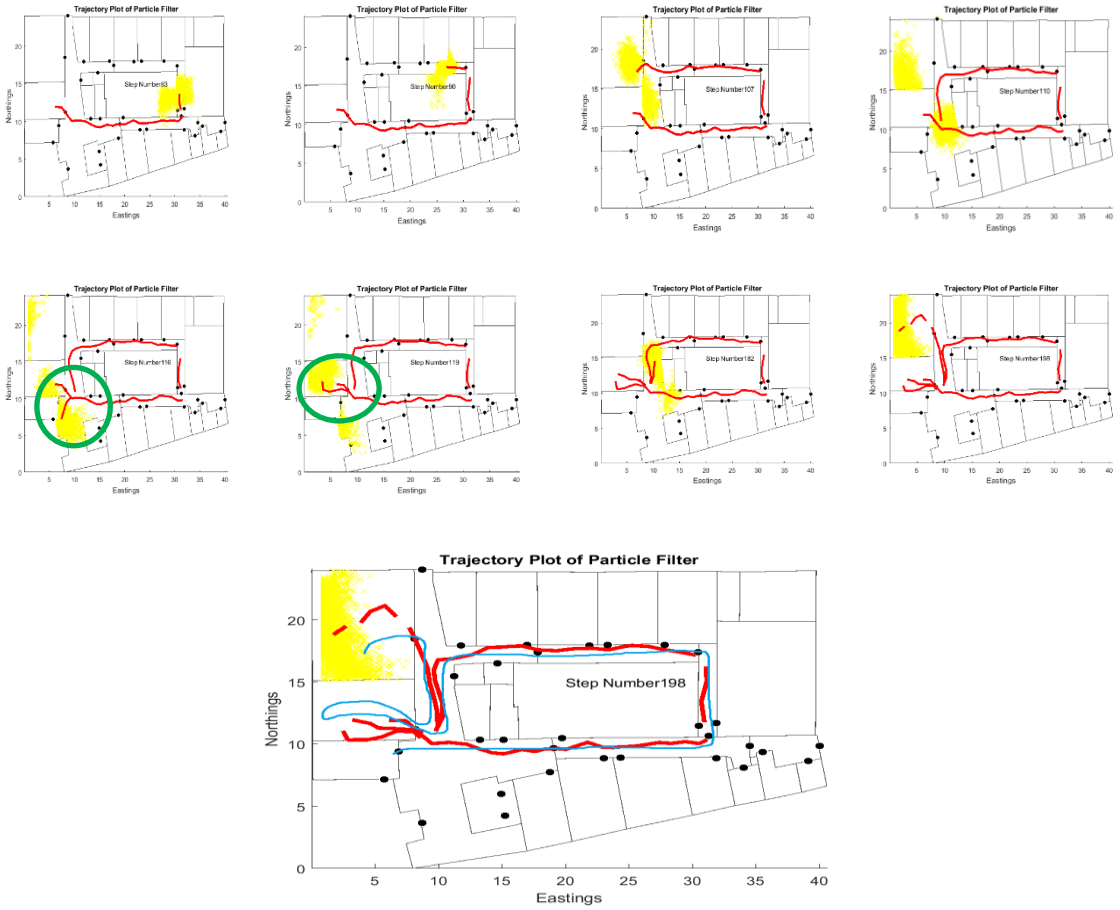


Figure 6-17 Plot showing particle drift and trajectory output from a trial segment, the red line is processed blue line is an actual path.

Step length and wrong step detection also create the possibility of trajectory going wrong. In this case, the plots marked green in Figure 6.18 shows the trajectory turning left a bit earlier before approaching the corridor on the left. This is possibly due to both generalisation of step length estimation and missed detection of steps during detection. Since the variability of the fingerprint map is already reduced and most of the particles on the corridor got de-weighted to zero due to the wall, the remaining impoverished particles got resampled to the ones already inside the room and thus altering the path completely by going inside the room. The trials were not in a controlled environment and conducted mimicking an everyday occupancy scenario with variable walking speed, posture and step length from the participants. As such, it is very likely to encounter missing steps during the step-like motion detection process, which is not possible to validate as well.

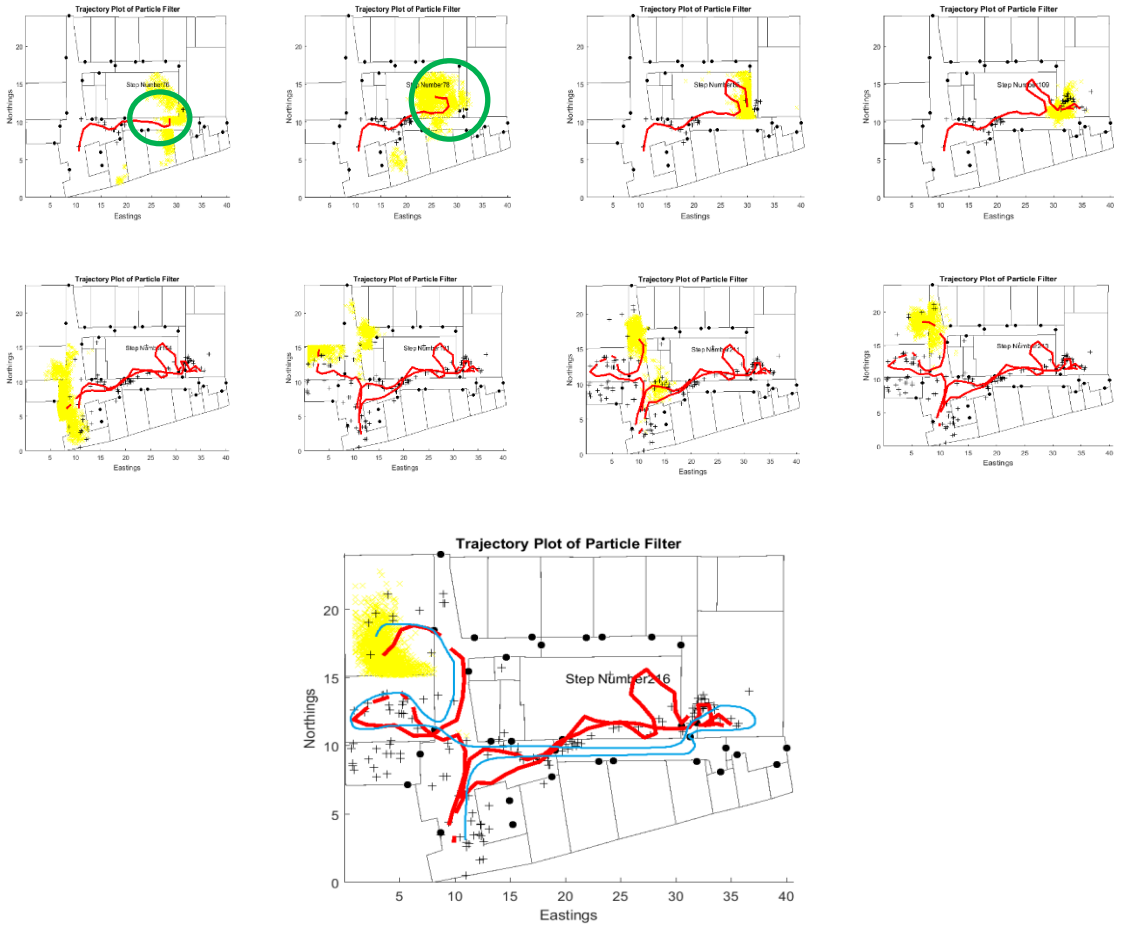


Figure 6-18 Plot showing particle drift and trajectory output from a trial segment, the red line is processed blue line is an actual path.

To get an understanding of the lack of variability of radio signals in large rooms such as the open plan area in floor B of the NGB and how it can affect the shape of the trajectory we need to look at the example of Figure 6.19. The plot shows the drift amongst the particle, completely altering the shape of the trajectory in the open plan area as it propagates epoch by epoch. It is essential to observe that during a quick transition between rooms, the Wi-Fi/BLE signal suffers from significant multipath, attenuation from physical obstacles and poor reception. Since the displacement of the body is happening at a quicker rate, the received signal strength cannot indicate the actual position-specific signal strength during a reception in the smartphone at each epoch. Variability of the overall signal strength also plays an important role in not constraining the particles in a smaller area, thus creating a more extensive overlapping of particle areas to choose the aggregate position from at each epoch.

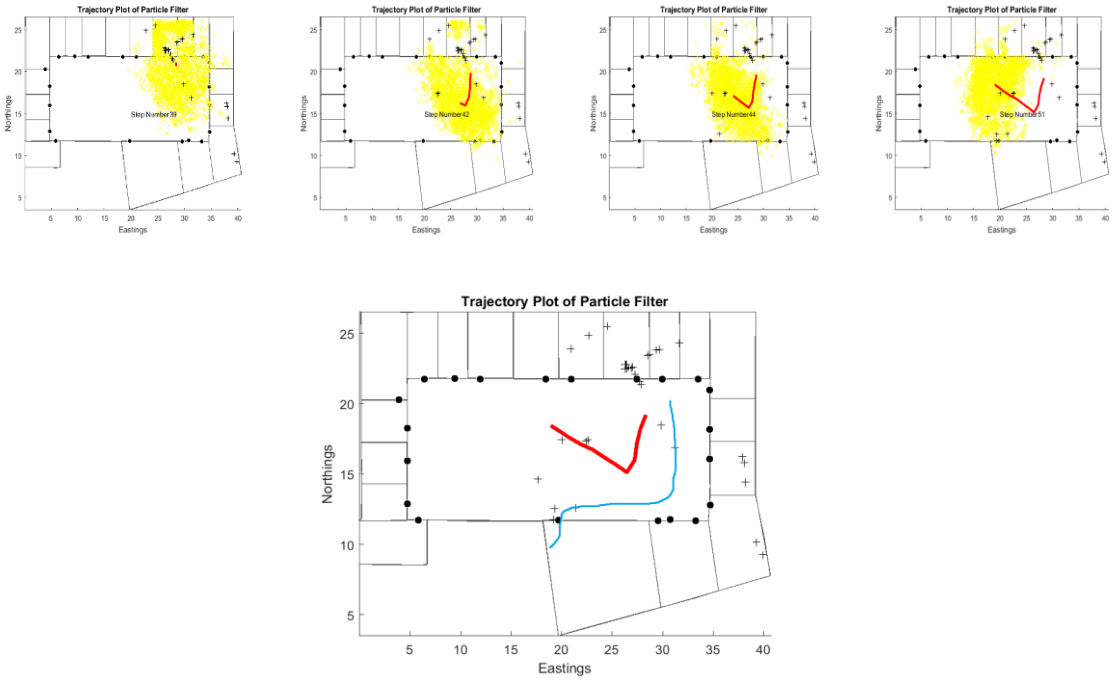


Figure 6-19 Plot showing particle drift and trajectory output from a trial segment, the red line is processed blue line is an actual path.

In most of the above cases, plots show correct trajectories of occupancy. There were occurrences of multiple distinct particle clusters in large open areas or corridors during turns. Also, since in our research, the step length model is rigid and we are detecting step-like motion and not actual step, participants with different stride patterns might cause particle propagation in the prediction state to overestimate or underestimate the new aggregate position at each epoch. Participants handling of the smartphone may also impact the correct estimation of heading and might cause the entire trajectory to go wrong. The map matching aided the positioning significantly, especially along the narrow corridors and smaller rooms with walls but also confused the particles when there were multiple doors close to each other. These and other radio signal related phenomenon cause significant positioning error or inaccurate aggregate-positioning output.

6.4.4 Validation

In this section, some of the trial plots discussed above are processed to show the time series of occupancy during the trial against actual occupancy, recorded by the researcher when shadowing the participants. The plots here help to validate the

trajectory shown above and show the time lag present between the processed and the recorded occupancy. Table 6.1 indicates room numbers against corresponding occupancy rooms and the plot legends. Time lag between the computed trajectory and recorded trajectory show the latency the particle filter engine suffers when computing the position estimation. Many factors come into effect such as missing step detection, step length and the quality of Wi-Fi and BLE radio signals when trying to identify the underlying cause. Also, time lag does not always imply lagging behind but sometimes due to overestimation can move the occupancy lines ahead of the recorded ones. We can see from the plots that the order of time lag is in seconds and not significantly higher, but from a navigation and positioning systems point of view, this is a drawback which may impact other external functionalities synchronised for the real-time update. Notably, application areas requiring time-specific occupancy information such as smart buildings need to get time-specific information to identify occupied and unoccupied periods of rooms, corridors and stairways to adjust heating, ventilation and air conditioning of the building for energy efficiency. In such applications, the occupancy information will be ideally used to develop stochastic time series models which should be able to tolerate up to a certain degree of time lag as long as it does not differ in the order of minutes and hours. The time lag can be adjusted and smooth out with some confidence level during the pre-processing data stage as such we find the level of time lag in this positioning system acceptable for some selected applications of smart buildings related to occupancy detection.

Table 6-1 Table shows the validation plot legends and the room numbers for respective occupancy corresponding to Figure 19. Room numbers do not correspond to actual rooms and assigned for ease of understanding.

Room Name	Corr1	Corr2	Corr3	Corr4	Garage	Store	A20	A19	B05	Stair 1	Stair 2	Stair 3
Room No.	31	10	11	18	8	12	17	9	20	-2	-1	-3

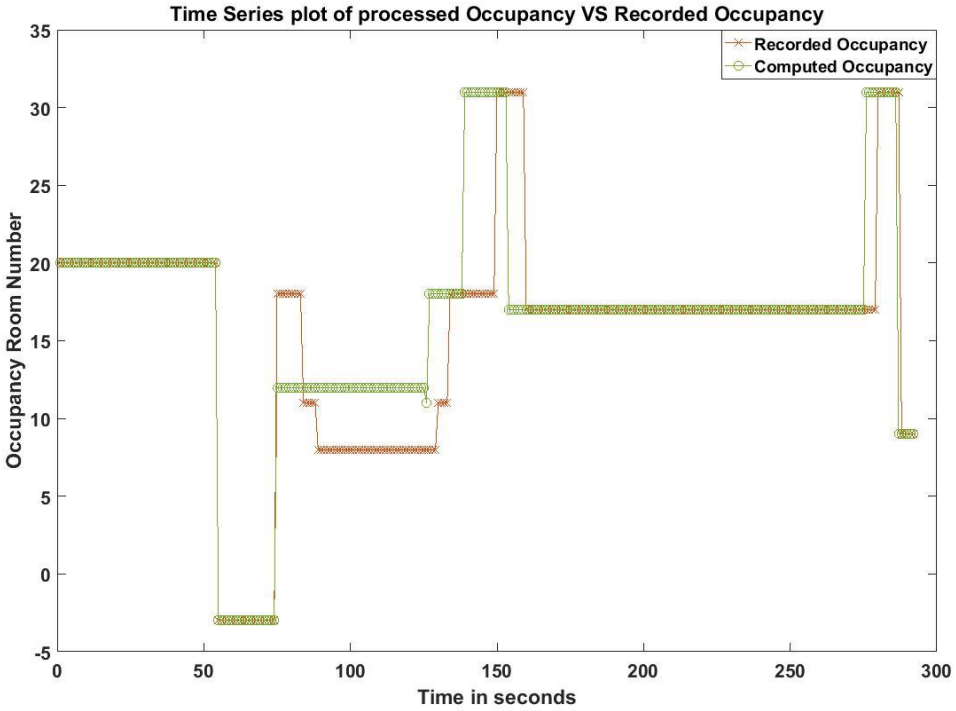


Figure 6-20 Trial validation plot of Figure 6.10 showing time series of occupancy.

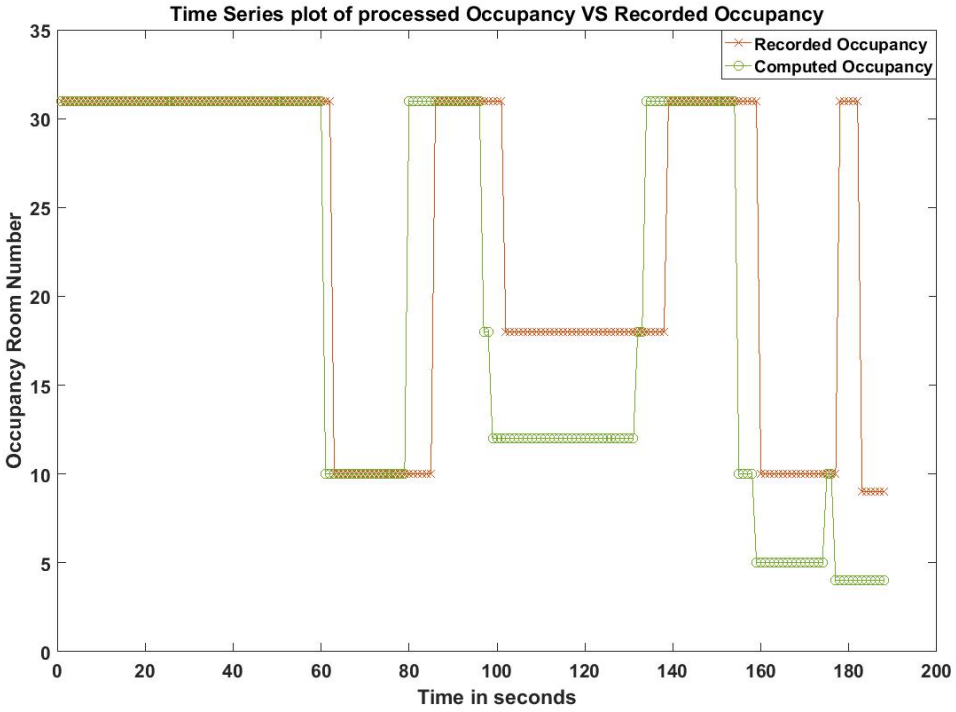


Figure 6-21 Trial validation plot of Figure 6.11 showing time series of occupancy.

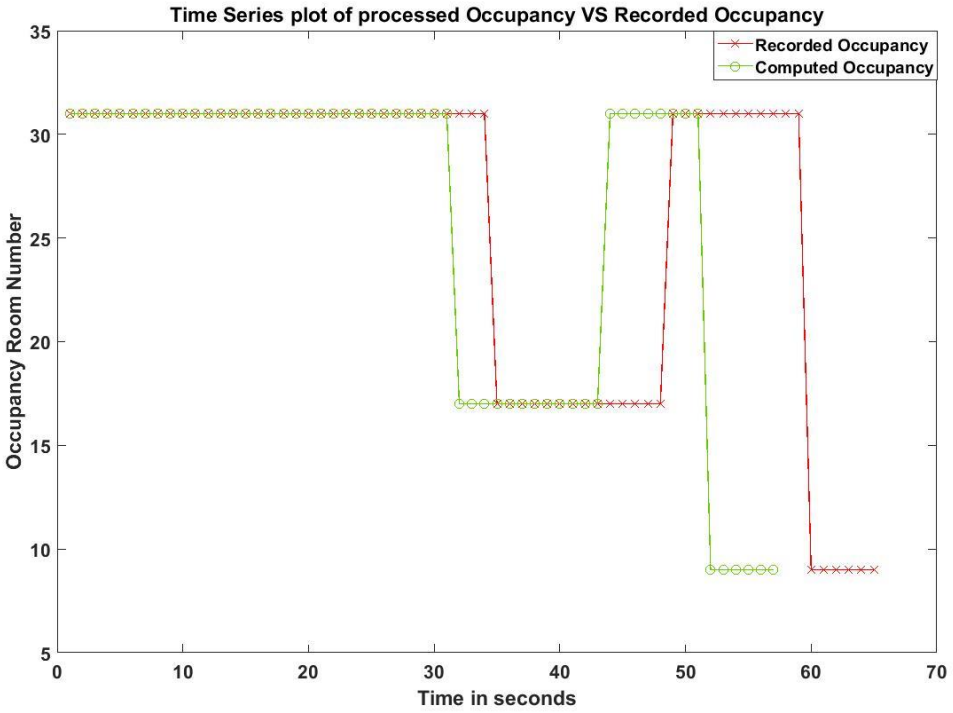


Figure 6-22 Trial validation plot of 2nd Figure 6.14 showing time series of occupancy.

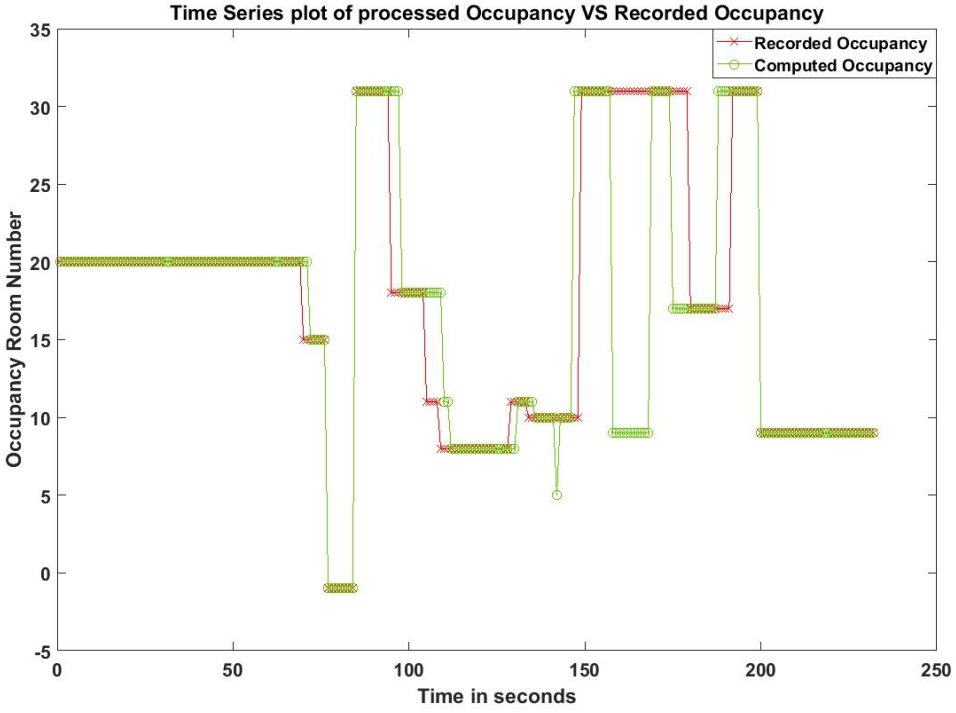


Figure 6-23 Trial validation plot of 2nd Figure 6.15 showing time series of occupancy.

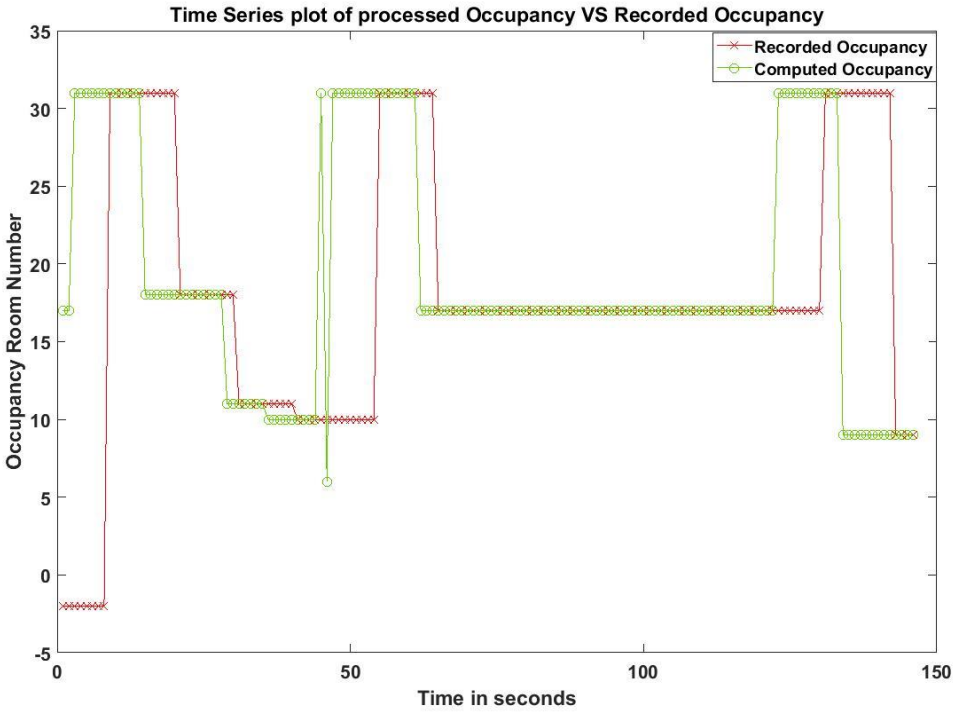


Figure 6-24 Trial validation plot of Figure 6.17 showing time series of occupancy.

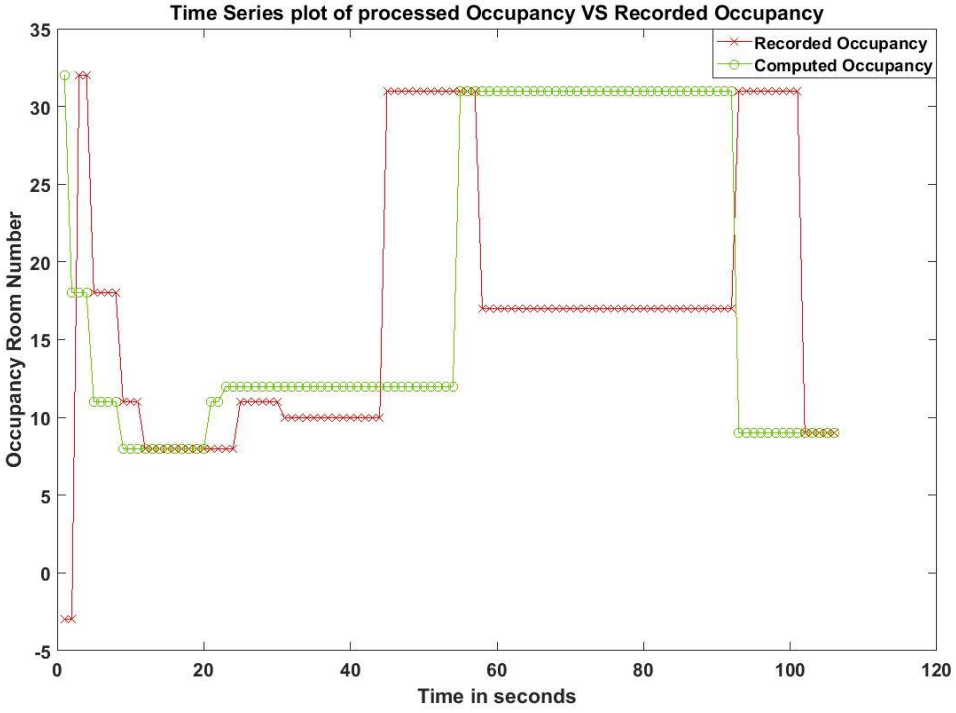


Figure 6-25 Trial validation plot of 2nd Figure 6.13 showing time series of occupancy.

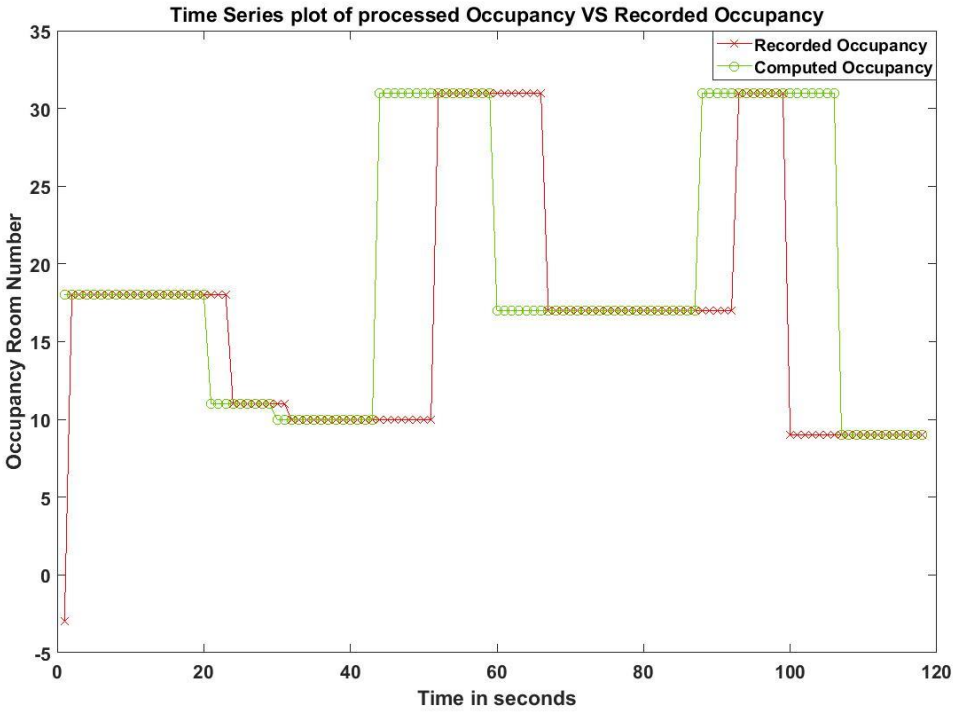


Figure 6-26 Trial validation plot of 1st Figure 6.16 showing time series of occupancy.

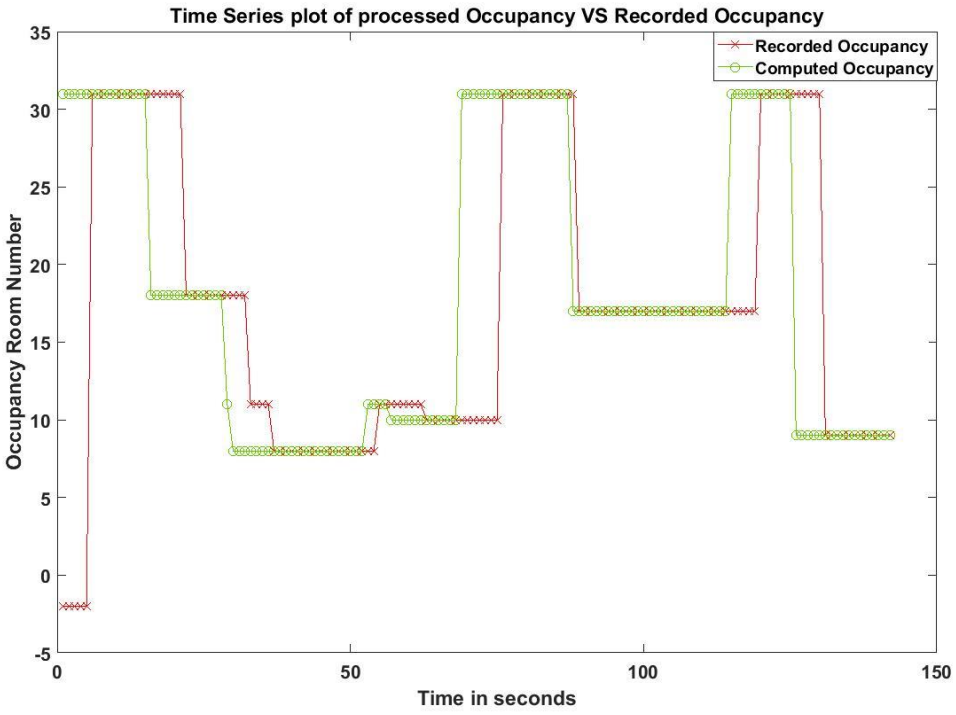


Figure 6-27 Trial validation plot of 2nd Figure 6.16 showing time series of occupancy.

6.5 Performance Specification and Analysis

To evaluate the performance of the positioning system when it comes to detecting occupancy, it is crucial to identify some key sets of the specification which can be used as a criterion to determine the performance metrics. This criterion may include but not limited to the correct identification of rooms, corridors, and stairs the participant occupies in the course of their occupancy in the building. In some cases, the accuracy level can be compromised for multiple zones comprising of multiple adjacent rooms and corridors when modelling building occupancy. Room level detection accuracy will help to identify the exact number of occupants similar to (Dodier *et al.*, 2006; Labeodan *et al.*, 2015; Jia *et al.*, 2017) if correctly identified. One of the most extensive validations of occupancy detection model is seen in the work of Page et al. (Page *et al.*, 2008) with single occupant office rooms and (Liao *et al.*, 2012)and (Z. Chen *et al.*, 2014) with multiple occupants and multiple zones. In both the latter cases, the researchers where developing occupancy models with zone level accuracy for state transition. As such we can list two level of performance specification necessary for developing any BOM.

1. Room level detection accuracy
2. Zone level detection accuracy

From our positioning solution, the continuous trajectory information has the potential to provide an apparent picture of an individual's occupancy and can also be fused with the standalone Wi-Fi/BLE observation to understand zone level occupancy like Figure 7.9. This is particularly true in situations of filter failures, or partially correct trajectories where we may not get a complete picture of the journey within room level accuracy but still manage to extract enough information to infer the overall occupancy pattern of the individual. These data can then be used to develop the occupancy model both at an aggregate level and individual level, which is nearly impossible with the existing methodologies of occupancy detection techniques discussed earlier in Chapter 3. Based on these understanding of the required performance metric we can

discuss the outcome of the trials carried out by non-expert participants to understand how the different algorithms of the sensor fusion performed when integrated, especially motion detection and heading estimate.

As mentioned at the beginning of this section, the main objective is to evaluate the robustness of this positioning system when tested by non-expert users with different motion traits; such as walking speed, height, body postures, and route choice. The overall performance can be seen in Table 6.2 for room level accuracy and Table 6.3 for zone level accuracy. We can list the performance indicator used to measure the quality of the trials against the performance specification required.

- Occurrences of completely incorrect trajectory are caused when all or a significant portion of the trajectory is computed incorrectly.
- Partially incorrect trajectory shows a wrong occupancy route computed for a part of the task, but the filter output may realign with the correct route afterwards providing enough accuracy for zone-level detection.
- Failure at initialisation implies a failure to collect data from one or more sensors due to a hardware issue in the smartphone.
- Correct trajectory implies position computed to reflect actual occupancy from the task and generally within 2 to 5 meters of positioning accuracy.

Also, there are instances of overall failures due to issues with sensor data quality such as incorrect heading estimation due to wrong time synchronisation causing the trajectory to start in the wrong direction eventually processing completely the wrong trajectory. This can also happen due to missing stair detection leading to misidentification of floor map fingerprint or significant gap in Wi-Fi or BLE data reception causing issues with data processing and in the process ending up with erroneous trajectory or system crash. Even with failures to detect occupancy trajectory accurately all the time, zone level detection accuracy was appreciable which is what most of the other occupancy detection methods, discussed in Chapter 3 tries to achieve.

Table 6-2 Lego Trial room level accuracy chart

Performance Indicator	Number of Trials
Correct estimation of occupancy	25
Failure at initialisation /data logger crashed	1
Incorrect occupancy estimation	9
Partially incorrect occupancy estimation	9
Missing stairway detection leading to incomplete data processing	1
Failure due to wrong heading estimate	3
Missing Wi-Fi/BLE signal data leading to incomplete data processing	1
Particle filter restart	1
Total	50

Table 6-3 Lego Trial zone level accuracy chart corresponding to Figure 7.9

Trial Number	Zone Detection	Trial Number	Zone Detection
Trial 1	(Z3) Floor B, St3, (Z4, Z3, Z1*) Floor A	Trial 24	(Z3,Z2^)Floor B,St3,(Z4,Z3,Z1,Z3,Z1,Z3,Z1)Floor A
Trial 2	(Z1, Z2, Z3) Floor B, St3, (Z4, Z3, Z1*) Floor A	Trial 25	(Z3) Floor B, St3, (Z4, Z3, Z1, Z3, Z1) Floor A
Trial 3	(Z2) Floor B, St1, (Z1, Z2, Z1*) Floor A	Trial 26	(Z3) Floor B, St3, (Z4, Z3,Z1,Z3,Z1,Z3*^)Floor A
Trial 4	(Z1, Z2, Z3) Floor B, St3, (Z4, Z3, Z1*) Floor A	Trial 27	(Z2, Z3) Floor B, St3, (Z4, Z3, Z1, Z3, Z1) Floor A
Trial 5	(Z3) Floor B, St3, (Z4, Z2, Z1*) Floor A	Trial 28	(Z2^) Floor B, St2, (Z1, Z3, Z1, Z3, Z1) Floor A
Trial6	(Z1, Z2) Floor B, (Z1, Z4, Z3, Z1*) Floor A	Trial 29	(Z1, Z2) Floor B, St1, (Z1, Z3, Z1, Z3, Z1) Floor A
Trial 7	(Z1) Floor A, St2, Z1*	Trial 30	(Z2, Z3) Floor B, St3, (Z4, Z3, Z1, Z3, Z1) Floor A
Trial 8	(Z2, Z1) Floor B, St2, (Z1*) Floor A	Trial 31	(Z2) Floor B, St1, (Z1, Z3, Z1, Z3, Z1) Floor A
Trial 9	(Z2, Z1) Floor B, St2, (Z1*) Floor A	Trial 32	(Z2) Floor B, St1, (Z1, Z3, Z1, Z3, Z1) Floor A
Trial 10	(Z3, Z2) Floor B, St1, (Z1*) Floor A	Trial 33	(Z1, Z3^) Floor B, St1, (Z1, Z3, Z1, Z3, Z1) Floor A
Trial 11	(Z3) Floor B, St1, (Z1*) Floor A	Trial 34	(Z2, Z1^) Floor B, St1, (Z1, Z3, Z1, Z3 Z1) Floor A
Trial 12	(Z1) Floor B, St2, (Z1*) Floor A	Trial 35	(Z3, Z2) Floor B, St1, (Z1, Z3, Z1*) Floor A
Trial 13	(Z3) Floor B, St3, (Z4, Z3, Z1*) Floor A	Trial 36	(Z3, Z2) Floor B, St1, (Z1, Z3, Z1, Z3, Z1) Floor A
Trial 14	(Z1, Z2) Floor A, St2, (Z1, Z3, Z1*) Floor A	Trial 37	(Z3, Z2) Floor B, St1, (Z1, Z3, Z1, Z1*^) Floor A
Trial 15	(Z1) Floor B, St2, (Z1, Z3, Z4, Z2, Z1*) Floor A	Trial 38	(Z2) Floor B, St1, (Z1,Z3,Z1,Z3,Z1,Z2,Z1) Floor A
Trial 16	(Z3) Floor B, St3, (Z4, Z3, Z4, Z2, Z1*) Floor A	Trial 39	(Z2, Z1^) Floor B, St1, (Z1,Z3,Z1,Z3,Z1) Floor A
Trial 17	(Z1) Floor B, St2, (Z1, Z3, Z4, Z2, Z1*) Floor A	Trial 40	(Z1, Z2, Z4, Z3, Z1, Z2, Z1, Z2, Z1) Floor B
Trial 18	(Z2, Z3) Floor B, St3, (Z4, Z3, Z1*) Floor A	Trial 41	(Z1, Z2, Z1, Z3, Z3^, Z4^, Z2^, Z1, Z2, Z1) Floor B
Trial 19	(Z2) Floor B, St1, (Z4, Z3, Z1*) Floor A	Trial 42	(Z1, Z2, Z1, Z3, Z1, Z2, Z1) Floor B
Trial 20	(Z3) Floor B, St3, (Z4, Z3, Z1*) Floor A	Trial 43	(Z1, Z2, Z1, Z3, Z1, Z2, Z1) Floor B
Trial 21	(Z2) Floor B, St3, (Z4, Z3, Z1*) Floor A	Trial 44	(Z1, Z2, Z1, Z3, Z1, Z2, Z1) Floor B
Trial 22	(Z3) Floor B, St3, (Z4, Z3,Z1*) Floor A	Trial 45	(Z1, Z2, Z1, Z3, Z1, Z2, Z1) Floor B
Trial 23	(Z3)Floor B, St3, (Z4, Z3, Z1*) Floor A		

Z = zone, St = stairway, * = movement within the same zone between multiple rooms, ^ = wrongly detected or missed zone

6.6 Discussion

The extensive multi-user trial showed promising results with the developed indoor positioning system based on their performance analysis. The positioning system proved capable of detecting occupancy of individuals both at room level and at zone level accuracy and provide useful trajectory information of route choices. The trials if extended over the entire day can provide a useful daily occupancy pattern of the building as well. This are very important information for an architect designing sustainable, smart buildings or built environment expert analysing building performance. Also, the errors in the positioning data for partially correct trajectories can be corrected to some extent by doing a post-process data analysis by incorporating landmarks and other environmental features that can help identify incorrectly detected occupancy. When it comes to the smartphone as a technology capable of providing positioning, the accuracy is generally poor. The sensors suffer from hardware latency, which may result in complete loss of data. Time synchronisation for all the sensor data is a big problem in the Android platform. Each sensor has its time parameter when receiving and logging data. It would be ideal for developing a bespoke device with all the required sensors packed together like Intel Edison or Raspberry Pi but with a customisable scan rate of Wi-Fi, Bluetooth, accelerometer, and gyroscope. The particle filter needs to be improved to account for the occurrences of multiple clusters due to reduced variability of the fingerprint radio signal. The overall accuracy may be further improved by increasing the number of Bluetooth beacons and placing them carefully with the range modified to reduce overlapping areas of similar signal strength. Also, the phone used in this research was an LG Nexus 5, which is a very old model but for keeping things simple we opted for just one model in this PhD. Latest smartphones may well be equipped with sensors of better sensitivity, as such would be another area to explore further in the future and compare the accuracy between different models of smartphones. The behaviour of participants also plays a significant role since their behaviour can be very unpredictable and challenging to models such as step detection, body posture, speed and angle of a turn at corridors. During ideal experimental setup, researchers are aware of the limitation of the sensors as such they

may try to conform to the instruction set as much as possible. Real-life movement is not constrained within some set of rules such as identifiable steps, slow turn around corners to get a good change of orientation and most importantly step length. In practice, people may turn at a different rate; step length may vary with sudden pause and walking speed may also vary. Movement is also affected by the familiarity of the place. In short, the trials tried to ensure participants are at their most natural state when completing the task thus we can understand the array of navigation and positioning issues and related environmental factors that affect the accuracy of our positioning system and what may be done in the future to mitigate or improve its accuracy.

In the next chapter, we will use these trial results to identify occupancy trajectory of the different participants. The trajectories will be used to understand patterns of route choice in the building and probabilities will be derived. These route choice probabilities will be used as input in a building occupant model. The model consists of a synthetic population of agents occupying a building and moving around mimicking everyday occupancy scenarios. The agent's movement and route choice in the simulation environment will be decided by the derived probabilities as well as random choices and whether the choices made have any impact on the building energy consumption will be analysed.

Chapter 7

A POTENTIAL USE OF POSITIONING DATA IN BUILDING SIMULATION

7.1 Introduction

This chapter discusses in detail the possible usage of the indoor positioning data collected from the Lego trial as one example described in the previous chapters. Due to the interdisciplinary nature of the PhD, it is important to show how the knowledge gained from the development and study of the indoor positioning system, developed for occupancy detection contributes to the understanding of occupant modelling, especially within the context of electricity usage prediction in a commercial building setting using modelling and simulation. To demonstrate its applicability, we use the data from the Lego trial in an agent-based occupant model of a multi-floor building with a synthetic population of agents acting as building occupants and performing some day-to-day activities. These activities require the agents to make route choice decisions when moving around the building within the simulation environment. The trajectory data from the Lego Trial is converted into probabilities of route choices and used as input for the agents to make independent decisions when transiting from one place to another within the simulation environment. At the same time, different patterns related to building energy consumption will be analysed and compared against real-world patterns, showing implications of trajectories and how we can incorporate positioning data as input to the model; route choice probabilities being one of them.

For model development and documentation we have used an agent-based social simulation framework, namely the Engineering Agent-Based Social Simulation (EABSS) framework developed by (Siebers *et al.*, 2017). We will discuss the use of the framework for the specific case of modelling building electricity usage. We will also explain the level of abstraction in the model to be developed for verification as a base

case and will present four case studies commencing with model validation against real-world data collected from the University of Nottingham, Estates Department. We then discuss in detail the varying electricity usage level for different scenarios of the model.

7.2 Agent-Based Modelling and Simulation

Social simulation is an emerging interdisciplinary field, seeing progress in modelling complex social scenarios, and generating a realistic output. Because of the increasing complexity of these models and their multi-disciplinarity, it is becoming essential to define a proper model development methodology (Cioffi-Revilla, 2010). Agent-based modelling is a tool for performing social simulation. It consists of a system of independent heterogeneous entities (so called agents) that behave and respond stochastically to changes in a modelled environment. These agents have their own decision-making capability based on a given set of rules. They may also interact with each other depending on the dynamics of the model and evolve over time to respond intelligently to changes in their surroundings. Thus they can realistically reproduce complex real-world scenarios in a simplified manner which mathematical models may fail to achieve (Bonabeau, 2002).

Before we move into the details of implementing a simulation model, it is important to develop a conceptual model (Robinson, 2014). As defined in Robinson (2004) the conceptual model outlines the model objectives, input, and output, content, assumptions and simplifications to the extent that the model can capture enough of the real world problem and is able to meet the objectives within a reasonable timescale.

To begin with, this process of developing a conceptual model can be very daunting. Help can be provided by using a standardised framework or methodology. In this study, we will make use of a novel model development framework by (Siebers *et al.*, 2017) that makes use of software engineering practices systematically and formally, known as the EABSS framework.

7.3 EABSS Framework

The EABSS framework is a structured approach to model development, making use of software engineering tools and techniques. The framework provides a step-by-step approach to conceptualise and develop agent-based models. The framework can be divided into three broad categories, Analysis (define objectives, scope, and key activities), Design (define stereotypes, object and agent templates, interaction, and artificial lab), and knowledge gathering.

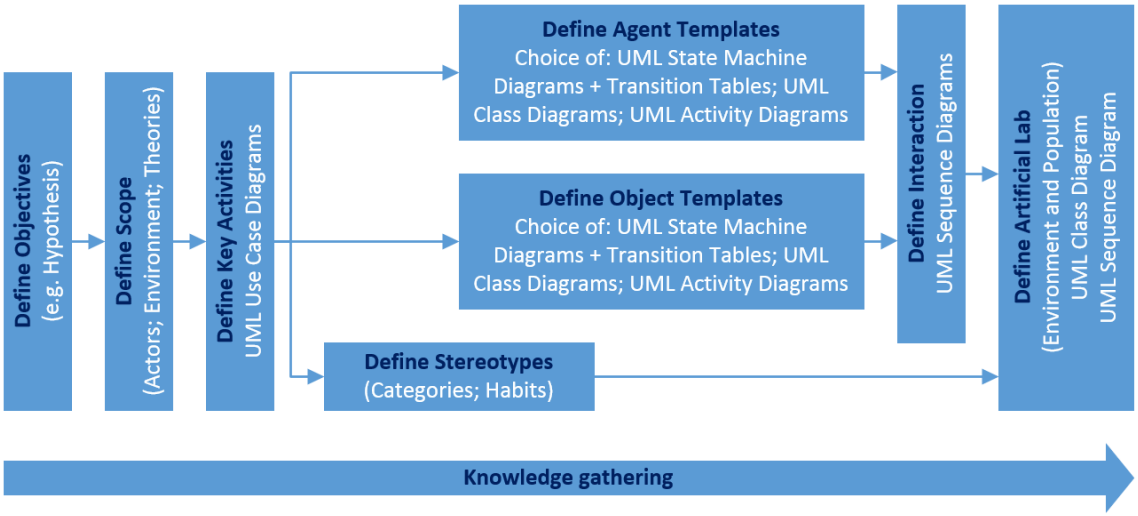


Figure 7-1 Structure of the EABSS framework as depicted in (Siebers *et al.*, 2017)

In the analysis part, the objectives, scope and key characteristics of the model are listed using Unified Modelling Language (UML) diagrams. In the design part, we define the activities and interaction between different elements of the system and their stereotypes making use of formal software engineering practices of state machine diagrams, class diagrams and UML activity diagrams. The knowledge section shows continuous information flow between the previous two sections and how it feeds into the main artificial lab of the simulation environment. In the next section, we will show how we used the EABSS framework for our own model development.

7.4 Applying the EABSS Framework

7.4.1 Motivation for the study

The world has seen an increasing demand for more sustainable buildings, both commercial and residential and has been striving to achieve energy efficiency in building design and performance. According to the United Nation's report stated in (Reinhart *et al.*, 2016), the populations of cities worldwide will be increasing at a rate of 2 million per week. Due to improved living conditions, jobs and basic amenities, more and more people are relocating to cities. This requires careful planning and maintenance of the city infrastructure and optimised allocation of energy resources such as water and electricity to avoid wastage. To ensure this, we need to understand and predict the energy requirements at the design stages of infrastructure to evaluate its post operation performance. Architects and built environment experts have been using building simulation tools to model occupant behaviour and their interaction with physical environments to understand the dynamics of energy consumption in buildings. The studies of (Menezes *et al.*, 2012) and (De Wilde, 2014) have shown that there is a significant gap in energy prediction and actual energy use when a building is occupied. The authors attribute these to discrepancies in model development such as oversimplification or excluding important input factors and prediction algorithms and measurement methodology that may have a significant impact when comparing real versus simulated output to evaluate building performance at the design stage. Occupancy pattern and behaviour also have a very significant impact on model prediction accuracy.

Energy consumption in buildings can be attributed to various factors, but in our model, we will be solely focusing on electricity usage from building lights. The management of building lights can be divided into three dominant policies.

- Manual: Here all the lights on/off state are maintained by the occupants themselves or by the building management authority dictating on/off state centrally at specific hours of the day. Typically, this causes wastage of electricity if occupants are not conscious or energy aware or if lights are kept

on during hours when unoccupied. A significant percentage of this electricity consumption comes from corridors and stairways.

- Automated: Here, passive infrared sensor (PIR) sensors are used to detect the presence of occupants and would act on the lighting state of rooms, corridors, and stairways accordingly. Depending on the presence of occupants the lights are switched on and after a predefined delay (may be configured for 10 minutes, 30 minutes etc.) based on the detection of occupancy nearby the lights are switched off automatically. If the switch off delay time is not optimal and too large, we will have the lights switched on unnecessarily even when unoccupied for long periods of time causing great electricity wastage. As such the light switch off delay time when the rooms are unoccupied may also play a factor in energy saving.
- Customised: This shows a mixed policy of control depending on the time of the day and specific zones of the building; especially in commercial buildings where there are lots of rooms and corridors. Some rooms and corridors may be automated and some under manual control.

There have been many studies related to the development of occupant behavioural modelling and how they interact with different building infrastructure such as light, fan and heating (e.g. Kashif *et al.*, 2013; Burak Gunay *et al.*, 2015; Langevin, Wen and Gurian, 2015). A comparison of existing models in Energy Plus, a building performance simulation tool, can be found in (Gunay *et al.*, 2016). Previous papers discussing agent-based models for predicting electricity energy consumption (e.g. Azar and Menassa, 2011; Zhang, Siebers and Aickelin, 2013; Zheng, Meinrenken and Lackner, 2014; Lin *et al.*, 2016; Kipping and Trømborg, 2017) mention different parameters such as energy management policy and strategy, regulations, electricity unit cost etc. and their impact in promoting green behavior and energy awareness amongst occupants. None of the papers discussed agent movement behaviour incorporating possible routes between state transitions, taken during the transition between rooms. This is also true for the non-agent based occupancy models discussing multi-zone and multi-occupant behaviours using in homogeneous Markov chains to determine agent movement

between multiple states based on transition probability of a *n* by *n* matrix as discussed in (Liao *et al.*, 2010) and (Z. Chen *et al.*, 2014). They discuss the importance of improving the model proposed by (Page *et al.*, 2008), which had a binary state of absence and presence in their own office. The authors introduced a multi-state transition covering general movements, such as going to the washroom, dropping by another office but they failed to address the importance of considering the intra-state transition. As such, a significant amount of electricity consumption may be overlooked entirely or underestimated significantly. It would be interesting to see when all the possible transition routes can be chosen during agent movement, how this would affect the electricity consumption prediction. Also, route choices are not always random; they may follow a predefined pattern depending on the familiarity of the occupants with the building floor plan. This pattern can be identified if the occupancy of individuals can be observed, which was done for our study in the form of spatially distributed tasks using a state-of-the-art indoor positioning system (see Chapter 6 for details). It would be interesting to see if these patterns of route choice impact the energy consumption related to light significantly. At the same time in automated lighting policy, the light switch off delay time also impacts how much electricity is wasted. In this chapter, we will investigate the above cases by developing an agent-based occupant model and carry out a simulation study. It will help to understand the potential impact on electricity consumption prediction from the case studies result.

7.4.2 Agent-Based Model Development

In this section, we will develop the conceptual model using the EABSS framework (Siebers *et al.*, 2017). The process of model development is described in Section 7.3.

(1) Analysis

The analysis of the EABSS framework investigates the defining the aim, hypothesis, experimental factors and responses. It also details the scope of the model and the activity of the model entities.

Aims:

1. Develop a building occupation model to analyse the local dynamics of electricity consumption over time when using different lighting policy settings
2. Understand how the contribution of indoor positioning data from observed individuals' trajectories, can help to estimate electricity usage in multi-floor offices such as academic buildings.

Hypotheses:

1. Using trajectory information during the agent's transition between rooms helps to predict a more realistic electricity usage.
2. Using route choice probabilities derived from occupancy trajectory information of individuals have a statistically significant impact in predicting electricity usage when compared to making a random choice.
3. When the light switch off delay time is increased significantly in the absence of occupants in the room/corridor electricity usage in the simulation will reach top level consumption, as indicated by estate's electricity usage data during peak hours.

Experimental factors:

Experimental factors are model inputs that we need to define and initialise when setting up the model at the very beginning before conducting an experiment. They will impact the output of the model and its responses during the simulation. In our model, we use the following experimental factors.

1. Lighting policy

Responses:

Responses are simulation results that we require to gain insight and to test the hypotheses stated for our model at the beginning. The following are our responses from the simulation.

1. Aggregate electricity consumption of the agent population (per half hour)
2. Aggregate building occupancy (per half hour).

Scope Table:

The scope table lists the model's scope within various categories and subcategories. The table provides inclusion and exclusion of different elements of each category with relevance to the models' abstraction with reasonable justifications. The categories can be defined based on discussion amongst participants such as focus group to make the model appropriately realistic, making sure each element has an impact on the system with relevance to the aims and objectives defined earlier. Redundant elements are removed to minimise ambiguity.

Category		Element	Decision	Justification
Actor		Faculty	Include as a group	Occupies Everyday
		Research fellow		
		PhD Students		
		Visitors	Exclude	Does not have regular presence. So no control
		MSc Students		
Physical Environment	Appliances	HVAC	Exclude	Does not impact the consumption of electricity due to the movement of occupants in the building, also not every element usage by occupants can be controlled.
		Computer		
		Microwave		
		Freeze/Freeze		
		Personal Appliances		
		Light	Include	Can be Controlled by the user and has a direct impact according to occupants presence in the area.
	Weather	Temperature	Exclude	Not required to prove the hypothesis
		Day/Night		
	Room	Kitchen	Include as other rooms	Common areas used for different reasons and impact electricity usage from lights.
		Toilet		
		Corridors		
		Activity rooms		
		Stairways	Include	Used for the transition between floors and also impacts electricity usage from lights.
		Own Office	Include	Required for every occupant.
		Out of building	Include	Required to include out of office breaks impacting possible electricity usage from light switch off/on.
Social/Psychological Aspect		Communication between occupants. General shout out during a seminar or lunch breaks	Include	Word of mouth communication to join seminar, presentation or joining colleagues during lunch, out of office breaks. May impact electricity usage from the light source depending on occupancy.
		Comparative Feedback	Exclude	Not required to prove the hypothesis
		Informative feedback		
		Apportionment level		
		Free-riding		
		Sanction		
		Anonymity		
		Informative feedback		

Table 7-1: The Scope of the Model and the elements available in the model environment with justification.

Activities:

The UML activity diagram defines the interaction between actors and between the actor and the physical environment as defined in the model. Here actors are agents defined in the model performing different tasks and exhibiting different behaviours. An adapted version of the UML use case diagram (where actors appear within the system boundaries) is used to define activities, as seen in Figure 7.2.

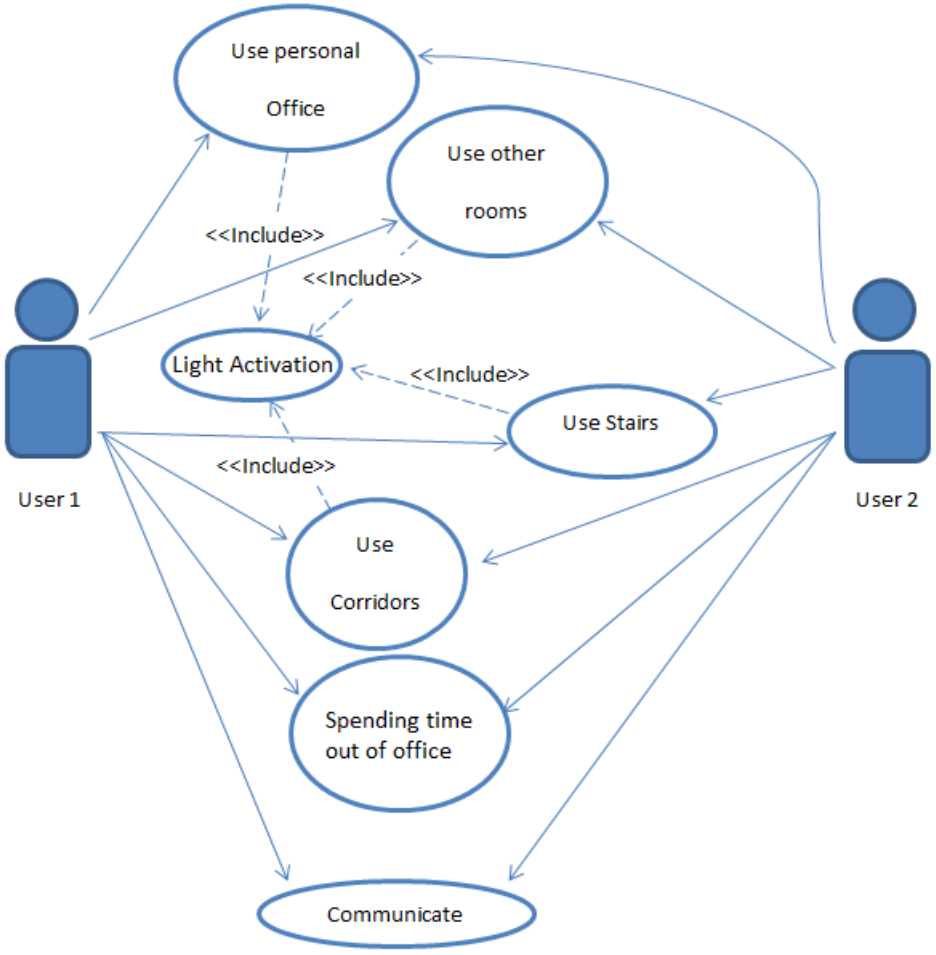


Figure 7-2: Activity diagram showing possible interaction between agents and between the agent and the physical world within the simulation environment.

(2) Design

Here we will discuss the design of the conceptual model describing the agent behaviour stereotype and agent templates, their interaction and transition between states within the simulation environment (artificial lab) in an object-oriented manner.

Stereotypes:

Table 7.2 defines the stereotypical behaviours shown by the agent population. We can classify the behaviours based on different characteristics of the populations such as demographics and habit. The table data is based on observation of the NGB occupancy.

Table 7-2: Agent population's behaviour stereotype in the simulation environment.

Stereotypes	Work Day	Arrival	Departure
Early Bird	Mon - Fri	6am – 8am	60% probability 4pm – 7pm
Timetable complier	Mon - Fri	9am – 10am	
Flexible	Mon - Fri	10am – 1pm	40% probability 1pm – 9pm
Hardworking	Mon – Fri + Sat/Sun	30% probability 9am – 10am	

UML State Machine Diagram for the User Agent:

The UML state machine diagram (also called state chart) shows the states an entity can be in as well as possible transitions between states and how they are triggered (? = condition; clock = timeout; envelope = message). Initially agents are out of building; at a certain time (depending on their stereotype) they will enter the building and go directly to their office. Only from there they can reach other facilities. Their office arrival and departure time is computed based on which they enter and exit the building. When the agent moves into and between different parts of the building, they need to pass through some transit state (eg: transitEntry1, transitReturn1) as seen in the Figure 7.3 below. Details of agent occupancy is explained later in section 7.6. The transit basically computes the route covering stairways, corridors, other rooms as seen in Figure 7.10 and Figure 7.11 to their destination. The destination can be other rooms or places inside the compound state of "inShortbreak","inLongBreak" and "inOffice" or entering and exiting the "insideBuilding" state altogether.

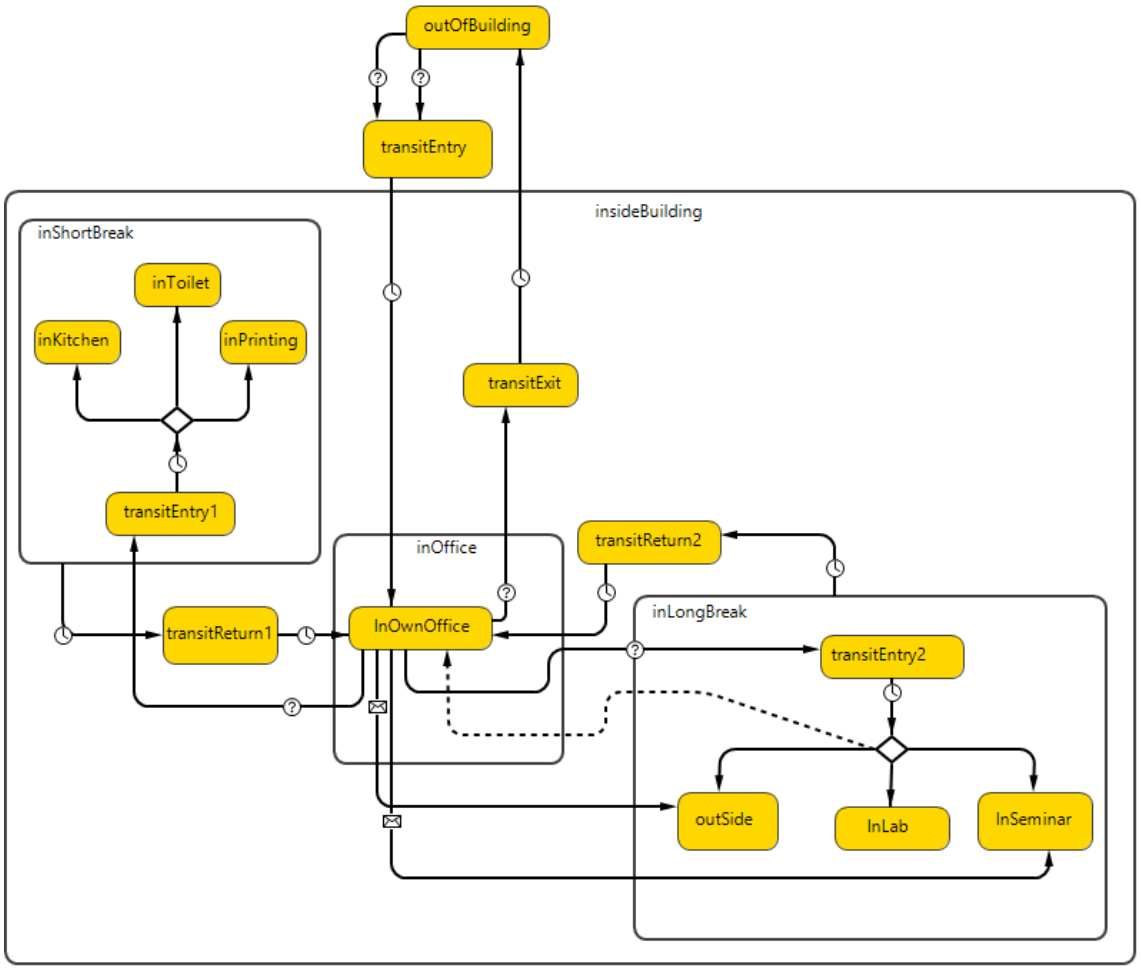


Figure 7-3: State chart showing the possible transition between various states in the office building.

UML State Machine Diagram for Light:

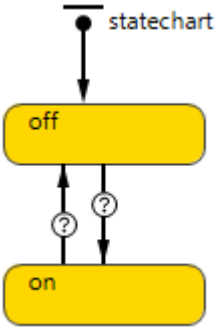


Figure 7-4: State chart showing the light switch on and off stage.

UML Transition Table:

The transition table elaborates the state machine diagram for each of the objects by defining the logic for every state change and what triggers the decision.

Table 7-3 State machine transition table of user agent shown in Figure 7.3.

From State	To State	Triggered by	When?
outOfBuilding	transitEntry	conditions	When Agent arrival time matches with the simulation time during weekdays or agent arrival time matches and the day is a weekend with a given probability.
transitEntry	inOwnOffice	timeout	Average travelling time of 5 min from entrance to own office inside the building and identifying the possible trajectory route in the Entry state
inOwnOffice	transitEntry1	condition	When current simulation time matches with a uniform distribution pick within agent arrival and leave time.
transitEntry1	inShortBreak	timeout	Identification of possible route to destination with an average travelling time of 5 min
inShortBreak	transitReturn1	timeout	Leave after between 5 to 10 min
transitReturn1	inOwnOffice	timeout	Identification of possible route to own office with an average travelling time of 5 min
inOwnOffice	transitEntry2	condition	When current simulation time matches with a uniform distribution pick within agent arrival and leave time.
transitEntry2	inLongBreak	timeout	Identification of possible route to destination with an average travelling time of 5 min
inLongBreak	transitReturn2	timeout	Leave after between 20 to 40 min
transitReturn2	inOwnOffice	imeout	Identification of possible route to own office with an average travelling time of 5 min
inLongBreak	inOwnOffice	condition	If room attendance is above threshold/full.
inOwnOffice	inLongBreak (Outside)	message+ guard	When message is received by an agent and probability of response (groupProb) satisfies.
inOwnOffice	inOtherRooms (Seminar Room)	message+ guard	When message is received by an agent and probability of response (*groupProb*) satisfies during Wednesday or Tuesday only.
inOwnOffice	Exit	condition	When leave time is reached
transitExit	outOfBuilding	timeout	Identification of route to out of building with an average travel time of 5 min.

Table 7-4: State machine transition table of light shown in Figure 7.4.

From State	To State	Triggered by	When?
off	on	condition	When light is ON
on	off	condition	When light is OFF

UML Class diagram:

The UML class diagram show the different attributes and functions of each of the actors already defined in the scope table. The arrow with the diamond symbol

indicates an aggregation association (linking objects that do not depend on each other but are directly related with each other).



Figure 7-5: UML Class diagram of Light and Office object

UML Sequence Diagram:

The UML sequence diagram captures interaction between actors and between actors and the physical world in more detail. It also shows the order of interaction and other methods of interaction such as message passing between entities and the lifeline of each interaction using vertical lines and solid line arrows.

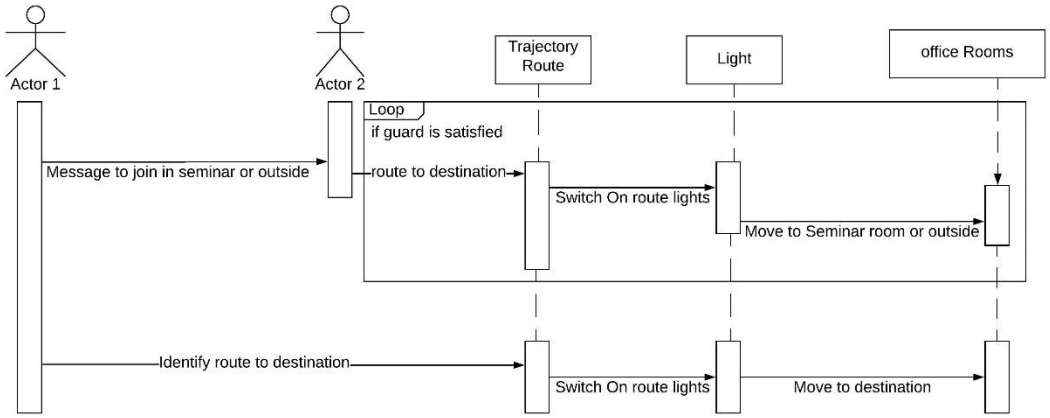


Figure 7-6: UML sequence diagram showing interaction sequences between actors and between the physical entities.

Artificial Lab:

The artificial lab is the primary environment where all the entities defined above are embedded with some global functionalities (statistics, agents, objects, read/write files) defined to capture outputs and capture experimental factors for inputs.

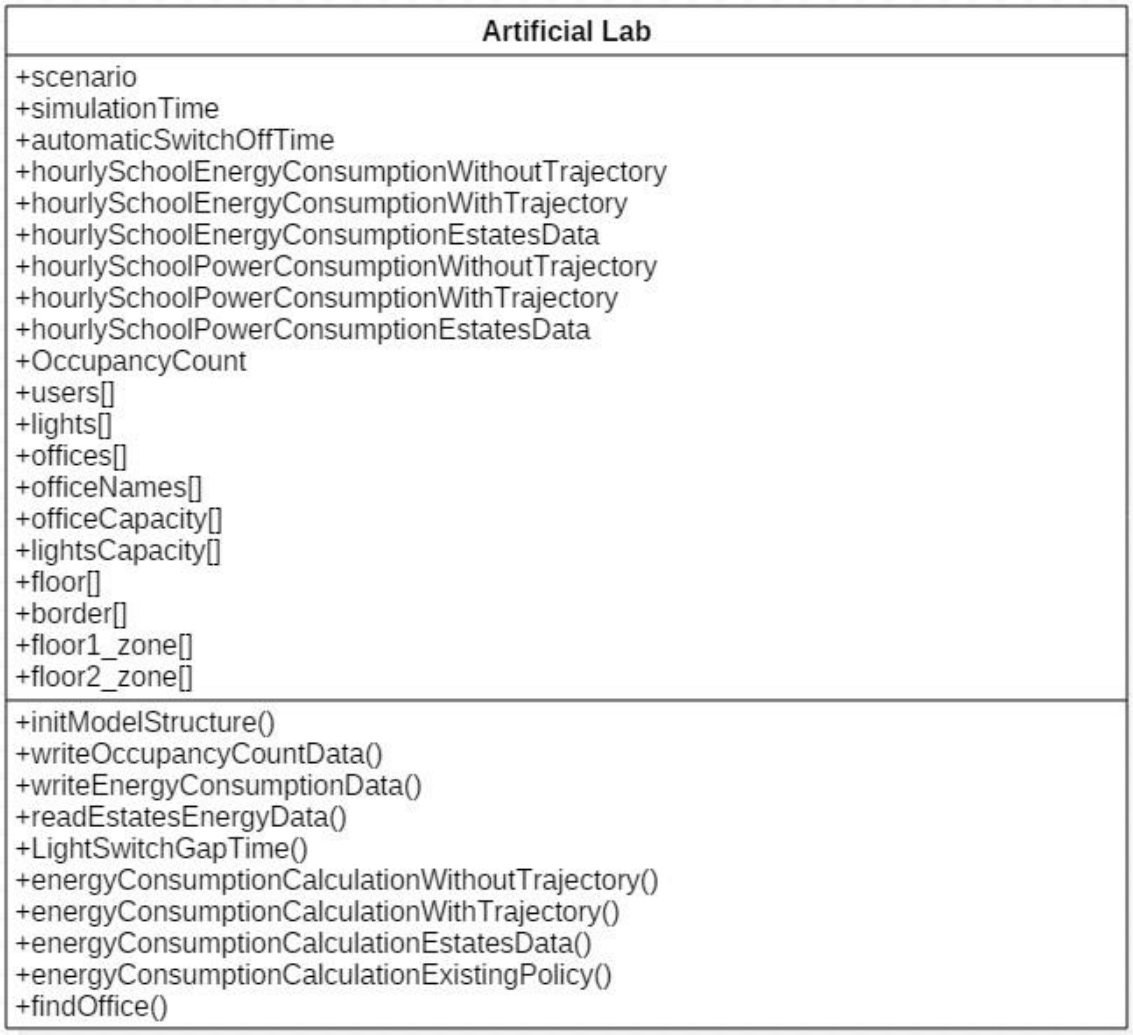


Figure 7-7: The artificial Lab class of the simulation model environment.

7.5 Implementation of the conceptual model

7.5.1 Assumptions and Simplifications

For the implementation of the conceptual model, we used AnyLogic (AnyLogic, 2018). AnyLogic is lightweight, easy to use with drag and drop features, written in Java, and supports both, inline coding and GUI input. It is a multi-paradigm simulation package that supports agent-based, discrete event, and system dynamics simulation as well as optimisations. AnyLogic supports all kind of simulations (for examples see Figure 7.8), related to market analysis, supply chain, health care, geo locations, map support, and many more. More details can be found in their website (AnyLogic, 2018).



Figure 7-8 Simulation examples from AnyLogic (AnyLogic, 2018)

Our occupant model implements a simplified version of the Nottingham Geospatial Building's first two floors only and its population as a case study in AnyLogic. The academic building houses not just faculty members, researchers, and PhD students but also a small number of SME offices on the first floor. As such, there is a diverse population of occupants exhibiting different behaviours with some having limited access to floors and rooms. For model simplification, we have selected some key rooms for agent transition to and from their respective offices, which are always accessed by the building occupiers of the two floors irrespective of their office desk locations as shown in Figure 7.10. They are listed below.

- Seminar room
- Presentation room
- Lab
- Equipment room
- Kitchen
- Toilets
- Printing services
- Stairways

Since we are only interested in observing the electricity consumption from Lights, the NGB lighting infrastructure is carefully observed physically and the original floor plan design is studied to identify the number of lights λ in each room and their associated power Φ_i. The building has a variety of light models and designs having different power capacity. So, for simplification, the power capacity in the model is kept constant at 60w, and the number of lights λ in each room is allocated according to the equation 7.1 below.

$$\lambda = \frac{\sum_1^i \Phi}{60} \qquad (7\text{-}1)$$

Here Φ is the power associated with each light in that room. The number of lights λ is calculated for each room and assigned during model implementation. Also, several occupants in each room are observed before allocation, which also includes office sharing between multiple occupants and an open plan office space as well.

The agents communicate with the agent population, in general, to invite colleagues for seminars and take out-of-office breaks. To avoid complexity, we have refrained from creating networks among agents representing close circles and friendship, which might be common among colleagues. Based on observation we have found occupants showing the almost negligible probability of forming large social circles or herding behaviour in this building and as such only kept general mass communication with a low probability of response.

For the transition to other rooms, route choices are implemented incorporating detailed trajectories between rooms and corridors, which also involved stairways depending on the model scenario. The destinations are separated in two blocks, 'inShortBreak' for a 5 to 10 minute break and 'inLongBreak' for a 20 to 40 minute break, as shown in the state chart diagram in Figure 7.3.

7.5.2 NGB Floor Plan and Route flow

It is important to understand how the Lego trial routes were set up when we mentioned different routes and starting point for the participants in Chapter 6. To

simplify the model, the NGB floor plan is partitioned into multiple zones, and the corridors and stairways are marked, as shown in Figure. 7.9. Floor A is divided into four zones and Floor B into three zones. It is expected that when participants travel from one zone to another, they will have their preferences of route choice. The partition of the floor maps and designation of the number of zones were completely arbitrary and done to simplify the Lego trial task and route preference identification. The same principle is used in the agent-based model when moving simulation agents from one place to another based on either random choice or transition probability derived from the trial data. Route choices may include going through other rooms, corridors and stairs.

A flow diagram of the many possible routes available during movement between and within floors can be seen in Figure 7.10. Zones in blue show zone wise partition in Floor A, zones in red shows zone wise partition in Floor B according to Figure 7.10. There were four corridors and three stairs used by the agents.

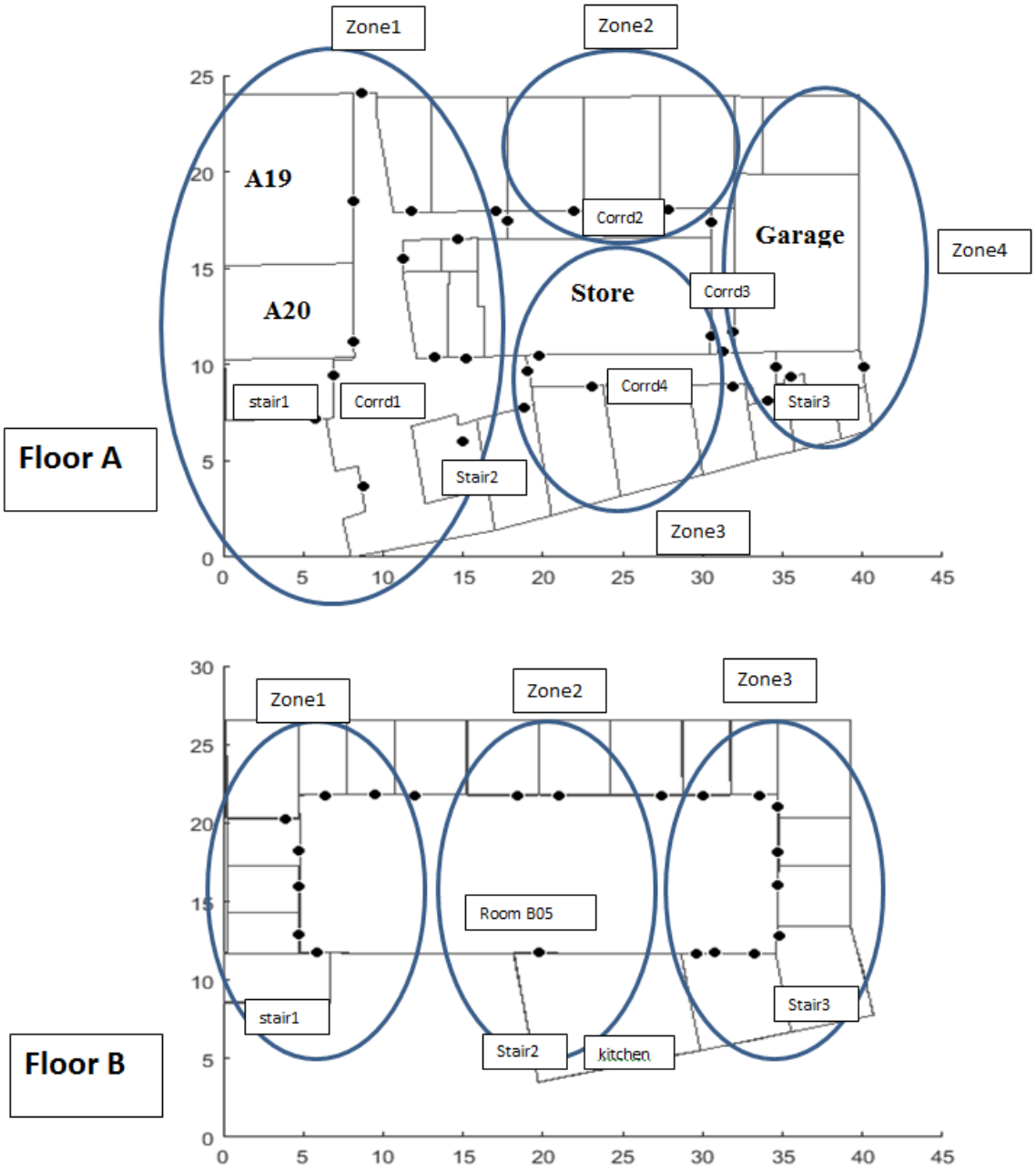


Figure 7-9: The floor plan of NGB and its partition into zones and rooms as seen during the simulation.

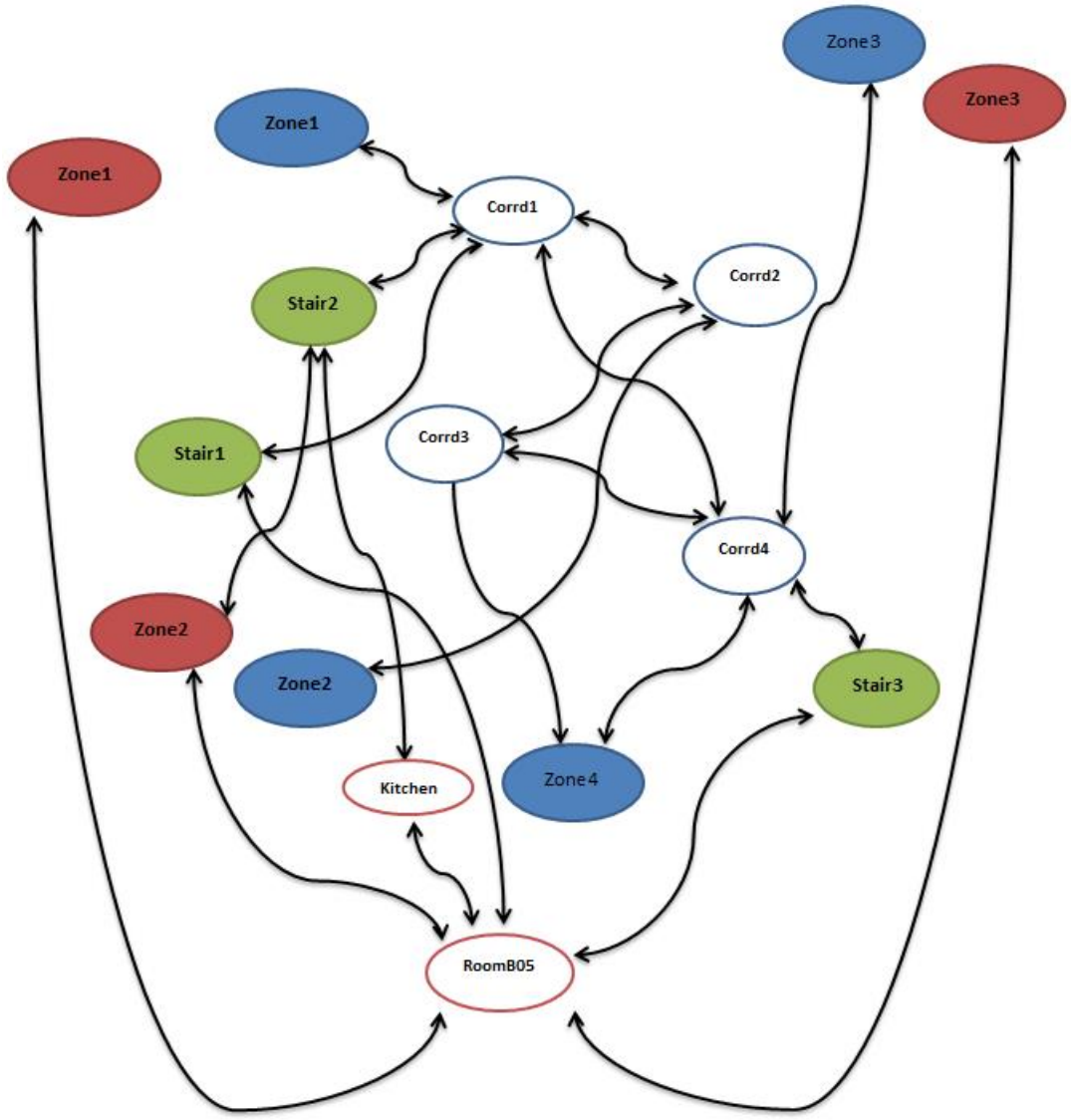


Figure 7-10: The possible route choices an occupant can make when moving within the two floors of the building.

It is evident that route choices are dependent on the initial location of people and vary due to personal preference and the instant reaction of the state of mind. Thus, to understand the route choices, the Lego trial experiment was carried out with spatially distributed tasks designed to cover different areas of the floor. The tasks had a different initial starting point and target zones and had four major transitions possible within the building.

1. Floor A → Floor B
2. Floor B → Floor A

3. Within Floor A
4. Within Floor B

The Lego trial positioning data was analysed once processed by the positioning system, and patterns of route choices made by the participants were identified. This would mean identification of routes taken by participants when moving between zones passing through rooms, corridors and stairs to complete their assigned task during the trials. The route choice probability computed from the trial data is shown in Table 7.5, 7.6, and 7.7. For simplicity of the model, the probability for the transition between zones from Floor A to Floor B is derived for trial data and assumed similar for the other way round, but transition probability within Floor A and Floor B are derived separately from the trial data since room layout is different for the two floors. Table 7.5, 7.6 and 7.7 shows the transition probability between zones consisting of multiple route choices for each different transition. These transition probabilities are used during route choices when selecting the routes for agent movement during the occupant simulation.

Table 7-5: List of possible routes and their associated probability when moving between zones from floor B to floor A. C1, C2, C3, C4 denotes corridors and S1, S2, S3 denotes stairs

Zone1F2	Zone1F1	Zone2F1	Zone3F1	Zone4F1
	C4,C1,B18,S3 = 0 C4,C3,C4,C1,B18,S3 = 0 C1,B18,S2 = 0.25 C1,B18,B14,S1 = 0.75	C1,C2,B18,S2 = 0.9 C1,C2,C3,C4,B18,B14,S1 =0 C1,C2,B18,B14,S1 = 0.1 C1,C2,B18,B14,S1 = 0 C1,C2,C3,C4,B18,S2 = 0 C1,C2,C4,B18,S3 = 0 C3,C2,C4,B18,S3= 0	C1,C4,B18,S2 = 0.8 C1,C2,C3,C4,B18,B14,S1 =0 C1,C2,C3,C4,B18,S2 = 0 C1,C4,B18,B14,S1 = 0.2 C4,B18,S3 = 0	C1,C2,C3,B18,S2 = 0 C1,C2,C3,B18,B14,S1 = 0 C1,C3,C4,B18,B14,S1 = 0.4 C1,C3,C4,B18,S2 = 0 C3,C4,B18,S3 = 0.6

Zone2F2	Zone1F1 C1,B18,S2= 0.2 C1,B18,B14,S1=0.8 C1,C4,B18,S3=0 C1,C2,C3,C4,B18,S3=0	Zone2F1 C1,C2,B18,S2=0.7 C1,C2,C3,C4,B18,B14,S1=0 C1,C2,B14,B18,S1=0.3 C1,C2,C3,C4,B18,S2=0 C1,C2,C4,B18,S3=0 C2,C3,C4,B18,S3=0	Zone3F1 C1,C4,B18,S2 = 0 C1,C2,C3,C4,B18,B14,S1=0 C1,C2,C3,C4,B18,S2=0.83 C1,C4,B18,B14,S1=0.166 C4,B18,S3=0	Zone4F1 C1,C2,C3,B18,S2=0 C1,C2,C3,B18,B14,S1=0 C1,C3,C4,B18,B14,S1=0.25 C1,C4,C3,B18,S2=0 C4,C3,B18,S3=0.75
Zone3F2	Zone1F1 C1,B18,S2=0 C1,B18,B14,S1=0.8 C1,C4,B18,S3=0.2 C1,C2,C3,C4,B18,S3=0	Zone2F1 C1,C2,B18,S2=0 C1,C2,C3,C4,B18,B14,S1=0 C1,C2,B18,B14,S1=0.3 C1,C2,C3,C4,B18,S2=0 C1,C2,C4,B18,S3=0 C2,C3,C4,B18,S3= 0.7	Zone3F1 C1,C4,B18,S2=0 C1,C2,C3,C4,B18,B14,S1=0 C1,C2,C3, C4,B18,S2=0 C1,C4,B18,B14,S1=0.2 C4,B18,S3=0.8	Zone4F1 C1,C2,C3,B18,S2=0.01 C1,C2,C3,B18,B14,S1=0 C1,C4,C3,B18,B14,S1=0 C1,C4,C3,B18,S2=0 C4,C3,B18,S3=0.99

Table 7-6: List of possible routes and their associated probability when moving between zones from floor A to floor B. C1, C2, C3, C4 denotes corridors and S1, S2, S3 denotes stairs

Zone1F1	Zone1F2 C4,C1,B18,S3 = 0 C4,C3,C4,C1,B18,S3 = 0 C1,B18,S2 = 0.25 C1,B18,B14,S1 = 0.75	Zone2F2 C1,B18,S2= 0.2 C1,B18,B14,S1=0.8 C1,C4,B18,S3=0 C1,C2,C3,C4,B18,S3=0	Zone3F2 C1,B18,S2=0 C1,B18,B14,S1=0.8 C1,C4,B18,S3=0.2 C1,C2,C3,C4,B18,S3=0
Zone2F1	Zone1F2 C1,C2,B18,S2 = 0.9 C1,C2,C3,C4,B18,B14,S1=0 C1,C2,B18,B14,S1 = 0.1 C1,C2,B18,B14,S1 = 0 C1,C2,C3,C4,B18,S2 = 0 C1,C2,C4,B18,S3 = 0 C3,C2,C4,B18,S3= 0	Zone2F2 C1,C2,B18,S2=0.7 C1,C2,C3,C4,B18,B14,S1=0 C1,C2,B14,B18,S1=0.3 C1,C2,C3,C4,B18,S2=0 C1,C2,C4,B18,S3=0 C2,C3,C4,B18,S3=0	Zone3F2 C1,C2,B18,S2=0 C1,C2,C3,C4,B18,B14,S1=0 C1,C2,B18,B14,S1=0.3 C1,C2,C3,C4,B18,S2=0 C1,C2,C4,B18,S3=0 C2,C3,C4,B18,S3=0.7
Zone3F1	Zone1F2 C1,C4,B18,S2 = 0.8 C1,C2,C3,C4,B18,B14,S1=0 C1,C2,C3,C4,B18,S2 = 0	Zone2F2 C1,C4,B18,S2 = 0 C1,C2,C3,C4,B18,B14,S1=0 C1,C2,C3,C4,B18,S2=0.83	Zone3F2 C1,C4,B18,S2=0 C1,C2,C3,C4,B18,B14,S1=0 C1,C2,C3, C4,B18,S2=0

	C1,C4,B18,B14,S1 = 0.2 C4,B18,S3 = 0	C1,C4,B18,B14,S1=0.166 C4,B18,S3=0	C1,C4,B18,B14,S1=0.2 C4,B18,S3=0.8
Zone4F1	Zone1F2 C1,C2,C3,B18,S2 = 0 C1,C2,C3,B18,B14,S1 = 0 C1,C3,C4,B18,B14,S1 = 0.4 C1,C3,C4,B18,S2 = 0 C3,C4,B18,S3 = 0.6	Zone2F2 C1,C2,C3,B18,S2=0 C1,C2,C3,B18,B14,S1=0 C1,C3,C4,B18,B14,S1=0.25 C1,C4,C3,B18,S2=0 C4,C3,B18,S3=0.75	Zone3F2 C1,C2,C3,B18,S2=0.01 C1,C2,C3,B18,B14,S1=0 C1,C4,C3,B18,B14,S1=0 C1,C4,C3,B18,S2=0 C4,C3,B18,S3=0.99

Table 7-7: List of possible routes and their associated probability when moving between zones in Floor A. C1, C2, C3, C4 denotes corridors and S1, S2, S3 denotes stairs.

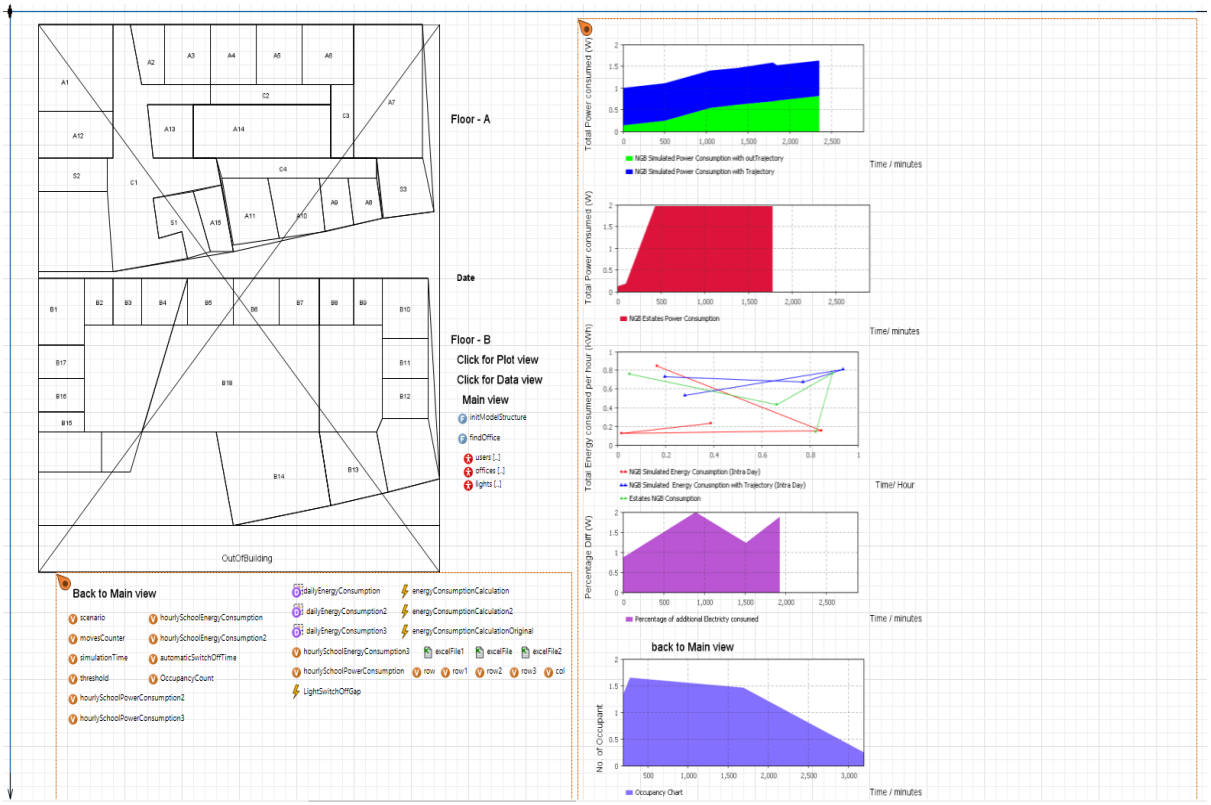
Zone1F1	Zone1F1 C1= 1	Zone2F1 C1,C2=0.99 C1,C2,C3,C4=0.01	Zone3F1 C1,C4=0.99 C1,C2,C3,C4=0.01	Zone4F1 C1,C4=0.01 C1,C3,C4=0.99
Zone2F1	Zone1F1 C1,C2 = 0.99 C1,C2,C3,C4=0.01	Zone2F1 C2=1	Zone3F1 C2,C3,C4=0.3 C1,C2,C4=0.7	Zone4F1 C2,C3 = 0.99 C1,C2,C3,C4=0.01

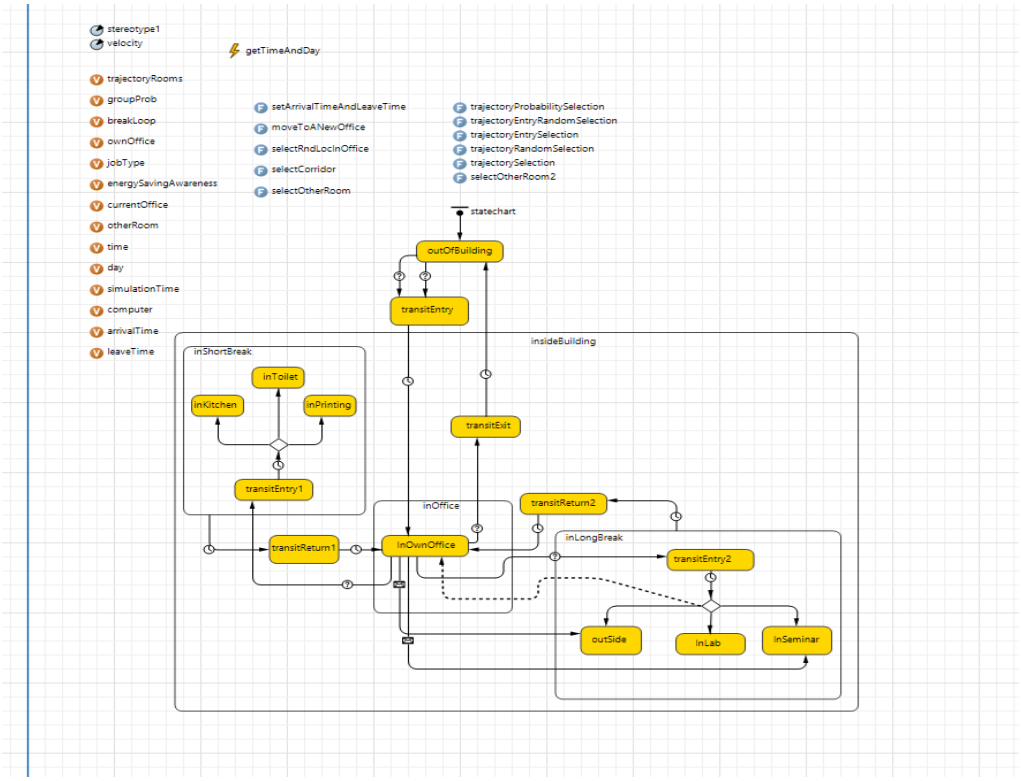
Zone3F1	Zone1F1 C1,C4=0.99 C1,C2,C3,C4=0.01	Zone2F1 C2,C3,C4= 0.3 C1,C2,C4=0.7	Zone3F1 C4=1	Zone4F1 C3,C4=0.99 C1,C2,C3,C4=0.01
Zone4F1	Zone1F1 C1,C3,C4=0.57 C1,C3,C4=0.43	Zone2F1 C3,C2=0.99 C1,C2,C3,C4=0.01	Zone3F1 C3,C4=0.99 C1,C2,C3,C4=0.01	Zone4F1 C3=1

7.5.3 The final simulation model

The picture below in Figure 7.11 shows the final model and its different parameters and plots. The user, office and light models with state transitions are also shown. No simulation is being run in this instance and is just a screen grab from the main window of the model. The model shows the two-floor plan of NGB used in simulation.

7.5 Implementation of the conceptual model





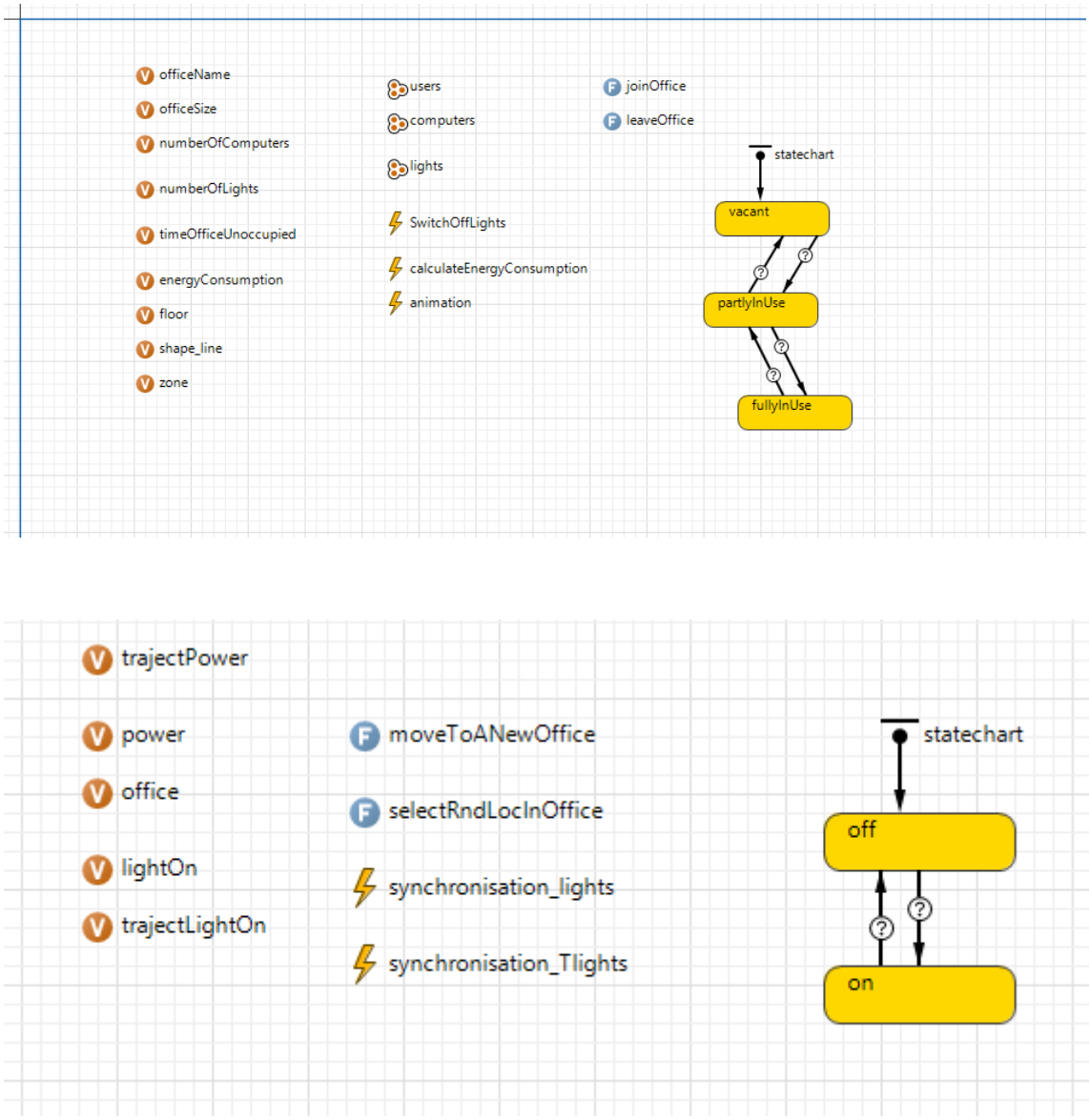


Figure 7-11 Final Simulation model main screen, user, office and light model respectively.

7.6 Experimentation

In this section we will conduct a hypothesis testing exercise by running computer simulation experiments with the model we developed. We will describe the experiments in more detail and then analyse and discuss the simulation outputs for each of the experiments. As a reminder, here are the hypotheses to be tested, as previously defined in Section 7.4.2.

- Hypothesis 1:

  At first, we simulate electricity usage of NGB with existing lighting policy as a base case and compare against actual electricity consumption data from Estates for validation and calibration of the model.

  To test the hypothesis, we then use the base case model to simulate electricity usage but using smart lighting policy (e.g., using PIR sensors) for the following case.

  - Simulate agent's movement without incorporating individual trajectories during the transition between rooms and corridors; teleporting agents to their destinations during simulation, as done by (Zhang *et al.*, 2013), thus ignoring the electricity consumed from lights switched on during movement through other rooms and corridors on the way.

- Hypothesis 2:

  To test the hypothesis, we use the base case model to simulate electricity usage but using smart lighting policy (e.g., using PIR sensors) in each of the following cases.

  - Simulate agent's movement incorporating individual trajectories during the transition between rooms and corridors, thus taking into consideration energy consumption during the transition between rooms. Compare and contrast the possible effect of electricity usage when using smart lighting policy in the following cases.
    - Using a random trajectory route choice during the transition.
    - Using probability defined trajectory route choice (derived from indoor positioning trial) during the transition.
    - Evaluate the statistical significance if any, from the two results.
    - Compare and contrast the energy usage in the two cases.

- Hypothesis 3:

  To test the hypothesis, we evaluate the automated light switch off delay (changing in steps of 5 minutes) in smart lighting policy and its impact to see if it ever reaches the top level consumption indicated by Estates' data.

The initial model, as described in Section 7.4, is used as a base case for the validation experiment, and then the building lighting policy is modified for each of the following experiments to test the related hypothesis.

For all experiments we use the following experimental settings:

- run length: 24 hours or 1440 minutes
- number of replications: 100

Initially we need to setup the offices, agent population and lights. We begin by creating the appropriate number of agents and allocate them to each of the office rooms in the NGB according to the floor plan in Figure 7.9. The number of agents allocated to each room is based on observation of the NGB offices in Floor A and Floor B. The number of lights in each room is assigned throughout the building with their defined electrical power configuration. The offices are assigned to their respective floors according to the floor plan in Figure 7.9. We then configure the agent behaviour stereotype and assign agents to a specific stereotype chosen from a uniform distribution. The stereotype behaviour seen in Table 7.2 defines the likelihood of arrival and departure time during the day. Then at the start of the experiment the arrival and departure time of each agent is assigned according to their stereotype. The arrival rate of agent is basically dependent on the stereotype the agent belongs to. A discrete uniform distribution is used to pick a random number. If that number falls within the entry and exit time range of the agent stereotype behaviour they are assigned as the entry and exit time. Similarly for occupancy behaviour within the building i.e. movement between other states and exit, uniform distribution is again used for agent occupancy decision making. This settings are true for all simulation experiments carried out.

7.6.1 Model Validation using existing Lighting Policy against Estates' Data

To understand the efficacy of the model, it is important to compare and validate the model against some truth data or real-world data as discussed in the book by (Robinson, 2004). In our case, the base model was designed to mimic the NGB lighting policy currently being utilised. Based on our observation of the building, we found it to be a mixture of PIR sensor controlled and centrally controlled. Some sections of the building lights are active 24 hours such as reception area, corridors in floor A, open plan space in floor B, stairways, kitchen etc. To verify this, electricity consumption data of NGB for lights were collected from the University of Nottingham Estates department for February. The data showed electricity usage (KWh) for every 30 minutes over 24 hours, which can be seen in the plot below in Figure 7.12.

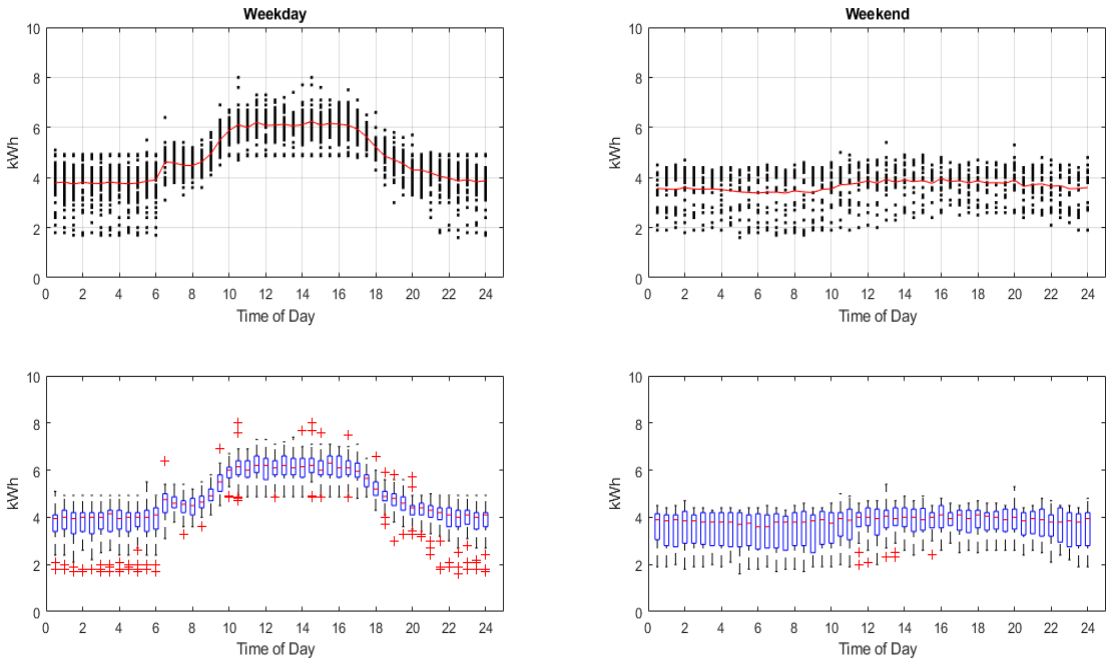


Figure 7-12. Actual electricity consumption of floor A and floor B of NGB combined for weekdays and weekends, respectively. The central red line in the upper plots shows the mean electricity consumption. Top two corresponds to mean plot and the bottom corresponds to box plot

It is interesting to see that almost two-third of the building energy is consumed at night when there is almost negligible or zero attendance. Thus, it is not surprising since

based on our observation, a major section of the building lights is kept switched on day and night.

For the first experiment we simulate with the base model. For the simplicity of the model, only weekday's energy data is simulated and compared. This is because the occupancy behaviour of NGB during weekends could not be observed reliably. As such the model stereotype parameters such as arrival rate, time of entry and exit and likelihood of occupants working during weekends will be vague and unrealistic. A screenshot of the main simulation window for model validation can be seen in Figure 7.13.

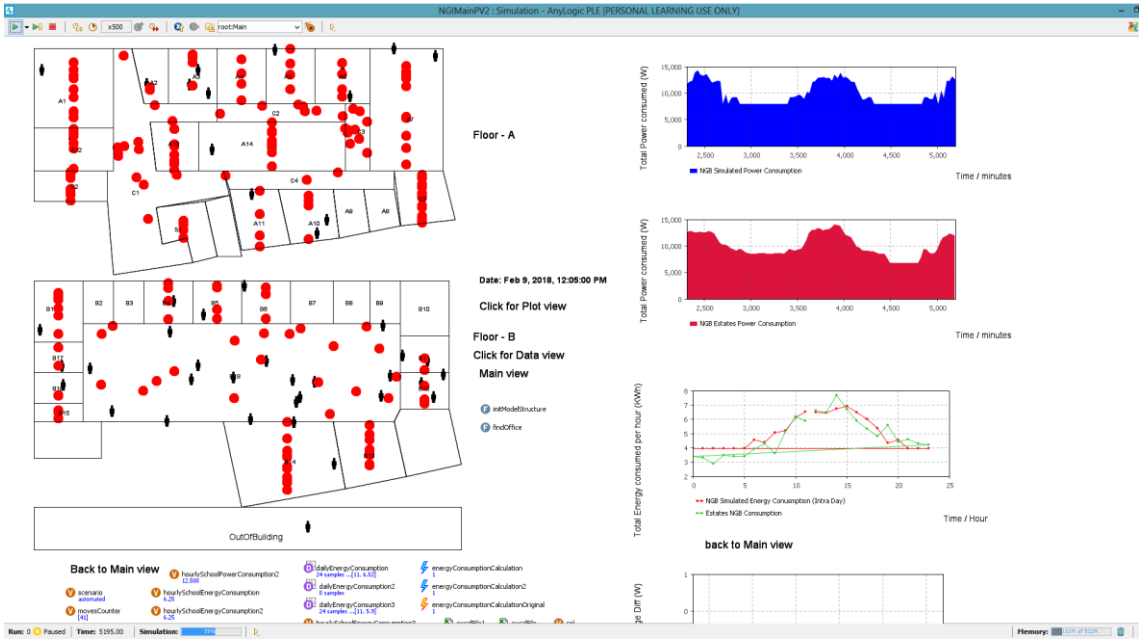


Figure 7-13. Screenshot showing the simulation main screen with agent movement during office hours on the left and the subsequent electricity consumption plots on the right.

Figure 7.14 is a snap shot (inset right, Figure 7.13) of the simulated electricity consumption data (W) updated every 30 minutes. Figure 7.15 (inset right, Figure 7.13) shows the actual electricity consumption data (W) from Estates from sample weekdays. Both the plots show some similarity in their pattern and electricity consumption. Figure 7.16 (inset right, Figure 7.13) shows the electricity consumption in (KWh) for both the simulated and Estates' data over 24 hours. We can see that the

patterns are similar, and that the similarity is at an acceptable level for running the next set of experiments and is not much different.

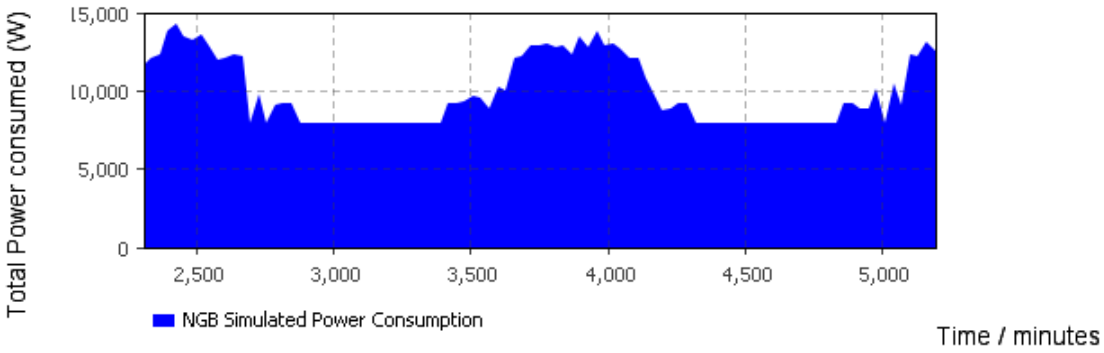


Figure 7-14 NGB simulated power consumption during weekdays only (inset right, Figure 7.13)

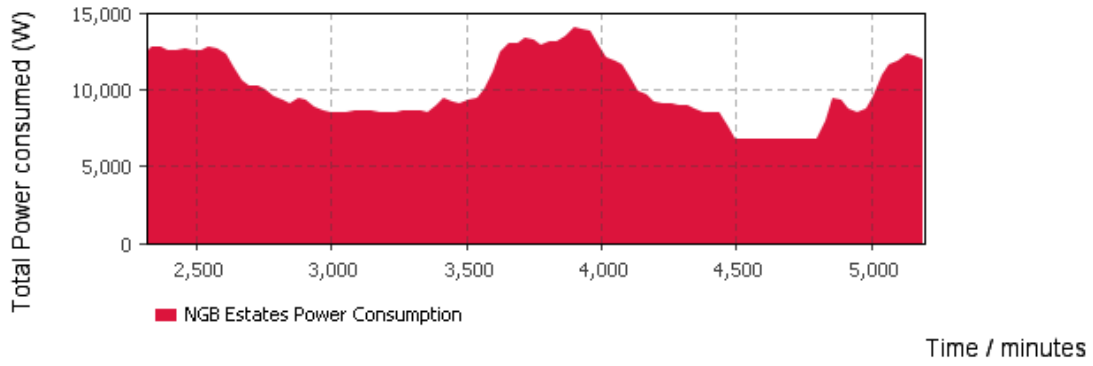


Figure 7-15. NGB Estates' power consumption during weekdays only. (inset right, Figure 7.13)

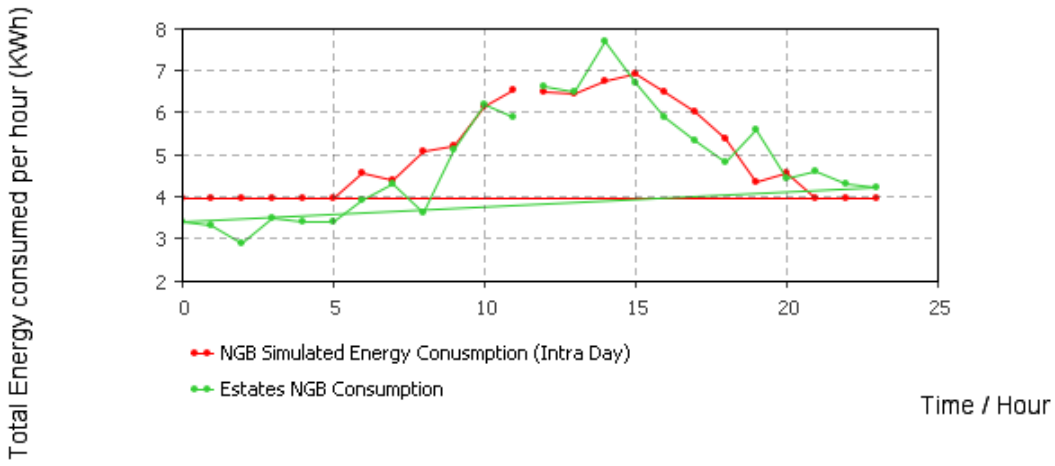


Figure 7-16. Simulation energy data vs Estate's energy data consumption over 24 hours. (inset right, Figure 7.13)

In reality, occupancy behaviour is a very complex phenomenon and varies among individuals and may exhibit collective behavioural patterns among occupant stereotypes as well. This is discussed in detail in the paper of (Luo *et al.*, 2017) where they have collected different occupant profiles and revealed the different occupation and behaviour preference, that occupancy behaviour patterns could vary one from another. The study focuses on performance analysis as well as verification of modelling regular occupancy behaviour patterns in office buildings and if the simulator could reproduce patterns of occupancy. In our study, we were not interested in looking into the details of occupancy modelling and its complexities in the building and followed a simple discrete uniform distribution to determine the agent's occupancy behaviour representing entry and exit time, their likelihood of coming to the office and transition between rooms and facilities.

To ensure the statistical significance of the result, the simulation was replicated 100 times with a random seed for each run and then compared with Estates' data. The plot in Figure 7.17 illustrates the electricity consumption predicted every 30 minutes over 24 hours.

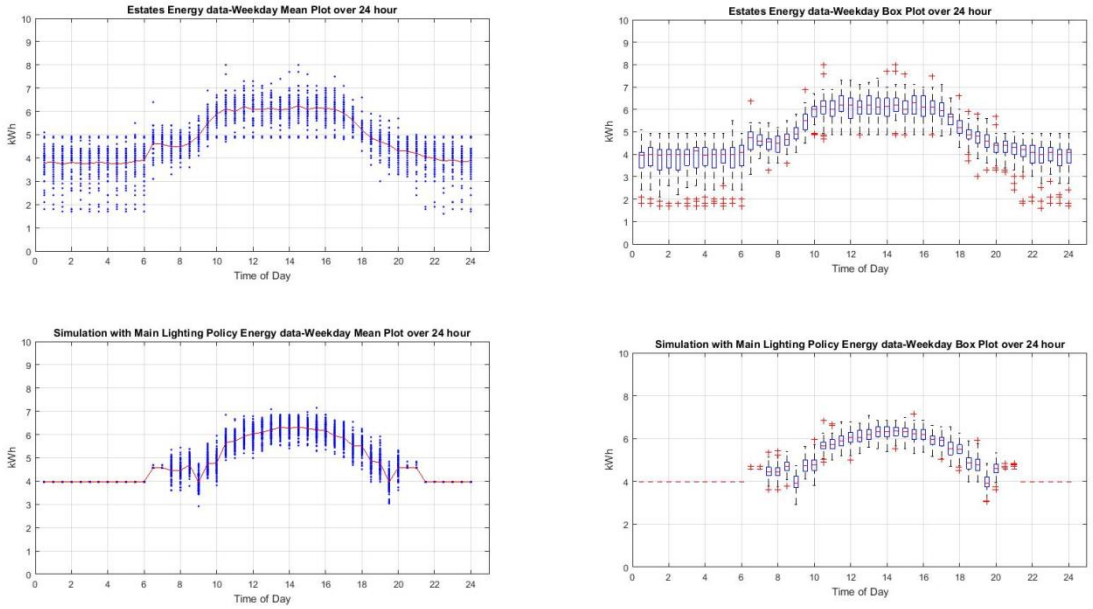


Figure 7-17 Simulation result after 100 repetitions compared against Estate's data every 30 min over 24 hours.

It can be seen in Figure 7.17 that the mean base energy consumption every half hour is around 4 KWh, which moves up to a little over 6 KWh during the peak times of the day. The energy consumption starts to rise from 6 am and starts to fall gradually from 6 pm. The variance of the electricity consumption data from Estate's record throughout the month is fairly high as seen in Figure 7.18. The model was slightly calibrated to ensure we have the same baseline for electricity consumption during the night. The lights in hallways, corridors, stairs etc. in the simulation environment were kept switched on mimicking the lighting policy of NGB but it was not possible to identify exactly how many since not all facilities were accessible at night for observation. As a result, the simulated electricity consumption was still falling below the mean consumption of Estate's data at night (near 4KWh) as seen in Figure 7.17. So, to ensure we have a similar baseline for comparison during the night time we introduced a constant value as miscellaneous electricity consumption in the base model. The simulated electricity output, although stochastic, shows less variance since it is less unpredictable compared to the real-world scenario. The mean electricity consumption from the simulation shown by the red line is around 6 KWh during peak times, nearly similar to Estate's data but the pattern varies slightly and seems flatter during the rise and fall. This difference can be explained due to various real-life factors such as intermittent absence by occupants is not taken into account during the model development, whereas during the simulation, these things are not considered, and all agents are present during weekdays. As a result, all the personal office spaces in the simulation are always occupied at some point of the time during the day, which might not be true in real life. Also, some of the major rooms listed for agent movement during simulation might not be occupied every day in real life. These and various other unforeseen everyday situations impact real-life energy consumption, which is evident from the significant variance in the Estate's energy data. We tried to normalise both the data sets to a common scale, without distorting differences in the ranges of values seen in Figure 7.18 but the outcome remained same. In general, the simulation results show the similarity of the simulated electricity output and Estate's pattern is at an acceptable level and that the similarity is at an acceptable level for failing to reject the

hypothesis. Although the variability is very different the mean of total electricity consumption is almost equal to that of Estates as illustrated in the box plot of Figure 7.19 thus satisfying the first objective of model validation.

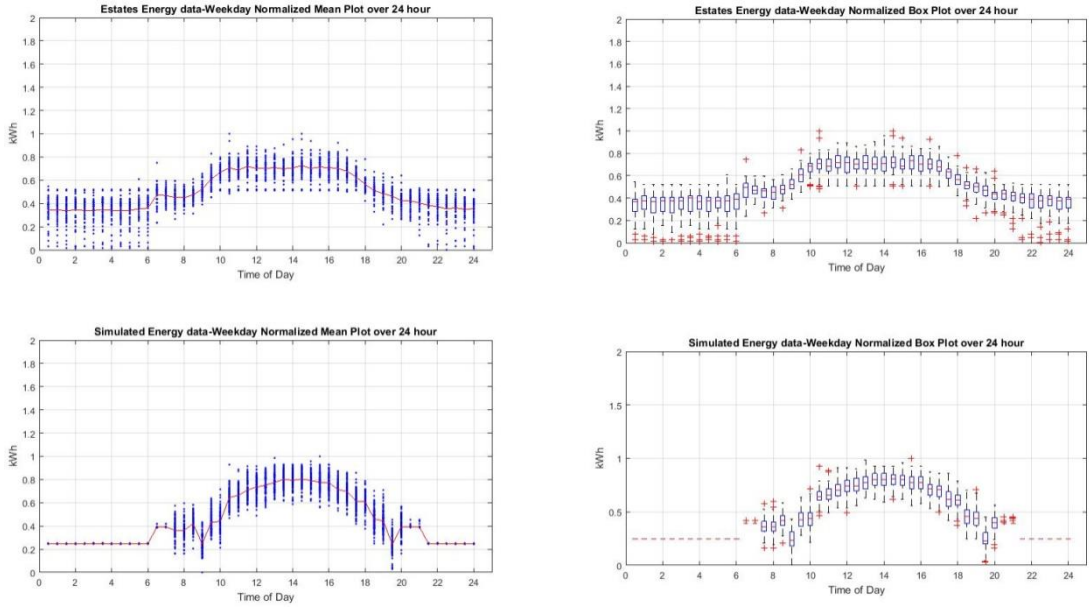


Figure 7-18 Normalised plot of Figure 7.16

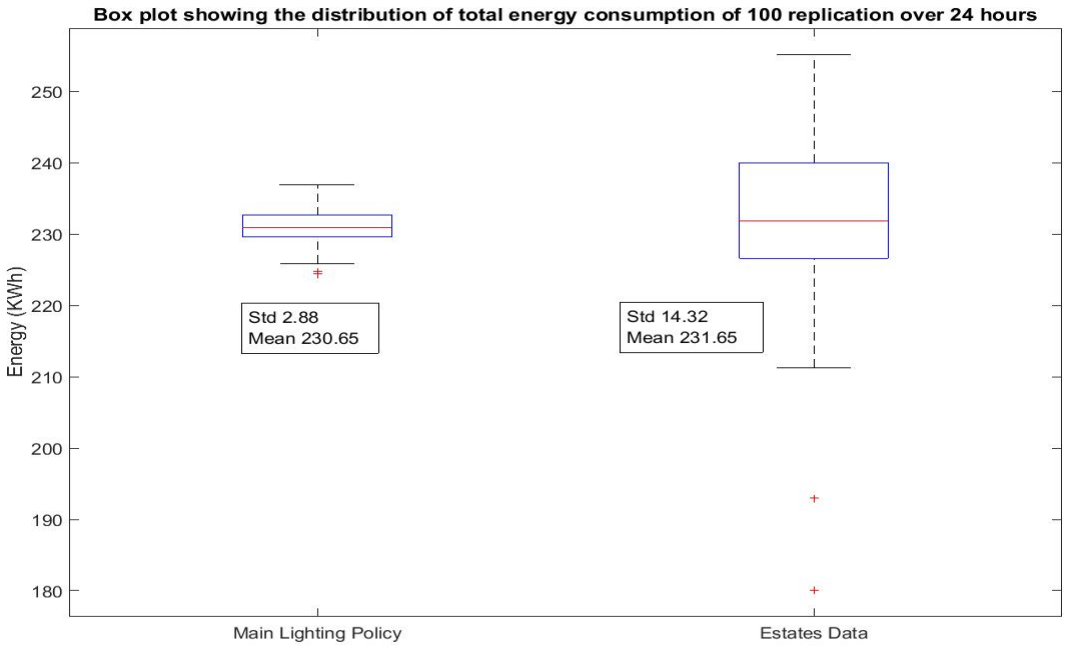


Figure 7-19 Box Plot showing the total energy consumption over 24 hours for 100 replications.

7.6.2 Experiment 1: Impact of trajectory route choice in Occupant Model

In the agent-based occupant model developed by Zhang et al. (2013) agent movement between rooms implied teleporting the agent to their destination through one corridor in between. In reality, to travel between rooms an agent might need to pass through multiple corridors; this means none of the corridor's electricity consumption from lighting usage is used in the calculation except one even though looking at the floor plan it was evident that some of the transition would require an agent to cross multiple corridors. An example illustration seen in Figure 7.20 going from A to B would require passing through corridor 2, 3 and 4 marked red, whereas in case of teleporting as in the case of Zhang et al. (2013) we will only use the electricity consumption from any one of the corridors randomly and move the agent from A to B. As a result, we always underestimate the electricity consumption.

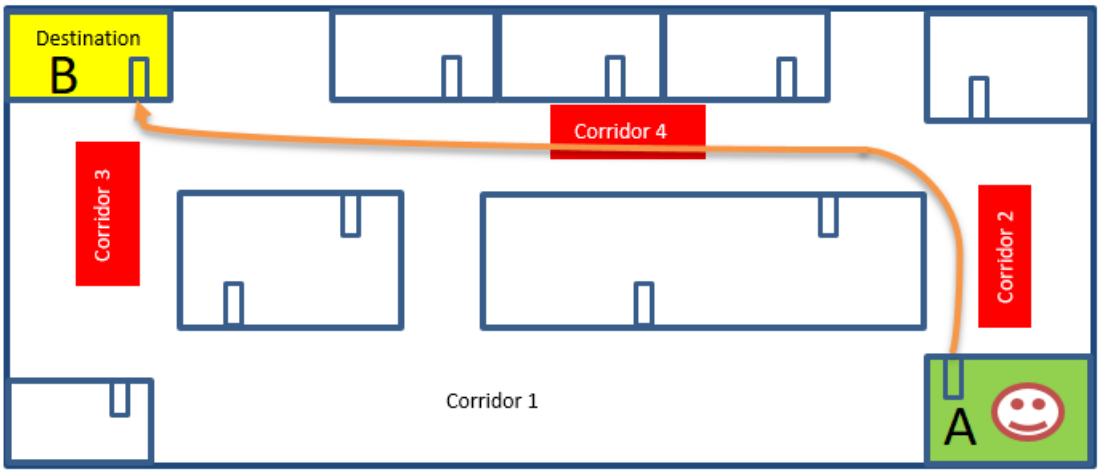


Figure 7-20 Graphical representation of transition between two rooms.

The model developed by Zhang et al. (2013) also only investigated a single floor scenario; in multiple floors, especially in large commercial buildings, there can be more than one stairway, multiple corridors, and rooms to go through. The Nottingham Geospatial Building is a perfect example with three stairways exiting at different zones of the building with multiple corridors. In this section, we will try to see the impact of passing through one or more corridors, stairs, rooms etc. during the transition by introducing trajectory routes for agent movement between rooms.

In the previous section, we validated the occupant model against real-world data from the Estates. So now we can use the model as a base case and work on the next hypothesis. With the existing lighting policy, most of the NGB lights are always in active mode, so there is no way to determine the impact on electricity consumption due to the agent's occupancy throughout the building. As such, we kept all the default setting of the model and changed the lighting configuration to smart lighting, i.e. PIR sensor controlled.

With the introduction of smart lighting policy for all lights in the simulation environment, we can now compare and contrast simulation results with and without trajectory route choices during agent movement. The list of trajectory routes was derived from Figure 7.10, as shown in Table 7.5, 7.6 and 7.7 for each of the transition between zones. During the simulation, route choices were made randomly from the available list for each zone, e.g. given an agent's current location, the transition from an existing zone to the destination zone is checked and for that move, the table is looked up for all possible routes available and one is randomly chosen. If trajectory choice is not included, agents would be teleported to their destination. A screenshot of the simulation window can be seen in Figure 7.21. Simulation results illustrated in Figure 7.22 show the electricity consumption difference between the two scenarios. The experiment was replicated 100 times with random seed for each of the two scenarios, and the aggregate results are plotted, as shown in Figure 7.23.

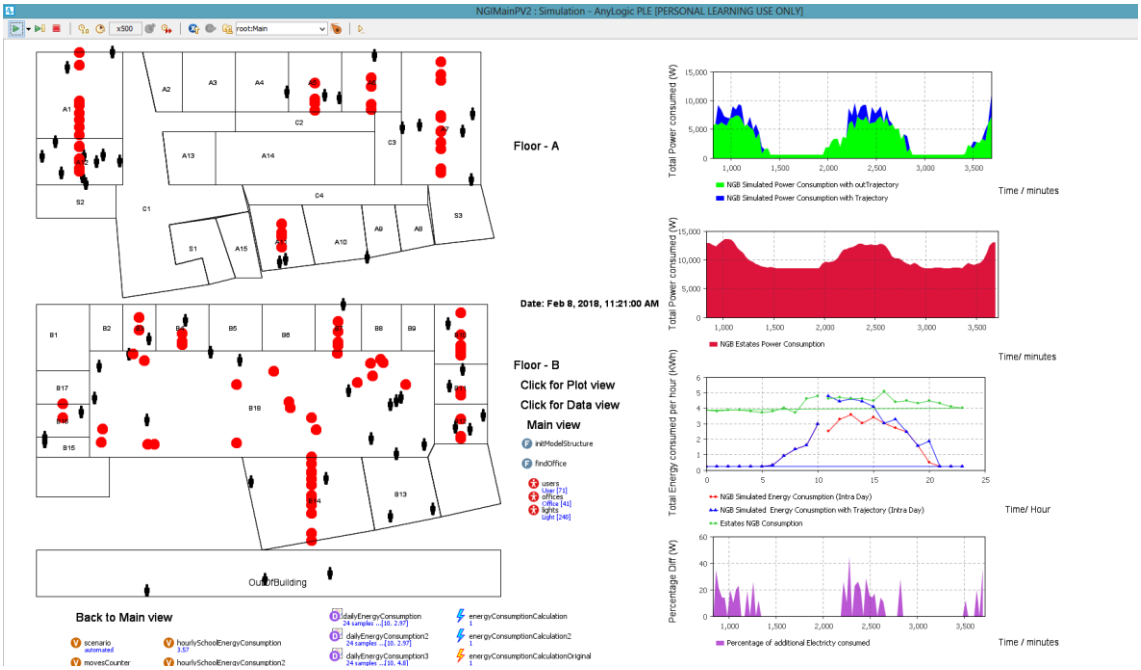


Figure 7-21 Image showing the main view of the simulation window comparing plots with and without trajectory

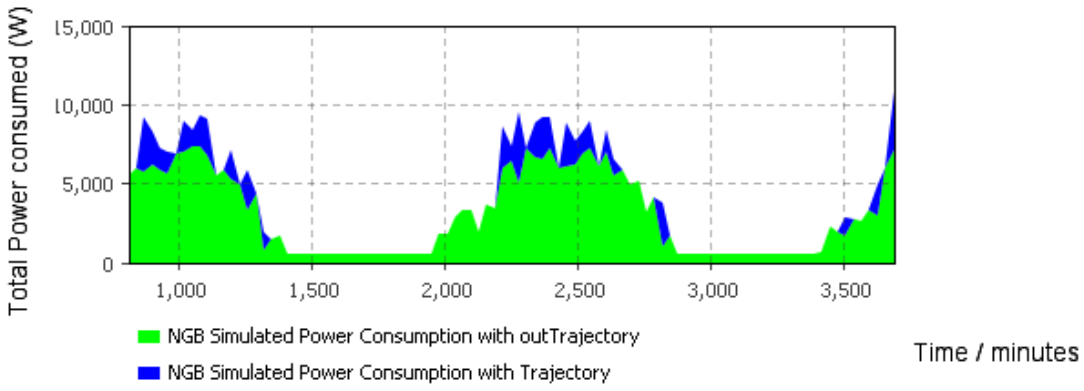


Figure 7-22 The difference between power consumption when using and not using trajectory route choice during agent movement is seen above. The blue is the extra energy usage when route choice is introduced.

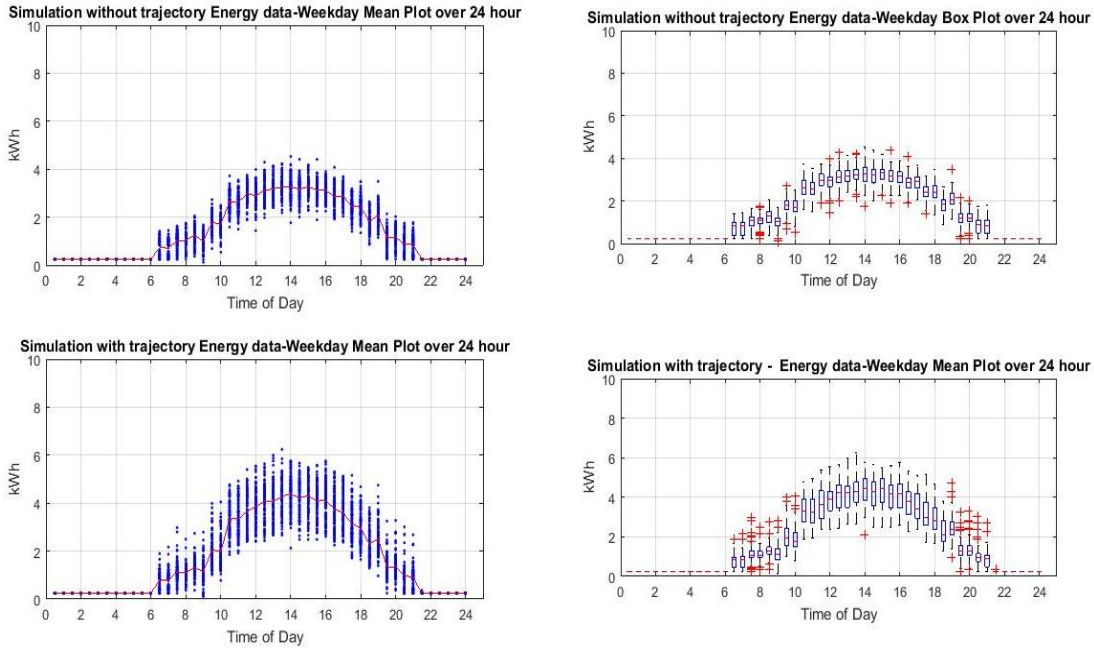


Figure 7-23 Showing energy consumption data without using trajectory and using trajectory information

Since smart lighting policy is adopted, zero electricity is consumed when the building is empty, and the lights respond to agent presence only. Electricity consumption starts to rise from 6 am morning and goes to zero by 9 pm as defined by the agent stereotype in Section 7.4.2. The shape of the curve for both the case is similar, but the box plot shows more variance with trajectory route choice when compared. This is simply because there is more than one route that an agent can choose during their movement, and the electricity consumption would vary depending on the length of the route. If the shorter route is taken, less energy would be consumed and vice versa. The peak energy consumption every half hour in the model without trajectory route choice is below 4KWh which when introduced reaches around 4KWh, thus showing a significant underestimation of energy consumption prediction when modelling without trajectory route choice.

7.6.3 Experiment 2: Random route choice vs probability-based route choice

Large commercial buildings may have lots of corridors and stairways, but they are not occupied all the time except when passing between rooms during office hours. Some

routes are shorter compared to others and occupants may prefer a specific route when travelling between rooms. It is also largely dependent on the location of the individual at that moment and how well they know the floor area. Not all destinations are next to their own office desk, and some may involve passing multiple corridors, rooms or stairways in the process. Such decisions of route choices are not always random taken as was the case in the previous section; instead, they may follow patterns or preferences among occupants. As such when comparing between random route choice and preference-based route choice, they may or may not have a significant impact on the overall electricity consumption in a smart building with PIR sensor-controlled lights, but it would be interesting to find out.

Indoor positioning in the form of the Lego trial helped us to understand and identify the preferences of route choice in the first two floors of the Nottingham Geospatial building. Data from the Lego trial was processed to identify route preferences among participants working in the office building. The data is then used to compute and tabulate all possible routes and their associated probabilities of preferences, as shown in Table 7.5, 7.6 and 7.7. In this section, two scenarios were investigated (i) with random route choice (ii) with probability specific route choice. Simulations were run with 100 replications for each of the cases, and the results were plotted, as shown below.

The left-hand side plots in Figure 7.24 illustrates the mean energy consumption every half hour varying over 24 hours for both the case of random route choice and probability specific route choice. The plot in the right illustrates the corresponding box plots showing the variance of energy for the 100 repetitions. It can be observed from the length of the bar that the variance for the random choice is higher during peak times of the day compared to probability specific route choice. Also, there seem to be a lot of outliers and smaller variance at the two ends of the box plots. This can be explained using the agent attendance plot in Figure 7.25 and 7.26.

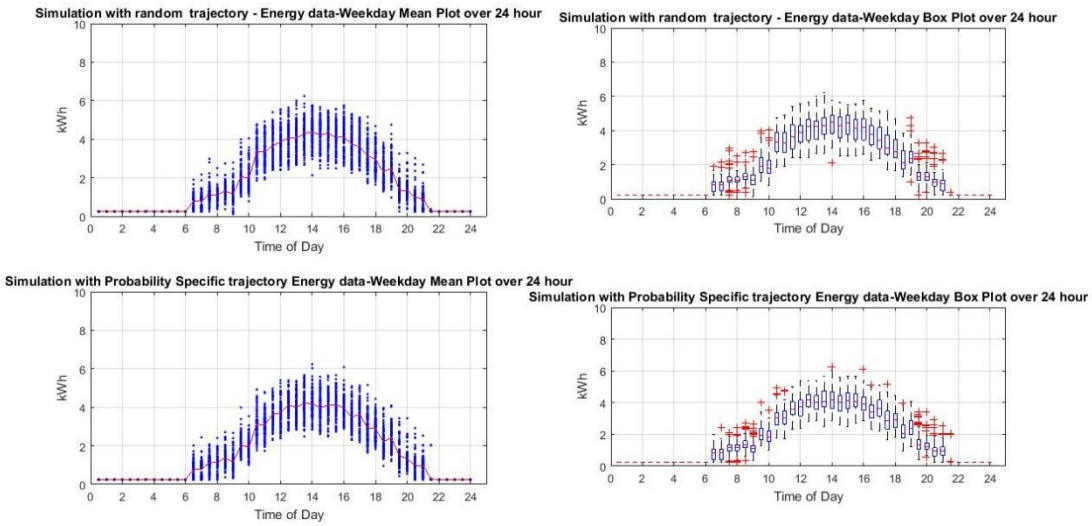


Figure 7-24 Showing the energy consumption between random and probability-based route choice

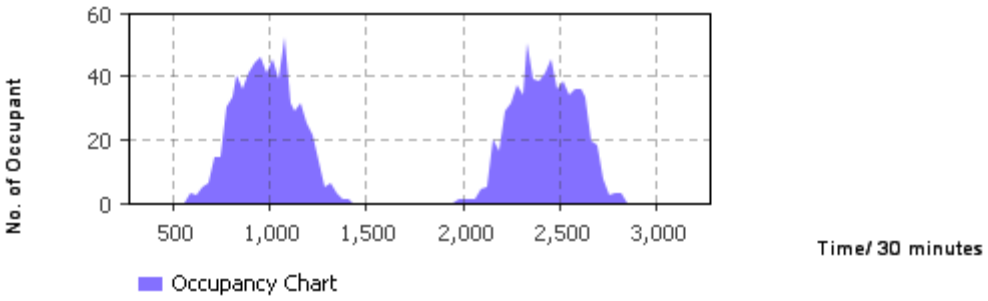


Figure 7-25 Snapshot of the agent attendance distribution over two days during the simulation run.

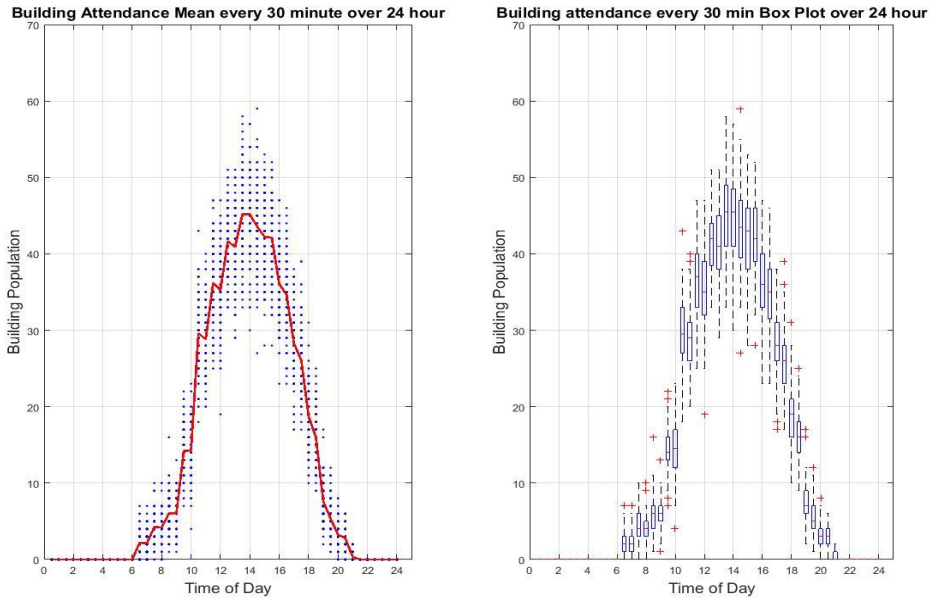


Figure 7-26 Building attendance plot with 100 replications over 24 hours showing both the mean and the box plot.

The building attendance population follows a Gaussian curve with a smaller attendance early morning slowly reaching a peak during midday and then falling as evening comes. The variance during peak times is higher mainly because of the stochastic nature of agent occupancy, when they are outside the building for break between and 12 and 3 pm. The smaller population early morning causes the variance to be smaller since fewer occupants are moving around the building. As the day progresses, the higher number of occupants causes more frequent movement within the building. That means most of the rooms will be occupied, and the stairways and corridors will be crossed more often, thus accounting for the higher variance.

The energy consumption illustrated in Figure 7.24 shows very little difference between the two cases, which is evident from Figure 7.27 showing the difference between scenarios. It can be seen there is a significant difference between not including trajectory and trajectory during agent movement but a minimal difference between random and probability specific route choice; as such it is important, we verify

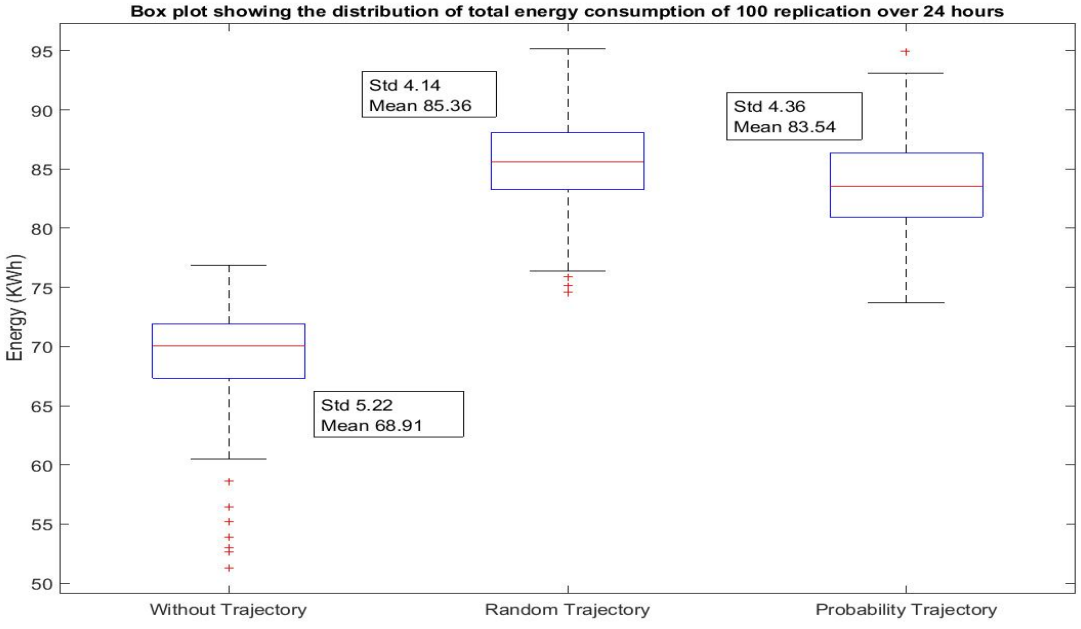


Figure 7-27 Box plot showing the difference in total energy consumption between different scenarios.

the statistical significance of the difference using a confidence interval. Since we are comparing two scenarios, the confidence interval for the difference between the results are calculated using the *paired – t* approach with 95% confidence as discussed by Robinson (2004).

$$CI = \overline{D} \mp t_{n-1.\alpha/2} \frac{S_D}{\sqrt{n}} \quad (7\text{-}2)$$

$$\overline{D} = \frac{\sum_{j=1}^{n}(X_{1j} - X_{2j})}{n} \quad (7\text{-}3)$$

$$S_D = \sqrt{\frac{\sum_{j=1}^{n}(X_{1j} - X_{2j} - \overline{D})^2}{n-1}} \quad (7\text{-}4)$$

Where:

CI = confidence interval

$\overline{D}$ = mean difference between scenario 1 (X_1) and scenario 2 (X_2)

X_{1j} = result from scenario 1 and replication j

X_{2j} = result from scenario 2 and replication j

S_D = standard deviation of the differences

n = number of replications performed (same for both scenarios)

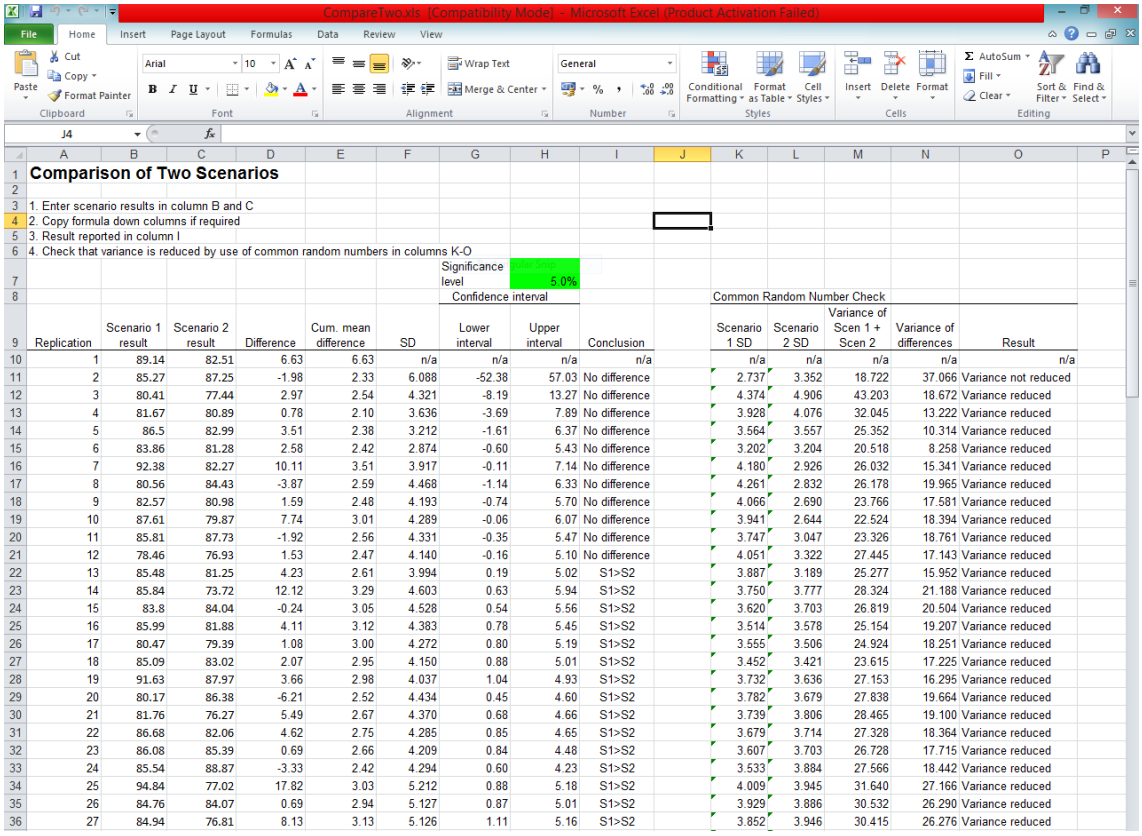
$t_{n-1.\alpha/2}$ = value from *t*- distribution with *n*-1 degree of freedom and significance level of $\alpha/2$

Scenario 1: Total energy consumption over 24 hours for 100 replications for random route choice.

Scenario 2: Total energy consumption over 24 hours for 100 replications for probability specific route choice.

Outcome: lower Interval = 0.63, upper interval = 3.03.

Thus, according to the paired confidence interval test, Scenario 1 electricity consumption is more than Scenario 2 electricity consumption and they are statistically significant. As such, we can conclude with 95% confidence that building route choice decision based on preferences instead of random choice has a statistically significant impact on energy consumption and saves energy. The reason for probability based route choice showing lower energy consumption compared to random route choice can be attributed to two factors. Firstly, the likelihood of routes having higher probability is chosen more often by the agents. This results in routes with common lighting period being taken most of the time throughout the day and avoiding less popular routes. Secondly some of the routes can be shorter as well consequently resulting in overall lower electricity consumption. The calculation of the combined paired confidence interval test scenario can be seen below. The interval outcome calculation is the combination of both the scenario data.



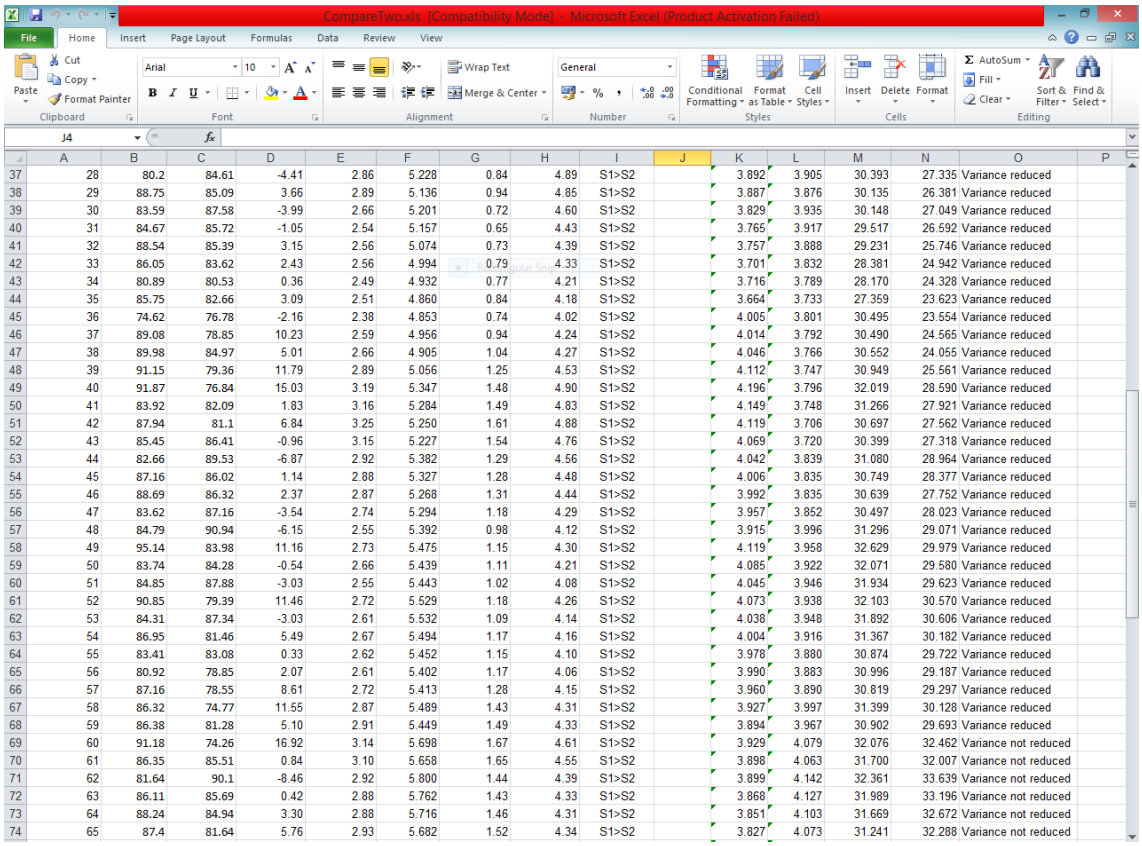
CompareTwo.xls [Compatibility Mode] - Microsoft Excel (Product Activation Failed)

Comparison of Two Scenarios

1. Enter scenario results in column B and C
2. Copy formula down columns if required
3. Result reported in column I
4. Check that variance is reduced by use of common random numbers in columns K-O

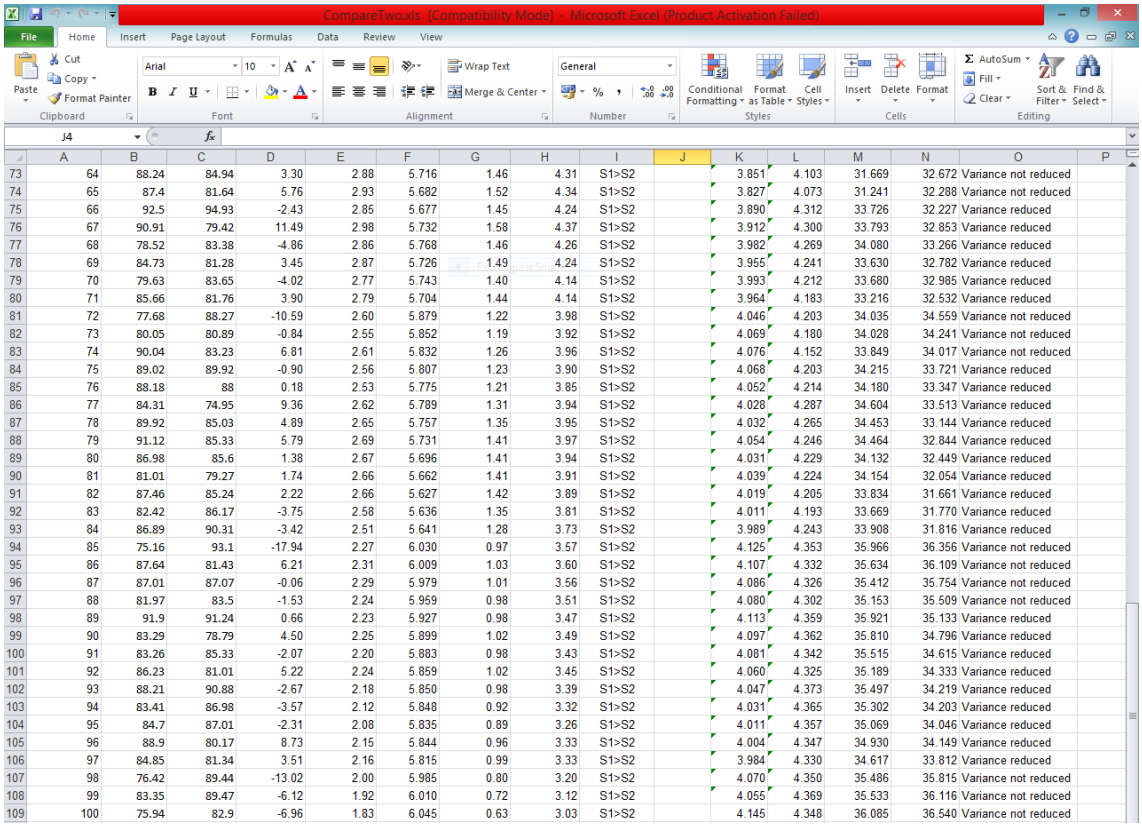
Significance level: 5.0%

		Confidence interval				Common Random Number Check			
Replication	Scenario 1 result	Scenario 2 result	Difference	Cum. mean difference	SD	Lower interval	Upper interval	Conclusion	Scenario 1 SD	Scenario 2 SD	Variance of Scen 1 + Scen 2	Variance of differences	Result
1	89.14	82.51	6.63	6.63	n/a	n/a	n/a	n/a	n/a	n/a	n/a	n/a	n/a
2	85.27	87.25	-1.98	2.33	6.088	-52.38	57.03	No difference	2.737	3.352	18.722	37.066	Variance not reduced
3	80.41	77.44	2.97	2.54	4.321	-8.19	13.27	No difference	4.374	4.906	43.203	18.672	Variance reduced
4	81.67	80.89	0.78	2.10	3.636	-3.69	7.89	No difference	3.928	4.076	32.045	13.222	Variance reduced
5	86.5	82.99	3.51	2.38	3.212	-1.61	6.37	No difference	3.564	3.557	25.352	10.314	Variance reduced
6	83.86	81.28	2.58	2.42	2.874	-0.60	5.43	No difference	3.202	3.204	20.518	8.258	Variance reduced
7	92.38	82.27	10.11	3.51	3.917	-0.11	7.14	No difference	4.180	2.926	26.032	15.341	Variance reduced
8	80.56	84.43	-3.87	2.59	4.468	-1.14	6.33	No difference	4.261	2.832	26.178	19.965	Variance reduced
9	82.57	80.98	1.59	2.48	4.193	-0.74	5.70	No difference	4.066	2.690	23.766	17.581	Variance reduced
10	87.61	79.87	7.74	3.01	4.289	-0.06	6.07	No difference	3.941	2.644	22.524	18.394	Variance reduced
11	85.81	87.73	-1.92	2.56	4.331	-0.35	5.47	No difference	3.747	3.047	23.326	18.761	Variance reduced
12	78.46	76.93	1.53	2.47	4.140	-0.16	5.10	No difference	4.051	3.322	27.445	17.143	Variance reduced
13	85.48	81.25	4.23	2.61	3.994	0.19	5.02	S1>S2	3.887	3.189	25.277	15.952	Variance reduced
14	85.84	73.72	12.12	3.29	4.603	0.63	5.94	S1>S2	3.750	3.777	28.324	21.188	Variance reduced
15	83.8	84.04	-0.24	3.05	4.528	0.54	5.56	S1>S2	3.620	3.703	26.819	20.504	Variance reduced
16	85.99	81.88	4.11	3.12	4.383	0.78	5.45	S1>S2	3.514	3.578	25.154	19.207	Variance reduced
17	80.47	79.39	1.08	3.00	4.272	0.80	5.19	S1>S2	3.555	3.506	24.924	18.251	Variance reduced
18	85.09	83.02	2.07	2.95	4.150	0.88	5.01	S1>S2	3.452	3.421	23.615	17.225	Variance reduced
19	91.63	87.97	3.66	2.98	4.037	1.04	4.93	S1>S2	3.732	3.636	27.153	16.295	Variance reduced
20	80.17	86.38	-6.21	2.52	4.434	0.45	4.60	S1>S2	3.782	3.679	27.838	19.664	Variance reduced
21	81.76	76.27	5.49	2.67	4.370	0.68	4.66	S1>S2	3.739	3.806	28.465	19.100	Variance reduced
22	86.68	82.06	4.62	2.75	4.285	0.85	4.65	S1>S2	3.679	3.714	27.328	18.364	Variance reduced
23	86.08	85.39	0.69	2.66	4.209	0.84	4.48	S1>S2	3.607	3.703	26.728	17.715	Variance reduced
24	85.54	88.87	-3.33	2.42	4.294	0.60	4.23	S1>S2	3.533	3.884	27.566	18.442	Variance reduced
25	94.84	77.02	17.82	3.03	5.212	0.88	5.18	S1>S2	4.009	3.945	31.640	27.166	Variance reduced
26	84.76	84.07	0.69	2.94	5.127	0.87	5.01	S1>S2	3.929	3.886	30.532	26.290	Variance reduced
27	84.94	76.81	8.13	3.13	5.126	1.11	5.16	S1>S2	3.852	3.946	30.415	26.276	Variance reduced



CompareTwo.xls [Compatibility Mode] - Microsoft Excel (Product Activation Failed)

28	80.2	84.61	-4.41	2.86	5.228	0.84	4.89	S1>S2	3.892	3.905	30.393	27.335	Variance reduced
29	88.75	85.09	3.66	2.89	5.136	0.94	4.85	S1>S2	3.887	3.876	30.135	26.381	Variance reduced
30	83.59	87.58	-3.99	2.66	5.201	0.72	4.60	S1>S2	3.829	3.935	30.148	27.049	Variance reduced
31	84.67	85.72	-1.05	2.54	5.157	0.65	4.43	S1>S2	3.765	3.917	29.517	26.592	Variance reduced
32	88.54	85.39	3.15	2.56	5.074	0.73	4.39	S1>S2	3.757	3.888	29.231	25.746	Variance reduced
33	86.05	83.62	2.43	2.56	4.994	0.79	4.33	S1>S2	3.701	3.832	28.381	24.942	Variance reduced
34	80.89	80.53	0.36	2.49	4.932	0.77	4.21	S1>S2	3.716	3.789	28.170	24.328	Variance reduced
35	85.75	82.66	3.09	2.51	4.860	0.84	4.18	S1>S2	3.664	3.733	27.359	23.623	Variance reduced
36	74.62	76.78	-2.16	2.38	4.853	0.74	4.02	S1>S2	4.005	3.801	30.495	23.554	Variance reduced
37	89.08	78.85	10.23	2.59	4.956	0.94	4.24	S1>S2	4.014	3.792	30.490	24.565	Variance reduced
38	89.98	84.97	5.01	2.66	4.905	1.04	4.27	S1>S2	4.046	3.766	30.552	24.055	Variance reduced
39	91.15	79.36	11.79	2.89	5.056	1.25	4.53	S1>S2	4.112	3.747	30.949	25.561	Variance reduced
40	91.87	76.84	15.03	3.19	5.347	1.48	4.90	S1>S2	4.196	3.796	32.019	28.590	Variance reduced
41	83.92	82.09	1.83	3.16	5.284	1.49	4.83	S1>S2	4.149	3.748	31.266	27.921	Variance reduced
42	87.94	81.1	6.84	3.25	5.250	1.61	4.88	S1>S2	4.119	3.706	30.697	27.562	Variance reduced
43	85.45	86.41	-0.96	3.15	5.227	1.54	4.76	S1>S2	4.069	3.720	30.399	27.318	Variance reduced
44	82.66	89.53	-6.87	2.92	5.382	1.29	4.56	S1>S2	4.042	3.839	31.080	28.964	Variance reduced
45	87.16	86.02	1.14	2.88	5.327	1.28	4.48	S1>S2	4.006	3.835	30.749	28.377	Variance reduced
46	88.69	86.32	2.37	2.87	5.268	1.31	4.44	S1>S2	3.992	3.835	30.639	27.752	Variance reduced
47	83.62	87.16	-3.54	2.74	5.294	1.18	4.29	S1>S2	3.957	3.852	30.497	28.023	Variance reduced
48	84.79	90.94	-6.15	2.55	5.392	0.98	4.12	S1>S2	3.915	3.996	31.296	29.071	Variance reduced
49	95.14	83.98	11.16	2.73	5.475	1.15	4.30	S1>S2	4.119	3.958	32.629	29.979	Variance reduced
50	83.74	84.28	-0.54	2.66	5.439	1.11	4.21	S1>S2	4.085	3.922	32.071	29.580	Variance reduced
51	84.85	87.88	-3.03	2.55	5.443	1.02	4.08	S1>S2	4.045	3.946	31.934	29.623	Variance reduced
52	90.85	79.39	11.46	2.72	5.529	1.18	4.26	S1>S2	4.073	3.938	32.103	30.570	Variance reduced
53	84.31	87.34	-3.03	2.61	5.532	1.09	4.14	S1>S2	4.038	3.948	31.892	30.606	Variance reduced
54	86.95	81.46	5.49	2.67	5.494	1.17	4.16	S1>S2	4.004	3.916	31.367	30.182	Variance reduced
55	83.41	83.08	0.33	2.62	5.452	1.15	4.10	S1>S2	3.978	3.880	30.874	29.722	Variance reduced
56	80.92	78.85	2.07	2.61	5.402	1.17	4.06	S1>S2	3.990	3.883	30.996	29.187	Variance reduced
57	87.16	78.55	8.61	2.72	5.413	1.28	4.15	S1>S2	3.960	3.890	30.819	29.297	Variance reduced
58	86.32	74.77	11.55	2.87	5.489	1.43	4.31	S1>S2	3.927	3.997	31.399	30.128	Variance reduced
59	86.38	81.28	5.10	2.91	5.449	1.49	4.33	S1>S2	3.894	3.967	30.902	29.693	Variance reduced
60	91.18	74.26	16.92	3.14	5.698	1.67	4.61	S1>S2	3.929	4.079	32.076	32.462	Variance not reduced
61	86.35	85.51	0.84	3.10	5.658	1.65	4.55	S1>S2	3.898	4.063	31.700	32.007	Variance not reduced
62	81.64	90.1	-8.46	2.92	5.800	1.44	4.39	S1>S2	3.899	4.142	32.361	33.639	Variance not reduced
63	86.11	85.69	0.42	2.88	5.762	1.43	4.33	S1>S2	3.868	4.127	31.989	33.196	Variance not reduced
64	88.24	84.94	3.30	2.88	5.716	1.46	4.31	S1>S2	3.851	4.103	31.669	32.672	Variance not reduced
65	87.4	81.64	5.76	2.93	5.682	1.52	4.34	S1>S2	3.827	4.073	31.241	32.288	Variance not reduced



CompareTwo.xls [Compatibility Mode] - Microsoft Excel (Product Activation Failed)

	A	B	C	D	E	F	G	H	I	J	K	L	M	N	O	P
73	64	88.24	84.94	3.30	2.88	5.716	1.46	4.31	S1>S2		3.851	4.103	31.669	32.672	Variance not reduced	
74	65	87.4	81.64	5.76	2.93	5.682	1.52	4.34	S1>S2		3.827	4.073	31.241	32.288	Variance not reduced	
75	66	92.5	94.93	-2.43	2.85	5.677	1.45	4.24	S1>S2		3.890	4.312	33.726	32.227	Variance reduced	
76	67	90.91	79.42	11.49	2.98	5.732	1.58	4.37	S1>S2		3.912	4.300	33.793	32.853	Variance reduced	
77	68	78.52	83.38	-4.86	2.86	5.768	1.46	4.26	S1>S2		3.982	4.269	34.080	33.266	Variance reduced	
78	69	84.73	81.28	3.45	2.87	5.726	1.49	4.24	S1>S2		3.955	4.241	33.630	32.782	Variance reduced	
79	70	79.63	83.65	-4.02	2.77	5.743	1.40	4.14	S1>S2		3.993	4.212	33.680	32.985	Variance reduced	
80	71	85.66	81.76	3.90	2.79	5.704	1.44	4.14	S1>S2		3.964	4.183	33.216	32.532	Variance reduced	
81	72	77.68	88.27	-10.59	2.60	5.879	1.22	3.98	S1>S2		4.046	4.203	34.035	34.559	Variance not reduced	
82	73	80.05	80.89	-0.84	2.55	5.852	1.19	3.92	S1>S2		4.069	4.180	34.028	34.241	Variance not reduced	
83	74	90.04	83.23	6.81	2.61	5.832	1.26	3.96	S1>S2		4.076	4.152	33.849	34.017	Variance not reduced	
84	75	89.02	89.92	-0.90	2.56	5.807	1.23	3.90	S1>S2		4.068	4.203	34.215	33.721	Variance reduced	
85	76	88.18	88	0.18	2.53	5.775	1.21	3.85	S1>S2		4.052	4.214	34.180	33.347	Variance reduced	
86	77	84.31	74.95	9.36	2.62	5.789	1.31	3.94	S1>S2		4.028	4.287	34.604	33.513	Variance reduced	
87	78	89.92	85.03	4.89	2.65	5.757	1.35	3.95	S1>S2		4.032	4.265	34.453	33.144	Variance reduced	
88	79	91.12	85.33	5.79	2.69	5.731	1.41	3.97	S1>S2		4.054	4.246	34.464	32.844	Variance reduced	
89	80	86.98	85.6	1.38	2.67	5.696	1.41	3.94	S1>S2		4.031	4.229	34.132	32.449	Variance reduced	
90	81	81.01	79.27	1.74	2.66	5.662	1.41	3.91	S1>S2		4.039	4.224	34.154	32.054	Variance reduced	
91	82	87.46	85.24	2.22	2.66	5.627	1.42	3.89	S1>S2		4.019	4.205	33.834	31.661	Variance reduced	
92	83	82.42	86.17	-3.75	2.58	5.636	1.35	3.81	S1>S2		4.011	4.193	33.669	31.770	Variance reduced	
93	84	86.89	90.31	-3.42	2.51	5.641	1.28	3.73	S1>S2		3.989	4.243	33.908	31.816	Variance reduced	
94	85	75.16	93.1	-17.94	2.27	6.030	0.97	3.57	S1>S2		4.125	4.353	35.966	36.356	Variance not reduced	
95	86	87.64	81.43	6.21	2.31	6.009	1.03	3.60	S1>S2		4.107	4.332	35.634	36.109	Variance not reduced	
96	87	87.01	87.07	-0.06	2.29	5.979	1.01	3.56	S1>S2		4.086	4.326	35.412	35.754	Variance not reduced	
97	88	81.97	83.5	-1.53	2.24	5.959	0.98	3.51	S1>S2		4.080	4.302	35.153	35.509	Variance not reduced	
98	89	91.9	91.24	0.66	2.23	5.927	0.98	3.47	S1>S2		4.113	4.359	35.921	35.133	Variance reduced	
99	90	83.29	78.79	4.50	2.25	5.899	1.02	3.49	S1>S2		4.097	4.362	35.810	34.796	Variance reduced	
100	91	83.26	85.33	-2.07	2.20	5.883	0.98	3.43	S1>S2		4.081	4.342	35.515	34.615	Variance reduced	
101	92	86.23	81.01	5.22	2.24	5.859	1.02	3.45	S1>S2		4.060	4.325	35.189	34.333	Variance reduced	
102	93	88.21	90.88	-2.67	2.18	5.850	0.98	3.39	S1>S2		4.047	4.373	35.497	34.219	Variance reduced	
103	94	83.41	86.98	-3.57	2.12	5.848	0.92	3.32	S1>S2		4.031	4.365	35.302	34.203	Variance reduced	
104	95	84.7	87.01	-2.31	2.08	5.835	0.89	3.26	S1>S2		4.011	4.357	35.069	34.046	Variance reduced	
105	96	88.9	80.17	8.73	2.15	5.844	0.96	3.33	S1>S2		4.004	4.347	34.930	34.149	Variance reduced	
106	97	84.85	81.34	3.51	2.16	5.815	0.99	3.33	S1>S2		3.984	4.330	34.617	33.812	Variance reduced	
107	98	76.42	89.44	-13.02	2.00	5.985	0.80	3.20	S1>S2		4.070	4.350	35.486	35.815	Variance not reduced	
108	99	83.35	89.47	-6.12	1.92	6.010	0.72	3.12	S1>S2		4.055	4.369	35.533	36.116	Variance not reduced	
109	100	75.94	82.9	-6.96	1.83	6.045	0.63	3.03	S1>S2		4.145	4.348	36.085	36.540	Variance not reduced	

Figure 7-28 Paired confidence interval test calculation for 100 replications.

7.6.4 Experiment 3: Impact of light switch off delay on energy consumption

One of the features of smart lighting is the PIR sensors' capability to detect movement within its proximity and respond by automatically switching on the connected light, but the connected light does not switch off immediately when it ceases to detect motion. There is a built-in automated delay to allow for a reasonable amount of time until the person has moved out of range. This delay can be configured according to the requirement and in theory, can have a noticeable impact on the peak energy consumption depending on the length of the delay. In the previous two sections with the smart lighting scenario, the minimum delay was set at 5 minutes. Based on our observation, this delay varies between rooms, open spaces and corridors, but all of them were more than 5 minutes. The simulation model that includes trajectory (smart lighting policy) never reaches the peak energy consumption indicated by Estates' data;

assuming all the lights would be switched ON during peak hours when the building capacity is reached.

In this section we will discuss the results from running some more experiments with the existing model, merely changing the settings of the automated light delay (in steps of 5 minutes), to see if the simulation ever reaches the top-level consumption indicated by the Estates' data. The following plots show energy consumption for each of the light delay settings; 10, 15 and 20 minutes. For each setting simulation was run for both random and probability specific trajectory choice with 100 replications and a random seed.

It can be observed from the Figures 7.29. 7.30 and 7.31 that with increasing light switch off delay the peak energy consumption increases and reaches the level indicated by the Estates' data, as shown in Figure 7.18. Also, for each switch off delay scenario, the energy peak for random trajectory route choice was slightly higher compared to probability specific route choice as illustrated in Figure 7.32.

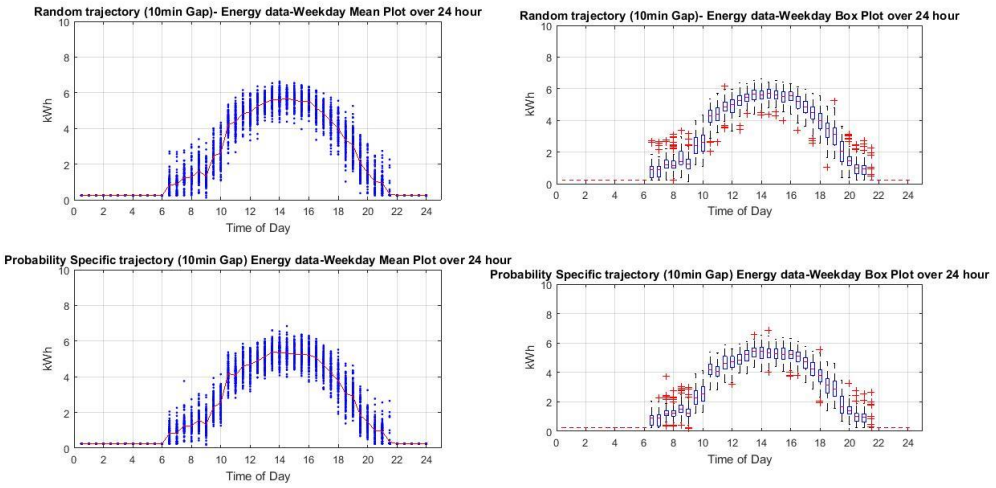


Figure 7-29 Energy consumption data for a 10-minute delay in automated lighting setting.

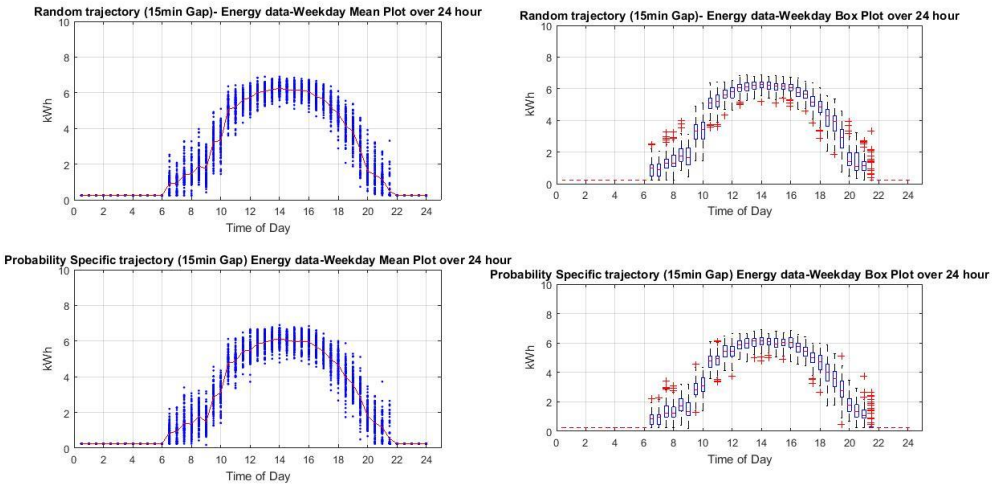


Figure 7-30 Energy consumption data for a 15-minute delay in automated lighting setting.

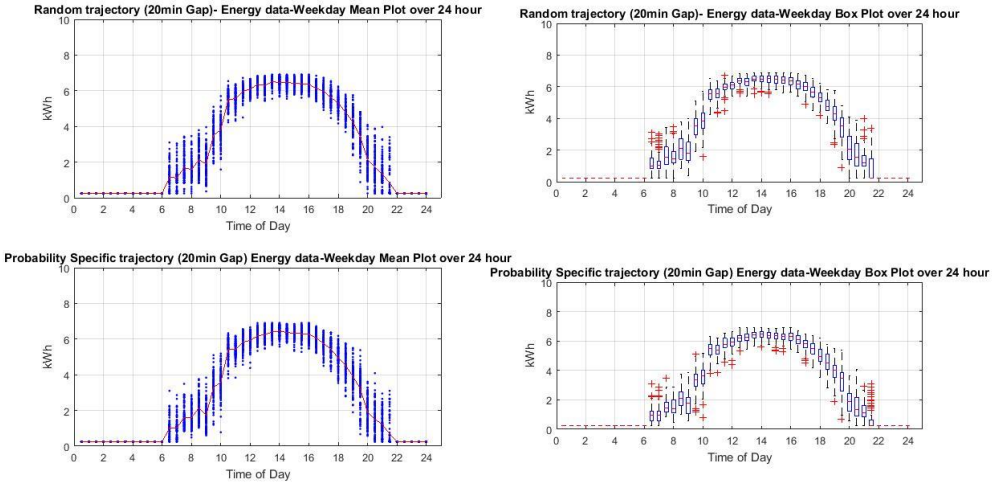


Figure 7-31 Energy consumption data for a 20-minute delay in automated lighting setting.

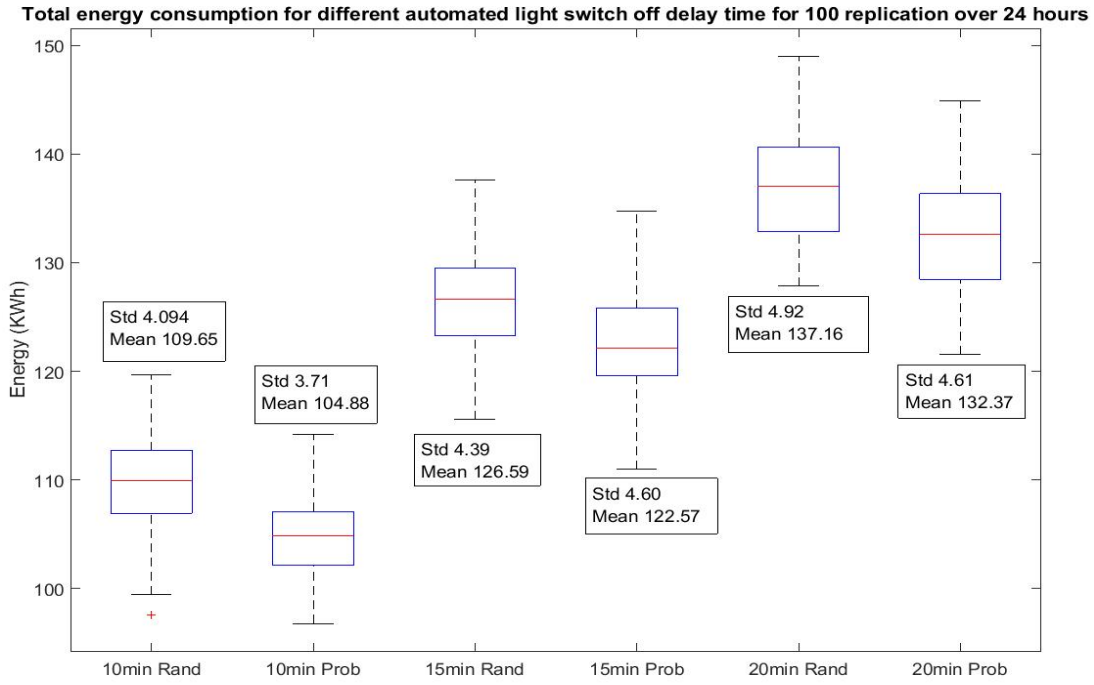


Figure 7-32 Energy consumption data for each of the automated lighting switch-off delay.

As such a paired confidence interval test was done to check the statistical significance of the difference and with 95% confidence for all the three cases, route choice with predefined probability showed significant impact and saved energy as shown in Table 7.8. Similar calculation method is followed for each case as seen in Figure 7.28.

Table 7-8 Showing the *paired – t* approach confidence interval test result

Scenario	Result	Conclusion
10 min switch off delay S1: Random S2: Probabilistic	Lower Interval: 3.73 Upper Interval: 5.92	S1 consumes more energy compared to S2 with 95 % confidence
15 min switch off delay S1: Random S2: Probabilistic	Lower Interval: 2.76 Upper Interval: 5.42	S1 consumes more energy compared to S2 with 95 % confidence

20 min switch off delay S1: Random S2: Probabilistic	Lower Interval: 3.21 Upper Interval: 5.84	S1 consumes more energy compared to S2 with 95 % confidence

7.7 Methodological Implications and Limitations

Recall that the research in this chapter investigated understanding the local dynamics of building electricity consumption over time for different lighting policies and how indoor positioning data from observed individuals' trajectories can help to estimate electricity usage in multi-floor offices. The initial model validation was done against actual energy consumption data collected from Estates, University of Nottingham and simulation results showed total mean energy consumption of 231KWh compared to Estates' data of 230KWh. The validated model was then calibrated as required and used as a base case with changing lighting scenario and used to prove the list of the hypothesis. We will discuss the outcome of the study concerning the three hypotheses initially set up.

1. **Using trajectory information during an agent's transition between rooms helps to predict more practical electricity usage:** The simulation at first considered typical agent state transition (teleporting) and then introduced trajectory routes. The results showed a significant difference between the two cases, according to Figure 7.26. Simulation results without trajectory show 68.5 KWh compared to 85.14 KWh with trajectory per day. This shows a typical electricity consumption underestimation of 16.64 KWh per day or 5028.32 KWh per year (only considering weekdays). Considering average variable unit electricity price of 13.86 pence / KWh for east midlands region according to the census provided in (*Compare 2020 Electricity Prices: Average UK Rates & Tariffs Per kWh*, no date), the model prediction underestimates roughly 697 GBP annually. Thus it proves the case that incorporating trajectory information

during agent movement between rooms help to minimise underestimation and predict more realistic electricity consumption data.

2. **Using route choice probability when compared to making a random choice**: Here we looked into the difference when instead of randomly choosing possible routes during agent transitions, we use route choice probability computed directly from actual occupancy data collected from the Lego trial using the Indoor positioning system. The outcome was a small difference between total electricity consumption of 83.54 KWh per day for probability specific route choice and to 85.36 KWh for random route choice as seen in Figure 7.26. The result shows a difference of 1.82 kWh per day or 567.84 KWh per year (weekdays). Statistically, we have proven that the difference is significant using the *paired-t approach of* the confidence interval test. In reality this is a very insignificant difference in electricity consumption per day and probably would not make much impact. One possible explanation for this small difference can be that we had similar number of lights allocated in each corridor and stairways based on our observation of the actual building (NGB). The spaces were always in use by the agents when transiting from one room to another during simulation. As such the overall outcome of probability-based route choice only helped to constrain their decision. If there was a significant difference between the number of lights in the corridors or if the building was much bigger like a hospital we probably would have found some significant differences, given some spaces are sparsely populated leading to the less frequent use of corridors, hallways or stairways in those parts.
3. **Automated light switch-off delay:** We assumed that when the delay time is increased significantly in the absence of occupants in the rooms/corridors, they reach top level consumption indicated by Estates' data. This is significant because the light switch off modelling time was initially taken to be 5 minutes, which is not realistic. In reality, this would typically be around at least 20 minutes, observed by physically exploring the building. As illustrated in the energy plot of Figure 7.27, 7.28 and 7.29 and a box plot of Figure 7.30, the

energy consumption distribution over the day reaches the peak as indicated by Estates' data when the light switch off delay is increased to 20 minutes showing a total energy consumption of 132 KWh (probability-based route choice) and 137 KWh (random route choice) per day. The output from probability-based route choice shows a difference of around 99 KWh per day or 30987 KWh per year (weekdays) when compared to Estates' mean electricity consumption of 231 KWh per day. This is a significant underestimation of electricity consumption when predicting building performance but including trajectory routes during state transition and light switch off delay helped to predict more realistic energy consumption from building lighting. This shows if all lights are PIR sensor controlled and the automated light switch-off delay is optimally configured then Estates could roughly save around 4295 GBP if the average price per unit electricity cost of 13.86 pence / KWh is considered according to the census (*Compare 2020 Electricity Prices: Average UK Rates & Tariffs Per kWh*, no date).

The model in this research has several shortcomings. Firstly, a realistic agent occupancy model is not implemented when compared to other models in the literature discussed in this chapter. The current model (base model) follows a random choice from a uniform distribution when determining agent occupancy and subsequent state transition. Real-life occupancy is very complex and exhibits varied occupancy behaviour, arrival and exit time and out of office breaks among individual occupants and occupant stereotypes. Secondly, the model does not incorporate short-time and long-time absence (such as vacations) within the model. This will impact how electricity is consumed in individual office rooms and other resources in the building thus making inaccurate predictions from the simulation. Third, in this research, we only investigated electricity consumption during weekdays. The electricity consumption differs during weekends since building occupancy would vary significantly. As a result, it is difficult to identify a definite pattern of occupancy without informed observation or reliable occupancy data. Finally, the model only investigated lighting energy sources. Including other energy sources such as

computers, fridge or microwave would help to provide a more complete picture of the overall building electricity consumption by occupants.

7.8 Potential Applications of Occupancy data

Modelling of building energy usage is typically done during building design stage and evaluated post occupancy period. Typical predictions obtained from energy estimation software's and statistical forecasting can deviate much from actual consumption mainly due to lack of understanding of occupants behaviour as well as exclusion of important details. In most of the cases it is assumed that occupant behaviours are constant for any type of building irrespective of building design, purpose, population, location and weather. Thus, to plan and design sustainable buildings and formulate energy policies in urban areas, it is of paramount importance that building occupancy is accurately predicted taking into consideration as much behavioural factors as possible (Azar *et al.*, 2011).

According to statistics provided by Barbour *et al.* (2019) over 40% of energy usage relates to buildings in the US and EU and may be much more if the whole world is considered. This is especially concentrated in urban areas which are rapidly expanding. Although energy model prediction is done at design stage, real life occupancy is hard to predict. Hence collection of occupancy data in post occupancy stage is vital to help us to understand the varying behaviour of occupants in different types of building and improve model accuracy. The data from this research can be analysed to understand not just occupancy pattern room-by-room or routes choices but also provide insights to the demographics of behavioural patterns of occupants at different times of the day and month specific to the type of building. This understanding can be applied for predictions in other similar buildings.

One of the most important application of occupancy data collected from this research is the development of an improved occupancy or presence model from existing ones such as the one stated in (Page *et al.*, 2008). The model should have the potential to incorporate multiple states of occupancy as well as route choices and also include

behavioural traits from different clusters of occupants when it comes to understanding building occupancy.

Use of accurate occupancy data to model and develop occupancy based heating systems is gaining popularity in building heating system design (Becker *et al.*, 2018). Occupancy data collected using indoor positioning methodology with sufficient accuracy has the potential to provide a detailed record of occupant journey in the building. The data collected in this research surely has the potential to be applied and improve the prediction capability of the models.

As discussed earlier in the work of (Clevenger *et al.*, 2006; Haldi *et al.*, 2011; Hong *et al.*, 2016) modelling of occupant behaviour is vital for improved modelling of building energy consumption, not just limited to lighting but also usage of appliances and electrical systems of everyday use such as TV, computer, washing machine and fridge. Occupancy presence model is an integral part for developing all these models and acts as an input for all. Since occupancy data collected in this research has the potential to provide detailed movement profiles of individuals, the possibility of interactions with building infrastructures such as window blinds and shading devices, window opening and light switching can be better understood.

Building occupancy data can also play a vital role in forecasting utility prices and play a constructive role in the development of smart grid systems. In post occupancy stage building management can benefit from the observation of occupancy data and plan for efficient operations and also be well prepared for any decisions related to future energy pricing and budgets. Also since our energy resources are limited it is important to manage existing ones effectively. As such focus is now on rolling out smart grids. Due to increased demand of electricity during peak times it is becoming important to balance the load distribution in real time between grids especially during peak times and accurate occupancy data can play a positive role (Newsham *et al.*, 2010).

The potential to effectively manage energy consumption in buildings is high. Since there is an expected gap between design and operational phase of a building (De Wilde, 2014) identifying the right policies and measures to improve energy

consumption is very important. Occupancy data can help to understand how the building layout and space allocation affects the configuration of the energy sources such as HVAC and lighting and the output of energy efficiency indicator also known as specific energy consumption (SEC) commonly measured in KWh/m^2 per annum. (Huovila *et al.*, 2017). Also accurate occupancy data can help improve the intelligence of building automation systems and enabling their designers to introduce more options by predicting the impact on occupant behaviour as seen in (Breslav *et al.*, 2013). Route choices collected from occupancy data can help to understand most commonly used spaces such as corridors, stairways in the building and actions to take in case of emergency scenarios such as fire evacuation. Effective management of facilities and storage of equipment's prone to cause danger in populated areas can be ensured. Accurate occupancy data can be used to improve mathematical models related to emergency evacuation simulations in large buildings such as shopping malls and hospitals (Løvs, 1998) (Pan *et al.*, 2007; Society of Fire Protection Engineers, 2019).

In this research occupancy data collection was limited due to ethical factors and time constraint. Extensive collection of occupancy data has the potential to be used as input in a variety of application areas related to the improvement of building energy efficiency, performance assessment and energy management (Kwok *et al.*, 2011; Huovila *et al.*, 2013; Ioannidis *et al.*, 2016; Mujtaba *et al.*, 2018). It can also act as a factor in raising awareness among occupants to be more socially responsible and change their behaviour when it comes to reducing energy consumption (van der Sandt, 2012; Zhang *et al.*, 2013).

7.9 Discussion

In this chapter, we have successfully shown the development of an agent-based occupation model and the value of using indoor positioning in the form of route choice probability derived from the Lego trial. The model looked into various electricity consumption scenarios from building lighting and used the input from positioning trial data in one of them to understand the implications, if any, on electrical energy consumption. The result of using probability specific route choice as opposed to

random route choice during agent movement showed a statistically significant difference in energy consumption. The random choice always showed higher energy consumption even in the automated light switch off scenarios with 95% confidence, but in reality, the difference is insignificant from a practical point of view as seen in Figure 7.26 and 7.30 and it will not make any significant impact since this can be easily adjusted during model calibration. It is important to keep in mind the case studies were chosen to demonstrate to the indoor positioning community how simulation and modelling of building energy prediction is done with one specific scenario of how indoor positioning data can be used. As such they may not exhibit the many potential application of positioning data some of which were discussed in section 7.8. Also due to time constraints of the PhD and privacy concern certain limitations were there regarding data collection and the duration of the trials.

Nevertheless, the positioning system developed in our project has the potential to be used to detect occupancy behaviour over the whole day with just the smartphone. We can process the data to understand real life individual occupancy behaviour and derive aggregate occupancy behaviour among similar groups of people which will be more realistic and will not require mathematical models or model calibration as seen in other models. These patterns can be understood using machine learning techniques such as clustering and infer different behavioural characteristics of actual participants instead of relying on surveys. As such, we can use the data to develop a more detailed occupancy model, acting as input to building occupant models. Future work would look to utilise the positioning system to develop a more detailed non-calibrated occupancy model from real word data which can be generalised to integrate with any other building floor plan and observe the impact on the energy simulation.

Chapter 8

CONCLUSION

To provide a concise and purposeful conclusion it is important to revisit the objectives of the thesis set out at the beginning in Chapter 1, and so check whether the objectives have been fulfilled and how they relate to the overall aim of the thesis, i.e. “improve building occupant modelling with the help of indoor positioning”. The objectives of the thesis are reviewed one by one and the relevant outcome for each stage of the research is discussed.

8.1 Summary of Research Results

8.1.1 Review of Objectives

(i) Develop easy to use Prototype Indoor Positioning System

The thesis explored the existing state of building occupant modelling and existing technology and techniques related to indoor positioning research. Based on that an informed decision was made with regards to the development of the positioning system and the choice of technology and techniques keeping in mind the scope of the thesis, time constraint, feasibility of usage and deployment factors discussed in Chapter 2 and 3. The methodology and technique used in developing the core framework of the prototype using Wi-Fi and BLE have been discussed in detail in Chapter 4. A bespoke Android specific data logger was developed and its technical specification detailed in this thesis. Details of the positioning infrastructure, *RSS* measurement characteristics from Wi-Fi and BLE beacons were covered. The fingerprinting technique was used to develop the radio map for both Wi-Fi and BLE and their performance analysed by carrying out static trials on the different floors of the building. Standard pattern matching algorithms were implemented for position computation using the trial data and their accuracy was evaluated.

Chapter 5 made use of these measurements and methods to implement algorithms required for developing the state-of-the-art multi-sensor positioning framework. Motion sensors from the smartphone, to be used for positioning data collection in this research have been analysed to get an estimate of the measurement noise and bias using the Allan variance method. Based on their satisfactory performance, motion detection and heading estimation algorithms were implemented and thoroughly tested. The particle filter engine was implemented and integrated with the Wi-Fi and BLE fingerprint radio map to develop a fully functional indoor positioning system with pedestrian dead reckoning capability. The algorithms implemented were carefully selected from existing literature and modified according to the needs of this study. They were simple to implement but capable of providing the required robustness and accuracy for the prototype positioning system necessary to satisfy the core objectives within the time frame of the research.

(ii) Validate prototype (personal and real-world trials)

To ensure that the prototype positioning system could collect occupancy positioning data from non-expert participants, it was important to validate the system first. Positioning related data was collected using the bespoke android specific data logger, which are then processed in the positioning framework to provide position updates of the participants during the trials. The validation results can be seen at the end of Chapter 5 and have been achieved by carrying out multiple experimental trials and comparing the positioning output from the system against ground truth obtained from a robotic total station. Chapter 6 carried out an extensive trial of the prototype positioning system for occupancy data collection, divided into two phases. The first phase saw the researcher carrying out short trials covering multiple floors of the building. In the second phase, non-expert participants were asked to participate in time-controlled trials covering multiple floors over 20 minutes without any guidance from the researcher. The trials mimicked day to day activities in the form a Lego building task for which the parts were spatially distributed throughout multiple floors. Participants were required to carry out the Lego building task with the data logger in

their pocket. The data logger kept running continuously in the background and logged measurements from Wi-Fi, BLE, accelerometer and gyro. At the end of the task, the measurements were collected from the phone and processed in the prototype positioning framework to get continuous positioning update and subsequently, occupancy information of the participant's movement during their tasks. These real-world trials ensured we get ecologically valid results and understand the potentials and imitations of the prototype system. During the trials, the researcher shadowed each participant as they went about doing their task and recorded their actual occupancy and time. The recorded data was then used to validate the computed positioning output of the participants by plotting the time series of recorded and computed occupancy for comparison. There were 22 participants (male and female) of varying physical characteristics such as height and walking pattern. In total, 50 trials were carried out covering multiple floors of the building involving stairs and corridors and various starting points to ensure all aspects of everyday office occupancy were experienced.

(iii) Demonstrate the use of collected occupancy data within building simulations

Chapter 7 demonstrated one application of the positioning data when developing a building occupant model. The positioning data collected from the Lego building task was used to generate probabilities of route choice in the building involving multiple stairs, corridors, kitchen areas and office rooms. The building occupant model was developed following an agent-based modelling approach using AnyLogic simulation tool. The floor plan of the NGB was used as the model environment and simulations were carried to analyse building performance in the form of electricity usage prediction. Electricity was chosen since it depends on the occupancy of the building and has direct relevance with the occupancy positioning data collected from the prototype system. The initial model output was validated against actual electricity usage data collected from the University Estates department. Then multiple case studies related to the local dynamics of electricity usage for different lighting

conditions were explored with at least one showing the potential impact from the use of positioning data in the form of route choice probability. For each of the case studies, the statistical significance of their simulation output and their impact is discussed, linking how positioning data can help improve building occupant modelling

8.1.2 Knowledge Contribution

Publication: *The following paper has been published in the conference IEEE/ION PLANS 2018, A smart phone based multi-floor indoor positioning system for occupancy detection.*

Contribution: *The contribution of the research has been to demonstrate the feasibility and practicality of deploying an indoor positioning system for building occupancy detection. At the same time identify and demonstrate possible contributions of the positioning data to be used as input in building occupant modelling for possible improvement.*

The research community working in the field of indoor positioning will be able to gain insights related to technical challenges and constraints faced and performance issues of the prototype positioning system developed in this research for the purpose of detecting building occupancy. They may be able to suggest improvements as well as advice more feasible alternatives when it comes to designing a more robust positioning system capable of detecting building occupant over longer periods of time.

The Built Environment and Energy Efficient Buildings and Building Management community will benefit from knowledge of another potentially effective method of building occupancy detection to the already existing ones and evaluate the advantages and disadvantages. They will gain insight on how the positioning data has been used in this research and what other ways the data can be used in research areas related to understanding building performance.

8.2 Limitations

The system has some limitations with regards to the integration of different positioning elements. Since the main objective of this research was to develop a prototype indoor positioning system capable of detecting occupancy, some constraints and limitations were placed at an early stage to ensure ease of implementation and simplicity when carrying out the trials. Based on that understanding, the following are highlighted as limitations in the system.

8.2.1 Motion Detection

Due to the smartphone being in the pocket during the experimental trials, it is complicated to identify zero crossings of the acceleration when the feet are stationary between each stride. It becomes even more complicated due to the unpredictable nature of the walking pattern of individuals, variable step length and pace. The acceleration peaks due to feet movement are not always consistent, and it is not always reliable to characterise a peak as a step taken. As such, the zero velocity update technique, the standard for foot-mounted inertial systems could not be used in our case. Complex algorithms involving machine learning techniques or dynamic acceleration peak analysis are complicated to implement and computationally slow. Those involving template matching using cross-correlation will not give reliable results with just one walking template pattern but rather would require multiple template patterns covering a wide array of movement characteristics to provide reliable results.

As such, methods were chosen which are simple to implement but reliable and accurate enough to achieve the objective satisfactorily and demonstrate their use successfully in the positioning framework. The system, instead of detecting actual steps detected step-like motion over 2 seconds. Based on the standard human velocity of 1.3 m/s, this gave the motion period divided into two separate windows per second. According to empirical observation, the distance covered involves movement with both the feet, as seen in Figure 5.15. The assumption made was that if a motion is detected over two seconds, then the person is in motion for that entire duration. This might not always be accurate. Also, the step length can vary depending on the situation; starting from rest, slowing down, turning or opening a door. Although the performance of the algorithm was satisfactory, instances of overestimation or underestimation of distance travelled from the particle filter every epoch was very common. Also, misidentification of any motion exacerbates the error even further since the particle propagation would be affected by twice the step length of approximately 1.3m in case of any errors. In terms of motion type, only regular walking was allowed, running or jogging was not, and the participants during the trial were instructed to maintain a natural walking pace depending on the circumstances.

8.2.2 Heading Estimate

The heading orientation estimate is one of the most essential elements of any dead reckoning solution. The problem with the smartphone is that it can be kept at different positions; handheld, bag, pocket etc. and may undergo varying local motion due to their placement. These factors affect the accuracy and implementation technique of the algorithm for heading estimation as well as the quality of the positioning. In this research, the phone's placement was constrained to inside the pocket of the participants when carrying out the trials to ensure less complexity in determining orientation at varying positions. In this case, since the particle filter engine is implemented with random heading during initialisation of the particles, a relative change in heading at each turn was required to update individual particles' heading and propagate them in the correct directions.

8.2.3 Particle filter and Sensor fusion

The particle filter engine was the only state estimation algorithm accounting for the uncertainty of positioning update every epoch and the particle weights updated from the radio map observation from Wi-Fi and BLE. A standard implementation of the filter was adopted which incorporated map matching constraints to restrict particles crossing over walls and doors. Features for dynamic step length change due to sudden obstruction, pause and doors were also included, since they affect the step length for the first few seconds after encountering such situations. The main limitation in the system is the weights assigned to the particle, which are of poor quality and dependent on the quality of the radio signals from Wi-Fi and BLE observation. Due to the inherent randomness, attenuation from multipath and fading of the radio signals, the filter can encounter blackouts or extremely poor radio signals at epochs which leads to the erroneous estimation of position update and can produce incorrect trajectories, force a filter restart or stall.

8.2.4 Interoperability

Another limitation of the current system is its lack of interoperability with other types of building, such as a residential houses or flats. The system is ideal for large

commercial buildings where there is ample room for movement and space. Residential buildings are generally much smaller and have smaller rooms and navigation areas for movement. Due to the extensive area coverage of Wi-Fi, it would be difficult to get enough variability of radio signal strength to ensure unique coverage areas. RFID tags or BLE beacons with reduced power level will work well as a proximity detector to identify entry and exit from rooms and thus does not require the development of a full-fledged indoor positioning system such as this one.

8.3 Future Work

Considering the limitations discussed above further work needs to be done to ensure improvement of the positioning systems reliability to detect building occupancy. Different phone carrying positions typical in an office environment and further improvement of motion detection also needs to be investigated to ensure stability for longer trials, which are critical for performance and impact.

The motion detection system needs to be improved by incorporating more robust methods to identify acceleration peaks corresponding to steps. Placement of additional motion sensors on the feet in addition to the ones from the smartphone may help to detect steps more accurately by combining the two results.

For heading estimation other phone carrying positions like hand held, needs to be considered since it is a very common posture for any individual with their smartphone. This will help to increase the potential of identifying more complex occupancy in the building. Comprehensive test needs to be carried out to ensure the algorithms are performing properly and also appropriate predictive measures may need to be placed if there are failures by looking at past sequence of heading directions and future ones at every epoch to detect heading changes which are uncharacteristic of human motion.

To improve the weighting of the particle filters switching to BLE only mode if Wi-Fi signal is poor and adding beacons in more frequent intervals throughout the floor may help contain particle drift within a reasonable boundary. A Kalman filter for position

update may also be added to the system to include a complimentary check with the particle filter position update and switching between them to get the most precise update at every epoch.

Additional future work suggestions would be to explore other indoor positioning technologies feasible for the application of occupancy detection and how they can further improve the capability of the positioning system and make it more robust for real-world deployment. The radio map needs to be updated from time to time to ensure any environmental changes such as changes in floor plan layout and furniture placement are taken into account. Also changes in receiver device type affect the variance of the collected radio signal data causing degradation in localisation accuracy. As such SLAM based radio mapping or crowdsourced update with the help of voluntary participants can be considered. More complex trials covering entire office hours need to be undertaken to ensure the robustness of the system ready for commercial deployment. Occupancy data derived from the positioning system can be further optimised by analysing the computed route with environmental tags and map matching techniques to remove outliers and realign any unusual route with the more likely one using predictive data modelling techniques. Of course this would mean the building maps and environmental tags will vary from building to building and would need to be created beforehand.

8.4 Conclusion

Research in the field of Indoor positioning is still at an early stage and continuously being updated with innovations and improvements. This research looked to tap into that progress and demonstrated a novel application of indoor positioning, showing how it can be used to improve modelling of building occupants. The research highlighted the limitations of some of the technology and techniques when used in this kind of real-world application.

Detecting occupancy in real life is difficult compared to any experimental setup. From the research we could see the uncertainty of position update from the particle filter with the BLE and Wi-Fi especially in large open plan rooms and corners when the

individual must make tight turns. The radio signal seems to undergo fast fading or complete outage from nearby radio stations as a result the position update from the particle filter drifts to erroneous position and leads to a completely altered path from the one actually taken.

Heading estimation with the phone in the pocket works fine if there are no tilt or rotation in the middle of the motions. The sudden rotation or tilt inside the pocket creates an additional offset which may cause the actual heading to point in a completely different direction thus causing the particles to drift as well. We have seen this occurring multiple times and if majority of the particles are resampled in that direction they may not be realigned back to the original route and even if they do so the position update would lag behind the true position and thus may fall short of the actual destination or turn prematurely. We have seen such examples in Figure 6.12 and 6.13 were the computed route does not enter the room all the way but turns away right in front of the door suggesting a lag between the computed and true position at that instance of time. There is also an inherent time lag as well for different sensor data due to hardware latency and time synchronisation which can be seen in the validation plot of chapter 6, section 6.44 discussed earlier.

In general, from the research it seems Wi-Fi and BLE may not be the most reliable positioning technology on their own as they suffered from frequent signal outage and severe interference from any moving body and obstruction very easily. They both are easy to deploy and cheap but not much reliable when it comes to unconstrained human movement in natural environment.

From the results of the occupancy model we have shown a potential application of the positioning data in the form of route choice probability. Even though the result showed statistically significant difference in simulated electricity usage when compared to random route choice, practically the difference was negligible. Nevertheless, the results from the positioning system developed did show the accuracy achievable and limitations that needs to be addressed for any further work. Even with failures to detect occupancy trajectory accurately all the time, zone level

detection accuracy was appreciable which is what most of the other occupancy detection methods, discussed in Chapter 3 tries to achieve.

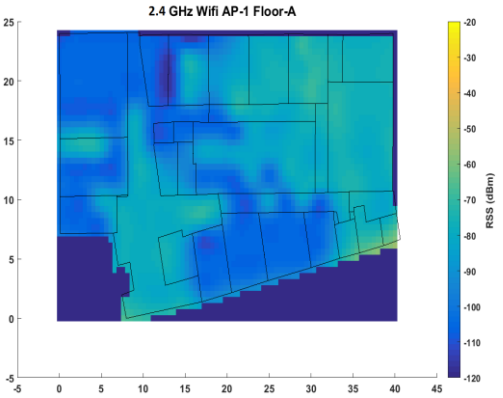
The inherent constraints embedded in a real-world scenario such as building occupancy is important to understand for any future improvement of the system related to the use of other indoor positioning technology and techniques. When it comes to building occupant modelling, irrespective of the outcome of the small scale application of positioning data seen in Chapter 7, it can be safely claimed that indoor positioning holds a lot of opportunity and potential for improvement of building occupant modelling. Identifying and utilising the appropriate technology and methodology will ensure real impact and improved outcome. If longer trials were done covering the entire office hours, we can potentially get insights into actual building occupancy of individuals. To identify impact from the positioning data we would need to analyse occupancy pattern of individuals from the positioning data and then develop an occupancy presence model. The model can be used as input to the building model and then evaluate its performance by comparing with models discussed in Chapter 3 to understand the true potential of indoor positioning data.

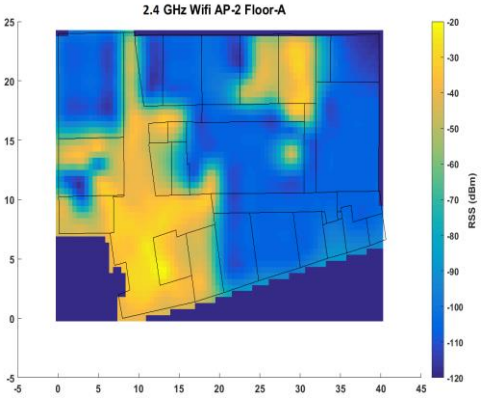
Compared to other methods for detecting building occupancy, indoor positioning provides information related to the trajectory of occupancy at an individual level, which is unique and essential for a multi-state presence model. Unlike continuous long term deployment of indoor positioning systems in typical LBS solutions such as hospitals, malls and museums, it only needs to be set up once in any building during the PROBE stage and collect occupancy data from time to time to understand patterns of occupancy and demographics from willing participants. It can help to develop more detailed occupancy models of both individuals and the aggregate population of the building, which can then be incorporated into building occupant models for energy prediction. These have long term implications in terms of energy predictions and other behavioural models of activities, as discussed earlier in Chapter 3. At the same time, there are implications related to privacy concerns of occupancy data collected during office hours, which needs to be addressed as well. Nevertheless, this research has

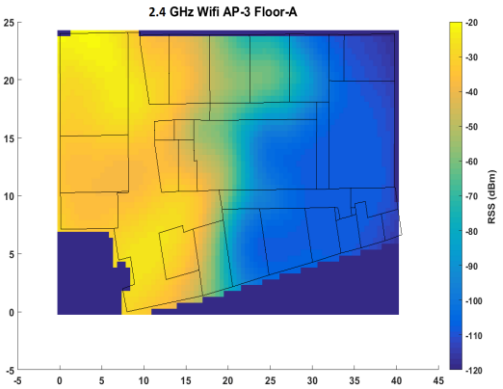
been able to successfully achieve its objectives and aim in developing an easy to use prototype indoor positioning system and demonstrating its application in building occupant modelling.

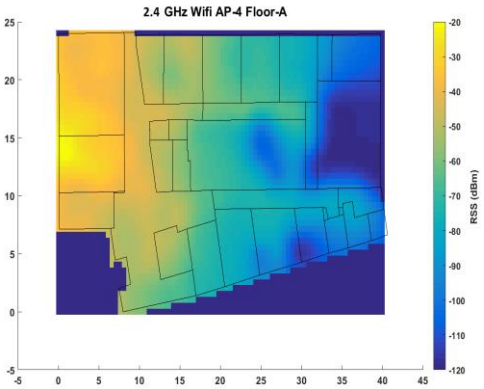
Appendix I

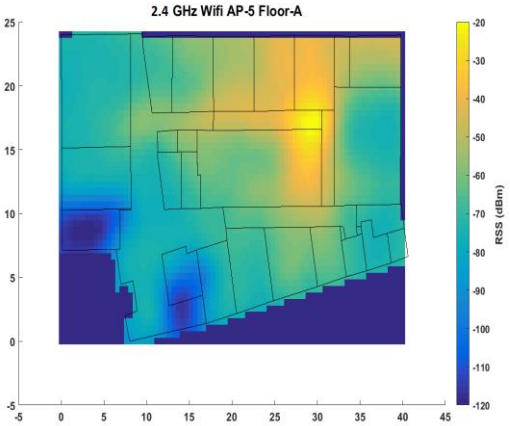
Radio Fingerprint Heat Map of NGB

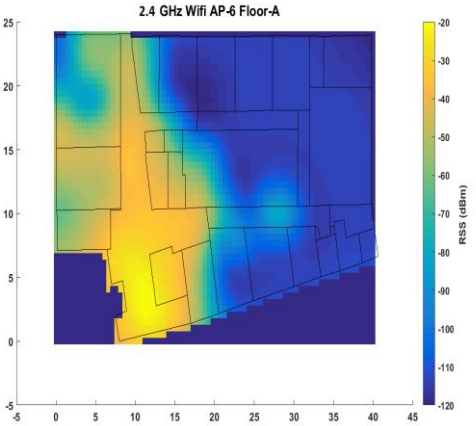












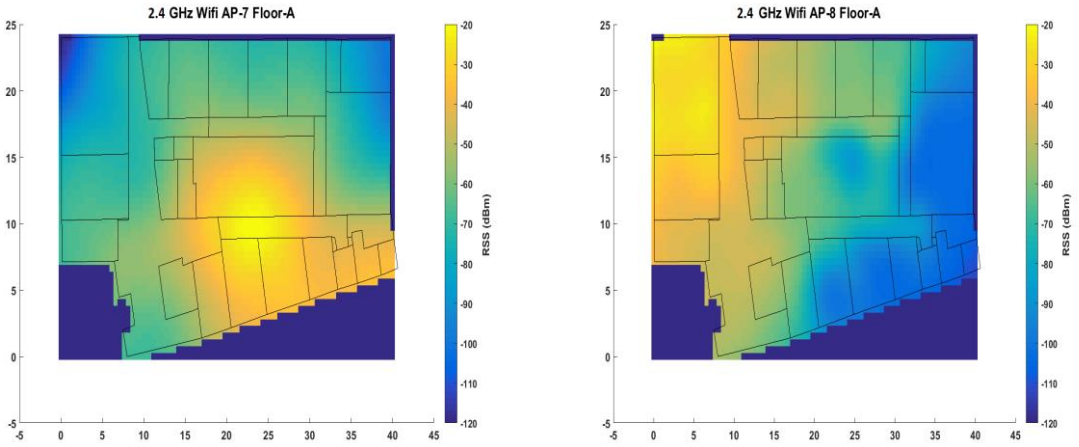
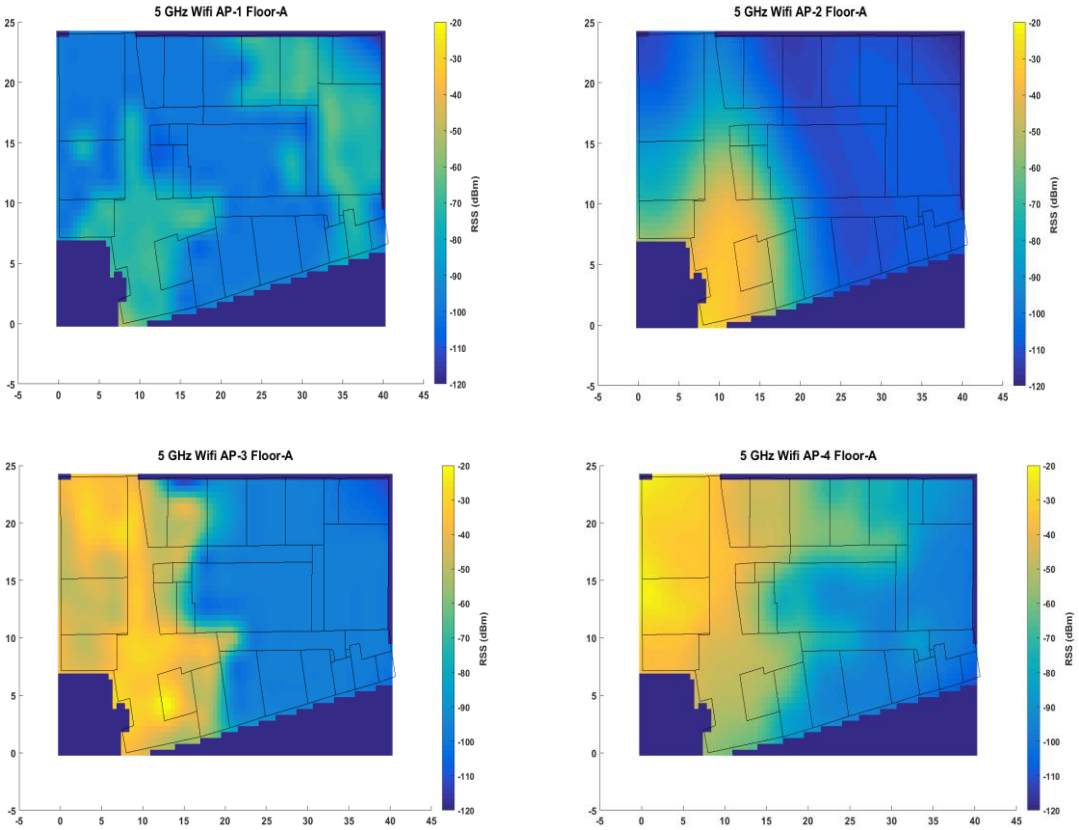


Figure 1 Heatmap for each of the 2.4 GHz Wi-Fi transmission showing the signal coverage in Floor-A



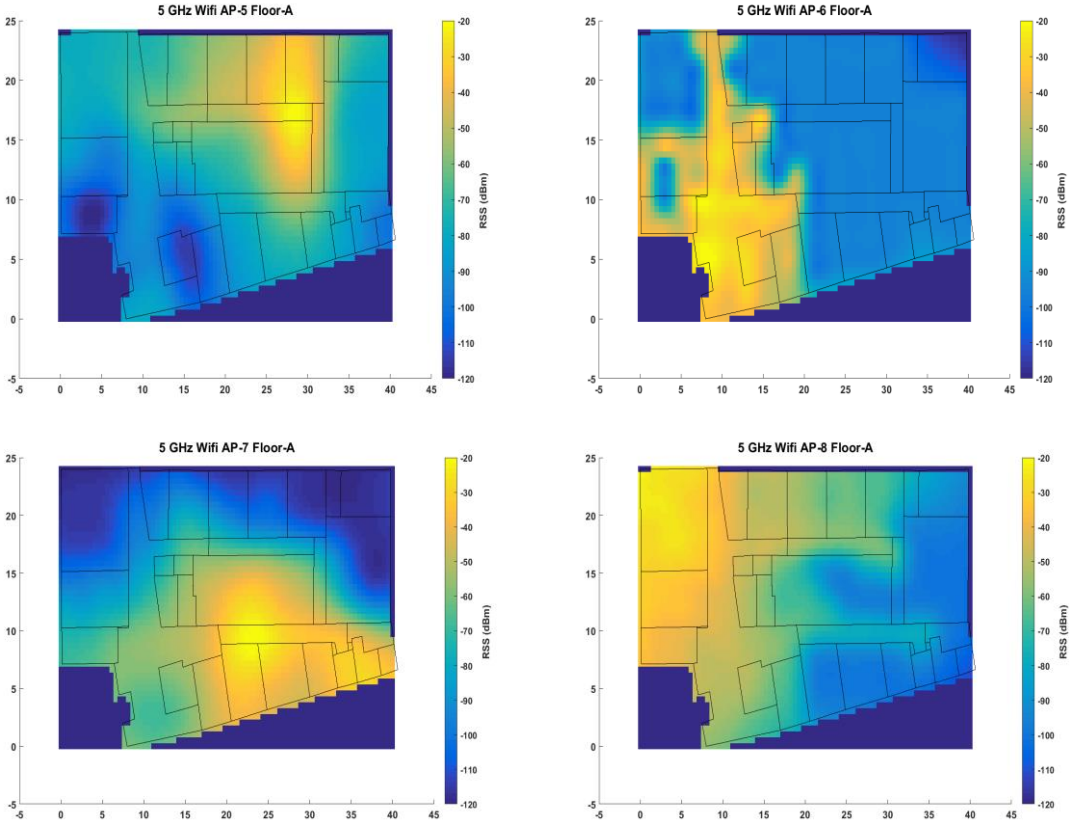
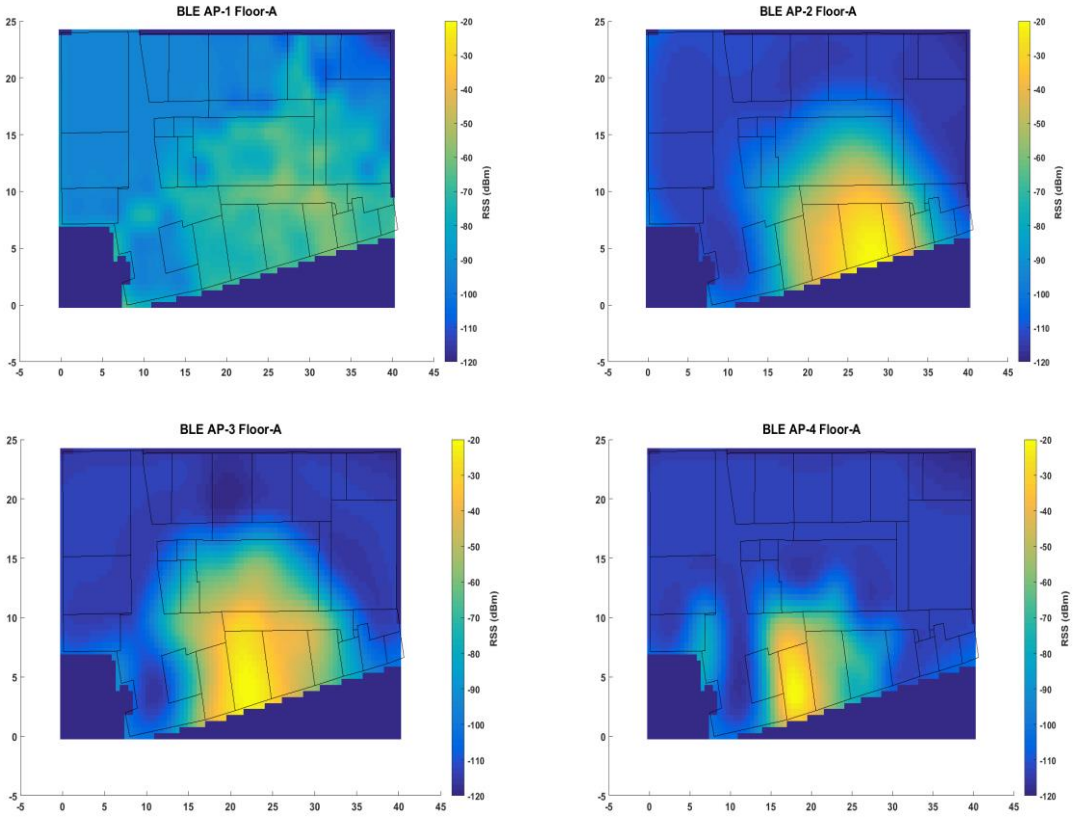
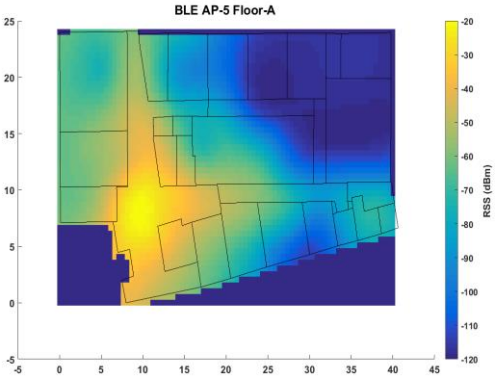
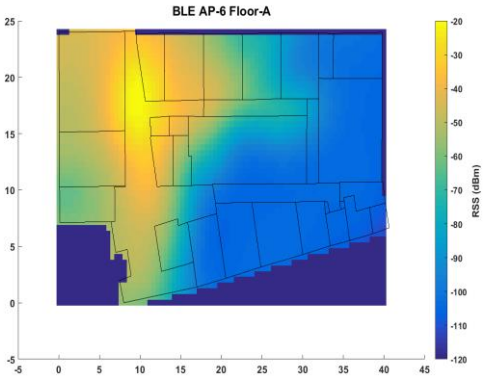
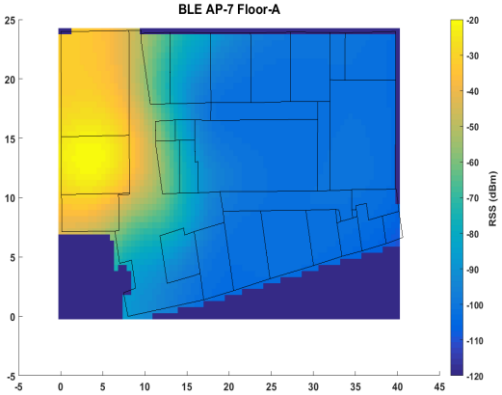


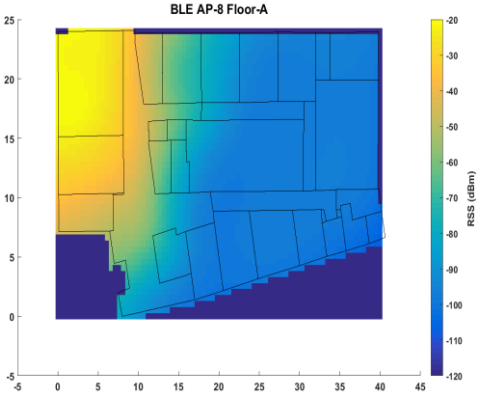
Figure 2 Heatmap for each of the 5 GHz Wi-Fi transmission showing the signal coverage in Floor-A

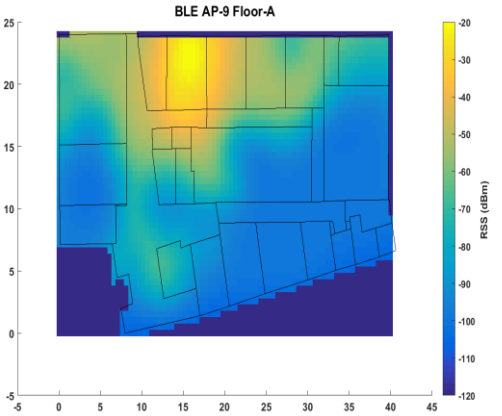


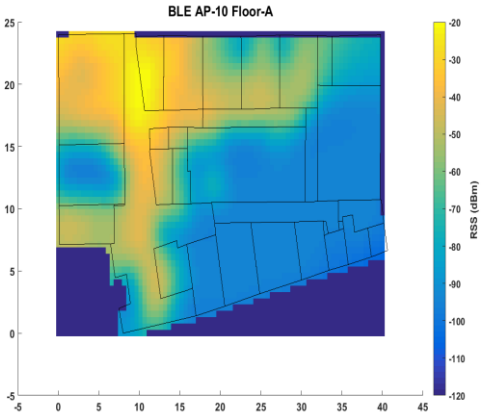

BLE AP-5 Floor-A
RSS (dBm)

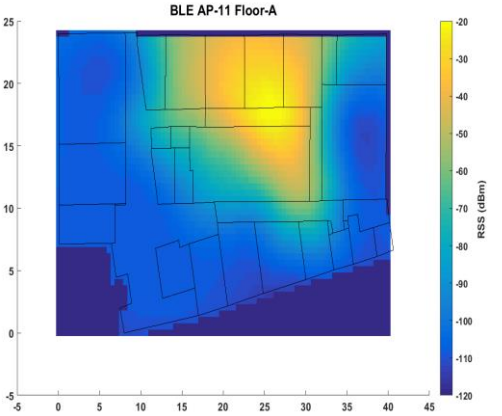

BLE AP-6 Floor-A
RSS (dBm)

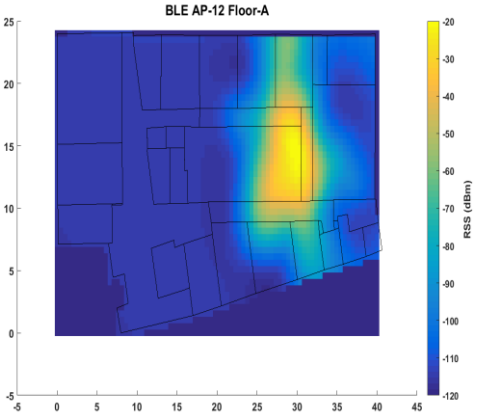

BLE AP-7 Floor-A
RSS (dBm)


BLE AP-8 Floor-A
RSS (dBm)


BLE AP-9 Floor-A
RSS (dBm)


BLE AP-10 Floor-A
RSS (dBm)


BLE AP-11 Floor-A
RSS (dBm)


BLE AP-12 Floor-A
RSS (dBm)

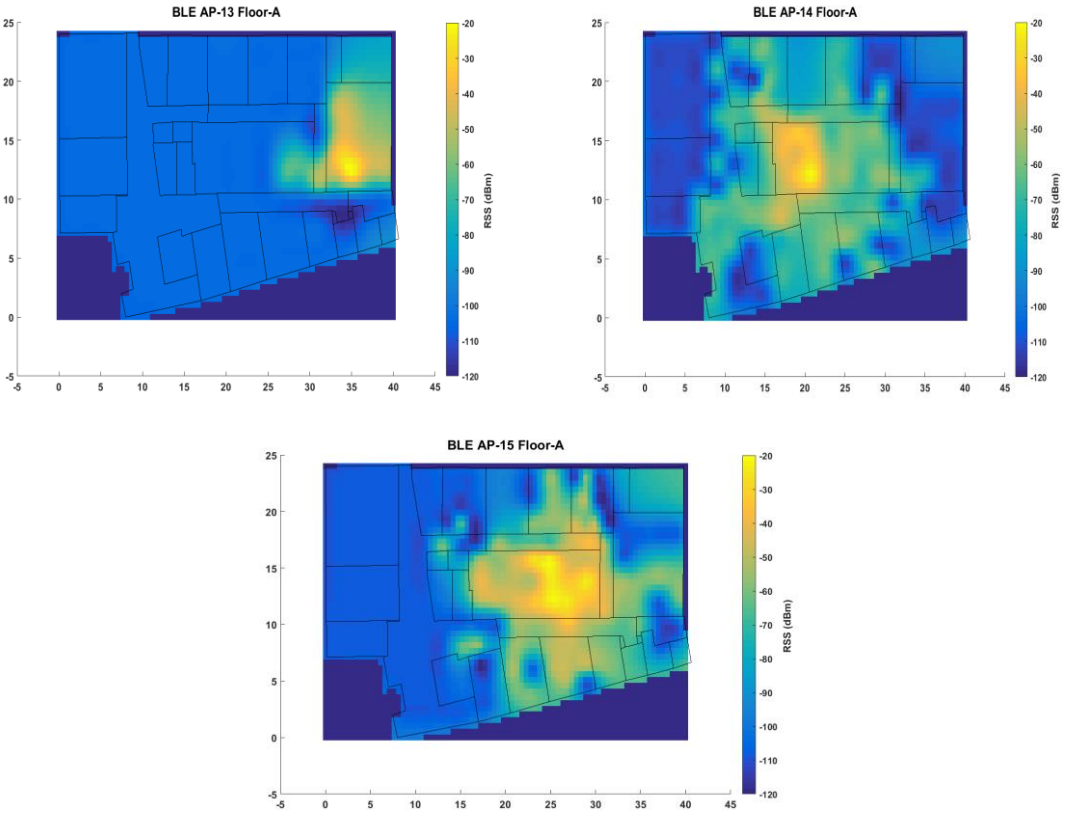
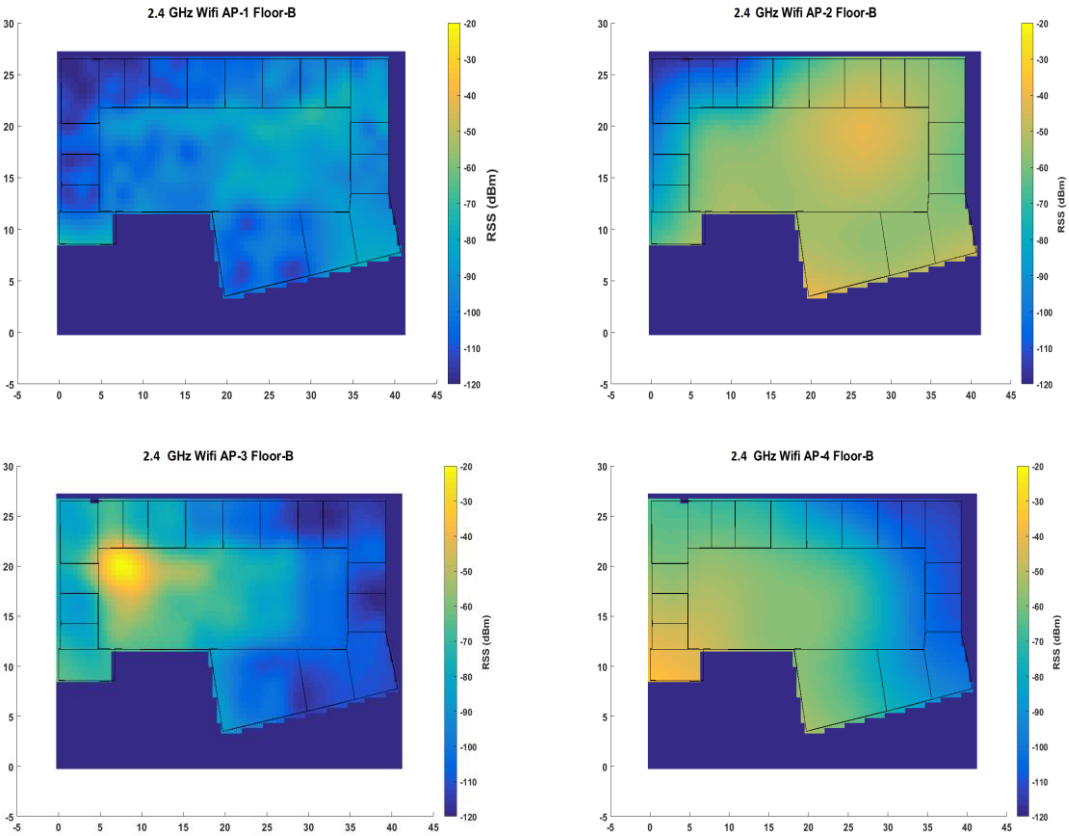


Figure 3 Heatmap for each of the BLE beacon showing the coverage of the signal strength in Floor- A



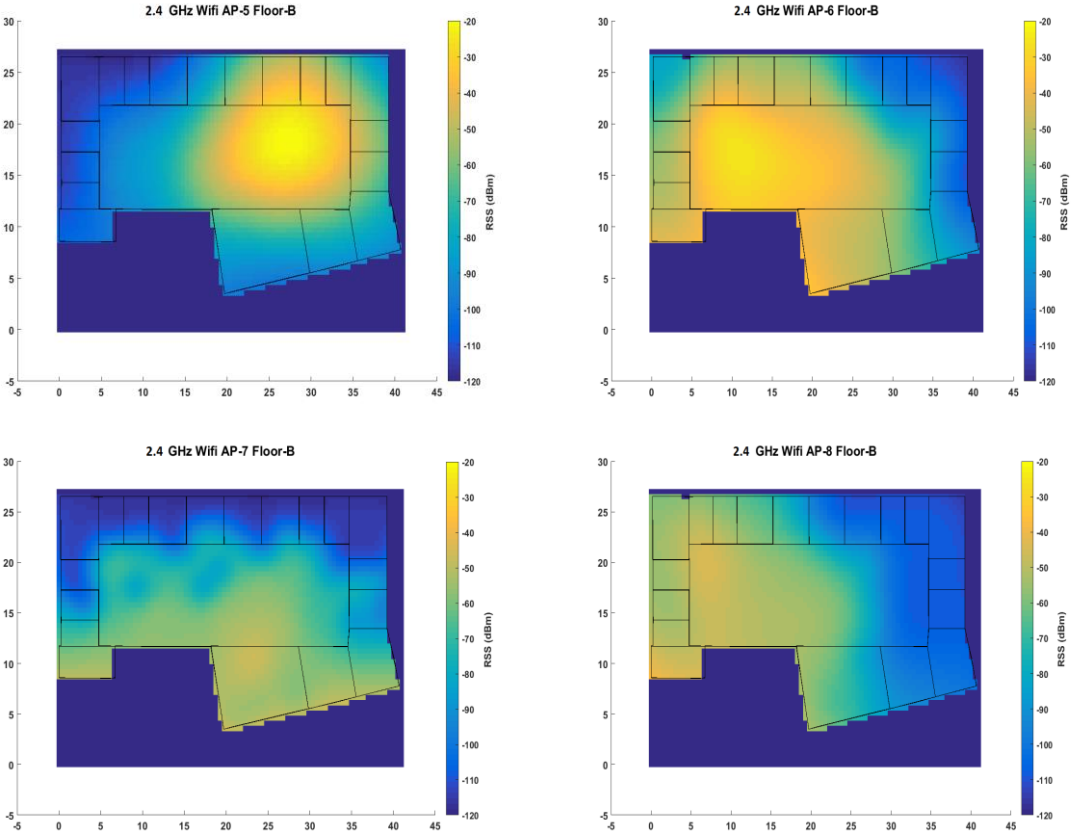
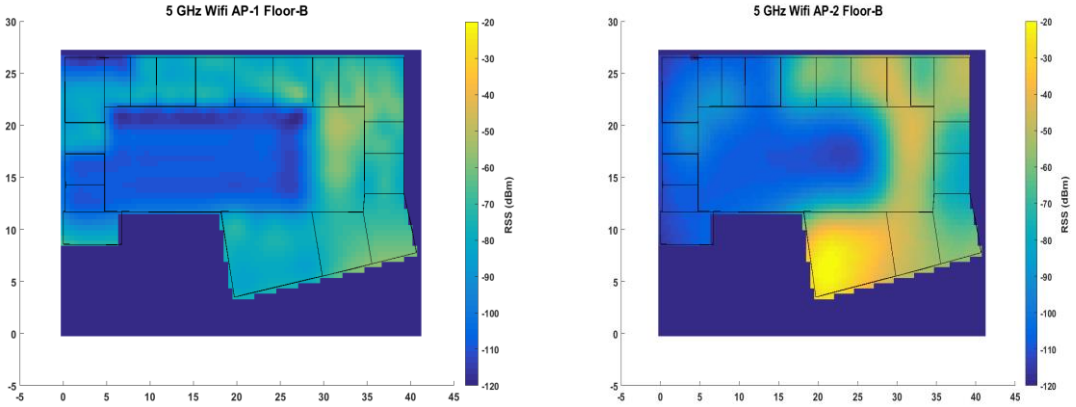


Figure 4 Heatmap for each of the 2.4 GHz Wi-Fi transmission showing the signal coverage in Floor-B



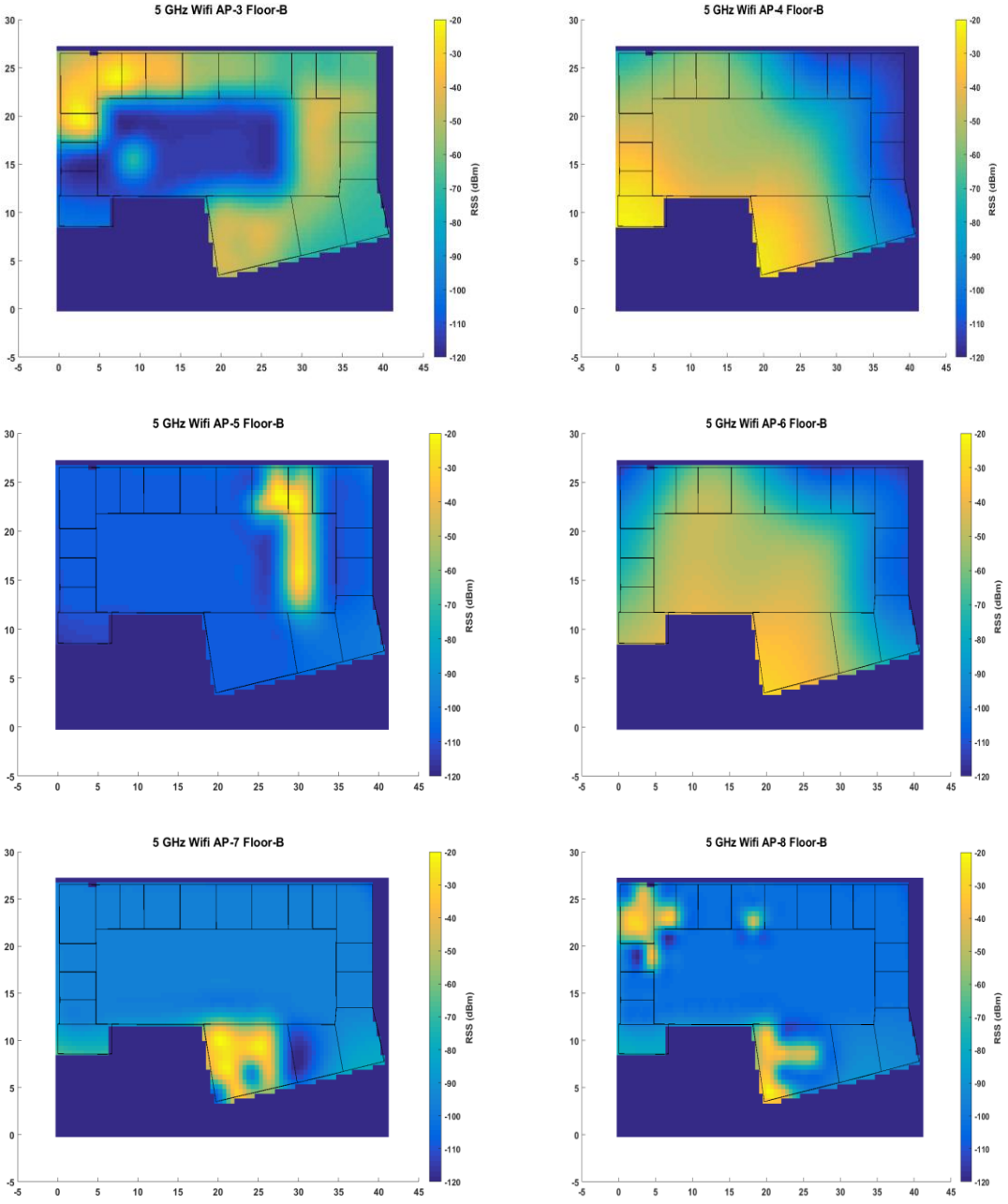
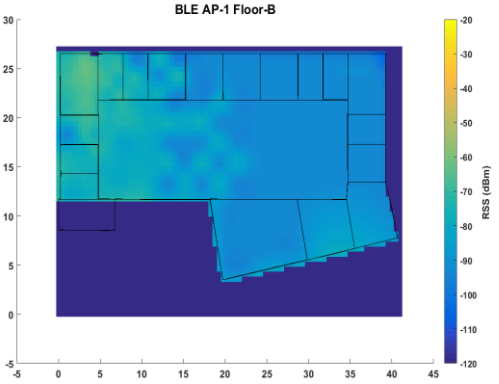
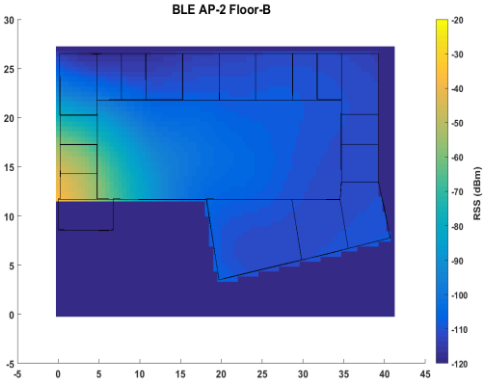
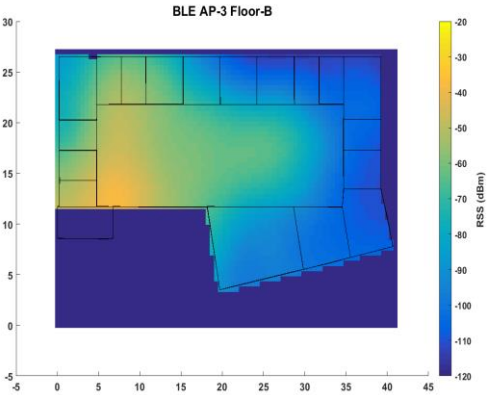
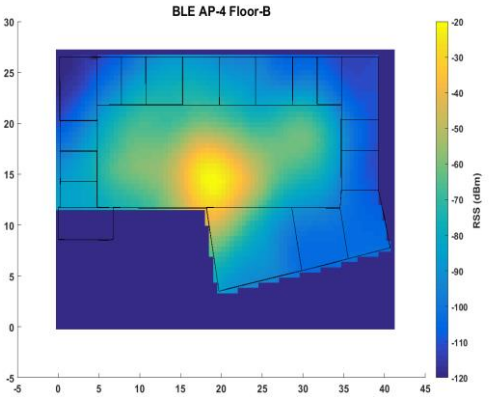


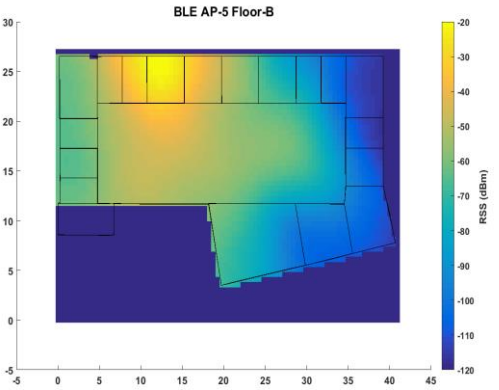
Figure 5 Heatmap for each of the 5 GHz Wi-Fi transmission showing the signal coverage in Floor-B

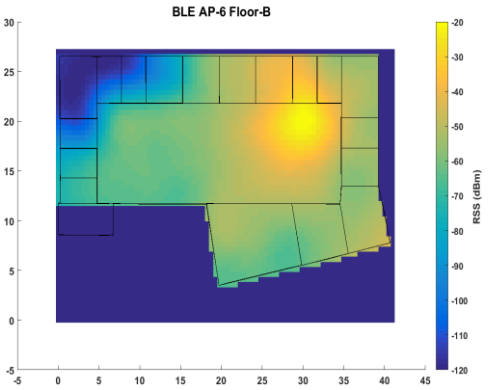

BLE AP-1 Floor-B
RSS (dBm)

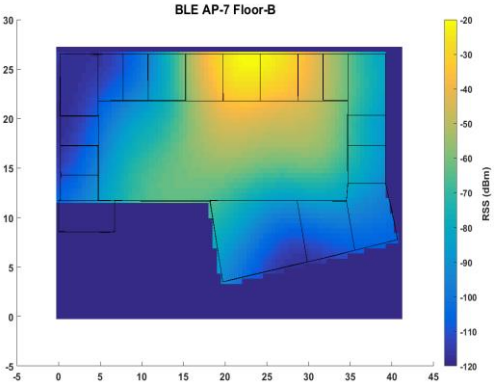

BLE AP-2 Floor-B
RSS (dBm)

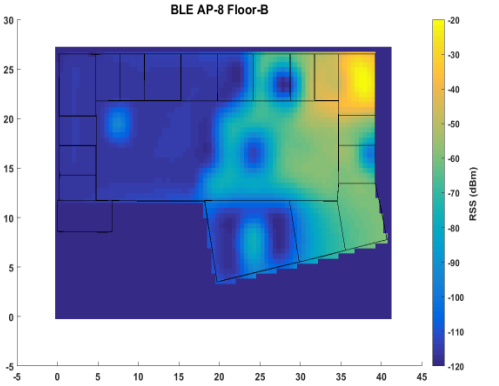

BLE AP-3 Floor-B
RSS (dBm)


BLE AP-4 Floor-B
RSS (dBm)


BLE AP-5 Floor-B
RSS (dBm)


BLE AP-6 Floor-B
RSS (dBm)


BLE AP-7 Floor-B
RSS (dBm)


BLE AP-8 Floor-B
RSS (dBm)

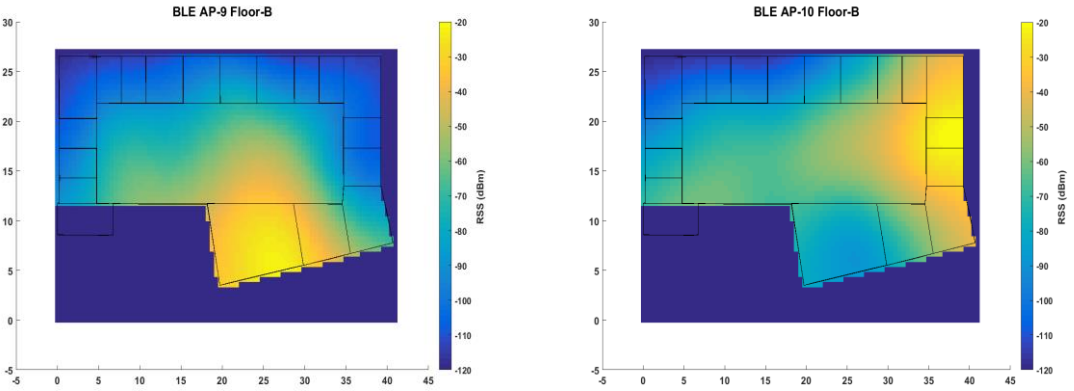


Figure 6 Heatmap for each of the BLE beacon showing the coverage of the signal strength in Floor- B

Appendix II

The figures below shows 45 trial plots out of 50. The other 5 could not be plotted because of incomplete data collection due to various issues mentioned in Table 6.2 earlier. Few selected plots are shown in chapter 6 to highlight various problems faced during the trials.

Lego Trial Result Plots

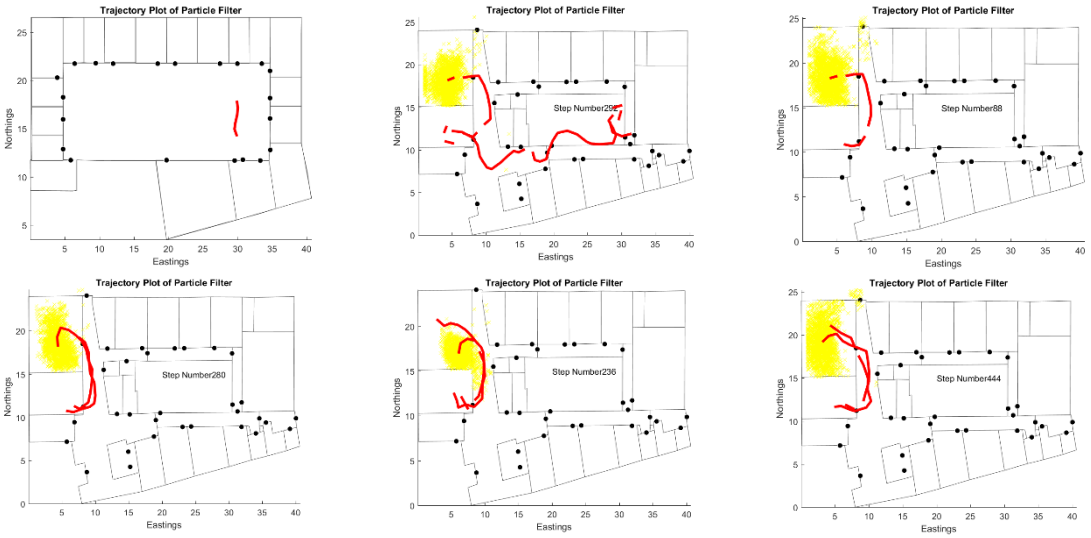


Figure 1: Trial 1 plot showing the sequence of trajectory taken by the participant

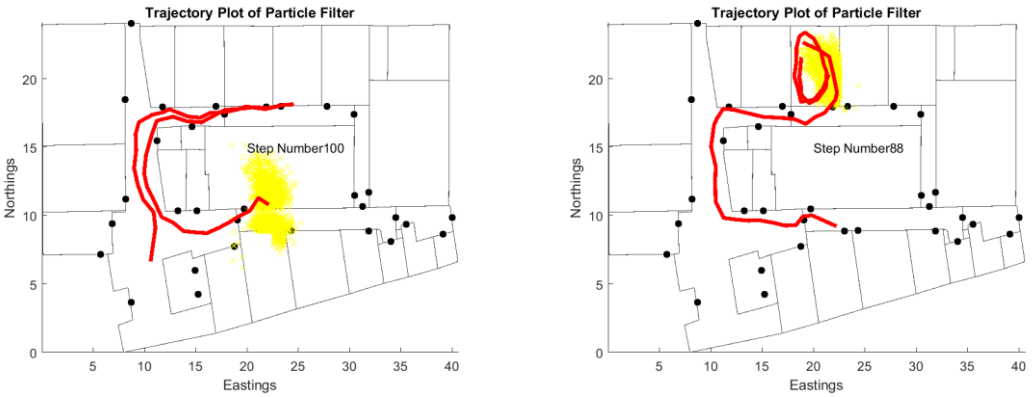


Figure 2: Trial 2 plot showing the sequence of trajectory taken by the participant

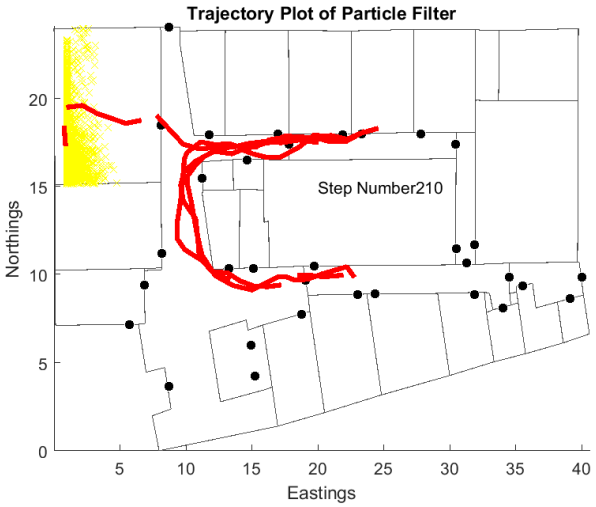


Figure 3: Trial 3 plot showing the sequence of trajectory taken by the participant

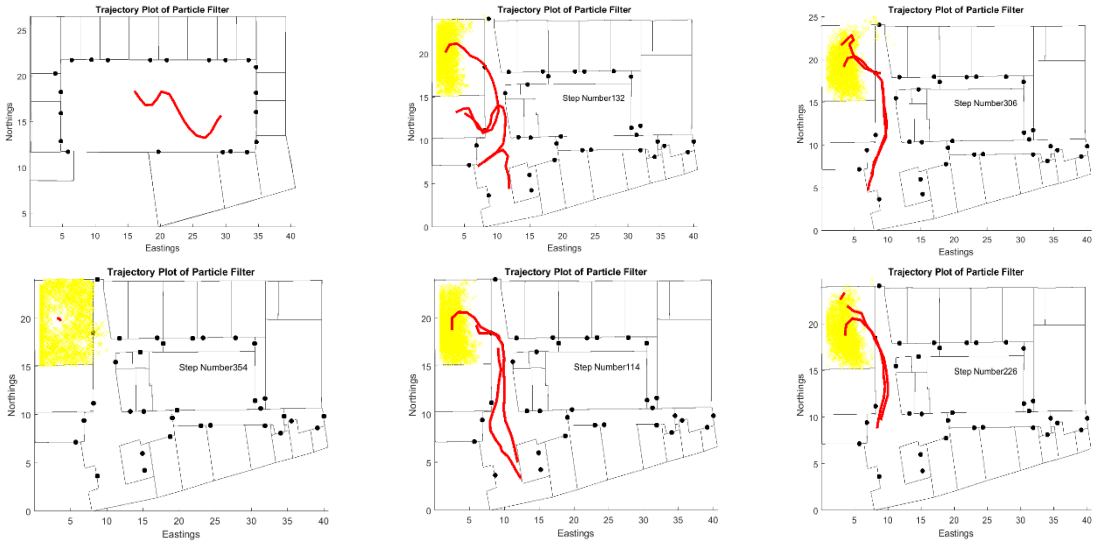
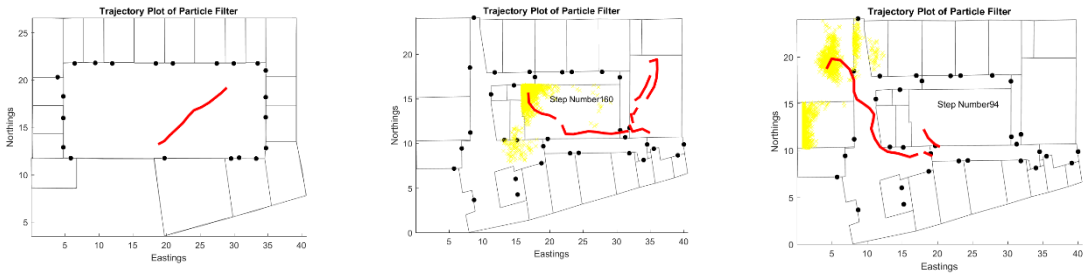


Figure 4: Trial 4 plot showing the sequence of trajectory taken by the participant



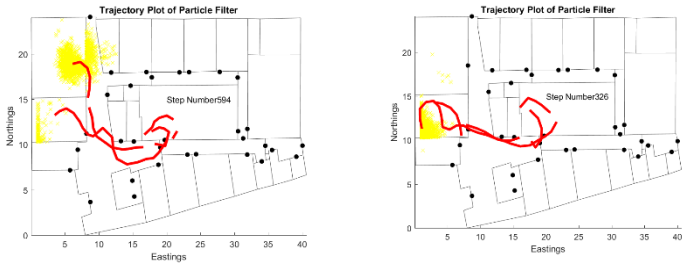


Figure 5: Trial 5 plot showing the sequence of trajectory taken by the participant

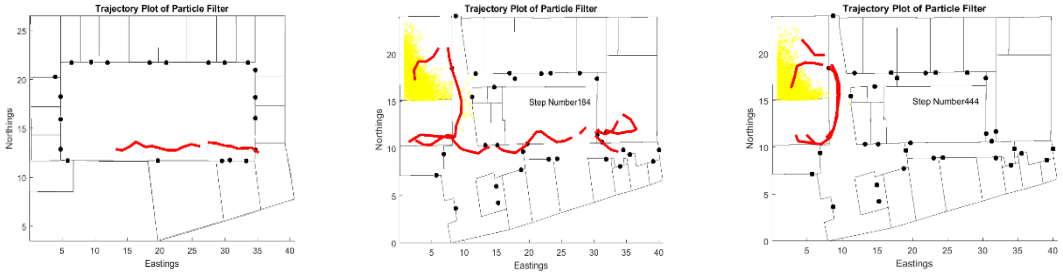


Figure 6: Trial 6 plot showing the sequence of trajectory taken by the participant

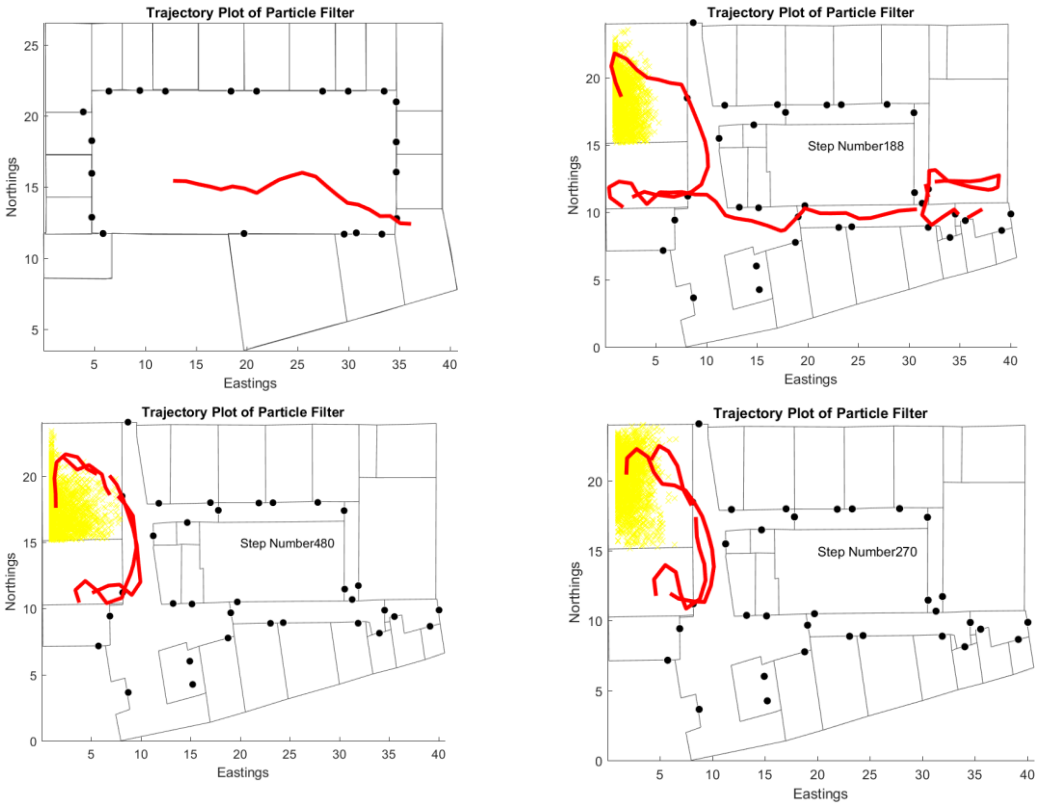


Figure 7: Trial 7 plot showing the sequence of trajectory taken by the participant

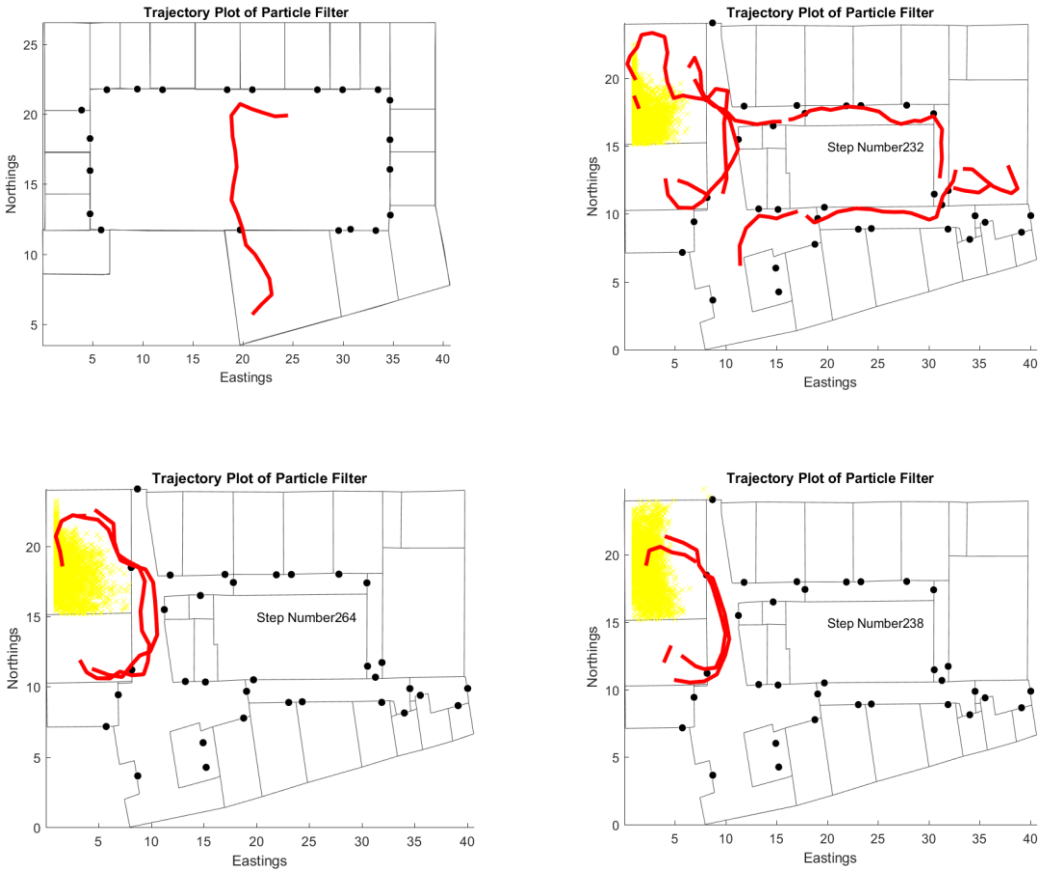
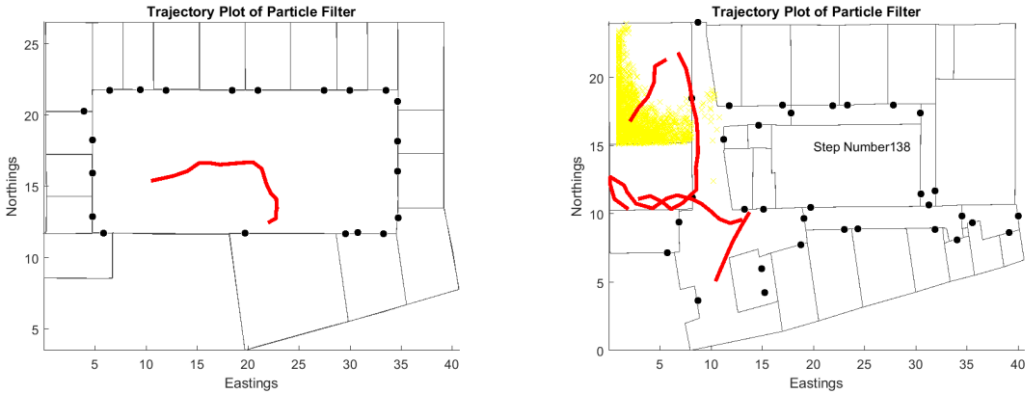


Figure 8: Trial 8 plot showing the sequence of trajectory taken by the participant



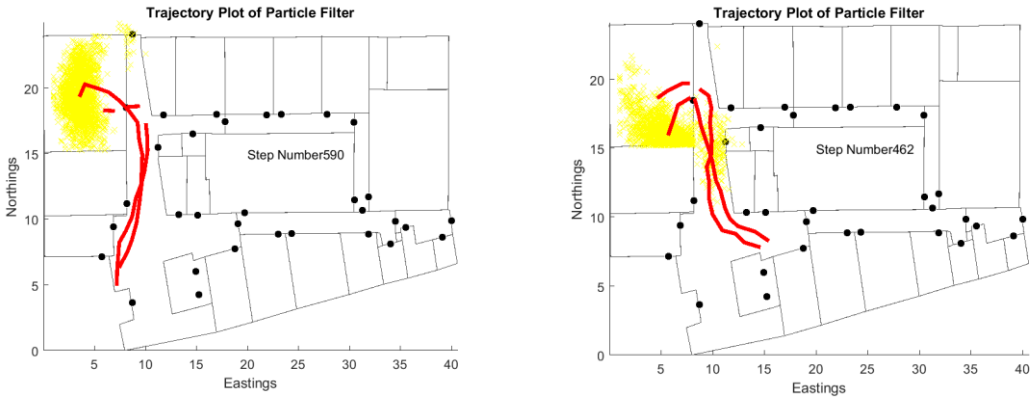


Figure 9: Trial 9 showing the sequence of trajectory taken by the participant

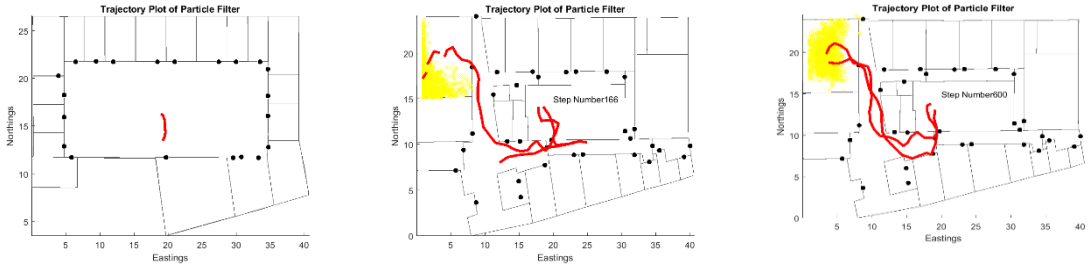


Figure 10: Trial 10 showing the sequence of trajectory taken by the participant

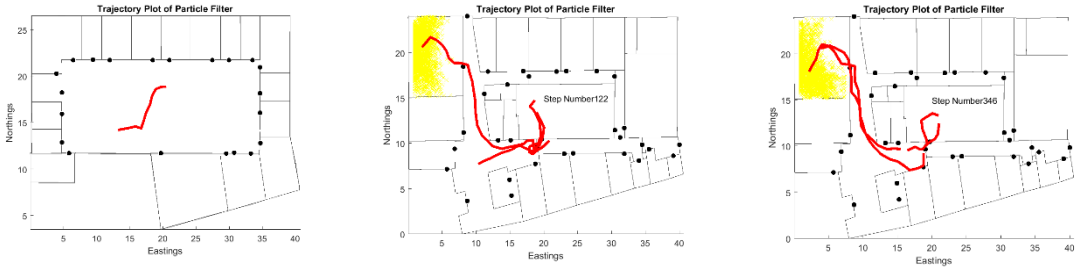


Figure 11: Trial 11 showing the sequence of trajectory taken by the participant

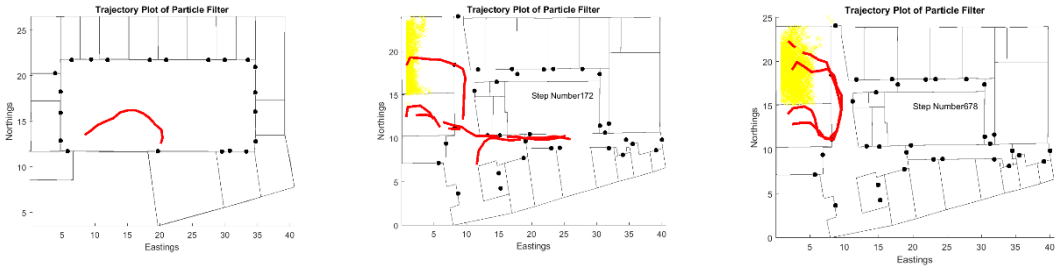


Figure 12: Trial 12 showing the sequence of trajectory taken by the participant

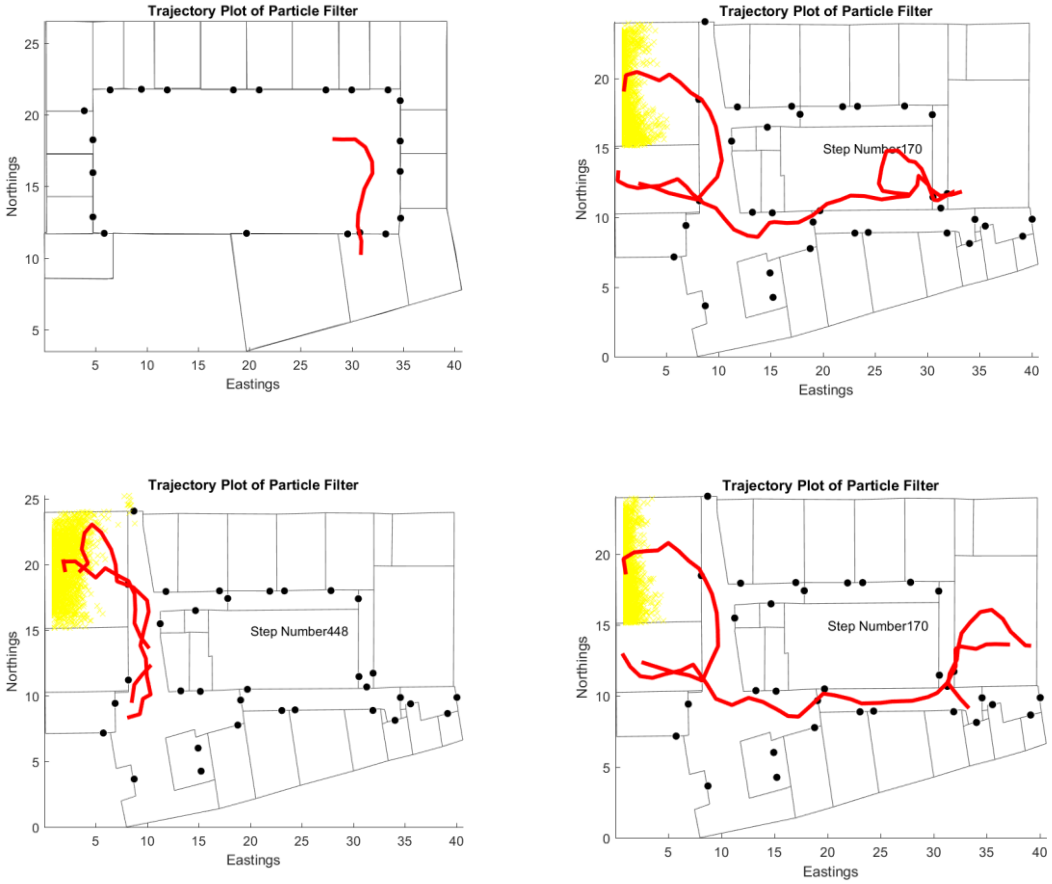


Figure 13: Trial 13 showing the sequence of trajectory taken by the participant

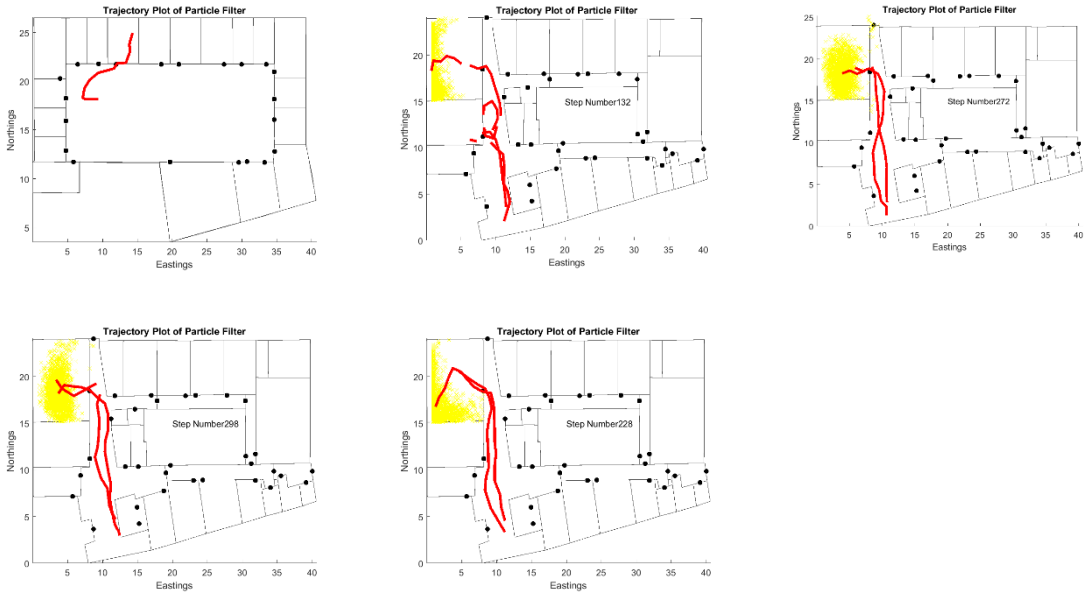


Figure 14: Trial 14 showing the sequence of trajectory taken by the participant

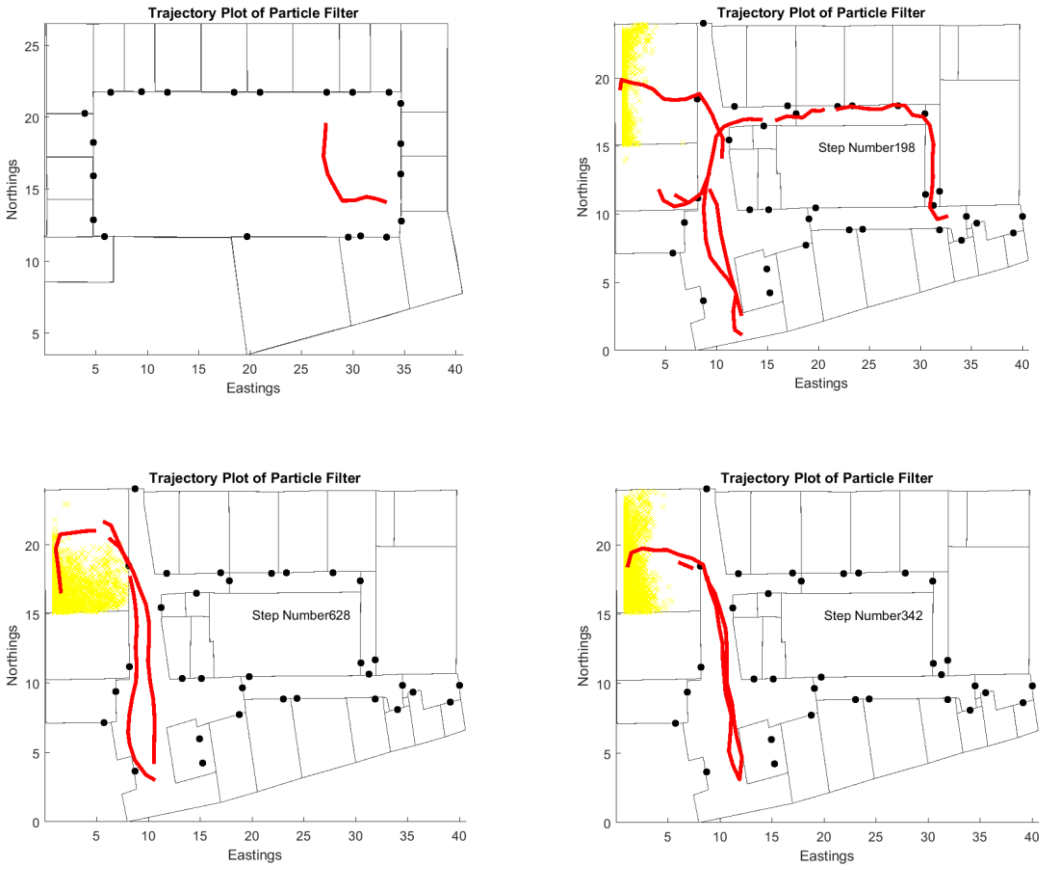


Figure 15: Trial 15 showing the sequence of trajectory taken by the participant

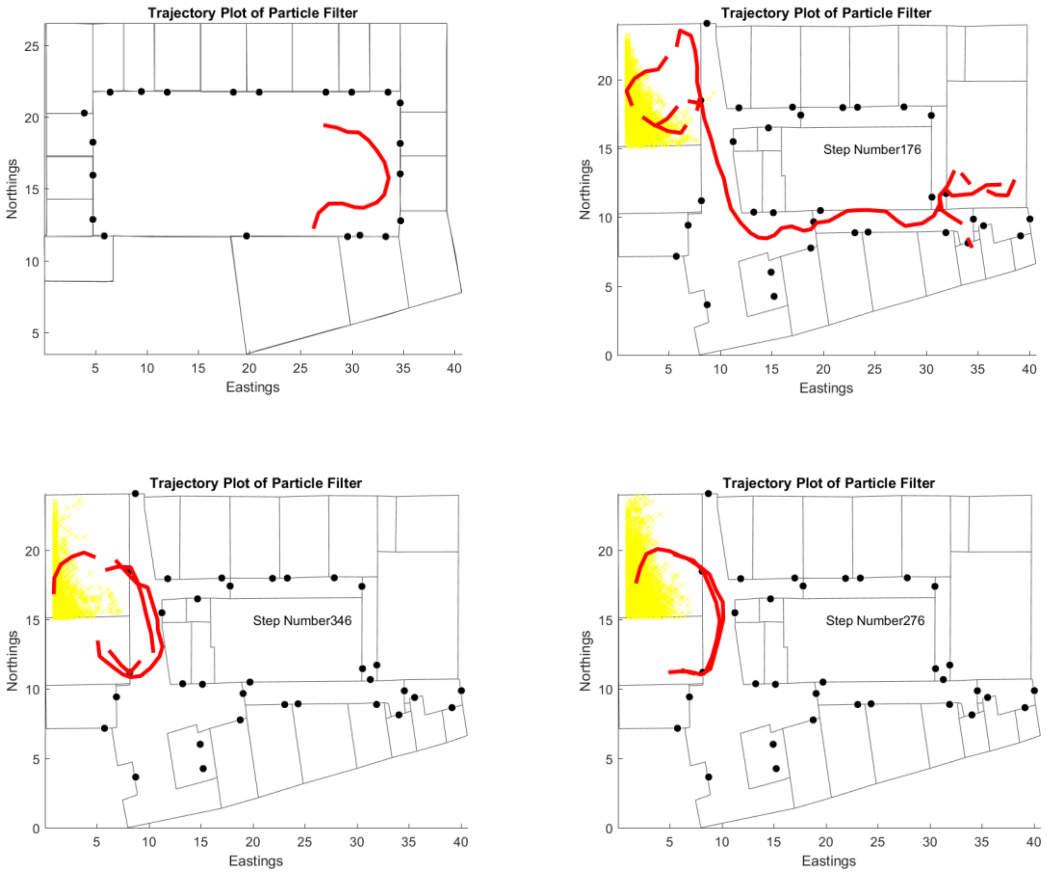


Figure 16: Trial 16 showing the sequence of trajectory taken by the participant

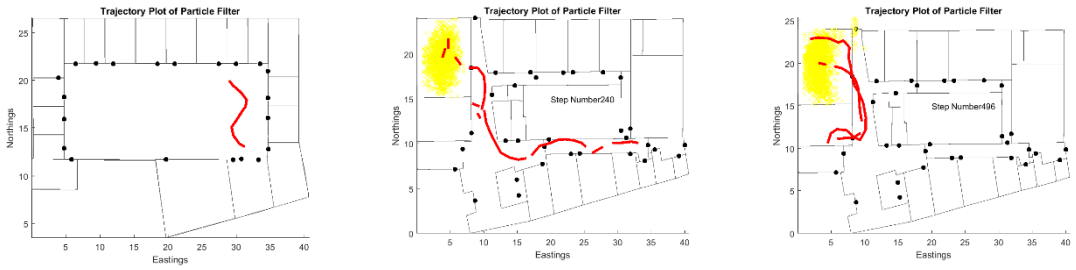


Figure 17: Trial 17 showing the sequence of trajectory taken by the participant

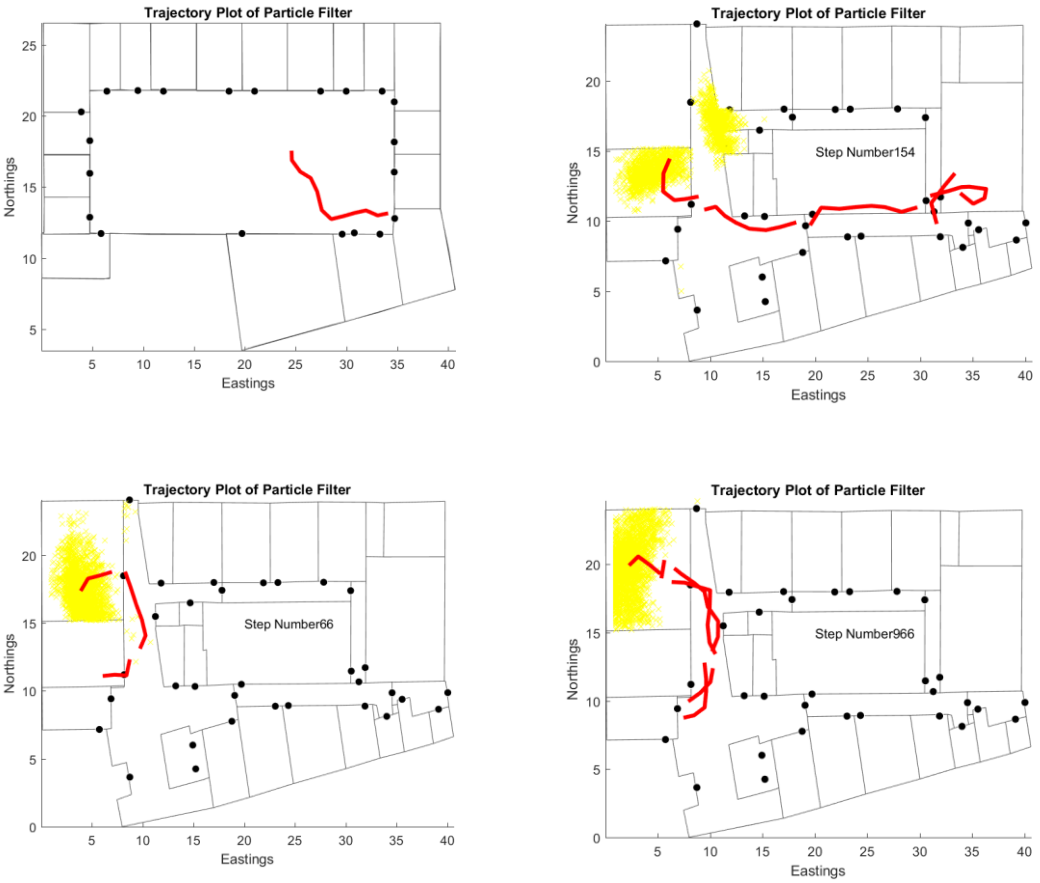
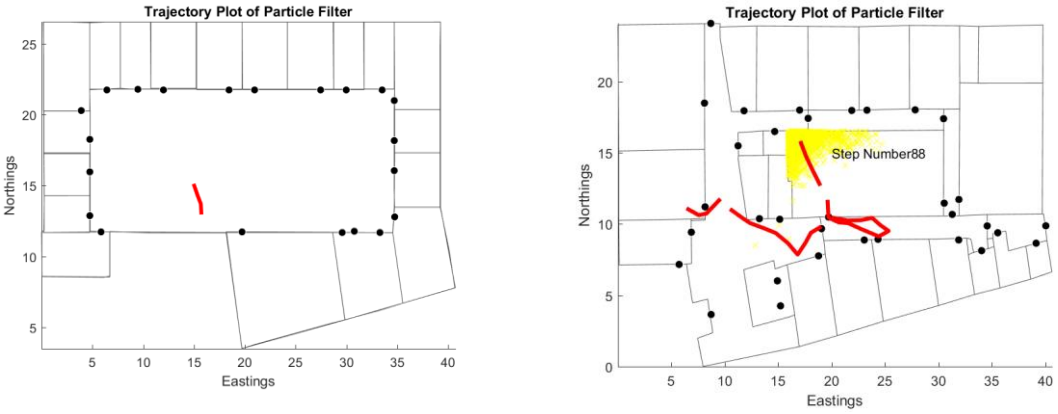


Figure 18: Trial 18 showing the sequence of trajectory taken by the participant



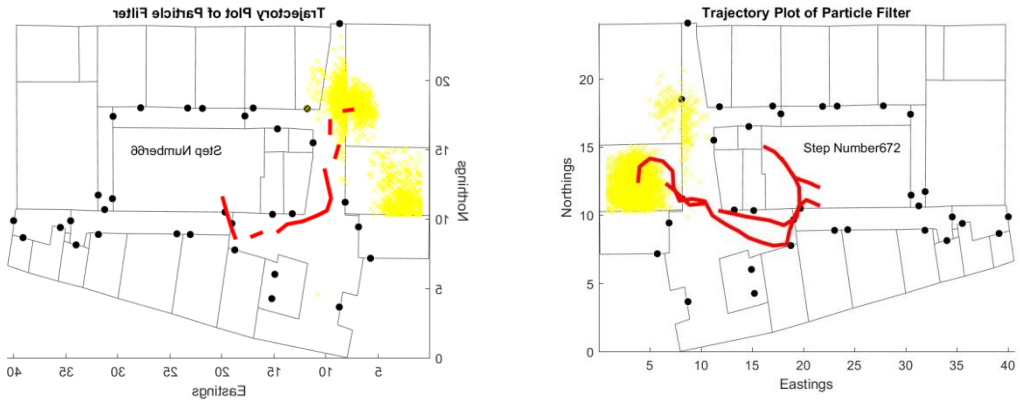


Figure 19: Trial 19 showing the sequence of trajectory taken by the participant

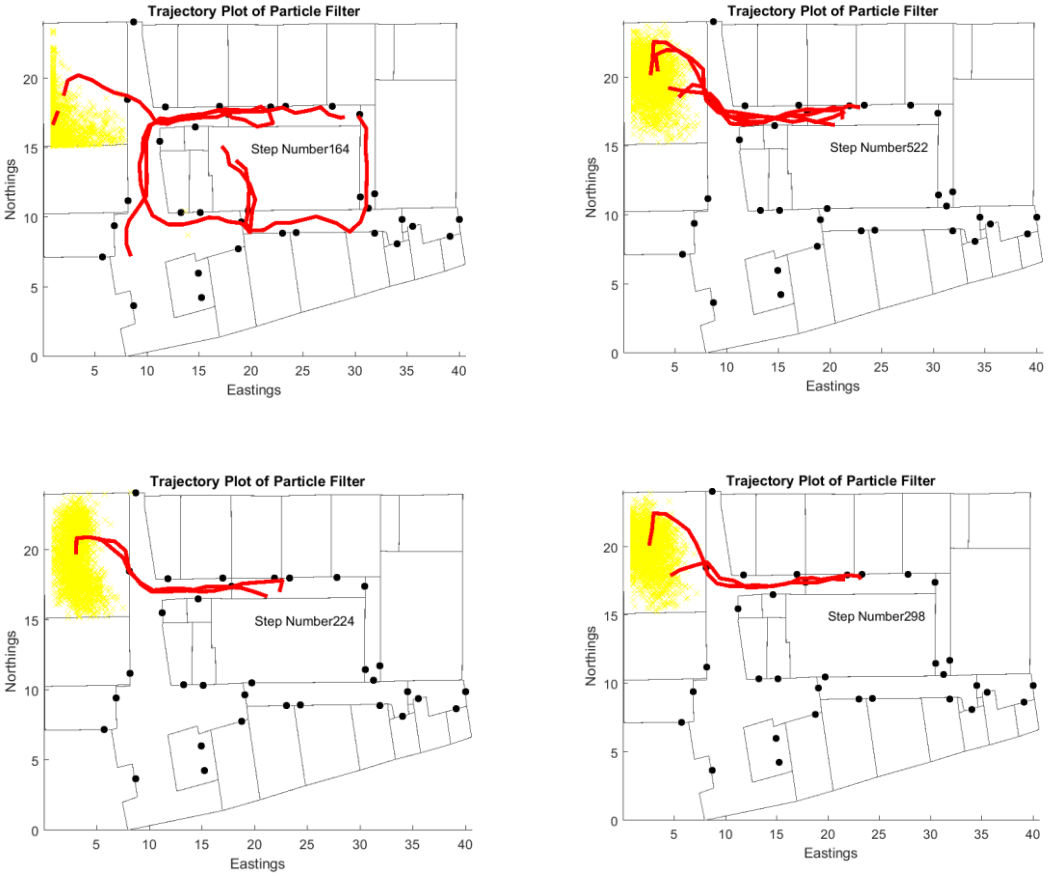


Figure 20: Trial 20 showing the sequence of trajectory taken by the participant

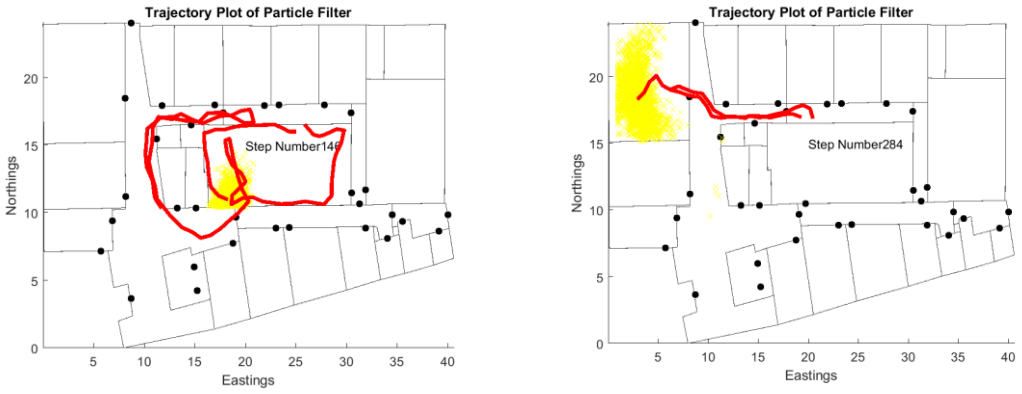


Figure 21: Trial 21 showing the sequence of trajectory taken by the participant

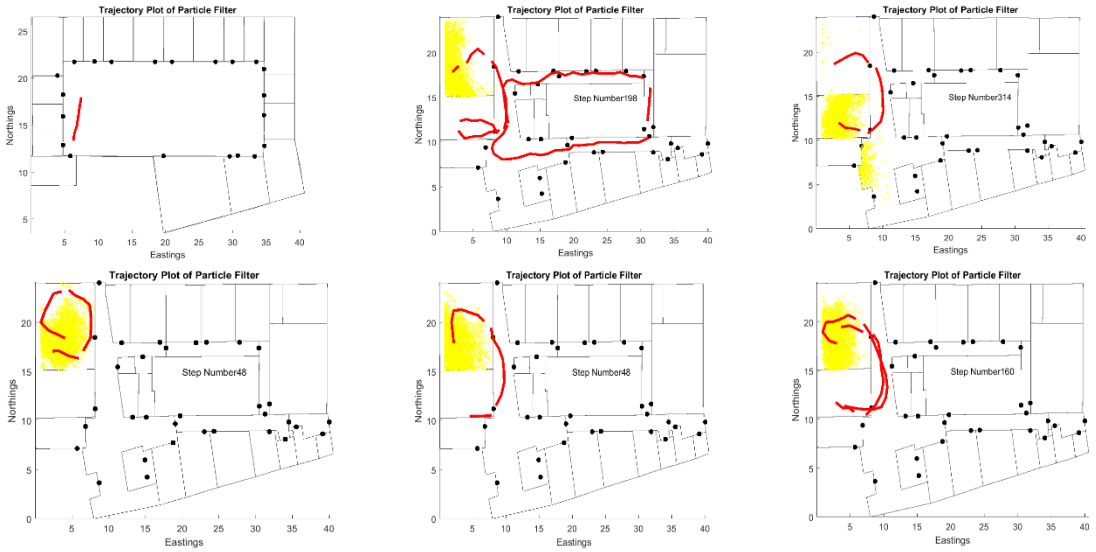
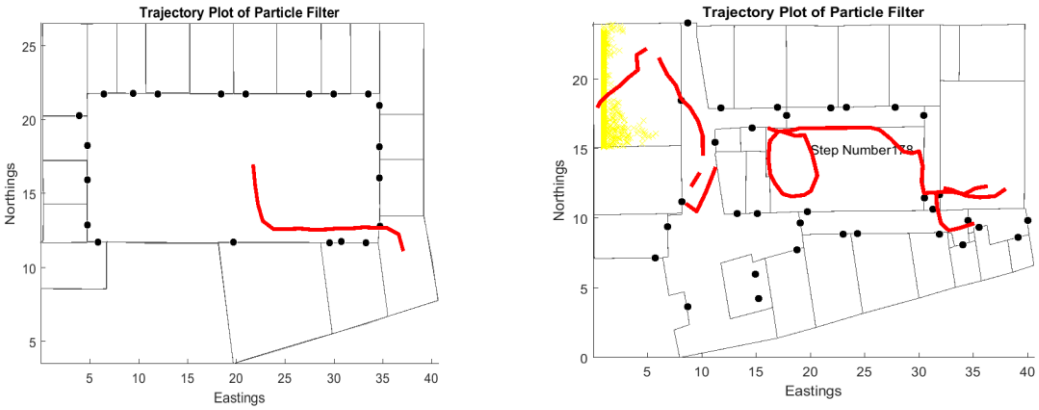


Figure 22: Trial 22 showing the sequence of trajectory taken by the participant



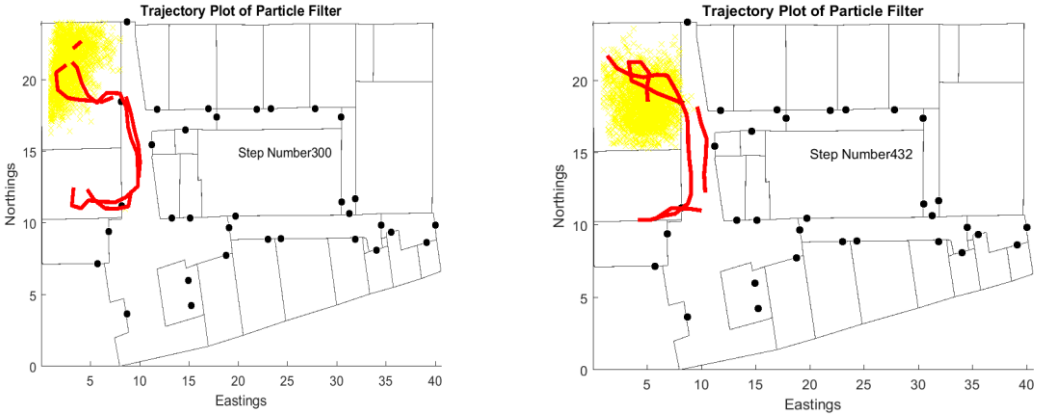


Figure 23: Trial 23 showing the sequence of trajectory taken by the participant

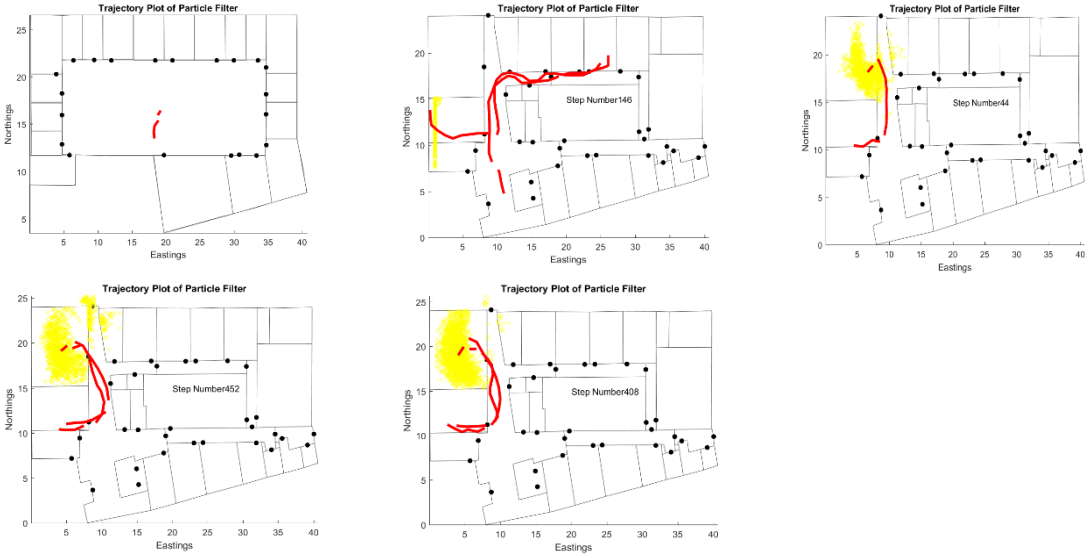
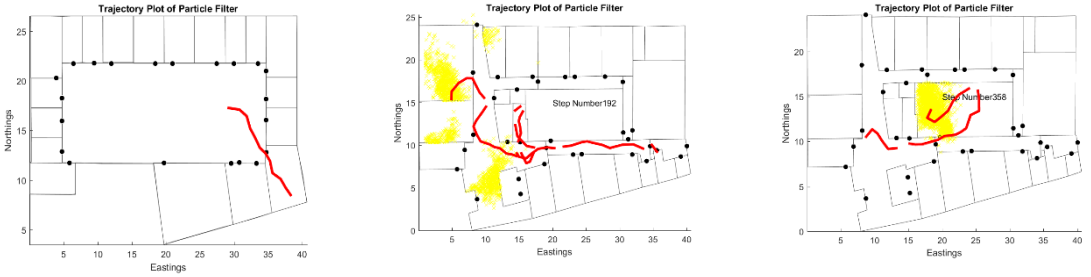


Figure 24: Trial 24 showing the sequence of trajectory taken by the participant



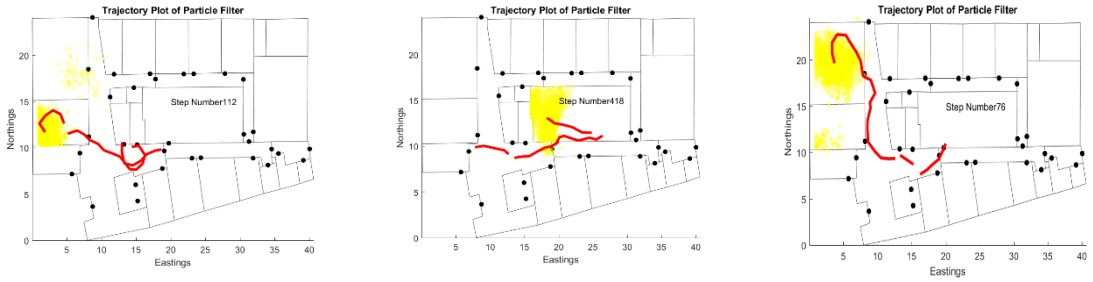


Figure 25: Trial 25 showing the sequence of trajectory taken by the participant

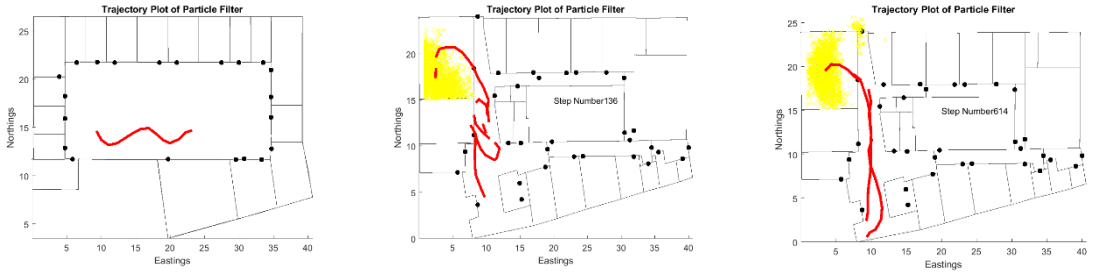


Figure 26: Trial 26 showing the sequence of trajectory taken by the participant

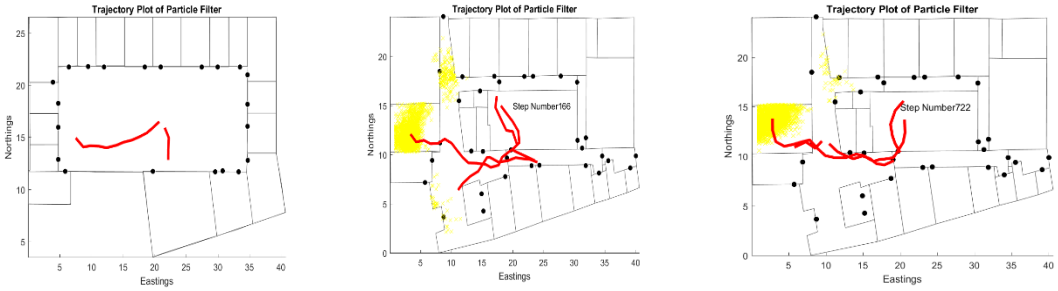
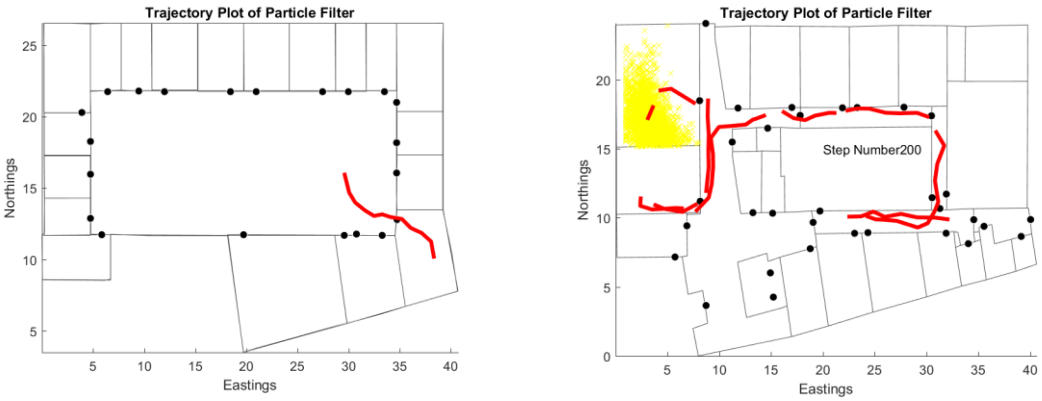


Figure 27: Trial 27 showing the sequence of trajectory taken by the participant



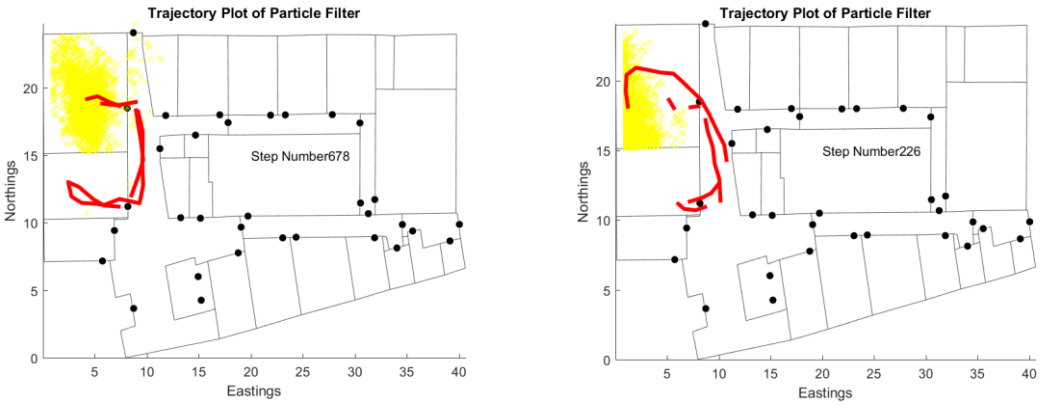


Figure 28: Trial 28 showing the sequence of trajectory taken by the participant

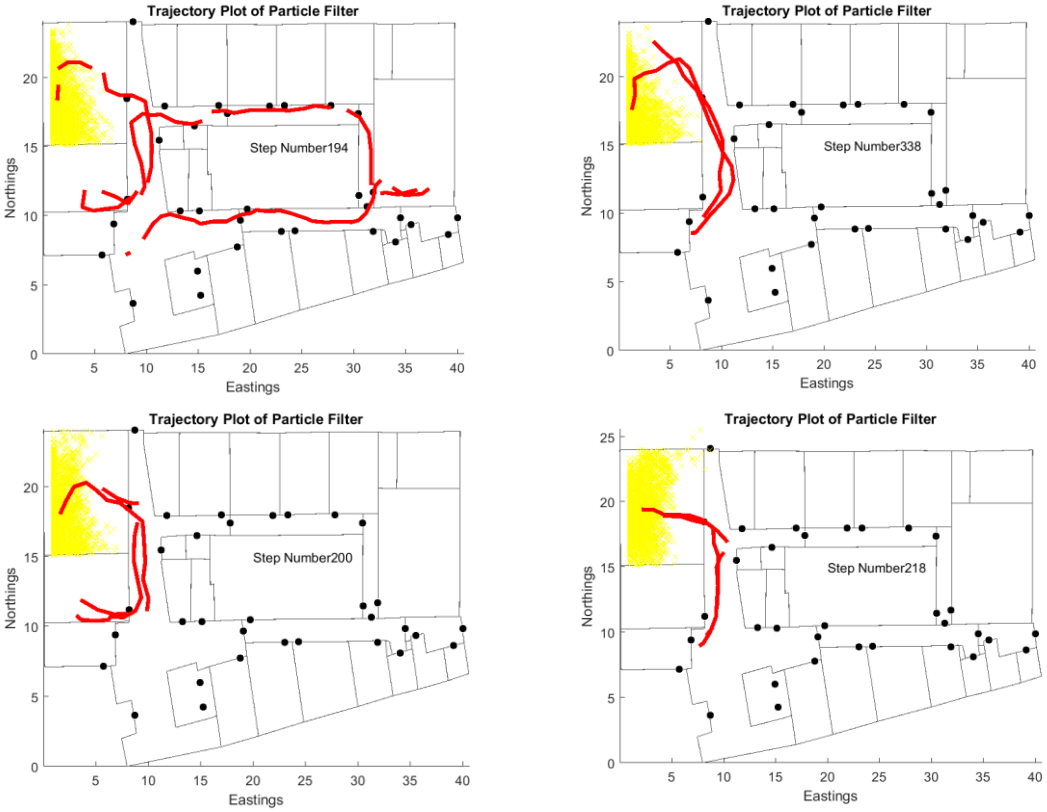


Figure 29: Trial 29 showing the sequence of trajectory taken by the participant

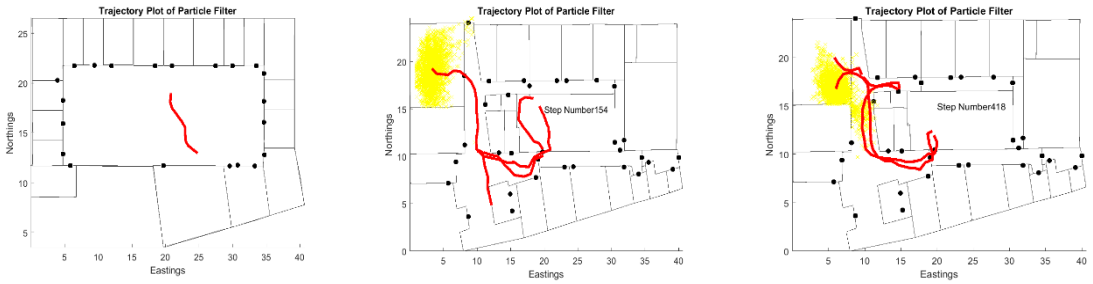


Figure 30: Trial 30 showing the sequence of trajectory taken by the participant

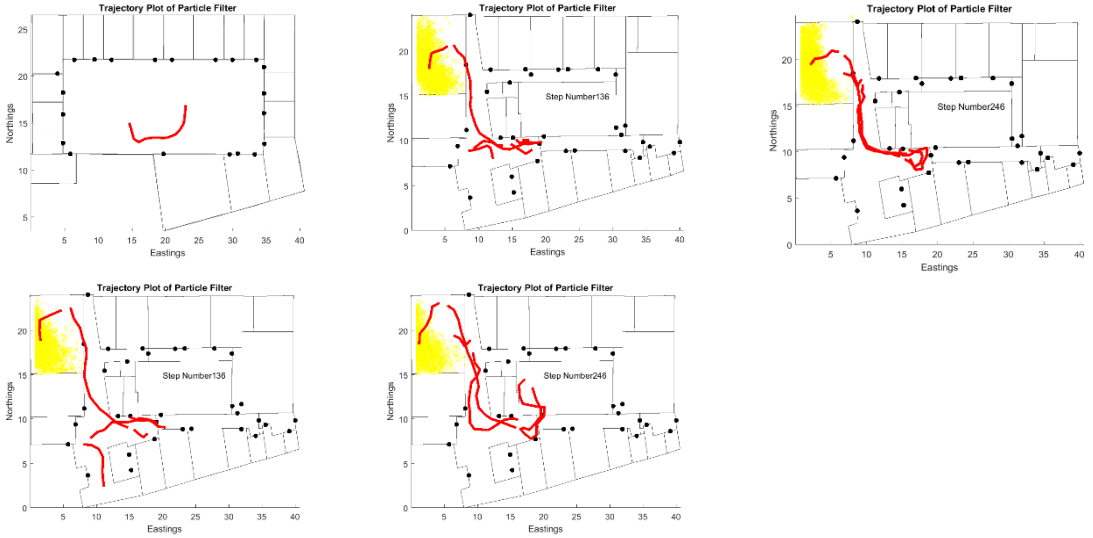


Figure 31: Trial 31 showing the sequence of trajectory taken by the participant

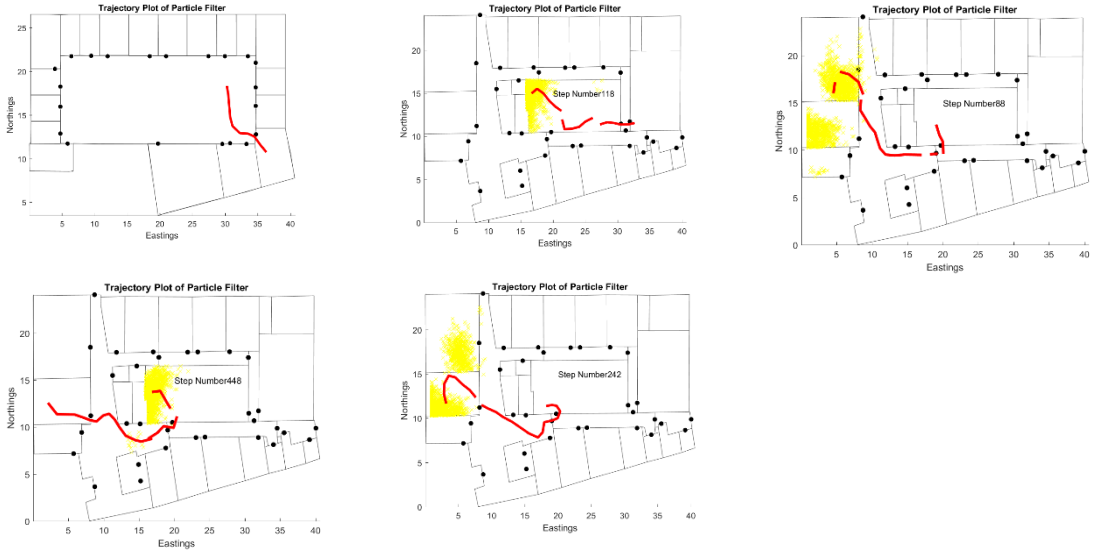


Figure 32: Trial 32 showing the sequence of trajectory taken by the participant

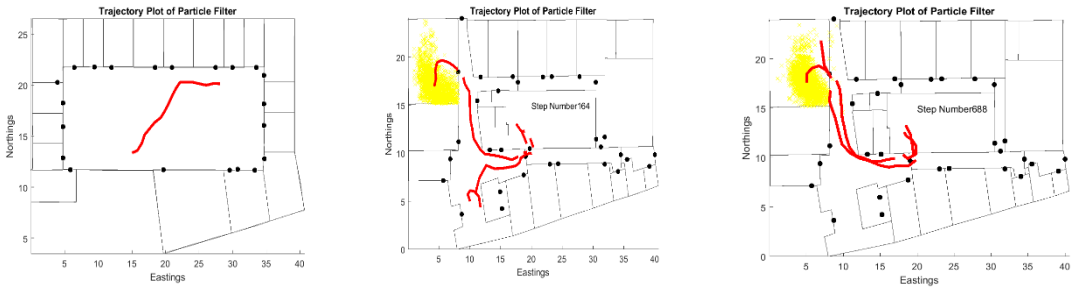


Figure 33: Trial 33 showing the sequence of trajectory taken by the participant

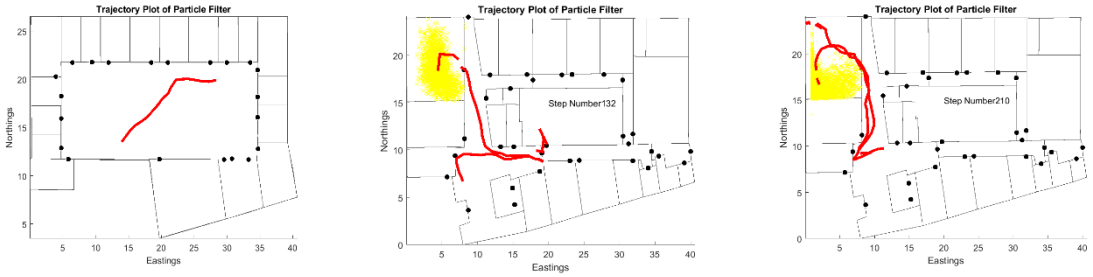


Figure 34: Trial 34 showing the sequence of trajectory taken by the participant

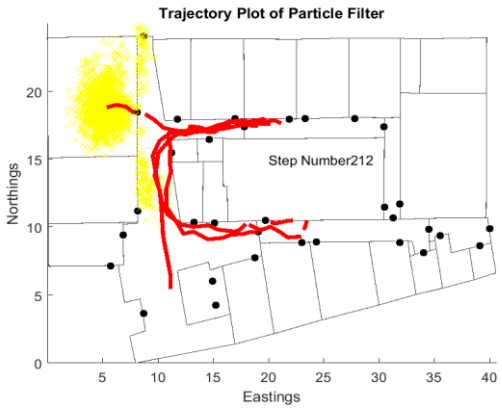


Figure 35: Trial 35 showing the sequence of trajectory taken by the participant

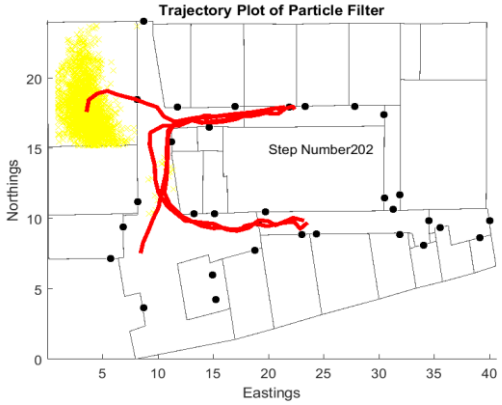


Figure 36: Trial 36 showing the sequence of trajectory taken by the participant

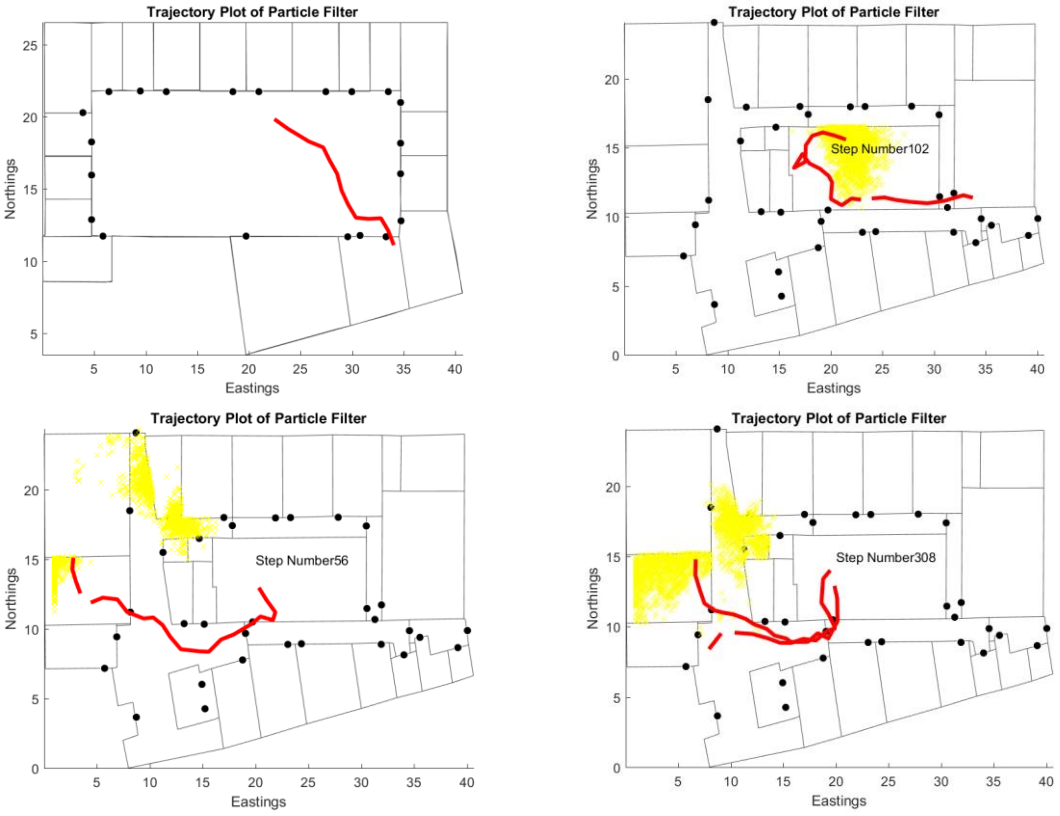


Figure 37: Trial 37 showing the sequence of trajectory taken by the participant

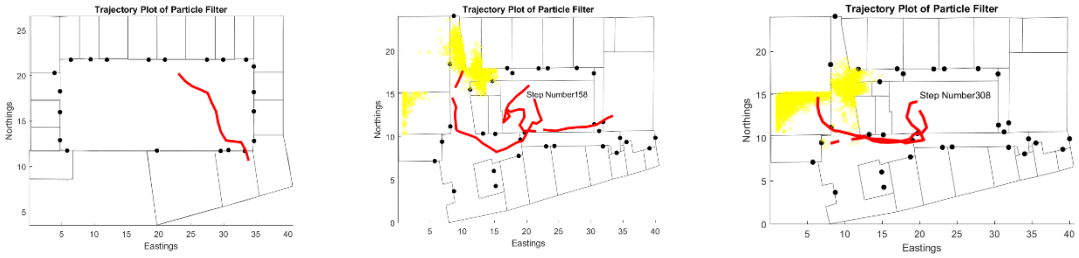


Figure 38: Trial 38 showing the sequence of trajectory taken by the participant

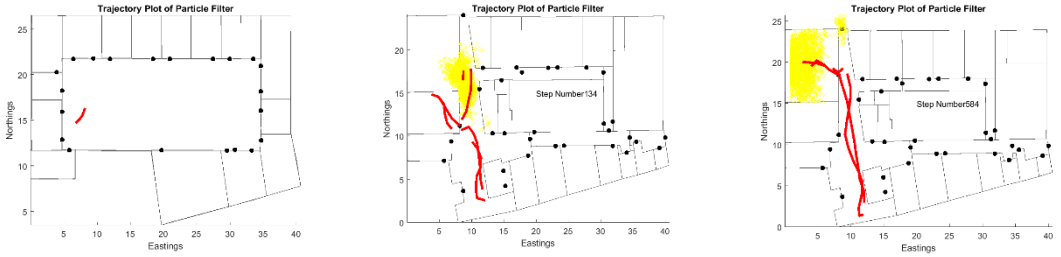


Figure 39: Trial 39 showing the sequence of trajectory taken by the participant

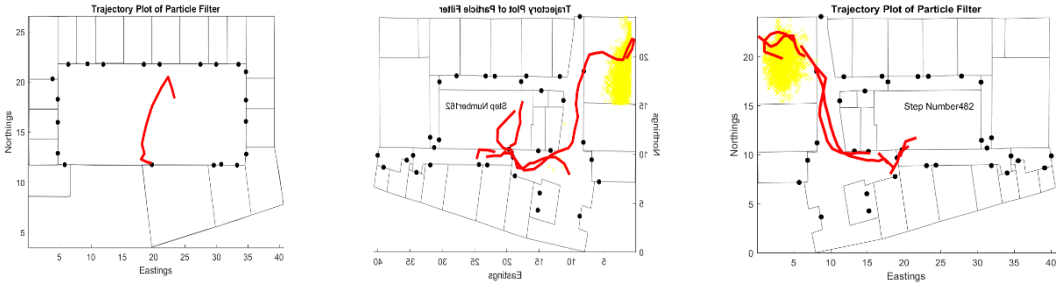


Figure 40: Trial 40 showing the sequence of trajectory taken by the participant

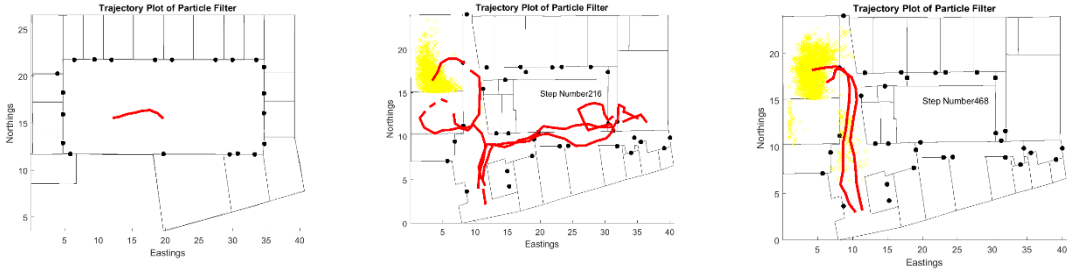


Figure 41: Trial 41 showing the sequence of trajectory taken by the participant

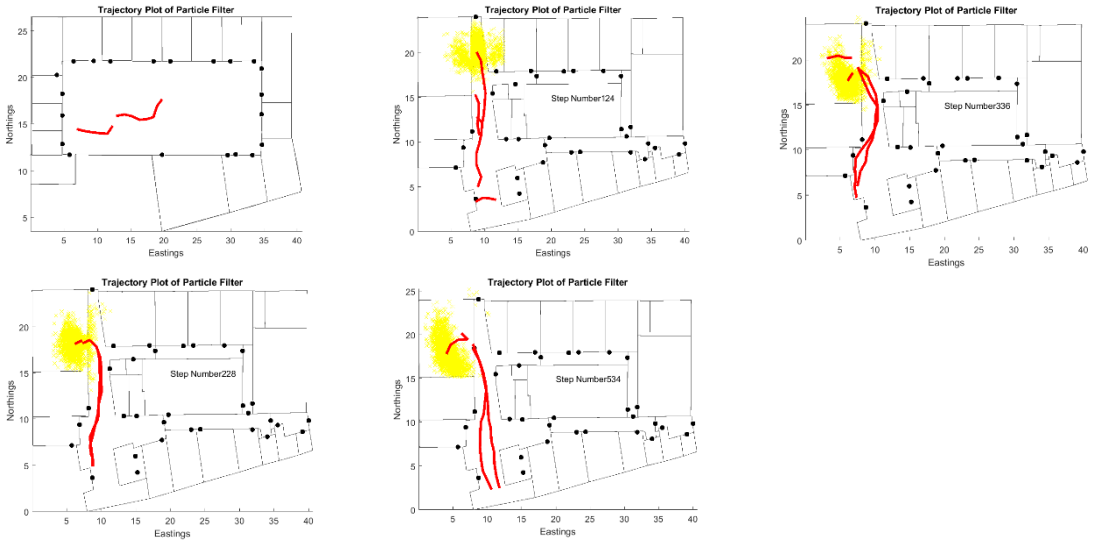


Figure 42: Trial 42 showing the sequence of trajectory taken by the participant

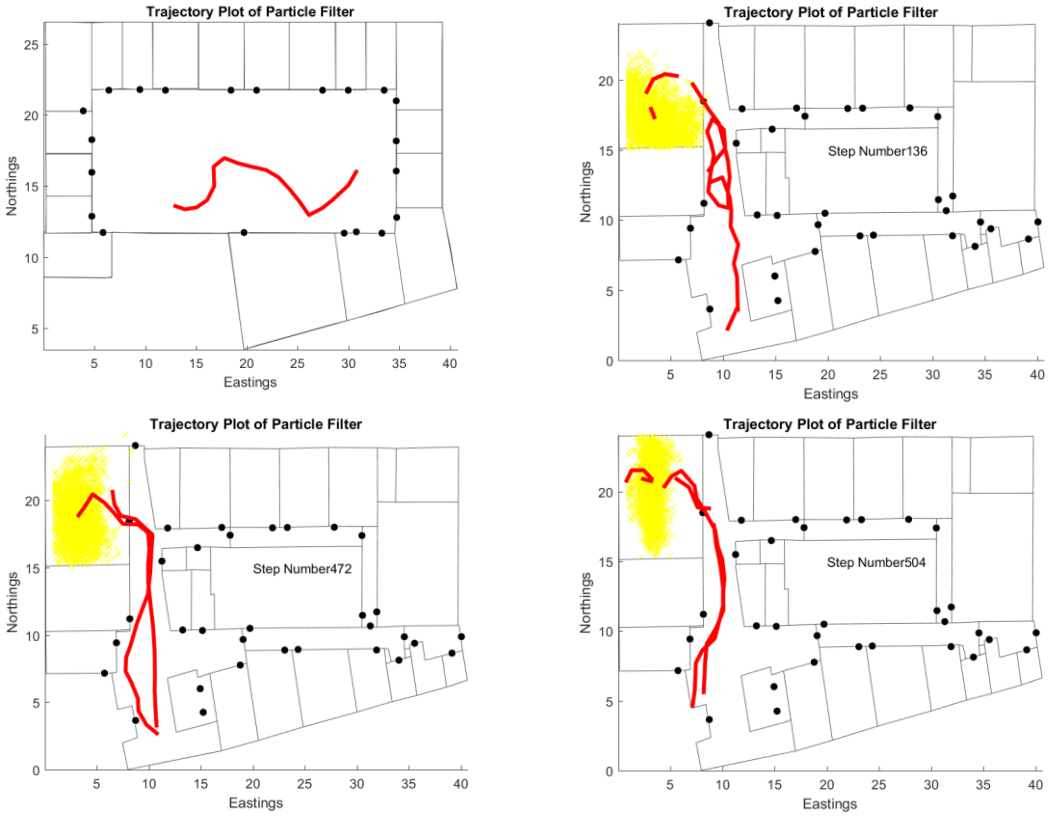


Figure 43: Trial 43 showing the sequence of trajectory taken by the participant

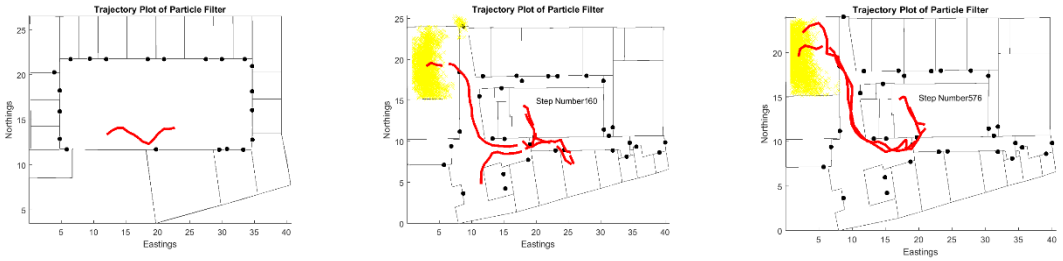


Figure 44: Trial 44 showing the sequence of trajectory taken by the participant

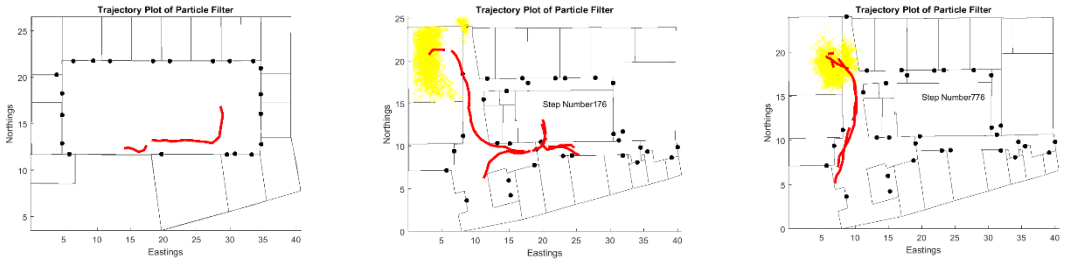


Figure 45: Trial 45 showing the sequence of trajectory taken by the participant

Reference

Abadleh, A., Al-Hawari, E. and Al-Sawalqah, H. (2017) *Step Detection Algorithm For Accurate Distance Estimation Using Dynamic Step Length*. Available at: https://arxiv.org/ftp/arxiv/papers/1801/1801.02336.pdf (Accessed: 13 March 2019).

Abadleh, A. H. (2018) 'Smartphone Based Distance Estimation Algorithm Using Dynamic Step Length', *International Journal on Communications Antenna and Propagation (IRECAP)*. Praise Worthy Prize, 8(4), p. 333. doi: 10.15866/irecap.v8i4.13894.

Abdul Rahim, K. (2012) 'Heading drift mitigation for low-cost inertial pedestrian navigation'. University of Nottingham. Available at: https://ethos.bl.uk/OrderDetails.do?uin=uk.bl.ethos.559704 (Accessed: 13 September 2019).

Abdulrahim, K., Hide, C., Moore, T. and Hill, C. (2011) 'Using Constraints for Shoe Mounted Indoor Pedestrian Navigation', *Journal of Navigation*. Cambridge University Press, 65(01), pp. 15–28. doi: 10.1017/S0373463311000518.

Adamopoulou, A. A., Tryferidis, A. M. and Tzovaras, D. K. (2016) 'A context-aware method for building occupancy prediction', *Energy and Buildings*, 110, pp. 229–244. doi: 10.1016/j.enbuild.2015.10.003.

Ai, B., Fan, Z. and Gao, R. X. (2014) 'Occupancy estimation for smart buildings by an auto-regressive hidden Markov model', in *Proceedings of the American Control Conference*. IEEE, pp. 2234–2239. doi: 10.1109/ACC.2014.6859372.

AnyLogic (2018) *AnyLogic*, *https://www.anylogic.com/*. Available at: https://www.anylogic.com/ (Accessed: 8 July 2019).

Ayub, S., Zhou, X., Honary, S., Bahraminasab, A. and Honary, B. (2012) 'Sensor placement modes for smartphone based pedestrian dead reckoning', in *Lecture Notes in Electrical Engineering*, pp. 123–132. doi: 10.1007/978-94-007-1839-5_14.

Azar, E. and Menassa, C. C. (2011) 'Agent-Based Modeling of Occupants and Their Impact on Energy Use in Commercial Buildings', *Journal of Computing in Civil Engineering*, 26(4), pp. 506–518. doi: 10.1061/(asce)cp.1943-5487.0000158.

Baniukevic, A., Jensen, C. S. and Lu, H. (2013) 'Hybrid Indoor Positioning with Wi-Fi and Bluetooth: Architecture and Performance', in *2013 IEEE 14th International Conference on Mobile Data Management*. IEEE, pp. 207–216. doi: 10.1109/MDM.2013.30.

Baniukevic, A., Sabonis, D., Jensen, C. S. and Lu, H. (2011) 'Improving Wi-Fi Based Indoor Positioning Using Bluetooth Add-Ons', *2011 IEEE 12th International Conference on Mobile Data Management*. Ieee, 1, pp. 246–255. doi: 10.1109/MDM.2011.50.

Bao, H. and Wong, W.-C. (2014) 'A Novel Map-Based Dead-Reckoning Algorithm for Indoor Localization', *Journal of Sensor and Actuator Networks*, 3(1), pp. 44–63. doi: 10.3390/jsan3010044.

Barbour, E., Davila, C. C., Gupta, S., Reinhart, C., Kaur, J. and González, M. C. (2019) 'Planning for sustainable cities by estimating building occupancy with mobile phones', *Nature Communications*. Nature Publishing Group, 10(1). doi: 10.1038/s41467-019-11685-w.

Basiri, A., Lohan, E. S., Pedro Figueiredo e Silva, Peltola, P., Hill, C. and Moore, T. (2014) 'Overview of positioning technologies from fitness-to-purpose point of view', in *International Conference on Localization and GNSS 2014 (ICL-GNSS 2014)*. IEEE, pp. 1–7. doi: 10.1109/ICL-GNSS.2014.6934176.

Basiri, A., Peltola, P., Figueiredo e Silva, P., Lohan, E. S., Moore, T. and Hill, C. (2015) 'Indoor positioning technology assessment using analytic hierarchy process for pedestrian navigation services', in *2015 International Conference on Location and GNSS (ICL-GNSS)*. IEEE, pp. 1–6. doi: 10.1109/ICL-GNSS.2015.7217157.

Becker, V., Kleiminger, W., Coroamă, V. C. and Mattern, F. (2018) 'Estimating the savings potential of occupancy-based heating strategies', *Energy Informatics*, 1(S1), pp. 11–12. doi: 10.1186/s42162-018-0022-6.

Bisio, I., Lavagetto, F., Marchese, M. and Sciarrone, A. (2013) 'Energy efficient WiFi-based fingerprinting for indoor positioning with smartphones', in *2013 IEEE Global Communications Conference (GLOBECOM)*. IEEE, pp. 4639–4643. doi: 10.1109/GLOCOMW.2013.6855683.

Bisio, I., Lavagetto, F., Marchese, M. and Sciarrone, A. (2016) 'Smart probabilistic fingerprinting for WiFi-based indoor positioning with mobile devices', *Pervasive and Mobile Computing*, 31. doi: 10.1016/j.pmcj.2016.02.001.

Bolliger, P., Partridge, K., Chu, M. and Langheinrich, M. (2009) 'Improving Location Fingerprinting through Motion Detection and Asynchronous Interval Labeling', in. Springer Berlin Heidelberg, pp. 37–51. doi: 10.1007/978-3-642-01721-6_3.

Bonabeau, E. (2002) 'Agent-based modeling: methods and techniques for simulating human systems.', *Proceedings of the National Academy of Sciences of the United States of America*. National Academy of Sciences, 99 Suppl 3(suppl 3), pp. 7280–7. doi: 10.1073/pnas.082080899.

Bourgeois, D. (no date) *DETAILED OCCUPANCY PREDICTION, OCCUPANCY-SENSING CONTROL AND ADVANCED BEHAVIOURAL MODELLING WITHIN WHOLE-BUILDING ENERGY SIMULATION*. Available at: http://www.gnu.org/ii (Accessed: 16 October 2018).

Brajdic, A. and Harle, R. (2013) 'Walk detection and step counting on unconstrained smartphones', in, p. 225. doi: 10.1145/2493432.2493449.

Brena, R. F., García-Vázquez, J. P., Galván-Tejada, C. E., Muñoz-Rodriguez, D., Vargas-Rosales, C. and Fangmeyer, J. (2017) *Evolution of Indoor Positioning Technologies: A Survey*, *Journal of Sensors*. doi: 10.1155/2017/2630413.

Breslav, S., Goldstein, R., Doherty, B., Rumery, D. and Khan, A. (2013) 'Simulating the sensing of building occupancy', in *Simulation Series*, pp. 110–117. Available at: https://www.researchgate.net/publication/262351107_Simulating_the_sensing_of_building_occupancy (Accessed: 19 February 2020).

Burak Gunay, H., Yan, D., Mahdavi, A., O'Brien, W., Tahmasebi, F., Feng, X. and Hong, T. (2015) 'Occupant behavior modeling for building performance simulation: Current state and future challenges', *Energy and Buildings*. Elsevier, 107, pp. 264–278. doi: 10.1016/j.enbuild.2015.08.032.

Buso, T., Fabi, V., Andersen, R. K. and Corgnati, S. P. (2015) 'Occupant behaviour and robustness of building design', *Building and Environment*, 94, pp. 694–703. doi: 10.1016/j.buildenv.2015.11.003.

Candanedo, L. M. and Feldheim, V. (2016) 'Accurate occupancy detection of an office room from light, temperature, humidity and CO2 measurements using statistical learning models', *Energy and Buildings*, 112, pp. 28–39. doi: 10.1016/j.enbuild.2015.11.071.

Cao, Y. (2008) *Bhattacharyya Distance Measure for Pattern Recognition - File Exchange - MATLAB Central*. Available at: https://uk.mathworks.com/matlabcentral/fileexchange/18662-bhattacharyya-distance-measure-for-pattern-recognition?focused=5100018&tab=function (Accessed: 5 January 2019).

Chandel, V., Choudhury, A. D., Ghose, A. and Bhaumik, C. (2014) 'AcTrak - Unobtrusive activity detection and step counting using smartphones', in *Lecture Notes of the Institute for Computer Sciences, Social-Informatics and Telecommunications Engineering, LNICST*. Springer, Cham, pp. 447–459. doi: 10.1007/978-3-319-11569-6_35.

Chapman, J., Siebers, P. O. and Robinson, D. (2018) 'On the multi-agent stochastic simulation of occupants in buildings', *Journal of Building Performance Simulation*, 11(5), pp. 604–621. doi: 10.1080/19401493.2017.1417483.

Chapman, J., Siebers, P. and Robinson (2014) *Coupling Multi-Agent stochastic simulation of occupants with building simulation*, *Proceedings of the Building Simulation and Optimization Conference*.

Chateau, J., Rousseau, P., Albiston, G., Cook, B., Papanastasiou, S. and Peytchev, E. (2014) 'Implementation and evaluation of particle filtering for indoor positioning', in *2014 IEEE Symposium on Computers and Communications (ISCC)*. IEEE, pp. 1–6. doi: 10.1109/ISCC.2014.6912587.

Chawathe, S. S. (2009) 'Low-latency indoor localization using bluetooth beacons', in *2009 12th International IEEE Conference on Intelligent Transportation Systems*. IEEE, pp. 1–7. doi: 10.1109/ITSC.2009.5309711.

Chen, G., Meng, X., Wang, Y., Zhang, Y., Tian, P. and Yang, H. (2015) 'Integrated WiFi/PDR/Smartphone Using an Unscented Kalman Filter Algorithm for 3D Indoor Localization', *Sensors*. Multidisciplinary Digital Publishing Institute (MDPI), 15(9), pp. 24595–24614. doi: 10.3390/s150924595.

Chen, L., Li, B., Zhao, K., Rizos, C. and Zheng, Z. (2013) 'An improved algorithm to generate a Wi-Fi fingerprint database for indoor positioning.', *Sensors (Basel, Switzerland)*, 13(8), pp. 11085–96. doi: 10.3390/s130811085.

Chen, R. and Guinness, R. (2014) *Geospatial Computing in Mobile Devices.* Artech House. Available at: https://trid.trb.org/view/1313887 (Accessed: 6 March 2019).

Chen, Z. and Soh, Y. C. (2014) 'Modeling building occupancy using a novel inhomogeneous Markov chain approach', in *IEEE International Conference on Automation Science and Engineering*. IEEE, pp. 1079–1084. doi: 10.1109/CoASE.2014.6899459.

Chen, Z., Zou, H., Jiang, H., Zhu, Q., Soh, Y. C. and Xie, L. (2015) 'Fusion of WiFi, smartphone sensors and landmarks using the kalman filter for indoor localization', *Sensors (Switzerland)*, 15(1), pp. 715–732. doi: 10.3390/s150100715.

Cioffi-Revilla, C. (2010) 'A Methodology for Complex Social Simulations', *Journal of Artificial Societies and Social Simulation*, 13(1). doi: 10.18564/jasss.1528.

Clevenger, C. M. and Haymaker, J. (2006) 'The Impact Of The Building Occupant On Energy Modeling Simulations', *In Joint International Conference on Computing and*

Decision Making in Civil and Building Engineering, pp. 1–10. doi: 10.1061/(ASCE)CP.1943-5487.0000323.

Compare 2020 Electricity Prices: Average UK Rates & Tariffs Per kWh (no date). Available at: https://powercompare.co.uk/electricity-prices/ (Accessed: 26 February 2020).

Corna, A., Fontanab, L., Nacci, A. A. and Sciuto, D. (2015) 'Occupancy Detection via iBeacon on Android Devices for Smart Building Management', in *Design, Automation & Test in Europe Conference & Exhibition (DATE), 2015*. New Jersey: IEEE Conference Publications, pp. 629–632. doi: 10.7873/DATE.2015.0753.

Dabove, P., Ghinamo, G. and Lingua, A. M. (2015) 'Inertial sensors for smartphones navigation.', *SpringerPlus*. Springer, 4, p. 834. doi: 10.1186/s40064-015-1572-8.

Dahlgren, E. and Mahmood, H. (2014) 'Evaluation of indoor positioning based on Bluetooth Smart technology', (June). Available at: http://publications.lib.chalmers.se/records/fulltext/199826/199826.pdf.

Davidson, P. and Piche, R. (2017) 'A Survey of Selected Indoor Positioning Methods for Smartphones', *IEEE Communications Surveys & Tutorials*, 19(2), pp. 1347–1370. doi: 10.1109/COMST.2016.2637663.

Davidson, P. and Piché, R. (2017) 'A Survey of Selected Indoor Positioning Methods for Smartphones', *IEEE Communications Surveys and Tutorials*, pp. 1347–1370. doi: 10.1109/COMST.2016.2637663.

Deng, Z. A., Hu, Y., Yu, J. and Na, Z. (2015) 'Extended Kalman filter for real time indoor localization by fusing WiFi and smartphone inertial sensors', *Micromachines*, 6(4), pp. 523–543. doi: 10.3390/mi6040523.

Deng, Z. A., Wang, G., Hu, Y. and Cui, Y. (2016) 'Carrying position independent user heading estimation for indoor pedestrian navigation with smartphones', *Sensors (Switzerland)*, 16(5). doi: 10.3390/s16050677.

Deng, Z. A., Wang, G., Hu, Y. and Wu, D. (2015) 'Heading estimation for indoor pedestrian navigation using a smartphone in the pocket', *Sensors (Switzerland)*. Multidisciplinary Digital Publishing Institute, 15(9), pp. 21518–21536. doi: 10.3390/s150921518.

Depatla, S., Muralidharan, A. and Mostofi, Y. (2015) 'Occupancy Estimation Using Only WiFi Power Measurements', *IEEE Journal on Selected Areas in Communications*, 33(7), pp. 1381–1393. doi: 10.1109/JSAC.2015.2430272.

DesignBuilder (2020) *DesignBuilder Software Ltd - Home*. Available at: https://designbuilder.co.uk// (Accessed: 10 February 2020).

Diao, L., Sun, Y., Chen, Z. and Chen, J. (2017) 'Modeling energy consumption in residential buildings: A bottom-up analysis based on occupant behavior pattern clustering and stochastic simulation', *Energy and Buildings*, 147, pp. 47–66. doi: 10.1016/j.enbuild.2017.04.072.

Do-Xuan, T., Tran-Quang, V., Bui-Xuan, T. and Vu-Thanh, V. (2015) 'Smartphone-based pedestrian dead reckoning and orientation as an indoor positioning system', in *International Conference on Advanced Technologies for Communications*. IEEE, pp. 303–308. doi: 10.1109/ATC.2014.7043402.

Dobbs, J. R. and Hencey, B. M. (2014) 'Model predictive HVAC control with online occupancy model', *Energy and Buildings*, 82, pp. 675–684. doi: 10.1016/j.enbuild.2014.07.051.

Dodier, R. H., Henze, G. P., Tiller, D. K. and Guo, X. (2006) 'Building occupancy detection through sensor belief networks', *Energy and Buildings*. doi: 10.1016/j.enbuild.2005.12.001.

Dong, B., Andrews, B., Lam, K. P., Höynck, M., Zhang, R., Chiou, Y.-S. and Benitez, D. (2010) 'An information technology enabled sustainability test-bed (ITEST) for occupancy detection through an environmental sensing network', *Energy and Buildings*, 42(7), pp. 1038–1046. doi: 10.1016/j.enbuild.2010.01.016.

Le Dortz, N., Gain, F. and Zetterberg, P. (2012) 'WiFi fingerprint indoor positioning system using probability distribution comparison', in *2012 IEEE International Conference on Acoustics, Speech and Signal Processing (ICASSP)*. IEEE, pp. 2301–2304. doi: 10.1109/ICASSP.2012.6288374.

Doucet, A. and Johansen, A. M. (2012) *A Tutorial on Particle Filtering and Smoothing: Fifteen years later*. Available at: https://www.stats.ox.ac.uk/~doucet/doucet_johansen_tutorialPF2011.pdf (Accessed: 5 March 2019).

Duarte, C., Van Den Wymelenberg, K. and Rieger, C. (2013) 'Revealing occupancy patterns in an office building through the use of occupancy sensor data', *Energy and Buildings*, 67, pp. 587–595. doi: 10.1016/j.enbuild.2013.08.062.

Dubin, J. C. (2013) *Achilles Tendinopathies in Runners : Causes , Treatment , and Prevention*, *Prevention*. Available at: https://dubinchiro.com/2013/10/achilles-tendinopathies-in-runners-causes-treatment-and-prevention/ (Accessed: 23 January 2018).

El-Sheimy, N., Hou, H. and Niu, X. (2008) 'Analysis and Modeling of Inertial Sensors Using Allan Variance', *IEEE Transactions on Instrumentation and Measurement*, 57(1), pp. 140–149. doi: 10.1109/TIM.2007.908635.

Faragher, R. (2012) 'Understanding the Basis of the Kalman Filter Via a Simple and Intuitive Derivation [Lecture Notes]', *IEEE Signal Processing Magazine*, 29(5), pp. 128–132. doi: 10.1109/MSP.2012.2203621.

Faragher, R. and Harle, R. (2014) 'An Analysis of the Accuracy of Bluetooth Low Energy for Indoor Positioning Applications', in *Proceedings of the 27th International Technical Meeting of The Satellite Division of the Institute of Navigation (ION GNSS+ 2014)*, pp. 201–210. Available at: http://www.ion.org/publications/abstract.cfm?jp=p&articleID=12411 (Accessed: 20 November 2015).

Faragher, R. and Harle, R. (2015) 'Location Fingerprinting With Bluetooth Low Energy Beacons', *IEEE Journal on Selected Areas in Communications*, 33(11), pp. 2418–2428. doi: 10.1109/JSAC.2015.2430281.

Faragher, R. M. and Harle, R. K. (2013) 'SmartSLAM - An efficient smartphone indoor positioning system exploiting machine learning and opportunistic sensing', in *26th International Technical Meeting of the Satellite Division of the Institute of Navigation, ION GNSS 2013*, pp. 1006–1019. Available at: https://www.ion.org/publications/abstract.cfm?articleID=11308 (Accessed: 10 February 2020).

Faria, D. B. (2005) 'Modeling Signal Attenuation in IEEE 802.11 Wireless LANs -Vol. 1'.

Feldmann, S., Ana, Z., Kyamakya, K. and Lue, Z. (no date) *An indoor Bluetooth-based positioning system: concept, Implementation and experimental evaluation*. Available at: https://www.researchgate.net/publication/220719209_An_Indoor_Bluetooth-Based_Positioning_System_Concept_Implementation_and_Experimental_Evaluation (Accessed: 30 October 2014).

Fet, N., Handte, M. and Marrón, P. J. (2013) 'A model for WLAN signal attenuation of the human body', in *Proceedings of the 2013 ACM international joint conference on Pervasive and ubiquitous computing - UbiComp '13*. New York, New York, USA: ACM Press, p. 499. doi: 10.1145/2493432.2493459.

Fetzer, T. *et al.* (2018) 'Smartphone-Based Indoor Localization within a 13th Century Historic Building', *Sensors*. Multidisciplinary Digital Publishing Institute, 18(12), p. 4095. doi: 10.3390/s18124095.

Ganti, D., Zhang, W. and Kavehrad, M. (2014) 'VLC-based indoor positioning system with tracking capability using Kalman and particle filters', in *2014 IEEE International Conference on Consumer Electronics (ICCE)*. IEEE, pp. 476–477. doi: 10.1109/ICCE.2014.6776093.

Gobana, F. W. (2018) 'Survey of Inertial/magnetic Sensors Based pedestrian dead

reckoning by multi-sensor fusion method', in *9th International Conference on Information and Communication Technology Convergence: ICT Convergence Powered by Smart Intelligence, ICTC 2018*. IEEE, pp. 1327–1334. doi: 10.1109/ICTC.2018.8539576.

GPML Library (2018) *Documentation for GPML Matlab Code*. Available at: http://www.gaussianprocess.org/gpml/code/matlab/doc/index.html (Accessed: 29 December 2018).

Groves, P. D. (Paul D. (2013) *Principles of GNSS, inertial, and multisensor integrated navigation systems*. Artech House.

Groves, P., Martin, H., Voutsis, K., Walter, D. and Wang, L. (2013) 'Context Detection, Categorization and Connectivity for Advanced Adaptive Integrated Navigation', *Proceedings of the 26th International Technical Meeting of The Satellite Division of the Institute of Navigation (ION GNSS+ 2013)*. The Institute of Navigation, pp. 1039–1056. Available at: http://discovery.ucl.ac.uk/1394967/1/ION_GNSS13_F2_1_Groves_et_al_1_0%28Context%29.pdf (Accessed: 4 March 2016).

Gul, M. S. and Patidar, S. (2015) 'Understanding the energy consumption and occupancy of a multi-purpose academic building', *Energy and Buildings*. Elsevier, 87, pp. 155–165. doi: 10.1016/j.enbuild.2014.11.027.

Gunay, H. B., O'Brien, W. and Beausoleil-Morrison, I. (2016) 'Implementation and comparison of existing occupant behaviour models in EnergyPlus', *Journal of Building Performance Simulation*, 9(6), pp. 567–588. doi: 10.1080/19401493.2015.1102969.

Gurrin, C. (2013) 'A Comprehensive Study of Bluetooth Fingerprinting-Based Algorithms for Localization', in *2013 27th International Conference on Advanced Information Networking and Applications Workshops*. IEEE, pp. 300–305. doi: 10.1109/WAINA.2013.205.

Haldi, F. and Robinson, D. (2008) 'On the behaviour and adaptation of office

occupants', *Building and Environment*, 43(12), pp. 2163–2177. doi: 10.1016/j.buildenv.2008.01.003.

Haldi, F. and Robinson, D. (2009) 'Interactions with window openings by office occupants', *Building and Environment*, 44(12), pp. 2378–2395. doi: 10.1016/j.buildenv.2009.03.025.

Haldi, F. and Robinson, D. (2010) 'Adaptive actions on shading devices in response to local visual stimuli', *Journal of Building Performance Simulation*, 3(2), pp. 135–153. doi: 10.1080/19401490903580759.

Haldi, F. and Robinson, D. (2011) 'The impact of occupants' behaviour on building energy demand', *Journal of Building Performance Simulation*. Taylor & Francis, 4(4), pp. 323–338. doi: 10.1080/19401493.2011.558213.

Hammersley, J. M. and Morton, K. W. (1954) 'Poor Man's Monte Carlo', *Journal of the Royal Statistical Society. Series B (Methodological)*. WileyRoyal Statistical Society, pp. 23–38. doi: 10.2307/2984008.

Han, X. and He, D. (2018) 'Research on Indoor Positioning Based on Fusion of WI-FI/PDR', in *Proceedings of the 3rd International Conference on Multimedia Systems and Signal Processing - ICMSSP '18*. New York, New York, USA: ACM Press, pp. 124–128. doi: 10.1145/3220162.3220183.

Harle, R. (2013) 'A Survey of Indoor Inertial Positioning Systems for Pedestrians', *IEEE Communications Surveys & Tutorials*, 15(3), pp. 1281–1293. doi: 10.1109/SURV.2012.121912.00075.

Hay, S. and Harle, R. (2009) 'Bluetooth Tracking without Discoverability', in. Springer, Berlin, Heidelberg, pp. 120–137. doi: 10.1007/978-3-642-01721-6_8.

Herrera, E. P., Trujillo, Y., Alvarez, R. and Sierra, D. (2017) 'Sampling frequency for step detection based on smartphone accelerometry', in *Proceedings - 14th International Symposium on Pervasive Systems, Algorithms and Networks, I-SPAN 2017, 11th International Conference on Frontier of Computer Science and Technology, FCST 2017*

and 3rd International Symposium of Creative Computing, ISCC 2017. IEEE, pp. 409–413. doi: 10.1109/ISPAN-FCST-ISCC.2017.89.

Hide, C. (2003) 'Integration of GPS and low cost INS measurements'. Available at: http://eprints.nottingham.ac.uk/12037/ (Accessed: 13 September 2019).

Ho, N.-H., Truong, P. H. and Jeong, G.-M. (2016) 'Step-Detection and Adaptive Step-Length Estimation for Pedestrian Dead-Reckoning at Various Walking Speeds Using a Smartphone', *Sensors*. Multidisciplinary Digital Publishing Institute, 16(9), p. 1423. doi: 10.3390/s16091423.

Ho, N. H., Truong, P. H. and Jeong, G. M. (2016) 'Step-detection and adaptive step-length estimation for pedestrian dead-reckoning at variouswalking speeds using a smartphone', *Sensors (Switzerland)*, 16(9). doi: 10.3390/s16091423.

Hong, F., Zhang, Y., Zhang, Z., Wei, M., Feng, Y. and Guo, Z. (2014) 'WaP: Indoor localization and tracking using WiFi-Assisted Particle filter', in *39th Annual IEEE Conference on Local Computer Networks*. IEEE, pp. 210–217. doi: 10.1109/LCN.2014.6925774.

Hong, T., Chen, Y., Belafi, Z. and D'Oca, S. (2018) 'Occupant behavior models: A critical review of implementation and representation approaches in building performance simulation programs', *Building Simulation*, 11(1), pp. 1–14. doi: 10.1007/s12273-017-0396-6.

Hong, T., Taylor-Lange, S. C., D'Oca, S., Yan, D. and Corgnati, S. P. (2016) 'Advances in research and applications of energy-related occupant behavior in buildings', *Energy and Buildings*, pp. 694–702. doi: 10.1016/j.enbuild.2015.11.052.

Hu, Z., Huang, G., Hu, Y. and Yang, Z. (2018) 'WI-VI fingerprint: WiFi and vision integrated fingerprint for smartphone-based indoor self-localization', in *Proceedings - International Conference on Image Processing, ICIP*. IEEE, pp. 4402–4406. doi: 10.1109/ICIP.2017.8297114.

Huang, C., Zhang, G., Jiang, Z., Li, C., Wang, Y. and Wang, X. (2015) 'Smartphone-based

indoor position and orientation tracking fusing inertial and magnetic sensing', in *International Symposium on Wireless Personal Multimedia Communications, WPMC*. IEEE, pp. 215–220. doi: 10.1109/WPMC.2014.7014819.

Huang, J., Millman, D., Quigley, M., Stavens, D., Thrun, S. and Aggarwal, A. (2011) 'Efficient, generalized indoor WiFi GraphSLAM', in *Proceedings - IEEE International Conference on Robotics and Automation*, pp. 1038–1043. doi: 10.1109/ICRA.2011.5979643.

Huovila, A., Tuominen, P. and Airaksinen, M. (2017) 'Effects of building occupancy on indicators of energy efficiency', *Energies*. MDPI AG, 10(5). doi: 10.3390/en10050628.

Huovila, A., Tyni, A. and Dooley, K. (2013) 'Building occupancy as an aspect of energy efficiency', in *Proceedings of SB13 Conference in Dubai*, pp. 8–10. Available at: https://www.researchgate.net/publication/326786036_Building_occupancy_as_an_aspect_of_energy_efficiency (Accessed: 19 February 2020).

Ilyas, M., Cho, K., Baeg, S.-H. and Park, S. (2016) 'Drift Reduction in Pedestrian Navigation System by Exploiting Motion Constraints and Magnetic Field.', *Sensors (Basel, Switzerland)*. Multidisciplinary Digital Publishing Institute (MDPI), 16(9). doi: 10.3390/s16091455.

Incel, O. (2015) 'Analysis of Movement, Orientation and Rotation-Based Sensing for Phone Placement Recognition', *Sensors*, 15(10), pp. 25474–25506. doi: 10.3390/s151025474.

indoo.rs (2010) *Indoor Positioning System for Enterprises | powered by indoo.rs*. Available at: https://indoo.rs/ (Accessed: 13 March 2019).

Ioannidis, D., Tropios, P., Krinidis, S., Stavropoulos, G., Tzovaras, D. and Likothanasis, S. (2016) 'Occupancy driven building performance assessment', *Journal of Innovation in Digital Ecosystems*. Elsevier BV, 3(2), pp. 57–69. doi: 10.1016/j.jides.2016.10.008.

Itu-R (2017) *Propagation data and prediction methods for the planning of indoor radiocommunication systems and radio local area networks in the frequency range 300*

MHz to 100 GHz P Series Radiowave propagation. Available at: https://www.itu.int/dms_pubrec/itu-r/rec/p/R-REC-P.1411-9-201706-I!!PDF-E.pdf (Accessed: 20 December 2016).

Jardak, N. and Samama, N. (2009) 'Indoor positioning based on GPS-repeaters: Performance enhancement using an open code loop architecture', *IEEE Transactions on Aerospace and Electronic Systems*, 45(1), pp. 347–359. doi: 10.1109/TAES.2009.4805284.

Jia, M., Srinivasan, R. S. and Raheem, A. A. (2017) 'From occupancy to occupant behavior: An analytical survey of data acquisition technologies, modeling methodologies and simulation coupling mechanisms for building energy efficiency', *Renewable and Sustainable Energy Reviews*, pp. 525–540. doi: 10.1016/j.rser.2016.10.011.

Jianyong, Z., Haiyong, L., Zili, C. and Zhaohui, L. (2014) 'RSSI based Bluetooth low energy indoor positioning', in *2014 International Conference on Indoor Positioning and Indoor Navigation (IPIN)*. IEEE, pp. 526–533. doi: 10.1109/IPIN.2014.7275525.

Jin, M., Koo, B., Lee, S., Park, C., Lee, M. J. and Kim, S. (2014) 'IMU-assisted nearest neighbor selection for real-time WiFi fingerprinting positioning', in *2014 International Conference on Indoor Positioning and Indoor Navigation (IPIN)*. IEEE, pp. 745–748. doi: 10.1109/IPIN.2014.7275556.

Jing, H. (2015) *Indoor Collaborative Positioning based on a Multi-sensor and Multi-user System*. University Of Nottingham. Available at: http://eprints.nottingham.ac.uk/30475/1/Thesis_HaoJing_4154111.pdf.

Jing, H., Pinchin, J., Hill, C. and Moore, T. (2016) 'Wi-Fi fingerprinting based on collaborative confidence level training', *Pervasive and Mobile Computing*, 30, pp. 32–44. doi: 10.1016/j.pmcj.2015.10.005.

Jouybari, A., Ardalan, A. A. and Rezvani, M. H. (2017) 'Experimental comparison between Mahoney and Complementary sensor fusion algorithm for attitude

determination by raw sensor data of Xsens IMU on buoy', in *International Archives of the Photogrammetry, Remote Sensing and Spatial Information Sciences - ISPRS Archives*, pp. 497–502. doi: 10.5194/isprs-archives-XLII-4-W4-497-2017.

Kaemarungsi, K. and Krishnamurthy, P. (2012) 'Analysis of WLAN's received signal strength indication for indoor location fingerprinting', *Pervasive and Mobile Computing*. Elsevier Science Publishers B. V., 8(2), pp. 292–316. doi: 10.1016/j.pmcj.2011.09.003.

Kaji, K. and Kawaguchi, N. (2012a) 'Design and Implementation of WiFi Indoor Localization based on Gaussian Mixture Model and Particle Filter', *2012 International Conference on Indoor Positioning and Indoor Navigation*, (November). Available at: http://ieeexplore.ieee.org/xpl/login.jsp?tp=&arnumber=6418943&url=http://ieeexplore.ieee.org/iel5/6409516/6418727/06418943.pdf?arnumber=6418943.

Kaji, K. and Kawaguchi, N. (2012b) 'Gaussian Mixture Model and Particle Filter', in *2012 International Conference on Indoor Positioning and Indoor Navigation (IPIN)*. IEEE, pp. 1–9. doi: 10.1109/IPIN.2012.6418943.

Kalman, R. E. (1960) 'A new Approach to Linear Filtering and Prediction Problems', *Transactions of the ASME-Journal of Basic Engineering*, 82, pp. 35–45. Available at: http://www.unitedthc.com/DSP/Kalman1960.pdf (Accessed: 4 March 2019).

Kang, W., Nam, S., Han, Y. and Lee, S. (2012) 'Improved heading estimation for smartphone-based indoor positioning systems', in *2012 IEEE 23rd International Symposium on Personal, Indoor and Mobile Radio Communications - (PIMRC)*. IEEE, pp. 2449–2453. doi: 10.1109/PIMRC.2012.6362768.

Kashif, A., Ploix, S., Dugdale, J. and Le, X. H. B. (2013) 'Simulating the dynamics of occupant behaviour for power management in residential buildings', *Energy and Buildings*. Elsevier, 56, pp. 85–93. doi: 10.1016/J.ENBUILD.2012.09.042.

Kim, C., So, H., Lee, T. and Kee, C. (2014) 'A pseudolite-based positioning system for legacy GNSS receivers', *Sensors (Switzerland)*. Molecular Diversity Preservation

International, 14(4), pp. 6104–6123. doi: 10.3390/s140406104.

Kim, D. Y., Kim, S. H., Choi, D. and Jin, S. H. (2015) 'Accurate indoor proximity zone detection based on time window and frequency with bluetooth low energy', in *Procedia Computer Science*. doi: 10.1016/j.procs.2015.07.199.

Kipping, A. and Trømborg, E. (2017) 'Modeling hourly consumption of electricity and district heat in non-residential buildings', *Energy*. Pergamon, 123, pp. 473–486. doi: 10.1016/J.ENERGY.2017.01.108.

Kok, M., Hol, J. D. and Schön, T. B. (2017) 'Using Inertial Sensors for Position and Orientation Estimation'. doi: 10.1561/2000000094.

kontakt.io (2013) *BLE Beacons and Tags - Kontakt.io*. Available at: https://kontakt.io/ble-beacons-tags/ (Accessed: 10 December 2018).

Kos, A., Tomažič, S. and Umek, A. (2016a) 'Evaluation of Smartphone Inertial Sensor Performance for Cross-Platform Mobile Applications.', *Sensors (Basel, Switzerland)*. Multidisciplinary Digital Publishing Institute (MDPI), 16(4). doi: 10.3390/s16040477.

Kos, A., Tomažič, S. and Umek, A. (2016b) 'Suitability of smartphone inertial sensors for real-time biofeedback applications', *Sensors (Switzerland)*, 16(3), p. 301. doi: 10.3390/s16030301.

Kriz, P., Maly, F. and Kozel, T. (2016) 'Improving Indoor Localization Using Bluetooth Low Energy Beacons', *Mobile Information Systems*, 2016. doi: 10.1155/2016/2083094.

Kupke, J., Willemsen, T., Keller, F. and Sternberg, H. (2016) 'Development of a step counter based on artificial neural networks', *Journal of Location Based Services*, pp. 161–177. doi: 10.1080/17489725.2016.1196832.

Kwok-Wai Cheung, Sau, J. H.-M. and Murch, R. D. (1998) 'A new empirical model for indoor propagation prediction', *IEEE Transactions on Vehicular Technology*, 47(3), pp. 996–1001. doi: 10.1109/25.704854.

Kwok, S. S. K., Yuen, R. K. K. and Lee, E. W. M. (2011) 'An intelligent approach to

assessing the effect of building occupancy on building cooling load prediction', *Building and Environment*. Elsevier Ltd, 46(8), pp. 1681–1690. doi: 10.1016/j.buildenv.2011.02.008.

Labeodan, T., Zeiler, W., Boxem, G. and Zhao, Y. (2015) 'Occupancy measurement in commercial office buildings for demand-driven control applications - A survey and detection system evaluation', *Energy and Buildings*. doi: 10.1016/j.enbuild.2015.02.028.

Lane, N., Miluzzo, E., Lu, H., Peebles, D., Choudhury, T. and Campbell, A. (2010) 'A survey of mobile phone sensing', *IEEE Communications Magazine*, 48(9), pp. 140–150. doi: 10.1109/MCOM.2010.5560598.

Langevin, J., Wen, J. and Gurian, P. L. (2015) 'Simulating the human-building interaction: Development and validation of an agent-based model of office occupant behaviors', *Building and Environment*. Pergamon, 88, pp. 27–45. doi: 10.1016/j.buildenv.2014.11.037.

Lassabe, F., Canalda, P., Chatonnay, P. and Spies, F. (2009) 'Indoor Wi-Fi positioning: techniques and systems', *Annals of Telecommunications - Annales Des Télécommunications*, 64(9–10), pp. 651–664. doi: 10.1007/s12243-009-0122-1.

Lee, H., Choi, S. and Lee, M. (2015) 'Step Detection Robust against the Dynamics of Smartphones', *Sensors*. Multidisciplinary Digital Publishing Institute, 15(10), pp. 27230–27250. doi: 10.3390/s151027230.

Lee, M. S., Ju, H. and Park, C. G. (2017) 'Map assisted PDR/Wi-Fi fusion for indoor positioning using smartphone', *International Journal of Control, Automation and Systems*, 15(2), pp. 627–639. doi: 10.1007/s12555-015-0342-2.

Lettieri, P. (2007) 'An introduction to particle systems', (May), pp. 1–25. doi: 10.1063/1.1510283.

Li, X., Wang, J. and Liu, C. (2015) 'A Bluetooth/PDR Integration Algorithm for an Indoor Positioning System', *Sensors*, 15(10), pp. 24862–24885. doi: 10.3390/s151024862.

Liao, C. L. C. and Barooah, P. (2010) 'An integrated approach to occupancy modeling and estimation in commercial buildings', *American Control Conference*. IEEE, pp. 3130–3135. doi: 10.1109/ACC.2010.5531035.

Liao, C., Lin, Y. and Barooah, P. (2012) 'Agent-based and graphical modelling of building occupancy', *Journal of Building Performance Simulation*, 5(1), pp. 5–25. doi: 10.1080/19401493.2010.531143.

Lin, H., Wang, Q., Wang, Y., Wennerstern, R. and Sun, Q. (2016) 'Agent-based Modeling of Electricity Consumption in an Office Building under a Tiered Pricing Mechanism', in *Energy Procedia*. Elsevier, pp. 329–335. doi: 10.1016/j.egypro.2016.12.056.

Liu, H., Darabi, H., Banerjee, P. and Liu, J. (2007) 'Survey of Wireless Indoor Positioning Techniques and Systems', *IEEE Transactions on Systems, Man and Cybernetics, Part C (Applications and Reviews)*, 37(6), pp. 1067–1080. doi: 10.1109/TSMCC.2007.905750.

Liu, J., Chen, R., Pei, L., Guinness, R. and Kuusniemi, H. (2012) 'A hybrid smartphone indoor positioning solution for mobile LBS', *Sensors (Switzerland)*, 12(12), pp. 17208–17233. doi: 10.3390/s121217208.

Løvs, G. G. (1998) 'Models of wayfinding in emergency evacuations', *European Journal of Operational Research*. ELSEVIER, 105(3), pp. 371–389. doi: 10.1016/S0377-2217(97)00084-2.

Lukianto, C., Hönniger, C. and Sternberg, H. (2010) 'Pedestrian smartphone-based indoor navigation using ultra portable sensory equipment', in *2010 International Conference on Indoor Positioning and Indoor Navigation, IPIN 2010 - Conference Proceedings*. IEEE, pp. 1–5. doi: 10.1109/IPIN.2010.5646697.

Luo, X., Lam, K. P., Chen, Y. and Hong, T. (2017) 'Performance evaluation of an agent-based occupancy simulation model', *Building and Environment*. Pergamon, 115, pp. 42–53. doi: 10.1016/j.buildenv.2017.01.015.

Luo, Y., Chen, Y. P. and Hoeber, O. (2011) 'Wi-Fi-Based Indoor Positioning Using Human-Centric Collaborative Feedback', in *2011 IEEE International Conference on*

Communications (ICC). IEEE, pp. 1–6. doi: 10.1109/icc.2011.5963278.

Luo, Y., Hoeber, O. and Chen, Y. (2013) 'Enhancing Wi-Fi fingerprinting for indoor positioning using human-centric collaborative feedback', *Human-centric Computing and Information Sciences*, 3(1), p. 2. doi: 10.1186/2192-1962-3-2.

Ma, R., Guo, Q., Hu, C. and Xue, J. (2015) 'An improved WiFi indoor positioning algorithm by weighted fusion', *Sensors (Switzerland)*, 15(9), pp. 21824–21843. doi: 10.3390/s150921824.

Mahdavi, A. and Tahmasebi, F. (2015) 'Predicting people's presence in buildings: An empirically based model performance analysis', *Energy and Buildings*, 86, pp. 349–355. doi: 10.1016/j.enbuild.2014.10.027.

Mahony, R., Hamel, T. and Pflimlin, J.-M. (2008) 'Nonlinear Complementary Filters on the Special Orthogonal Group', *IEEE Transactions on Automatic Control*, 53(5), pp. 1203–1218. doi: 10.1109/TAC.2008.923738.

Manna, C., Fay, D., Brown, K. N. and Wilson, N. (2013) 'Learning occupancy in single person offices with mixtures of multi-lag markov chains', in *Proceedings - International Conference on Tools with Artificial Intelligence, ICTAI*. IEEE, pp. 151–158. doi: 10.1109/ICTAI.2013.32.

Mautz, R. (2012) 'Indoor positioning technologies'. ETH Zurich, Department of Civil, Environmental and Geomatic Engineering, Institute of Geodesy and Photogrammetry. doi: 10.3929/ETHZ-A-007313554.

Menezes, A. C., Cripps, A., Bouchlaghem, D. and Buswell, R. (2012) 'Predicted vs. actual energy performance of non-domestic buildings: Using post-occupancy evaluation data to reduce the performance gap', *Applied Energy*. Elsevier, 97, pp. 355–364. doi: 10.1016/J.APENERGY.2011.11.075.

Michel, T., Fourati, H., Geneves, P. and Layaida, N. (2015) 'A comparative analysis of attitude estimation for pedestrian navigation with smartphones', in *2015 International Conference on Indoor Positioning and Indoor Navigation (IPIN)*. IEEE, pp. 1–10. doi:

10.1109/IPIN.2015.7346767.

Miyamoto, S. and Ogawa, H. (2014) 'Human Activity Recognition System Including Smartphone Position', *Procedia Technology*, 18, pp. 42–46. doi: 10.1016/j.protcy.2014.11.010.

Moder, T., Reitbauer, C., Dorn, M. and Wieser, M. (2017) 'Calibration of smartphone sensor data usable for pedestrian dead reckoning', in *2017 International Conference on Indoor Positioning and Indoor Navigation, IPIN 2017*. IEEE, pp. 1–8. doi: 10.1109/IPIN.2017.8115910.

Moghtadaiee, V. and Dempster, A. G. (2012) 'WiFi fingerprinting signal strength error modeling for short distances', in *2012 International Conference on Indoor Positioning and Indoor Navigation (IPIN)*. IEEE, pp. 1–6. doi: 10.1109/IPIN.2012.6418852.

Mourcou, Q., Fleury, A., Franco, C., Klopcic, F. and Vuillerme, N. (2015) 'Performance evaluation of smartphone inertial sensors measurement for range of motion', *Sensors (Switzerland)*, 15(9), pp. 23168–23187. doi: 10.3390/s150923168.

Muhammad, M. N., Salcic, Z. and Wang, K. I.-K. (2016) 'Real-time PDR based on resource-constrained embedded platform', in *Proceedings of the International Conference on Sensing Technology, ICST*. IEEE, pp. 779–784. doi: 10.1109/ICSensT.2015.7438502.

Mujtaba, A., Khalil, I. U. and Ahsan, M. (2018) *(PDF) Building Energy Management using Occupant detection*, *3rd Abasyn International Conference on Business and Technology*. Available at: https://www.researchgate.net/publication/324137344_Building_Energy_Management_using_Occupant_detection (Accessed: 19 February 2020).

NASA (2008) *NASA - BRAHMS - TUNE UP YOUR WORKPLACE*. Available at: https://www.nasa.gov/centers/ames/research/lifeonearth/lifeonearth-brahms.html (Accessed: 10 February 2020).

Newsham, G. R. and Birt, B. (2010) 'Detecting Total Building Occupancy for More

Efficient Operation'. doi: 10.4224/40000712.

Nguyen-Huu, K., Song, C. G. and Lee, S.-W. (2018) 'Smartphone Holding Styles Based Step Detection and Length Estimation'. Available at: https://www.semanticscholar.org/paper/Smartphone-Holding-Styles-Based-Step-Detection-and-Hang-Eun/113eaacf7918b6123528065ae330216e4931b658 (Accessed: 13 March 2019).

Niwa, H., Kodaka, K., Sakamoto, Y., Otake, M., Kawaguchi, S., Fujii, K., Kanemori, Y. and Sugano, S. (2008) 'GPS-based indoor positioning system with multi-channel pseudolite', in *Proceedings - IEEE International Conference on Robotics and Automation*. IEEE, pp. 905–910. doi: 10.1109/ROBOT.2008.4543320.

Ochiai, M., Fujii, M., Ito, A., Watanabe, Y. and Hatano, H. (2014) 'A study on indoor position estimation based on fingerprinting using GPS signals', in *2014 International Conference on Indoor Positioning and Indoor Navigation (IPIN)*. IEEE, pp. 727–728. doi: 10.1109/IPIN.2014.7275552.

Oksar, I. (2014) 'A Bluetooth signal strength based indoor localization method', in *Systems, Signals and Image Processing (IWSSIP), 2014 International Conference on*, pp. 251–254. Available at: http://ieeexplore.ieee.org/articleDetails.jsp?arnumber=6837678.

Oliveira-Lima, J. A., Morais, R., Martins, J. F., Florea, A. and Lima, C. (2016) 'Load forecast on intelligent buildings based on temporary occupancy monitoring', *Energy and Buildings*, 116, pp. 512–521. doi: 10.1016/j.enbuild.2016.01.028.

OlliW (2016) 'OlliW's Bastelseiten » IMU Data Fusing_ Complementary, Kalman, and Mahony Filter', pp. 1–18. Available at: http://www.olliw.eu/2013/imu-data-fusing/ (Accessed: 29 December 2017).

Ozsoy, K., Bozkurt, A. and Tekin, I. (2013) 'Indoor positioning based on global positioning system signals', *Microwave and Optical Technology Letters*, 55(5), pp. 1091–1097. doi: 10.1002/mop.27520.

Page, J. (2007) 'Simulating occupant presence and behaviour in buildings'. EPFL. doi: 10.5075/epfl-thesis-3900.

Page, J., Robinson, D., Morel, N. and Scartezzini, J.-L. (2008) 'A generalised stochastic model for the simulation of occupant presence', *Energy and Buildings*, 40(2), pp. 83–98. doi: 10.1016/j.enbuild.2007.01.018.

Page, J., Robinson, D. and Scartezzini, J. (2007) 'Stochastic simulation of occupant presence and behaviour in buildings', *researchgate.net*. Available at: http://www.researchgate.net/profile/Jean-Louis_Scartezzini/publication/37453662_Stochastic_Simulation_of_Occupant_Presence_and_Behaviour_in_Buildings/links/09e41513990cd19d37000000.pdf (Accessed: 15 February 2015).

Pan, X., Han, C. S., Dauber, K. and Law, K. H. (2007) 'A multi-agent based framework for the simulation of human and social behaviors during emergency evacuations', *AI and Society*, 22(2), pp. 113–132. doi: 10.1007/s00146-007-0126-1.

Papadopoulos, S. and Azar, E. (2016) 'Integrating building performance simulation in agent-based modeling using regression surrogate models: A novel human-in-the-loop energy modeling approach', *Energy and Buildings*, 128, pp. 214–223. doi: 10.1016/j.enbuild.2016.06.079.

Pappi, I. N., Paterakis, N. G., Catalao, J. P. S., Panapakidis, I. and Papagiannis, G. (2015) 'Analysis of the energy usage in university buildings: The case of Aristotle university campus', in *2015 Australasian Universities Power Engineering Conference: Challenges for Future Grids, AUPEC 2015*. IEEE, pp. 1–5. doi: 10.1109/AUPEC.2015.7324856.

Park, S. Y., Heo, S. J. and Park, C. G. (2017) 'Accelerometer-based smartphone step detection using machine learning technique', in *2017 International Electrical Engineering Congress, iEECON 2017*. IEEE, pp. 1–4. doi: 10.1109/IEECON.2017.8075875.

Parys, W., Saelens, D. and Hens, H. (2011) 'Coupling of dynamic building simulation

with stochastic modelling of occupant behaviour in offices - a review-based integrated methodology', *Journal of Building Performance Simulation*, 4(4), pp. 339–358. doi: 10.1080/19401493.2010.524711.

Peltola, P., Hill, C. and Moore, T. (2017) 'Adaptive real-time dual-mode filter design for seamless pedestrian navigation', in *2017 International Conference on Localization and GNSS (ICL-GNSS)*. IEEE, pp. 1–6. doi: 10.1109/ICL-GNSS.2017.8376257.

Pinchin, J., Brown, M., Blum, J., Shaw, D. and Blakey, J. (2014) 'Integrating WiFi based positioning with a job management system to study task management behaviour', in *2014 IEEE/ION Position, Location and Navigation Symposium - PLANS 2014*. IEEE, pp. 193–200. doi: 10.1109/PLANS.2014.6851375.

Pinchin, J., Hide, C. and Moore, T. (2012) 'A particle filter approach to indoor navigation using a foot mounted inertial navigation system and heuristic heading information', in *2012 International Conference on Indoor Positioning and Indoor Navigation (IPIN)*. IEEE, pp. 1–10. doi: 10.1109/IPIN.2012.6418916.

Poole, I. (2006) *Wi-Fi Channels, Frequency Bands and Bandwidth | Electronics Notes*. Available at: https://www.electronics-notes.com/articles/connectivity/wifi-ieee-802-11/channels-frequencies-bands-bandwidth.php (Accessed: 27 December 2018).

Preiser, W. F. E. (1995) 'Post-occupancy evaluation: How to make buildings work better', *Facilities*. MCB UP Ltd, 13(11), pp. 19–28. doi: 10.1108/02632779510097787.

Pritt, N. (2013) 'Indoor positioning with maximum likelihood classification of Wi-Fi signals', in *2013 IEEE SENSORS*. IEEE, pp. 1–4. doi: 10.1109/ICSENS.2013.6688619.

Quan, W., Li, J., Gong, X. and Fang, J. (2015) *INS/CNS/GNSS integrated navigation technology*. Available at: https://books.google.co.uk/books?id=eIdfBgAAQBAJ&pg=PA7&lpg=PA7&dq=navigation+filter+algorithm&source=bl&ots=1ENF2bxUMo&sig=ACfU3U0xJXY9qXnUiN6LUqNOZHmW8Br0Rw&hl=en&sa=X&ved=2ahUKEwiQy4yF2ujgAhWFuHEKHWvFBjY4ChDoATABegQIBhAB#v=onepage&q=navigation filter a (Accessed: 4 March 2019).

rabbit.com (2007) *An introduction to Wi-Fi*. Available at: http://ftp1.digi.com/support/documentation/0190170_b.pdf (Accessed: 27 December 2018).

Rajkiran, S. and Balakrishnan, C. (2015) 'RSSI estimation using Bluetooth in smart phones', in *2015 2nd International Conference on Electronics and Communication Systems (ICECS)*. IEEE, pp. 1431–1434. doi: 10.1109/ECS.2015.7124822.

Rasmussen, C. E. and Williams, C. K. I. (2006) 'Gaussian Processes for Machine Learning', in. Available at: www.GaussianProcess.org/gpml (Accessed: 29 December 2018).

Reinhart, C. F. (2004) 'Lightswitch-2002: a model for manual and automated control of electric lighting and blinds', *Solar Energy*, 77(1), pp. 15–28. doi: 10.1016/j.solener.2004.04.003.

Reinhart, C. F. and Cerezo Davila, C. (2016) 'Urban building energy modeling - A review of a nascent field', *Building and Environment*. Pergamon, pp. 196–202. doi: 10.1016/j.buildenv.2015.12.001.

Renaudin, V. and Combettes, C. (2014) 'Magnetic, acceleration fields and gyroscope quaternion (MAGYQ)-based attitude estimation with smartphone sensors for indoor pedestrian navigation', *Sensors (Switzerland)*. Multidisciplinary Digital Publishing Institute, 14(12), pp. 22864–22890. doi: 10.3390/s141222864.

Robinson, D. and Haldi, F. (2011) 'Modelling Occupants' Presence and Behaviour – Part I', *Journal of Building Performance Simulation*. Taylor & Francis, 4(4), pp. 301–302. doi: 10.1080/19401493.2011.599157.

Robinson, D. and Haldi, F. (2012) 'Modelling Occupants' Presence and Behaviour–Part II', *Journal of Building Performance Simulation*. Available at: http://www.tandfonline.com/doi/full/10.1080/19401493.2011.599158 (Accessed: 15 February 2015).

Robinson, S. (2004) *Simulation : the practice of model development and use*. Wiley.

Available at: https://books.google.com.bd/books/about/Simulation.html?id=DapH9XLwN4kC&redir_esc=y (Accessed: 26 September 2018).

Rodas, J., Escudero, C. J. and Iglesia, D. I. (2008) 'Bayesian filtering for a bluetooth positioning system', in *2008 IEEE International Symposium on Wireless Communication Systems*. IEEE, pp. 618–622. doi: 10.1109/ISWCS.2008.4726130.

Roetenberg, D., Luinge, H. J., Baten, C. T. M. and Veltink, P. H. (2005) 'Compensation of magnetic disturbances improves inertial and magnetic sensing of human body segment orientation', *IEEE Transactions on Neural Systems and Rehabilitation Engineering*, 13(3), pp. 395–405. doi: 10.1109/TNSRE.2005.847353.

del Rosario, M., Redmond, S. and Lovell, N. (2015) 'Tracking the Evolution of Smartphone Sensing for Monitoring Human Movement', *Sensors*, 15(8), pp. 18901–18933. doi: 10.3390/s150818901.

S Douglas, J. (2014) 'Energy Performance Analysis of University Buildings: Case Studies at Sheffield University, UK', *Journal of Architectural Engineering Technology*. OMICS International, 03(03), pp. 1–13. doi: 10.4172/2168-9717.1000129.

Saeedi, S. and El-Sheimy, N. (2015) 'Activity Recognition Using Fusion of Low-Cost Sensors on a Smartphone for Mobile Navigation Application', *Micromachines*, 6(8), pp. 1100–1134. doi: 10.3390/mi6081100.

Sánchez-Rodríguez, D., Hernández-Morera, P., Quinteiro, J., Alonso-González, I., Sánchez-Rodríguez, D., Hernández-Morera, P., Quinteiro, J. M. and Alonso-González, I. (2015) 'A Low Complexity System Based on Multiple Weighted Decision Trees for Indoor Localization', *Sensors*. Multidisciplinary Digital Publishing Institute, 15(6), pp. 14809–14829. doi: 10.3390/s150614809.

van der Sandt, P. H. (2012) 'Saving energy through education & awareness in the Hospitality Sector', in *2012 Southern African Energy Efficiency Convention (SAEEC)*. IEEE, pp. 1–6. doi: 10.1109/SAEEC.2012.6408586.

Shi, J., Ren, M., Wang, P. and Meng, J. (2018) 'Research on PF-SLAM indoor pedestrian localization algorithm based on feature point map', *Micromachines*, 9(6), p. 267. doi: 10.3390/mi9060267.

Shih, H. C. (2014) 'A robust occupancy detection and tracking algorithm for the automatic monitoring and commissioning of a building', *Energy and Buildings*, 77, pp. 270–280. doi: 10.1016/j.enbuild.2014.03.069.

Shin, S. H., Park, C. G., Kim, J. W., Hong, H. S. and Lee, J. M. (2007) 'Adaptive step length estimation algorithm using low-cost MEMS inertial sensors', in *Proceedings of the 2007 IEEE Sensors Applications Symposium, SAS*. IEEE, pp. 1–5. doi: 10.1109/SAS.2007.374406.

Siebers, P.-O. and Klügl, F. (2017) *'What Software Engineering has to offer to Agent-Based Social Simulation'. In: Edmonds B and Meyer R (Eds). Simulating Social Complexity: A Handbook - 2e*. Available at: http://www.cs.nott.ac.uk/~pszps/docs/pos-SSC_Ch6_Sec3.pdf (Accessed: 18 August 2019).

Smith, S. W. (2019) *Notation and Format of the Real DFT*. Available at: https://www.dspguide.com/ch8/2.htm (Accessed: 19 September 2019).

Society of Fire Protection Engineers (2019) 'Managing the Movement of Building Occupants', in *SFPE Guide to Human Behavior in Fire*. Springer International Publishing, pp. 131–147. doi: 10.1007/978-3-319-94697-9_13.

Solà, J. (2017) 'Quaternion kinematics for the error-state Kalman filter'. Available at: http://www.iri.upc.edu/people/jsola/JoanSola/objectes/notes/kinematics.pdf (Accessed: 29 December 2017).

Solin, A., Cortes, S., Rahtu, E. and Kannala, J. (2017) 'Inertial Odometry on Handheld Smartphones'. Available at: http://arxiv.org/abs/1703.00154 (Accessed: 28 December 2017).

Stoppel, C. M. and Leite, F. (2014) 'Integrating probabilistic methods for describing occupant presence with building energy simulation models', *Energy and Buildings*,

68(PARTA), pp. 99–107. doi: 10.1016/j.enbuild.2013.08.042.

Sun, K. and Hong, T. (2017) 'A simulation approach to estimate energy savings potential of occupant behavior measures', *Energy and Buildings*, 136, pp. 43–62. doi: 10.1016/j.enbuild.2016.12.010.

Syed, U. B. and Arslan, T. (2011) '3-Dimensional Approach to WiFi Indoor Positioning', in *Proceedings of the 24th International Technical Meeting of The Satellite Division of the Institute of Navigation (ION GNSS 2011)*, pp. 2861–2865. Available at: http://www.ion.org/publications/abstract.cfm?jp=p&articleID=9840 (Accessed: 30 October 2014).

Thacker, N. and Lacey, A. (1998) 'Tutorial: The Kalman filter', *Imaging Science and Biomedical …*, pp. 133–140. Available at: http://web.mit.edu/kirtley/kirtley/binlustuff/literature/control/Kalman filter.pdf (Accessed: 4 March 2019).

Tian, Q., Salcic, Z., Wang, K. I.-K. and Pan, Y. (2015) 'A hybrid indoor localization and navigation system with map matching for pedestrians using smartphones', *Sensors (Switzerland)*, 15(12), pp. 30759–30783. doi: 10.3390/s151229827.

Tian, Q., Salcic, Z., Wang, K. I.-K., Pan, Y. and Yim, J. (2013) 'A hybrid indoor localization and navigation system with map matching for pedestrians using smartphones', *International Journal of Smart Home*, 15(5), pp. 9–18. doi: 10.3390/s151229827.

Tian, Z., Zhang, Y., Zhou, M. and Liu, Y. (2014) 'Pedestrian dead reckoning for MARG navigation using a smartphone', *EURASIP Journal on Advances in Signal Processing*. SpringerOpen, 2014(1), p. 65. doi: 10.1186/1687-6180-2014-65.

Titterton, D. H. and Weston, J. L. (2004) *Strapdown Inertial Navigation Technology, Second Edition*. Available at: http://www.navtechgps.com/assets/1/7/1147.pdf (Accessed: 7 February 2019).

U.S. Department of Energy (2016) 'EnergyPlus: External interface(s) application guide'. Available at: http://simulationresearch.lbl.gov/bcvtb. (Accessed: 23 March 2019).

Valenti, R. G., Dryanovski, I. and Xiao, J. (2015) 'Keeping a good attitude: A quaternion-based orientation filter for IMUs and MARGs', *Sensors (Switzerland)*, 15(8). doi: 10.3390/s150819302.

Vazquez, F. I. and Kastner, W. (2010) 'Usage profiles for sustainable buildings', *2010 IEEE 15th Conference on Emerging Technologies & Factory Automation (ETFA 2010)*. Ieee, pp. 1–8. doi: 10.1109/ETFA.2010.5641214.

Vectornav (2008) *What is a quaternion?* Available at: http://www.vectornav.com/docs/default-source/documentation/vn-100-documentation/AN002.pdf?sfvrsn=19ee6b9_10 (Accessed: 18 May 2017).

VectorNav (2008) *VectorNav Technolgies*. Available at: https://www.vectornav.com/support/library/imu-and-ins (Accessed: 6 March 2019).

Wang, B., Liu, X., Yu, B., Jia, R. and Gan, X. (2018) 'Pedestrian dead reckoning based on motion mode recognition using a smartphone', *Sensors (Switzerland)*. Multidisciplinary Digital Publishing Institute (MDPI), 18(6), p. 1811. doi: 10.3390/s18061811.

Wang, C., Yan, D. and Jiang, Y. (2011) 'A novel approach for building occupancy simulation', *Building Simulation*. Tsinghua Press, 4(2), pp. 149–167. doi: 10.1007/s12273-011-0044-5.

Wang, D., Federspiel, C. C. and Rubinstein, F. (2005) 'Modeling occupancy in single person offices', *Energy and Buildings*, 37(2), pp. 121–126. doi: 10.1016/j.enbuild.2004.06.015.

Wang, Q., Ye, L., Luo, H., Men, A., Zhao, F. and Huang, Y. (2019) 'Pedestrian stride-length estimation based on LSTM and denoising autoencoders', *Sensors (Switzerland)*, 19(4), p. 840. doi: 10.3390/s19040840.

Wang, S. S. (2018) 'A BLE-based pedestrian navigation system for car searching in indoor parking garages', *Sensors (Switzerland)*. Multidisciplinary Digital Publishing Institute, 18(5), p. 1442. doi: 10.3390/s18051442.

Wang, Y. and Shao, L. (2017) 'Understanding occupancy pattern and improving building energy efficiency through Wi-Fi based indoor positioning', *Building and Environment*. Pergamon, 114, pp. 106–117. doi: 10.1016/j.buildenv.2016.12.015.

Ward, I., Ogbonna, A. and Altan, H. (2008) 'Sector review of UK higher education energy consumption', *Energy Policy*, 36(8), pp. 2939–2949. doi: 10.1016/j.enpol.2008.03.031.

Wei, Y., Zhang, X., Shi, Y., Xia, L., Pan, S., Wu, J., Han, M. and Zhao, X. (2018) 'A review of data-driven approaches for prediction and classification of building energy consumption', *Renewable and Sustainable Energy Reviews*, 82, pp. 1027–1047. doi: 10.1016/j.rser.2017.09.108.

Werner, M., Kessel, M. and Marouane, C. (2011) 'Indoor positioning using smartphone camera', in *2011 International Conference on Indoor Positioning and Indoor Navigation, IPIN 2011*. IEEE, pp. 1–6. doi: 10.1109/IPIN.2011.6071954.

De Wilde, P. (2014) 'The gap between predicted and measured energy performance of buildings: A framework for investigation', *Automation in Construction*. Elsevier, 41, pp. 40–49. doi: 10.1016/j.autcon.2014.02.009.

Xu, R., Chen, W., Xu, Y. and Ji, S. (2015) 'A new indoor positioning system architecture using gps signals', *Sensors (Switzerland)*, 15(5), pp. 10074–10087. doi: 10.3390/s150510074.

Yadav, N. and Bleakley, C. (2014) 'Accurate orientation estimation using AHRS under conditions of magnetic distortion', *Sensors (Switzerland)*. Multidisciplinary Digital Publishing Institute, 14(11), pp. 20008–20024. doi: 10.3390/s141120008.

Yang, Z., Becerik-Gerber, B., Li, N. and Orosz, M. (2014) 'A systematic approach to occupancy modeling in ambient sensor-rich buildings', *SIMULATION*, 90(8), pp. 960–977. doi: 10.1177/0037549713489918.

Yang, Z., Pan, Y. and Zhang, L. (2017) 'Hybrid orientation filter aided indoor tracking for pedestrians using a smartphone', in *IEEE International Conference on Control and*

Automation, ICCA. IEEE, pp. 107–112. doi: 10.1109/ICCA.2017.8003043.

Yim, J. (2013) 'A smartphone indoor positioning method', *International Journal of Smart Home*, 7(5), pp. 9–18. doi: 10.14257/ijsh.2013.7.5.02.

Yiu, S., Dashti, M., Claussen, H. and Perez-Cruz, F. (2017) 'Wireless RSSI fingerprinting localization', *Signal Processing*, 131, pp. 235–244. doi: 10.1016/j.sigpro.2016.07.005.

Yousefi, F., Gholipour, Y. and Yan, W. (2017) 'A study of the impact of occupant behaviors on energy performance of building envelopes using occupants' data', *Energy and Buildings*, 148, pp. 182–198. doi: 10.1016/j.enbuild.2017.04.085.

Yu, J., Na, Z., Liu, X. and Deng, Z. (2019) 'WiFi/PDR-integrated indoor localization using unconstrained smartphones', *Eurasip Journal on Wireless Communications and Networking*. SpringerOpen, 2019(1), p. 41. doi: 10.1186/s13638-019-1365-9.

Zhang, P., Zhao, Q., Li, Y., Niu, X., Zhuang, Y. and Liu, J. (2015) 'Collaborative WiFi fingerprinting using sensor-based navigation on smartphones', *Sensors (Switzerland)*. Multidisciplinary Digital Publishing Institute, 15(7), pp. 17534–17557. doi: 10.3390/s150717534.

Zhang, T., Siebers, P.-O. and Aickelin, U. (2013) 'Modelling Electricity Consumption in Office Buildings: An Agent Based Approach'. Available at: http://arxiv.org/abs/1305.7437 (Accessed: 26 September 2018).

Zheng-Chun, W., Zhi, X., Pin, L., Jian-Xin, X., Xin, H. and Li-Min, X. (2018) 'A method of inertial integrated navigation based on low cost MEMS sensors', in *2018 IEEE/ION Position, Location and Navigation Symposium, PLANS 2018 - Proceedings*. IEEE, pp. 1372–1378. doi: 10.1109/PLANS.2018.8373529.

Zheng, M., Meinrenken, C. J. and Lackner, K. S. (2014) 'Agent-based model for electricity consumption and storage to evaluate economic viability of tariff arbitrage for residential sector demand response', *Applied Energy*. Elsevier, 126, pp. 297–306. doi: 10.1016/j.apenergy.2014.04.022.

Zhou, H. and Van, N. N. (2014) 'Indoor Fingerprint Localization Based on Fuzzy C-Means Clustering', in *2014 Sixth International Conference on Measuring Technology and Mechatronics Automation*. IEEE, pp. 337–340. doi: 10.1109/ICMTMA.2014.83.

Zhou, M., Krishnamurthy, P., Xu, Y. and Ma, L. (2011) 'Physical Distance vs. Signal Distance: An Analysis towards Better Location Fingerprinting', in *2011 IEEE International Conference on High Performance Computing and Communications*. IEEE, pp. 977–982. doi: 10.1109/HPCC.2011.143.

Zhou, X. C., Chen, J. X., Dong, Y., Lu, X. R., Cui, J. W. and Zheng, B. Y. (2014) 'Pedestrian navigation with foot-mounted inertial sensors in wearable body area networks', in *2014 Asia-Pacific Signal and Information Processing Association Annual Summit and Conference, APSIPA 2014*. IEEE, pp. 1–7. doi: 10.1109/APSIPA.2014.7041547.

Zhu, N., Zhao, H., Feng, W. and Wang, Z. (2015) 'A novel particle filter approach for indoor positioning by fusing WiFi and inertial sensors', *Chinese Journal of Aeronautics*, 28(6), pp. 1725–1734. doi: 10.1016/j.cja.2015.09.009.

Zhu, X. and Feng, Y. (2013) 'RSSI-based Algorithm for Indoor Localization', *Communications and Network*. Scientific Research Publishing, 05(02), pp. 37–42. doi: 10.4236/cn.2013.52B007.

Zhuang, Y., Yang, J., Li, Y., Qi, L. and El-Sheimy, N. (2016) 'Smartphone-Based Indoor Localization with Bluetooth Low Energy Beacons', *Sensors*, 16(5), p. 596. doi: 10.3390/s16050596.

Zuraimi, M. S., Pantazaras, A., Chaturvedi, K. A., Yang, J. J., Tham, K. W. and Lee, S. E. (2017) 'Predicting occupancy counts using physical and statistical Co2-based modeling methodologies', *Building and Environment*, 123, pp. 517–528. doi: 10.1016/j.buildenv.2017.07.027.